TEHNIČKI GLASNIK

TEHNIČKI GLASNIK / TECHNICAL JOURNAL – GODIŠTE / VOLUME 13 – BROJ / NUMBER 1

OŽUJAK 2019 / MARCH 2019 – STRANICA / PAGES 1-80

/

SVEUČILIŠTE SJEVER / UNIVERSITY NORTH – CROATIA – EUROPE

ISSN 1846-6168 (PRINT) / ISSN 1848-5588 (ONLINE)

TECHNICAL JOURNAL

ISSN 1846-6168 (Print) ISSN 1848-5588 (Online)

TEHNIČKI GLASNIK - TECHNICAL JOURNAL

Scientific-professional journal of University North

Volume 13 Number 1
Varaždin, March 2019 Pages 1–80

Editorial Office:
Sveučilište Sjever – Tehnički glasnik
Sveučilišni centar Varaždin
104. brigade 3, 42000 Varaždin, Hrvatska
Tel. ++385 42 493 328, Fax.++385 42 493 333
E-mail: tehnickiglasnik@unin.hr
https://tehnickiglasnik.unin.hr
https://www.unin.hr/djelatnost/izdavastvo/tehnicki-glasnik/
https://hrcak.srce.hr/tehnickiglasnik

Founder and Publisher:
Sveučilište Sjever / University North

Print:
Centar za digitalno nakladništvo, Sveučilište Sjever

All manuscripts published in journal have been reviewed.
Manuscripts are not returned.

The journal is free of charge and four issues per year are published.
Circulation: 100 copies

Journal is indexed and abstracted in:
Web of Science Core Collection (Emerging Sources Citation Index - ESCI), EBSCOhost Academic Search Complete, EBSCOhost – One Belt, One Road Reference Source Product, ERIH PLUS, CITEFACTOR – Academic Scientific Journals, Hrčak - Portal znanstvenih časopisa RH

Registration of journal:
The journal "Tehnički glasnik" is listed in the HGK Register on the issuance and distribution of printed editions on the 18th October 2007 under number 825.

Preparation ended:
March 2019

Legend:
(1) University North, (2) Mechanical Engineering Faculty in Slavonski Brod, (3) Faculty of Graphic Arts Zagreb, (4) Faculty of Civil Engineering Osijek, (5) Faculty of Engineering Rijeka, (6) Faculty of Mechanical Engineering and Naval Architecture Zagreb, (7) Faculty of Metallurgy Sisak, (8) Tomas Bata University in Zlín, (9) Department of Physics of the University of Josip Juraj Strossmayer in Osijek, (10) Faculty of Humanities and Social Sciences Osijek, (11) Karlovac University of Applied Sciences, (12) University of Applied Sciences Velika Gorica, (13) Department of Polytechnics - Faculty of Humanities and Social Sciences Rijeka, (14) Faculty of Electrical Engineering and Computer Science - University of Maribor, (15) Faculty of Civil Engineering - University of Maribor, (16) University College of Teacher Education of Christian Churches Vienna/Krems, (17) Mechanical Engineering Faculty Tuzla, (18) Mechanical Engineering Faculty Sarajevo, (19) University of Travnik - Faculty of Technical Studies, (20) Higher Education Technical School of Professional Studies in Novi Sad, (21) University of Novi Sad - Faculty of Technical Sciences, (22) Faculty of Mechanical Engineering - University of Montenegro, (23) Brno University of Technology, (24) Odessa State Academy of Civil Engineering and Architecture, (25) Faculty of Civil Engineering - University of Mostar, (26) Faculty of Manufacturing Technologies with the seat in Prešov - Technical University in Košice

Note from the new member of the International Editorial Council

Dear Colleagues,

Industry 4.0 is a hot topic for today's society, especially for engineers. Robotics, automation, smart factory logistics, intelligent systems, internet of things, big data - those are the terms we use and deal with every day.

Academia and industrial partners solve technical challenges related to the implementation of Industry 4.0 to practice. Germany, where the Industry 4.0 revolution was launched in 2013 during the fair in Hanover, invests 40 billion euro per year to 4.0 applications. At the bottom of Mount Fuji there are factories where robots are self-replicated. In 2005, world-wide digital data reached 130 exabytes; the prediction for 2020 is 15,000 exabytes. We transfer big data to smart data. Production efficiency increases. We organize forums where we share our achievements so far.

In addition to all the effort, care, time, and energy invested so far, the question arises: Are we mentally ready for Industry 4.0?

The revolution (from Latin *revolvere*), according to its definition, is a fast, sudden, distinctive change. The first industrial revolution started in the UK in the 18th century and brought the labour from manufacturers to factories; steam engine constructed by James Watt was the turning point. The second, technological revolution, with mass production pioneers in automation, brought the greatest achievements in both natural and human sciences based on which our developed society was built. The third, digital revolution, started in the new millennium, and was the first in the history of the human civilization to change the concept of communication.

Each revolution caused people to fear it and to protest against it. Workers, later called luddites (according to Ned Ludd who broke his sewing machine) because they were destroying machines in factories, started massive protests already at the end of the 18th century. As we may learn from the history, such resistance and aversion existed in all the industrial revolutions.

Now, we are faced with the same situation, but this time not on the streets or in the factories, but on our current communication platform – social media. Robots are scaring one part of our society.

The origin of the word *robot* comes from Czech. In 1920, the Czech dramatist Karel Čapek wrote the play R.U.R. In this play, Rossum's Universal Robots, artificial people, overtake the world power. This novel was put into the category of science fiction. Now, a hundred years later, it addresses the questions and issues we have to answer in a satisfactory way.

Necessarily, our students will go directly to the epicentre of Industry 4.0, where more than 50% of present professions will be forgotten. With no doubt, they will have sufficient technical background to cope with the challenges and technical tasks waiting for them. In addition, I believe and hope we are preparing them to handle the social aspects of our new reality, where the borders between the real world and virtual world diminish.

What is the next step? Today's advanced technology and qualified workforce represent numerous opportunities that manufacturers can use to optimize their production processes. With the advent of industrial robots, such as co-robots, factory employees will continue to play an important role as a co-supervisor and ensure that work is done safely and without problems.

Business owners who are already creating smart factories will soon understand the need to consider what follows. In today's fast-growing manufacturing environment, companies must be at the top of their game by continually innovating their products or modernizing their production processes. Industry 5.0 has now begun to be rooted in factories, and cooperation between men and

machines will continue to prosper. The future has infinite possibilities of cooperation between the man and the robot.

Industry 5.0 is a revolution in the alignment of people and machines and in finding ways for them to work together to improve the means and efficiency of production. Simply ridiculous, the fifth revolution may already be in process among companies that only adhere to the principles of Industry 4.0.

Berenika Hausnerova

In Zlin, Czech Republic
January 31, 2019

Prof. Ing. Berenika HAUSNEROVÁ, Ph.D.
Department of Production Engineering
Tomas Bata University in Zlín
Faculty of Technology
Vavrečkova 275
760 01 Zlín, Czech Republic

https://ft.utb.cz/en/contacts/prof-ing-berenika-hausnerova-ph-d-2/

About ICMAE 2019

The 10th International Conference on Mechanical and Aerospace Engineering (ICMAE) will be held in Brussels during ***July 22nd-25th 2019***, following the successful conference in Budapest last year.

ICMAE is a global event focused on Mechanical and Aerospace Engineering. The support and participation of SCIEI members and participants has made ICMAE continue to be one of top conferences among Aerospace Engineering area. It focuses on all aspects in the area – e.g. research, achievements, industry, market, etc. Please see web site www.icmae.org for more detailed information.

With a solid reputation, ICMAE is event where you can meet and network with engineering leaders, business innovators, researchers, academics and policy makers from across the globe.

Previous ICMAE conferences: Kuala Lumpur / Bangkok / Paris / Moscow / Madrid / Rome / London / Prague / Budapest - www.icmae.org/history.html.

Submission:
Online at **EasyChair link**:
https://easychair.org/conferences/?conf=icmae2019

Contacts:
For General Questions ***Ms. Celine. Xi***
secretary@icmae.org

For Committee Member and Special Session Application ***Ms. Renne Gao*** committee@icmae.org

ICMAE 2019 Chairs

Advisory Chair	
Ruggero Maria Santilli	*USA*
Conference Chairs	
Dashnor Hoxha	*France*
Ian McAndrew	*United Kingdom*
Technical Program Chairs	
Anh Dung Ngo	*Canada*
Necdet Bildik	*Turkey*
Technical Program Co-Chairs	
Huafeng Ding	*China*
Michaela Musilova	*Slovakia*
Huisheng Shi	*China*
Steering Co-chairs	
Simon Barrans	*United Kingdom*
Eldad Avital	*United Kingdom*
Hamid Bahai	*United Kingdom*
Zheng Hong	*Canada*
Katarina Monkova	*Slovakia*
International Publicity Co-chairs	
Kamel Mehdi	*Tunisia*
Peter Pavol Monka	*Slovakia*
Yoshifumi Yokoi	*Japan*
Adriana Franca	*Brazil*
Luling An	*China*

ICMAE 2019 Technical Committee

Michaela Musilová *Slovakia* | ***Yuri N. Skiba*** *Mexico* | ***Maya Mitkova*** *Kuwait* | ***Önder TURAN*** *Turkey* | ***Anthony R. McAndrew*** *UK* | ***Kenji Uchiyama*** *Japan* | ***Linda Vee Weiland*** *Asia* | ***Mark Allen Friend*** *USA* | ***Tan Sui*** *UK*

ICMAE 2019 Venue

ICMAE´19 offers you very friendly and interesting venue of Brussels recognized as European Union Capitol, European top international-meetings city, and one of the top financial centres of Western Europe. The Brussels area is known as one of the richest business and cultural destinations in Europe. Brussels is known for its cuisine and gastronomy as well as its historical and architectural landmarks. Main attractions include its historic *Grand Place*, *Manneken Pis*, *Atomium*, and cultural institutions such as *La Monnaie* and the *Museums of Art and History*. It is also a capital of the comic strip.

Science and technology in Brussels is well developed with the presence of several universities and research institutes. More science parks associated with the universities are spread over the Brussels-Capital Region. The most important of them are Research Parks: *Da Vinci* RP/ *Erasmus* RP/ *Mercator* RP/ *Vesalius* RP.

It is possible to visit many Science & Technology Museums in Brussels. The *Royal Belgian Institute of Natural Sciences* houses the world's largest hall completely dedicated to dinosaurs. The *Planetarium of the Royal Observatory of Belgium* is one of the largest in Europe.

And who know – maybe ICMAE´19 presentation of your professional work will mark the city of Brussels for the future as place where "**YourName Breaking Concept**" was born!

ICMAE Topics:

Aerospace Mechatronics and Avionics Systems | Advanced theoretical models | Advances in aerospace technology | Aeroelasticity and loads | Mechanical Engineering in Aerospace | Applied Plasma and Fusion | Aerodynamics and Aeroacoustics | Airport Management and Operations | Aircraft Maintenance Management | Applied aerodynamics and fluid mechanics | Aviation human factors | Computational fluid dynamics | Electronic Systems | Technologies in navigation, avionics, radar, sonar, telemetry, sensors, security systems, simulators, automatic test, and command and control | Aerospace Communications | Aircraft Navigation | Astronomical Image Processing | Attitude maneuver control | Aerospace Engineering and Management | Satellite subsystems & components | Sensing & sensor technologies | Sensor platform & network | Space communications

ICMAE´19 Deadlines:

Submission due	April 10th 2019
Acceptance / Rejection	April 30th 2019
Final Registration	May 15th 2019
Conference Date	July 22nd-25th 2019

Publications:

- All successfully reviewed and accepted papers presented at ICMAE´19 will be published in **IEEE conference proceedings** and reviewed by the IEEE conference publication program for **IEEE Xplore**, **EI Compendex** and **Scopus**.
- Publication of two selected papers in extended contents in special issue "Recent Advances in Cellular Materials" of journal **Materials** ((ISSN 1996-1944) indexed in **Current Contents – Web of Sciences** (IF 2,467)) **with a discount of 75%.**
- The most excellent papers with extension will be selected and recommended to **International Journal of Mechanical Engineering and Robotics Research** (IJMERR – ISSN 2278-0149), indexed by **Scopus**.
- Special Issue publication in **Aerospace** (ISSN 2226-4310), indexed in **ESCI - Web of Science** from Vol. 3, and **Inspec (IET)** from Vol. 4 (2017). Covered in **Scopus** from Vol. 4. Registered papers will be recommended to this Journal. **Three excellent papers can be published for free.**

*Document version: **TUKE FMT PPM** 190316_1730*

ISSN 1846-6168 (Print), ISSN 1848-5588 (Online)
https://doi.org/10.31803/tg-20180131161141

Original scientific paper

GREEN SYNTHESIZED SILVER NANOPARTICLES LOADED PVA/STARCH CRYOGEL SCAFFOLDS WITH ANTIBACTERIAL PROPERTIES

Didem DEMİR, Seda CEYLAN, Gülşah GÜL, Zeynep İYİGÜNDOĞDU, Nimet BÖLGEN

Abstract: In this study, Polyvinyl alcohol/Starch (PVA/Starch) cryogel scaffolds were combined with antibacterial silver nanoparticles (AgNPs), and the antimicrobial properties of composite scaffolds were determined for potential in tissue engineering applications. The porous PVA/Starch scaffolds were prepared by cryogelation technique. The nanoparticles were prepared by green synthesis from Aloe barbadensis leaf extract and characterized. The antibacterial, antifungal and antiyeast properties of AgNPs and AgNPs loaded PVA/Starch cryogel scaffolds were investigated. The highest antimicrobial activity of composite scaffold was found against Pseudomonas aeruginosa. Based on our studies, the results indicate that biodegradable, biocompatible and antimicrobial AgNPs loaded PVA/Starch scaffolds have potential to be used at an infection site in tissue engineering applications.

Keywords: aloe barbadensis; antimicrobial activity; green synthesis; PVA/Starch scaffold; silver nanoparticles

1 INTRODUCTION

Over the past few decades, green process for the synthesis of nanoparticles has attracted wide interest because of its inherent features such as rapidity, simplicity, being eco-friendly and cheap [1]. A wide variety of applications include the use of nanoparticles due to their unique optical, electrical, mechanical, magnetic and chemical properties [2-4]. Due to their unique properties, metal nanoparticles, such as Ag, Au, Pt and Pd, are extensively used in pharmaceutical industry, clothing, cosmetics, optics, catalysis, mirrors, photography, electronics, food industry, and many other fields [5, 6]. Green biosynthesis has significant importance in the progress of nanotechnology. Several physical and chemical methods have been previously proposed to be used to synthesize nanoparticles. However, biosynthesis is an easy, alternative, eco-friendly and inexpensive approach compared to the previous methods. In addition, green synthesis method provides the production of nanoparticles with a well-defined shape and controllable size [1]. There are three main green synthesis perspectives in the production of AgNPs including the selection of solvent medium, reducing agent and nontoxic stabilizers [5]. One of the green methods of nanoparticle synthesis is the utilization of various plants and their parts [1]. The plant extract mediated synthesis of nanoparticles does not involve specific media and culture conditions and the reaction time is very short compared to other synthesis methods [7]. Gardea-Torresdey et al. reported the possibility of the synthesis of nanoscale metals by using plants. Later, various plants have been used to synthesize silver nanoparticles, such as *Azadirachta indica, Delonix elata, Tephrosia purpurea, Melia dubia, Tribulus terrestris, Artemisia nilagirica, Boerhaavia diffusa, Ficus religiosa, Piper pedicellatum* and *Melia azedarach* [1, 8].

The fabrication of scaffolds for tissue engineering applications with antibacterial properties is essential during implantation, surgery and wound healing process. Ideally, the scaffolds should have the ability to regenerate new tissue, treat the infection by delivering an antibacterial agent, and could provide a targeted treatment for the infection site [9]. Silver nanoparticles are loaded in different kinds of scaffolds (such as bacterial cellulose nanoparticles and chitosan-nanohyroxyapatite scaffold) to be applied as biomaterials with capability of reducing the bacterial and fungal infections [10, 11]. The incorporation of AgNPs into cryogels would attract a great deal of attention because of the resulting scaffolds' antimicrobial activity.

Cryogels are one the most promising types of scaffolds due to their interconnected and homogeneous macroporous structure which leads to three-dimensional cell growth, diffusion of nutrients and waste transfer during tissue regeneration [12]. Therefore, in this study we synthesized and characterized AgNPs by green synthesis approach with antimicrobial (antibacterial, antifungal and antiyeast) properties from aloe barbadensis leaf extract, combined them with PVA/Starch cryogel scaffolds, and demonstrated their antibacterial potential for tissue engineering applications.

2 MATERIALS AND METHOD

2.1 Chemicals

Silver nitrate was obtained from Merck, Germany. Aqueous solution of silver nitrate and other diluted solutions were prepared with distilled water. For the antimicrobial studies, nutrient agar (NA) and potato dextrose agar (PDA) were obtained from Merck, Germany. For the synthesis of scaffold, PVA with a molecular weight of 89,000-98,000 g/mol (99% hydrolyzed) was purchased from Sigma Aldrich, USA. Starch was obtained from Emir Chemicals, Turkey. Sodium dodecyl sulfate (SDS) was obtained from Merck, Germany. Both powder and liquid AgNPs, and AgNPs loaded PVA/Starch scaffolds were tested against bacterial and fungal species. The list of microorganisms used is presented in Table 1. Bacterial and yeast species were obtained from ATCC bacterial culture guide, and fungal species were provided by the Department of Genetics and Bioengineering, Faculty of

Engineering and Architecture, Yeditepe University (Istanbul, Turkey).

Table 1 The list of microbial species tested in antimicrobial studies

Bacteria	Yeast	Fungi
Pseudomonas aeruginosa ATCC 27853	*Candida albicans* ATCC 102312	*Aspergillus niger*
Escherichia coli ATCC 25922		
Staphylococcus aureus ATCC 29213		

2.2 Preparation of *Aloe Barbadensis* Leaf Extract

The freshly collected leaves of *Aloe barbadensis* were washed with tap water to remove the dust particles present on the surface and then rinsed with distilled water. The cleaned leaves were chopped into small pieces and dried for 2 days at 40 °C in the oven. The completely dried leaves were powdered with mortar for further usage in the preparation of leaf extract. 10 g of the powdered leaves were mixed with 100 ml of distilled water at 60 ± 1 °C for 30 min. After cooling, the mixture was filtered with a cheese cloth and the aqueous filtrate was centrifuged. The clear leaf extract of *Aloe barbadensis* was used for synthesis of AgNPs.

2.3 Synthesis of AgNPs

In order to synthesize AgNPs, 50 mL of the leaf extract was added drop by drop to 500 mL of 10 mM silver nitrate solution with stirring magnetically at room temperature for 30 min, as shown in the experimental set-up in Fig. 1. After incubation of the solution for 48 hours at dark conditions, the yellow color of the mixture of silver nitrate and leaf extract was changed to deep brown, which designates the formation of AgNPs. After the synthesis of AgNPs, the solution containing colloidal nanoparticles was centrifuged at 45x100 r/min for 5 min to separate AgNPs. The collected particles were subsequently dispersed in distilled water. Finally, AgNPs were dried at 110 °C in the oven for 24 h, and were stored at +4 °C in the refrigerator for further usage.

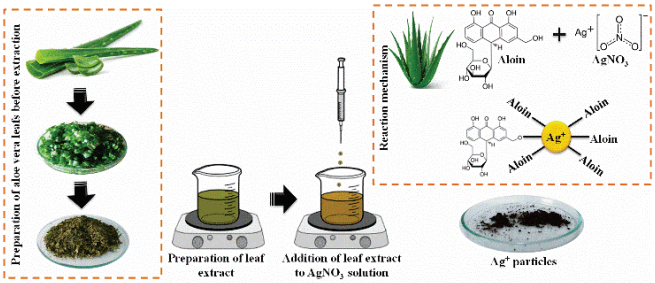

Figure 1 Experimental set-up of AgNPs synthesis from Aloe barbadensis leaf extract

2.4 Preparation of PVA/Starch Cryogel Scaffold

PVA/Starch cryogels were prepared by cryogelation technique as described in our previous study [13]. Briefly, PVA/Starch solution was fixed at 8% (w/v) polymer concentration at 90:10 (w:w) polymer ratio. SDS was added to the prepared polymer solution and homogeneous mixture was incubated at cryostat and freezer, then lyophilized before use. Synthesis, characterization, cytotoxicity and genotoxicity evaluation of PVA/Starch cryogels were investigated in previous study [13].

2.4 Characterization Studies of AgNPs

The synthesized AgNPs were characterized by UV-Vis Spectrophotometer (Chebios Optimum-One UV-VIS Spectrometer, Italy), which is the most widely used technique for structural characterization of metal nanoparticles. Fourier Transform Infrared Spectrometer (FTIR, Perkin Elmer, USA) for *Aloe barbadensis* leaf extract and AgNPs was obtained at a resolution of 4 cm^{-1} in the wavelength range 4000 to 450 cm^{-1}. The particle size distribution of AgNPs was performed by Zeta Sizer (Malvern, Nano ZS90, England) using Dynamic Light Scattering (DLS) technique.

2.4 Antimicrobial Activity of AgNPs and AgNPs Loaded PVA/Starch Scaffolds

Inhibition of microbial growth by the AgNPs and AgNPs loaded PVA/Starch scaffolds were tested against selected microorganisms. Antimicrobial activity tests were carried out using disc diffusion assay as described previously [14]. The blank discs were impregnated with 19 µL of liquid nanoparticles and blank disks were wetted with 19 µL of sterile distilled water and impregnated with powder nanoparticle samples. Liquid and powder AgNPs loaded blank disks were placed on the inoculated agar. PVA/Starch scaffolds were cut in 0.1 cm height and 50 µL of AgNPs solution was dropped on the scaffolds. AgNPs solution embedded scaffolds were placed into the inoculated plates. Ofloxacin (5 µg/disc) for bacteria and nystatin (100 µg/disc) for fungi were used as positive control. The inoculated plates were incubated at 36 ± 1 °C for 24 h for bacterial and yeast strains and at 27 ± 1 °C for 72 h for fungal isolate.

3 RESULTS AND DISCUSSION

3.1 Synthesis and Characterization of AgNPs

AgNPs were synthesized using *Aloe barbadensis* leaf extract as a reducing agent according to the method described in the previous section. Synthesis of AgNPs was proven with a color change from yellow to deep brown after 48 h of the addition of *Aloe barbadensis* leaf extract to silver nitrate solution. This color change is due to the excitation of surface plasmon resonance (SPR) vibrations of the AgNPs. The SPR vibrations of synthesized AgNPs were recorded by UV-Vis spectrum analysis of the reaction medium at different time points (12, 24 and 48 h). As shown in Fig. 2, a characteristic and well-defined SPR vibration was obtained at 430 nm, which is in agreement with the findings from previous studies [15, 16]. In addition, it was observed that increasing the reaction time increased the intensity of absorbance.

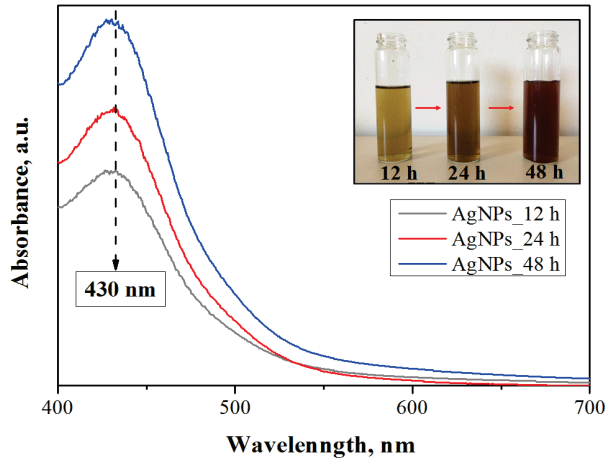

Figure 2 UV-Vis spectra of AgNPs solution at different reaction time points

FTIR analysis can be used for characterization of the synthesized AgNPs [17]. FTIR analysis of leaf extract and synthesized AgNPs is presented in Fig. 3. The absorption peaks of *Aloe barbadensis* leaf extract located at 1040, 1415, 2854 and 2919 cm^{-1} correspond to the presence of various compounds including proteins, amino acids, organic acids, vitamins, flavonoids, alkaloids, polyphenols, terpenoids, and polysaccharides. FTIR spectrum of AgNPs demonstrated sharp absorption peaks at 1619 and 3320 cm^{-1} which corresponds to amide and alcoholic hydroxide groups, respectively [6]. FTIR results confirmed that the *Aloe barbadensis* leaf extract can reduce and stabilize Ag^{1+} ions into zero valent Ag^0 nanoparticles. The flavonoid compounds in the extract of *Aloe barbadensis* might be responsible for this reduction [18, 19].

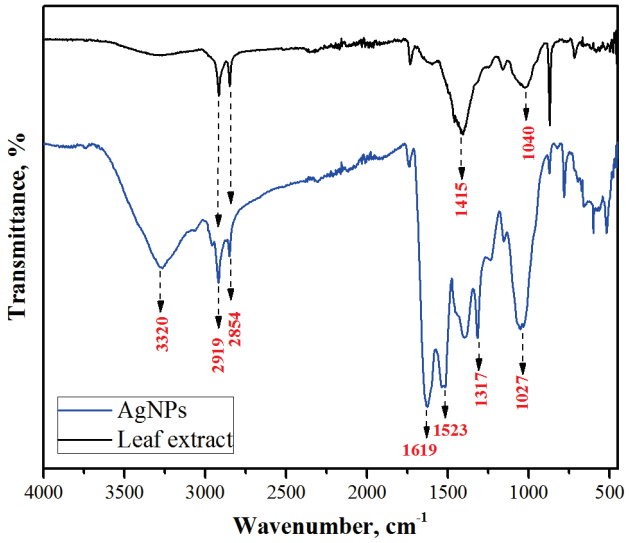

Figure 3 FTIR spectra of leaf extract and AgNPs

DLS measurements were done to determine the hydrodynamic size of the nanoparticles. Before DLS measurement, final reaction mixture containing the AgNPs was diluted with three fold distilled water. The particle size distribution curve (Fig. 4) demonstrated the various sizes of the particles ranging from 5.848 to 25.37 nm with an asymmetric distribution. The average particle size of the nanoparticles was 8.84 nm. In previous reports, the particle size of green synthesized AgNPs from various plant extracts increased from a nanometer to a hundred of nanometers. These studies proposed that by changing the composition of a reaction mixture or reaction conditions, the characteristic properties of nanoparticles such as size, shape, morphology and surface charge, could be controlled. In addition, the hydrodynamic diameter is presented as an important parameter, for understanding the size of nanoparticles and their performance in biological assays [20].

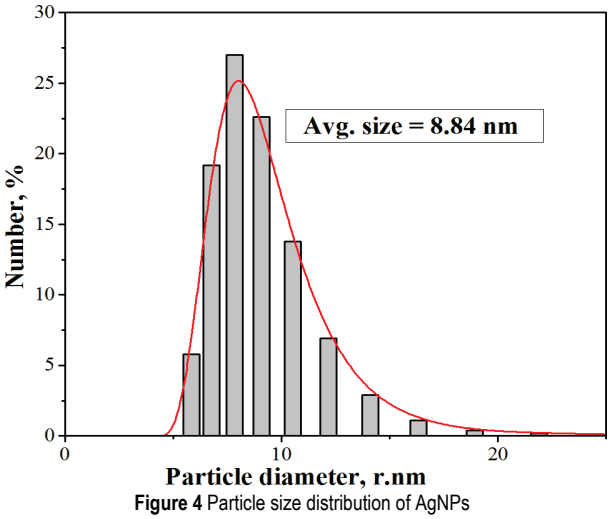

Figure 4 Particle size distribution of AgNPs

3.2 Antimicrobial Activity of Synthesized AgNPs and AgNPs Loaded PVA/Starch Cryogel Scaffolds

Antimicrobial activity of the powder and liquid nanoparticles, and AgNPs loaded scaffolds were investigated both quantitatively and qualitatively based on disc diffusion assays by evaluating the presence of inhibition zones and zone diameters. Antimicrobial activity test results were shown in Tab. 2.

Fig. 5 and Fig. 6 show the results of the antimicrobial tests regarding microorganisms. Disc diffusion assays revealed that both powder and liquid nanoparticles displayed remarkable antimicrobial activity on tested gram positive and gram negative bacterial and fungal species.

PVA/starch cryogel scaffolds which are promising materials for bone tissue engineering or wound dressing applications were synthesized and characterized in our previous study. Fourier transform infrared spectroscopy and scanning electron microscopy (SEM) were used to investigate the chemical structure and pore morphology of the scaffolds. Degradation profile and swelling ratio of the scaffolds were also determined. 3-(4,5-dimethylthiazoyl-2-yl)-2,5-diphenyltetrazolium bromide assay and SEM were used to investigate the biocompatibility of the scaffolds and cell morphology. In order to evaluate DNA fragmentation, genotoxicity test was also performed [13]. They were found to be biocompatible and have ability to enhance the attachment and growth of Mouse Embryonic Fibroblast cells. In the current study, the PVA/Starch cryogel scaffolds were impregnated with green synthesized AgNPs in order to

enhance their functions by adding antimicrobial properties. The composite PVA/Starch/AgNPs cryogel scaffolds were found to be effective against tested bacteria (both gram-positive and gram-negative), yeast and fungus (Tab. 2, Fig. 6). The composite cryogel scaffolds with antibacterial properties would have potential in preventing contamination risks in tissue engineering applications.

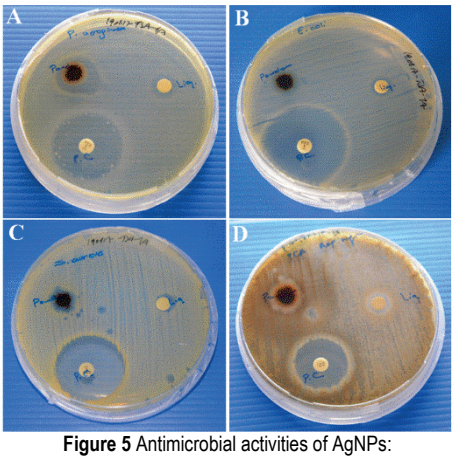

Figure 5 Antimicrobial activities of AgNPs:
A) *P. aeruginosa,* B) *E. coli,* C) *S. aureus,* D) *A. niger*

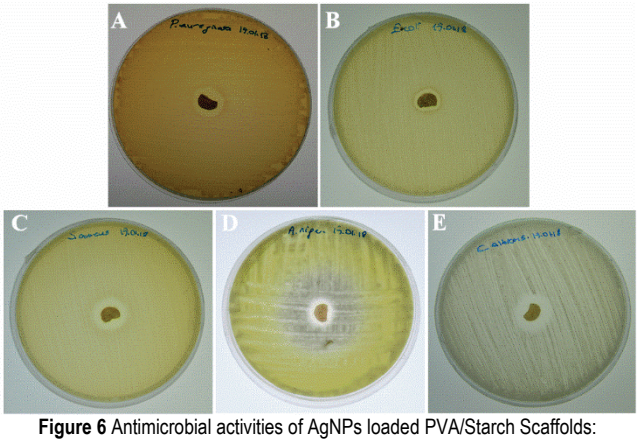

Figure 6 Antimicrobial activities of AgNPs loaded PVA/Starch Scaffolds:
A) *P. aeruginosa,* B) *E. coli,* C) *S. aureus,* D) *A. niger,* E) *C. albicans*

Antimicrobial activity of various scaffolds, including AgNPs impregnated, against gram-positive and gram-negative bacteria including *E. coli, S. aureus, and P. aeruginosa* and yeast (*C. albicans*) have been stated [21-25]. The selected bacteria, except *A. niger*, are responsible for nosocomial infections [21-26]. Moreover, *Candida* species are among the most opportunistic fungal pathogens responsible for invasive fungal infections. The antimicrobial activity of wound dressing or bone transplantation material is a favorable parameter for preventing surgical contaminations. AgNPs usage in tissue engineering scaffolds were reported previously [27, 28]. Jiang et al. produced nanohydroxyapatite/ polyurethane composite scaffolds with different amounts of silver phosphate particles for bone regeneration and tested them with *S. aureus* and *E. Coli*. Their results revealed that incorporation of silver phosphate particles into the scaffolds could impart excellent antibacterial activity to commonly existing bacteria [29]. Polycaprolactone and gelatine were also used to produce fibrous scaffolds and the scaffolds were coated with silver in different concentrations of silver nitrate aqueous solution. Scaffolds demonstrated antibacterial effects towards *Bacillus cereus* (B. cereus) and *E. coli* [30]. Moreover, nanosilver particles-collagen/chitosan hybrid scaffolds were produced for wound healing applications and applied in full-thickness skin defects in Sprague-Dawley rats to investigate the therapeutic effects of the scaffolds. The studies demonstrated that nanosilver particles-collagen/chitosan scaffolds promoted wound healing by regulating fibroblast migration and macrophage activation [31].

Table 2 Antimicrobial activity of powder and liquid nanoparticles and AgNPs loaded PVA/Starch scaffolds on microorganisms determined based on disc diffusion assay

Microbial Species	Zone of inhibition (mm)			
	Liquid	Powder	Scaffold	PC
Pseudomonas aeruginosa	12	22	20	30
Escherichia coli	10	14	12.5	30
Staphylococcus aureus	9	12	15	40
Candida albicans	NT	NT	17.5	24
Aspergillus niger	12	17	12	25

NT: not tested

As a result, the synthesized AgNPs loaded PVA/starch scaffolds could be helpful to treat both the development of infections due to microbial contamination of the scaffold throughout the surgery and the development of latent infections for biomedical applications.

4 CONCLUSION

The green synthesis of AgNPs using plant extracts is an eco-friendly method when compared to chemical and physical synthesis. The present study shows that leaf extract of *Aloe barbadensis* can be used efficiently for the synthesis of AgNPs. Green synthesized AgNPs loaded PVA/Starch cryogels were synthesized as novel tissue engineering scaffolds. Antimicrobial properties of the composite scaffold demonstrated its potential for preventing contamination risks in tissue engineering applications.

Acknowledgement

This work was supported by The Scientific Research Projects Unit of Mersin University (2018-1-TP3-2731). Authors would like to thank Yeditepe University Genetics and Bioengineering Department for providing microbial species.

5 REFERENCES

[1] Raja, S., Ramesh, V., & Thivaharan, V. (2017). Green biosynthesis of silver nanoparticles using Calliandra haematocephala leaf extract, their antibacterial activity and hydrogen peroxide sensing capability. *Arabian Journal of Chemistry*, 10, 253-261. https://doi.org/10.1016/j.arabjc.2015.06.023

[2] Bagherzade, G., Tavakoli, M. M., & Namaei, M. H. (2017). Green synthesis of silver nanoparticles using aqueous extract of saffron (Crocus sativus L.) wastages and its antibacterial

activity against six bacteria. *Asian Pacific Journal of Tropical Biomedicine, 7*(3), 227-233. https://doi.org/10.1016/j.apjtb.2016.12.014

[3] Khaghani, S. & Ghanbari, D. (2016). Magnetic and photo-catalyst Fe_3O_4–Ag nanocomposite: green preparation of silver and magnetite nanoparticles by garlic extract. Journal of Materials Science: Materials in Electronics, 8(3), 2877-2886. https://doi.org/10.1007/s10854-016-5872-8

[4] Hungund, B. S., Dhulappanavar, G. R., & Ayachit, N. H. (2015). Comparative Evaluation of Antibacterial Activity of Silver Nanoparticles Biosynthesized Using Fruit Juices. *Nanomedicine & Nanotechnology, 6*(2), 1-6. https://doi.org/10.4172/2157-7439.1000271

[5] Shameli, K., Bin Ahmad, M., Al-Mulla, E. A. J., Ibrahim, N. A., Shabanzadeh, P., Rustaiyan, A., Abdollahi, Y., Bagheri, S., Abdolmohammadi, S., Usman, M. S., & Zidan, M. (2012). Green Biosynthesis of Silver Nanoparticles Using Callicarpa maingayi Stem Bark Extraction. *Molecules, 17*(7), 8506-8517. https://doi.org/10.3390/molecules17078506

[6] Medda, S., Hajra, A., Dey, U., Bose, P., & Mondal, N. K. (2015). Biosynthesis of silver nanoparticles from Aloe vera leaf extract and antifungal activity against Rhizopus sp. and Aspergillus sp. *Applied Nanoscience, 5*(7), 875-880. https://doi.org/10.1007/s13204-014-0387-1

[7] Sadhasivam, L. & Durairaj, J. R. (2014). Evaluation profile of silver nanoparticle synthesized by Aloe Vera extract. *International Journal of ChemTech Research, 6*(9), 4379-4385.

[8] Yadav, J. P., Kumar, S., Budhwar, L., Yadav, A. and Yadav, M. (2016). Characterization and antibacterial activity of synthesized silver and iron nanoparticles using Aloe vera. *Journal of Nanomedicine & Nanotechnology, 7*(3), 1-7.

[9] El-Kady, A. M., Rizk, R. A., El-Hady, B. M. A., Shafaa, M. W., & Ahmed, M. M. (2012). Characterization and antibacterial properties of novel silver releasing nanocomposite scaffolds fabricated by the gas foaming/salt-leaching technique. *Journal of Genetic Engineering and Biotechnology, 10*(2), 229-238. https://doi.org/10.1016/j.jgeb.2012.07.002

[10] Barud, S. H., Regiani, T., Marques, R. F. C., Lustri, W. R., Messaddeq, Y., & Ribeiro, S. J. L. (2011). Antimicrobial Bacterial Cellulose-Silver Nanoparticles Composite Membranes. *Journal of Nanomaterials*, 2011, Article ID 721631, 8 pages. https://doi.org/10.1155/2011/721631

[11] Saravanan, S., Nethala, S., Pattnaik, S., Tripathi, A., Moorthi, A., & Selvamurugan, N. (2011). Preparation, characterization and antimicrobial activity of a bio-composite scaffold containing chitosan/nanohydroxyapatite/nano-silver for bone tissue engineering. *International Journal of Biological Macromolecules, 49*(2), 188-193. https://doi.org/10.1016/j.ijbiomac.2011.04.010

[12] Demir, D. & Bölgen, N. (2017). Synthesis and characterization of injectable chitosan cryogel microsphere scaffolds. *International Journal of Polymeric Materials and Polymeric Biomaterials, 66*(13), 686-696. https://doi.org/10.1080/00914037.2016.1255614

[13] Ceylan, S., Göktürk, D., Demir, D., Özdemir, M. D., & Bölgen, N. (2018). Comparison of additive effects on the PVA/Starch cryogels: Synthesis, characterization, cytotoxicity and genotoxicity studies. *International Journal of Polymeric Materials and Polymeric Biomaterials, 67*(14), 855-864. https://doi.org/10.1080/00914037.2017.1383254

[14] Iyigundogdu, Z. U., Demir, O., Asutay, A. B., & Sahin, F. (2017). Developing Novel Antimicrobial and Antiviral Textile Products. *Applied Biochemistry and Biotechnology, 181*(3), 1155-1166. https://doi.org/10.1007/s12010-016-2275-5

[15] Metuku, R. P., Pabba, S., Burra, S., Hima Bindu, S. V. S. S. S. L., Gudikandula, K., & Singara Charya, M. A. (2014). Biosynthesis of Silver Nanoparticles from Schizophyllum Radiatum HE 863742.1: Their Characterization and Antimicrobial Activity. *3 Biotech, 4*(3), 227-234. https://doi.org/10.1007/s13205-013-0138-0

[16] Zomorodian, K., Pourshahid, S., Sadatsharifi, A., Mehryar, P., Pakshir, K., Rahimi, M. J., & Arabi Monfared, A. (2016). Biosynthesis and Characterization of Silver Nanoparticles by Aspergillus Species. *BioMed Research International*, 2016, Article ID 5435397, 6 pages.

[17] Ahmed, S. & Ikram, S. (2015). Silver Nanoparticles: One Pot Green Synthesis Using Terminalia Arjuna Extract for Biological Application. *Journal of Nanomedicine and Nanotechnology, 6*(4), 1-6.

[18] Anandalakshmi, K., Venugobal, J., & Ramasamy, V. (2016). Characterization of silver nanoparticles by green synthesis method using Pedalium murex leaf extract and their antibacterial activity. *Applied Nanoscience, 6*(3), 399-408. https://doi.org/10.1007/s13204-015-0449-z

[19] Zuas, O., Hamim, N., & Sampora, Y. (2014). Bio-synthesis of silver nanoparticles using water extract of Myrmecodia pendans (Sarang Semutplant). *Material Letters, 123*, 156-159. https://doi.org/10.1016/j.matlet.2014.03.026

[20] Erjaee, H., Rajaian, H., & Nazifi, S. (2017). Synthesis and characterization of novel silver nanoparticles using Chamaemelum nobile extract for antibacterial application. *Advances in Natural Sciences: Nanoscience and Nanotechnology*, 8, 025004, 9 pages.

[21] El-Kady, A. M., Rizk, R. A., Abd El-Hady, B. M., Shafaa, M. W., & Ahmed, M. M. (2012). Characterization and antibacterial properties of novel silver releasing nanocomposite scaffolds fabricated by the gas foaming/salt-leaching technique. *Journal of Genetic Engineering and Biotechnology, 10*(2), 229-238. https://doi.org/10.1016/j.jgeb.2012.07.002

[22] Madhumathi, K., Sudheesh Kumar, P. T., Abhilash, S., Sreeja, V., Tamura, H., Manzoor, K., Nair, S. V., & Jayakumar, R. (2010). Development of novel chitin/nanosilver composite scaffolds for wound dressing applications. *Journal of Materials Science: Materials in Medicine, 21*(2), 807-813. https://doi.org/10.1007/s10856-009-3877-z

[23] Yazdimamaghani, M., Vashaee, D., Assefa, S., Shabrangharehdasht, M., Tahmasbi Rad, A., Eastman, M. A., Walker, K. J., Madihally, S. V., Köhler, G. A., & Tayebi, L. (2014). Green synthesis of a new gelatin-based antimicrobial scaffold for tissue engineering. *Materials Science and Engineering C, 39*, 235-244. https://doi.org/10.1016/j.msec.2014.03.007

[24] Xing, Z. C., Chae, W. P., Baek, J. Y., Choi, M. J., Jung, Y., & Kang, I. K. (2010). In vitro assessment of antibacterial activity and cytocompatibility of silver-containing phbv nanofibrous scaffolds for tissue engineering. *Biomacromolecules, 11*(5), 1248-1253. https://doi.org/10.1021/bm1000372

[25] D'Britto, V., Kapse, H., Babrekar, H., Prabhune, A. A., Bhoraskar, S. V., Premnathb, V., & Prasad, B. L. V. (2011). Silver nanoparticle studded porous polyethylene scaffolds: bacteria struggle to grow on them while mammalian cells thrive. *Nanoscale, 3*(7), 2957-2963. https://doi.org/10.1039/c1nr10154d

[26] Vonberg, R. P. & Gastmeier, P. (2007). Hospital-acquired infections related to contaminated substances. *Journal of Hospital Infection, 65*(1), 15-23. https://doi.org/10.1016/j.jhin.2006.09.018

[27] Marsich, E., Bellomo, F., Turco, G., Travan, A., Donati, I., & Paoletti, S. (2013). Nano-composite scaffolds for bone tissue

engineering containing silver nanoparticles: preparation, characterization and biological properties. *Journal of Materials Science: Materials in Medicine, 24*(7), 1799-1807. https://doi.org/10.1007/s10856-013-4923-4

[28] Jin, G., Prabhakaran, M. P., Nadappuram, B. P., Singh, G., Kai, D., & Ramakrishna, S. (2012). Electrospun Poly (L-Lactic Acid)-co-Poly (ϵ-Caprolactone) Nanofibres Containing Silver Nanoparticles for Skin-Tissue Engineering. *Journal of Biomaterials Science, Polymer Edition, 23*(18), 2337-2352.

[29] Jiang, J., Li, L., Li, K., Li, G., You, F., Zuo, Y., Li, Y., & Li, J. (2016). Antibacterial nanohydroxyapatite/polyurethane composite scaffolds with silver phosphate particles for bone regeneration. *Journal of Biomaterials Science, Polymer Edition, 27*(16), 1584-1598. https://doi.org/10.1080/09205063.2016.1221699

[30] Lim, M. M. & Sultan, N. (2016). In vitro cytotoxicity and antibacterial activity of silver-coated electrospun polycaprolactone/gelatine nanofibrous scaffolds. *3 Biotech, 6*(211), 1-10. https://doi.org/10.1007/s13205-016-0531-6

[31] You, C., Li, Q., Wang, X., Wu, P., Ho, J. K., Jin, R., Zhang, L., Shao, H., & Han, C. (2017). Silver nanoparticle loaded collagen/chitosan scaffolds promote wound healing via regulating fibroblast migration and macrophage activation. *Nature: Scientific reports, 7*(10489), 1-11.

Authors' contacts:

Didem DEMİR
Department of Chemical Engineering,
Mersin University, Mersin, Turkey
didemdemir@mersin.edu.tr

Seda CEYLAN
Department of Bioengineering,
Adana Science and Technology University, Adana, Turkey
sceylan@adanabtu.edu.tr

Gülşah GÜL
Department of Chemical Engineering,
Mersin University, Mersin, Turkey
Sah_8865@hotmail.com

Zeynep İYİGÜNDOĞDU
Department of Bioengineering,
Adana Science and Technology University, Adana, Turkey
ziyigundogdu@adanabtu.edu.tr

Nimet BÖLGEN, Corresponding author
Department of Chemical Engineering,
Mersin University, Mersin, Turkey
nimetbolgen@yahoo.com
nimet@mersin.edu.tr

ISSN 1846-6168 (Print), ISSN 1848-5588 (Online)
https://doi.org/10.31803/tg-20180514083545

Original scientific paper

THE STRESS-STRAIN STATE OF HORIZONTAL JOINTS OF WALL PANELS

Anatolii KOSTYUK, Dariya KOVTUNENKO, Aleksei KOVTUNENKO

Abstract: The article is devoted to the experimental and numerical research of the stress-strain state of wall panels joints from foam concrete of natural hardening. The eccentricity of the load and the quantity of indirect reinforcement meshes are adopted as factors that have a significant effect on the stress-strain state of the joint elements. The load in the experimental research and numerical simulation was applied in steps of 0.1 of the estimated value of the destructive force. Numerical modelling was carried out with consideration of the physical nonlinearity of the wall panel materials. A significant increment in the displacement of the design scheme nodes at the current loading stage was taken as a destruction criterion in numerical modelling. It is noted that the installation of indirect reinforcement meshes leads to a reduction of transverse deformations of the wall panel, but does not significantly affect the bearing capacity of the joint.

Keywords: eccentricity; foam concrete of natural hardening; horizontal joints; indirect reinforcement; stress-strain state; wall panel

1 STATE OF THE MATTER

The foam concrete is widely used in modern construction. It is possible to achieve high thermal performance in enclosing structures due to its structure. The production and use of large wall panels of foam concrete for low-rise construction will shorten the time of construction and installation works and allow to receive housing which will be comfortable at any time of the year.

There are several design solutions for joints (Fig. 1), consisting of wall panels and overlapping plates, which can be divided into contact (Fig. 1a), platform (Fig. 1b, c) and combined (contact-platform) (Fig. 1d, e) joints. A feature of the last type of joints is the presence of both a platform and a contact part. Joints of wall panels are designed with one- and two-sided arrangements of slabs (Fig. 1c, e).

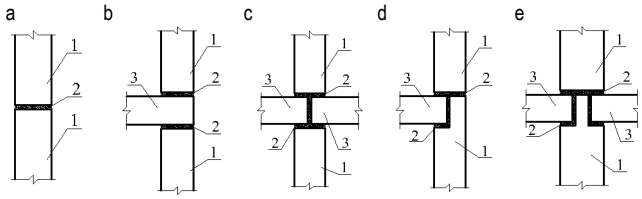

Figure 1 Designs of wall panels joints:
a, b, d, - joint of external walls; a, c, d - joint of internal walls; a - contact joint; b, c - platform joint; d, e, - combined joints; b, d - joints with one-sided support of the slab; c, e - joints with two-sided support of slabs.

The transfer of vertical forces in horizontal joints between panels represents the most difficult task of large-panel construction. The studies listed below concern the analysis of the support zone strength of panels made of heavy or light concrete from various factors, as well as the stress-strain state of the joint as a whole.

The research of butt joints in buildings from large panels was carried out since the 1930s by Soviet and European scientists. Among them, the works of [2-5, 7-16] and many others should be noted. All these works are devoted to the stress-strain state in the wall panels, under the influence of a certain set of factors affecting it. However, each of the works examines only one of the joint types and does not cover the simultaneous effect of the load application eccentricity and the presence of indirect reinforcement.

The aim of the work is to study the stress-strain state of three variants of butt joints of wall panels made of foam concrete of natural hardening.

The following tasks were accomplished to achieve this goal:

1. Experimental research of combined joint,
2. Analysis of experimental results,
3. Numerical simulation using a software package,
4. Comparison of the results of two experiments.

2 EXPERIMENTAL RESEARCH

The authors of this article carried out experimental research of combined joints of wall panels taking into consideration two important factors: the eccentricity of the load application and the amount of indirect reinforcement. The combined joint design was chosen as the main one because it includes a contact and a platform parts. This feature allows studying simultaneously three types of joint design.

The samples for the experimental research were made consisting of three parts (Fig. 2):

1. Overlying panel
2. Underlying panel
3. Floor slab

The dimensions of the sample elements are taken along the geometrical similarity to the actual parameters of the panels and their joints. The thickness of the wall panels is 200 mm (100 mm contact part and 100 mm platform part). The thickness of the floor slab is 150 mm. The width of the samples was adopted 600 mm with consideration of the press bearing pad dimensions. Supporting areas in the contact and platform parts of the sample overlying wall panel are located close to each other, so it can be assumed that the load on the sample is applied to its entire width l_c = 200 mm. The height of the overlying panel is assumed to be $3l_c$ = 600 mm. The

maximum possible support width in the platform part of the underlying panel is 100 mm. The required height of the underlying panel is $3l_c = 300$ mm. The ledge height of the underlying panel is 160 mm. Finally, the height of the underlying panel together with the ledge is 600 mm, based on the production conditions. The cantilever ledge of the floor slab fragment is 510 mm.

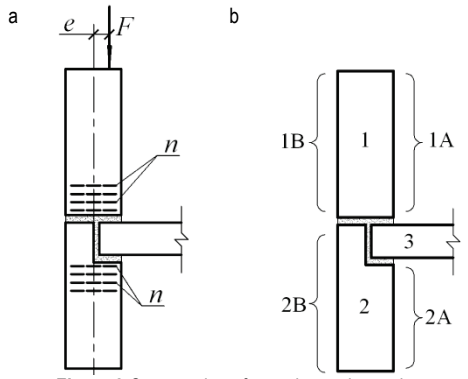

Figure 2 Construction of experimental samples:
a -factors considered in the experiment; b - layout of the joint elements;
1 - overlying panel; 2 - underlying panel; 3 –floor slab; 1A - the inner surface of the overlying panel; 1B - the outer surface of the overlying panel; 2A - the inner surface of the underlying panel; 2B - the outer surface of the underlying panel.

The wall panels of test samples are made of natural hardening foam concrete with density from 700 to 1000 kg/m³. The slab is made of heavy concrete of class C 25/30. The indirect reinforcement of the wall panels is made of reinforcing wire mesh ∅3 mm class Bp-I with a characteristic yield strength $f_y = 608$ MPa and modulus of elasticity $E = 30.51 \times 10^5$ MPa.

By analysis of the experiment results it is concluded that indirect reinforcement prevents the formation and development of a vertical crack from cement mortar joint between wall panels. At the same time, the bearing capacity of the sample as a whole does not change.

The increasing of loads eccentricity towards the platform part leads to decreasing of the contact area of the panels in the contact part (formation of the horizontal crack in the cement mortar) and redistribution of load onto the platform part. As a result, the destruction of the joint occurs along the platform part.

More detailed results of experimental research of the stress-strain state of the wall panels support zones with the identification of the most probable destruction schemes are given in [6].

3 NUMERICAL SIMULATION

In addition to the experimental tests, the authors carried out a numerical research of the stress-strain state of the support zones of wall panels. The software package Lira 9.4 that implements the finite element method was used for that purpose.

The following finite elements that allow the construction of a flat model were used at modelling:

1. Physically nonlinear universal rectangular finite element of a flat problem (beam-wall) (No. 223) was used for modelling of the body of a foam concrete panels, heavy concrete floor slab and cement mortar.
2. Physically nonlinear universal spatial rod finite element (No. 210) was used for modelling of meshes of indirect reinforcement.

The analysis was made taking into consideration non-linear properties of the materials with a stepwise increment of the load. The physical nonlinearity of the material was taken into account by the "σ-ε" diagram, which has an exponential dependence. The design values of mechanical properties of the materials were determined from the results of experimental compression tests of cube and prism samples, as well as tension tests of reinforcing bars. A significant increment of the design scheme nodes displacement at the current load stage was assumed as a criterion of the joints destruction.

The counter plots of the principal stresses distribution (Fig. 3) can be represented as a result of the joint samples analysis by software package Lira PC.

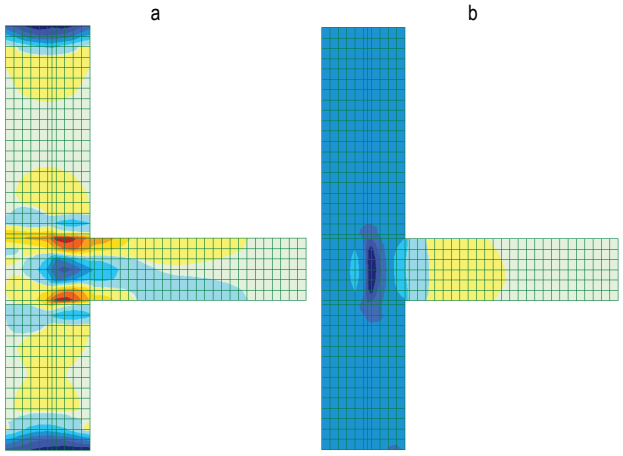

Figure 3 Principal stresses for sample JCP-0-0:
a – principal stresses σ_1; b – principal stresses σ_3

According to the counter plots of the principal stresses (Fig. 3), the support zones of the wall panels are in the condition of biaxial compression, which determines the nature of failure observed in the experimental research.

The dependences of the relative deformations on the load level (Fig. 4) are plotted to compare the results of a numerical study with the experimental research.

Statistical analysis (Tab. 1) of results comparison of samples numerical modelling and experimental research showed that the accepted model in SP "LIRA" describes the stress-strain state of joints of wall panels from natural hardening foam concrete with sufficient accuracy.

A numerical experiment was planned and carried out to generalize the results of the experimental research of the wall panel joint samples. The three types of horizontal joints of wall panels from natural hardening foam concrete with a stepwise increase of load up to the limit value were provided by the experiment plan.

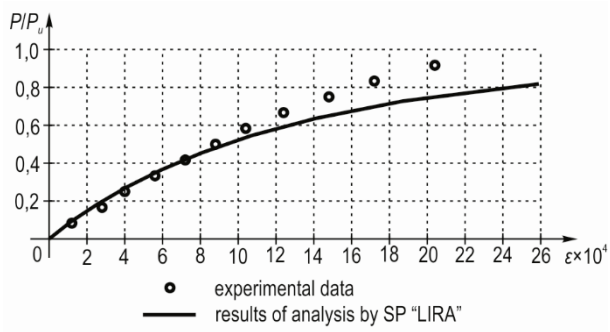

Figure 4 Diagram of the strain dependence on the load level for inner surface of overlying panel of the sample JCP 2-20 (1).

Table 1 Comparison of bearing capacity of combined horizontal joints

Sample code	Cubic strength $f_{cd,cube}$, MPa	Bearing capacity of joint, kN		
		by test results F_{exp}	based on the results of numerical studies F_{teor}	F_{exp}/F_{teor}
JCP-0-0	2.39	60.00	53.33	1.12
JCP -2-0	0.89	33.33	20.00	1.67
JCP -4-0	1.99	46.67	53.33	0.87
JCP -0-20	1.42	33.33	26.67	1.25
JCP -2-20-1	2.95	73.33	66.67	1.1
JCP -2-20-2	2.84	46.67	40.00	1.17
JCP -2-20-3	4.16	86.67	80.00	1.08
JCP -4-20	3.26	46.67	53.33	0.87
JCP -0-40	2.14	33.33	46.67	0.71
JCP -2-40	1.66	53.33	40.00	1.33
JCP -4-40	4.61	73.33	80.00	0.92

The physical and mechanical characteristics of the materials obtained during the experimental research were used. The averaged data for all the necessary parameters were used at planning a numerical experiment. The identical characteristics of the materials for all models of wall panel horizontal joints were used to obtain the objective results for comparison.

The following physical and mechanical material characteristics were used at modelling:

1. For foam concrete of wall panels:
- Density - 8 kN/m^3
- Modulus of elasticity (E_0) - 2902769 kN/m^2
- Ultimate value of tensile stresses σ (+) = 309.8901 kN/m^2
- Ultimate value of the compressive stresses σ (−) = 2402.629 kN / m^2

2. For heavy concrete of floor slab:
- Density - 25 kN/m^3
- Modulus of elasticity (E_0) - 24026290 kN/m^2
- Ultimate value of tensile stresses σ (+) = 1402.351 kN/m^2;
- Ultimate value of the compressive stresses σ (−) = 15004.17 kN/m^2.

3. For cement mortar of joint
- Density - 15 kN/m^3
- Modulus of elasticity (E_0) - 11473780 kN/m^2
- Ultimate value of tensile stresses σ (+) = 550.1531 kN/m^2
- Ultimate value of the compressive stresses σ (−) = 3500.974 kN/m^2

4. For wire rods of reinforcement meshes:
- Density - 78.5 kN/m^3
- Modulus of elasticity (E_0) - 2×10^8 kN/m^2
- Diameter - 3 mm

The loads distributed by linearly dependent were applied in stages by steps of 0.1 of the assumed destructive load.

With the purpose of creating a mathematical model of the corresponding physical work of the wall panels joint, the loads were transferred to the joint through a rigid bar with following characteristics:
- Density - 1×10^5 kN/m^3;
- Modulus of elasticity (E_0) - 2902770 kN/m^2;

Dependency diagrams of longitudinal and transverse deformations in wall panels on the load are plotted (Fig. 5-14) based on the numerical models analysis results of the wall panels horizontal joints.

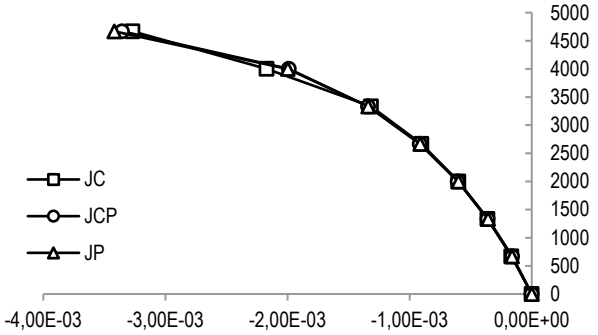

Figure 5 Diagrams of the strain dependence on the applied load for inner surface of overlying panel of samples with two meshes of indirect reinforcement and with eccentricity equal to 20 mm.

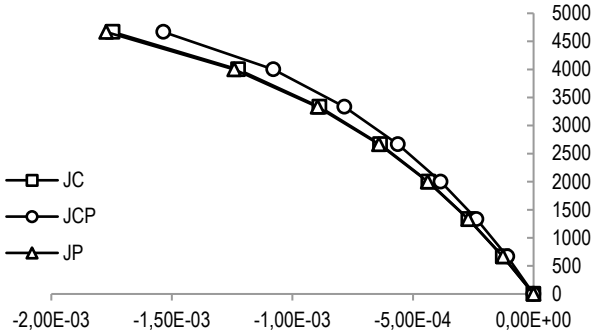

Figure 6 Diagrams of the strain dependence on the applied load for inner surface of underlying panel of samples with two meshes of indirect reinforcement and with eccentricity equal to 20 mm.

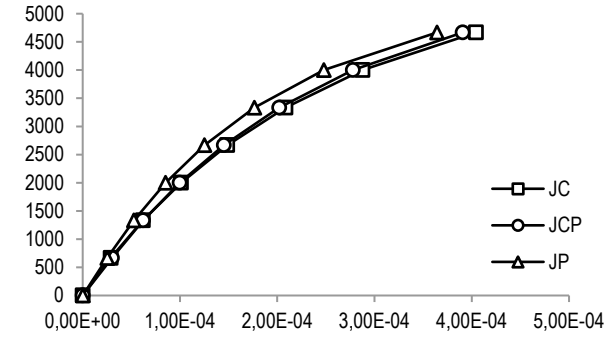

Figure 7 Diagrams of the transverse strain dependence on the applied load for section of overlying panel on distance of 20 mm from cement mortar of samples with two meshes of indirect reinforcement and with eccentricity equal to 20 mm.

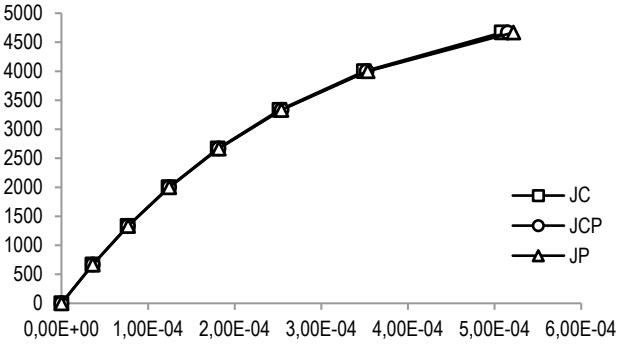

Figure 8 Diagrams of the transverse strain dependence on the applied load for the section of overlying panel on distance of 170 mm from cement mortar of samples with two meshes of indirect reinforcement and with eccentricity equal to 20 mm.

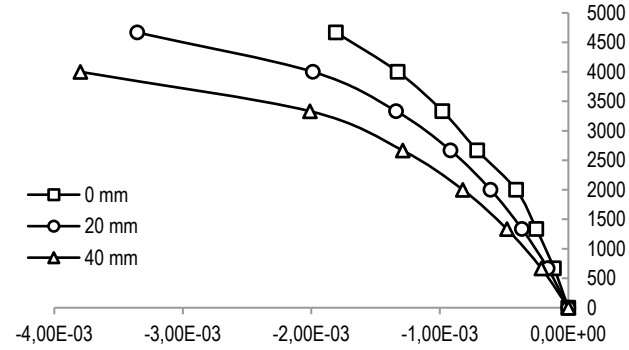

Figure 9 Diagrams of the strain dependence on the applied load for inner surface of overlying panel of combined design samples with two meshes of indirect reinforcement

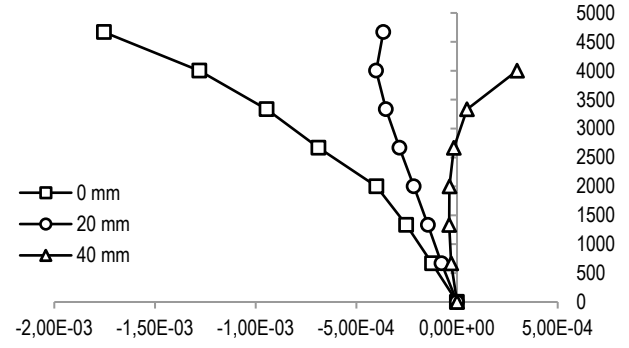

Figure 10 Diagrams of the strain dependence on the applied load for outer surface of overlying panel of combined design samples with two meshes of indirect reinforcement

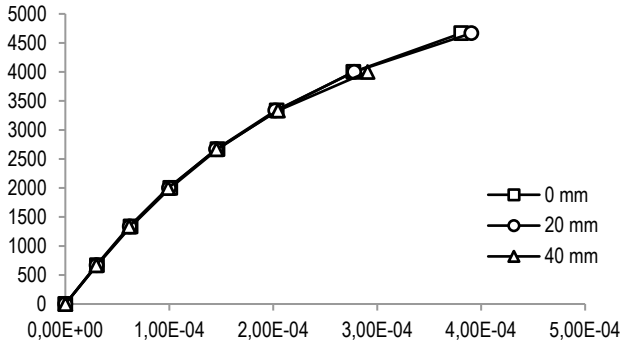

Figure 11 Diagrams of the transverse strain dependence on the applied load for the section of overlying panel on distance of 20 mm from cement mortar of combined design samples with two meshes of indirect reinforcement.

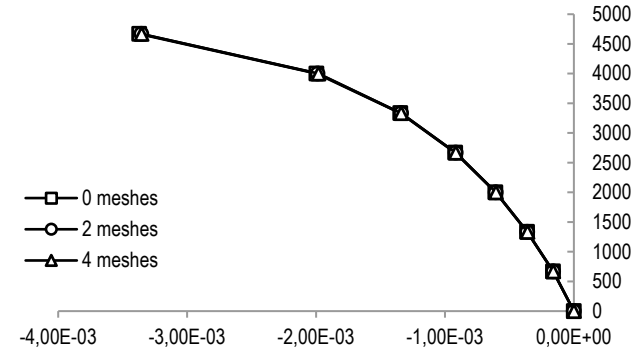

Figure 12 Diagrams of the strain dependence on the applied load for inner surface of overlying panel of combined design samples with eccentricity equal to 20 mm

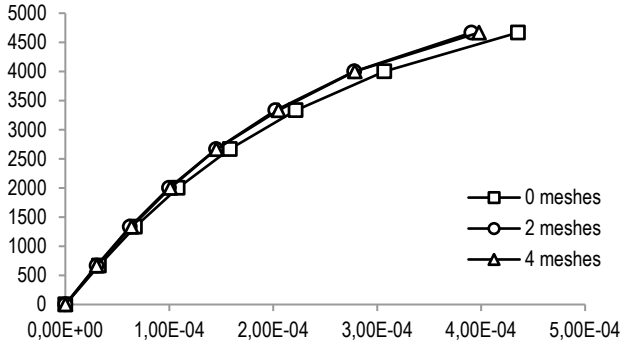

Figure 13 Diagrams of the transverse strain dependence on the applied load for the section of overlying panel on distance of 20 mm from cement mortar of combined design samples with eccentricity equal to 20 mm.

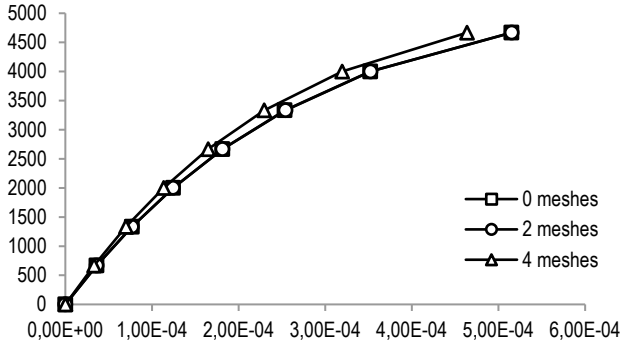

Figure 14 Diagrams of the transverse strain dependence on the applied load for the section of underlying panel on distance of 20 mm from cement mortar of combined design samples with eccentricity equal to 20 mm.

4 CONCLUSION

The following conclusions can be made by analysing the obtained diagrams:

1. The longitudinal deformations are reduced by 12% on the outer surface of the bottom panel and increased by an average of 10% on the inner surface as the result of redistribution of internal forces into a more rigid platform part of the combined joint.
2. The design of the platform joints of the wall panels provides greater stiffness of the joint in the direction transverse to the axis of the wall panels, and as a result, the transverse deformations in the support part ($h \leq 0.5$b) of the wall panel are reduced by 13-17%.
3. The wall panel horizontal joints design does not exert any influence on the overall bearing capacity of joints.
4. The installation of the indirect reinforcement meshes resulted in the reduction of transverse deformations in the support zone of the wall panels by 8-12% in all the three types of joint design.
5. The installation of the indirect reinforcement meshes does not affect longitudinal deformations in the body of the wall panels and the bearing capacity of the horizontal joints as a whole.
6. Increasing of loads eccentricity towards the inner surface of the wall panels leads to an increase of the compression deformation on the inner surface of the overlying panel and the outer surface of the underlying panel. As a result, the compression deformation on the opposite sides of the wall panels is decreasing up to the emergence of tensile deformation on the outer side of the overlying panel.
7. The transverse deformations increase to 5% in the underlying panel and up to 20% in the overlying panel with increasing eccentricity. The effect of the eccentricity decreases as the considered cross-section is removed from the place where the load is applied.
8. The loads preceding the development of plastic deformations decrease from $0.5P_u$ (for the sample without eccentricity) to $0.33P_u$ (for the sample with eccentricity equal to 40 mm).
9. The bearing capacity of the horizontal joints of the wall panels decreases by 12.5% for joints where $e = 20$ mm, and by 25% for samples where $e = 40$ mm with increasing eccentricity.

5 REFERENCES

[1] Barboza, A. d S. R. & El Debs, M. K. (2006). Load-bearing capacity of mortar joints between precast elements. *Magazine of Concrete Research, 58*(9), 589-599. https://doi.org/10.1680/macr.2006.58.9.589

[2] Grasser, F. & Daschner, F. (1972). Die Druckfestigkeit von Mörtel fugenzwischen Beton Fertigteilen. *Deutscher Ausschuss für Stahlbeton*, 221-228.

[3] Drozdov, P. F., Gorshkov, Yu. K., & Panshin, L. L. (1975). Compressed mortar joints. *Housing construction*, 6, 9-10.

[4] Gorachek, E. & Lishak, I. (1980). *Strength and rigidity of butt joints of panel structures*. Moscow, stroiizdat, 191-199.

[5] Korchagin, O. P. (1986). *The ultimate condition of large-panel buildings caused by the thawing of mortar joints*. Work of constructions of residential buildings from large-sized elements: a collection of scientific works. Central Research Institute of Housing, 104-106.

[6] Kostyuk, A. & Kovtunenko, D. (2016). Experimental research of combined joints of wallboards from natural hardening foam concrete. *Technical Journal, 10*(3-4), 124-127.

[7] Kotov, I. T. (1968). Investigations of the influence of the assembly seam on the strength of panel walls. Durability of large-panel structures. 100-106.

[8] Lishak, V. I. & Agranovsky, V. D. (1984). *Influence of thickness and strength of solution joints on the bearing capacity of horizontal joints*. Constructive systems of full-assembled residential buildings: a collection of scientific papers. Central Research Institute of Building Constructions, 106-111.

[9] Morozov, Yu. B. & Sedlovets, G. F. (1971). Investigation of strength and deformations of horizontal joints of wall panels. Investigation of strength and calculation of multi-storey buildings. MNIITEP Moscow, Russia.

[10] Sokolov, B. S. & Nikitin, G. P. (2007). Perfection of the procedure for calculating combined joints of building panels. *Bulletin of Tomsk State Architectural and Construction University*, 1, 81-90.

[11] Sedov, A. N. (2009). *Structural and technological features of reinforcement of combined joints in large-panel buildings during reconstruction*. Author's abstract. Thesis for a scientific degree PhD. KazGASU Kazan, Russia.

[12] Sementsov, S. A. (1961). Strength of knots of interface of walls and ceilings in large-panel buildings. *Concrete and Reinforced Concrete*, 1, 14-18.

[13] Sokolov, B. S. (1992). A new approach to calculating the strength of concrete elements under local load action. *Concrete and Reinforced Concrete*, 10, 22-25.

[14] Spiridonov, V. V. (1957). Bearing capacity of horizontal joints of large-panel buildings. *Concrete and Reinforced Concrete*, 5, 199-202.

[15] Spiridonov, V. V. (1957). Bearing capacity of horizontal joints of large-panel buildings. *Concrete and Reinforced Concrete*, 5, 199-202.

[16] Shapiro, G. I. & Shapiro, A. G. (2008). Calculation of the strength of platform joints of panel buildings. *Industrial and Civil Construction*, 1, 55-57.

Authors' contacts:

Anatolii KOSTYUK, Professor
Odessa State Academy of Civil Engineering and Architecture
Address: Ukraine, Odessa, Didrikhsona St., 4
Tel./Fax,e-mail: +380 505 523 855, isi@ogasa.org.ua

Dariya KOVTUNENKO, Assistant
Odessa State Academy of Civil Engineering and Architecture
Address: Ukraine, Odessa, Didrikhsona St., 4
Tel./Fax,e-mail: +380 673 655 520, kovtunenko.d.o@gmail.com

Aleksei KOVTUNENKO, Assistant Professor
Odessa State Academy of Civil Engineering and Architecture
Address: Ukraine, Odessa, Didrikhsona St., 4
Tel./Fax,e-mail: +380 963 960 557, kovtunenko.aleksei.od@gmail.com

ISSN 1846-6168 (Print), ISSN 1848-5588 (Online)
https://doi.org/10.31803/tg-20180522160526

Original scientific paper

FEATURES OF SILOS CALCULATIONS AT ASYMMETRIC WIND LOAD BY USING THE MOMENTLESS THEORY

Oleksandr LAPENKO, Anton MAKHINKO, Natalia MAKHINKO

Abstract: The paper deals with the features of silos calculations as shells of rotation under asymmetric semi-uniform load. In accordance with the equation of equilibrium by using the momentless theory, the expressions for maximum value of linear longitudinal efforts in radial and meridional (longitudinal) direction and linear shearing force have been obtained. Analysis of design factor series of linear efforts and shearing force has been carried out in the paper. The opportunity of using the momentless theory to evaluate changes of linear efforts in radial direction and shearing forces has been presented. The quantitative assessment of a normal tension in laminas of silo body from the influence of maximum linear efforts and their connection with the tension from the pressure of the bulk material at the top of the capacity have been given. Full radial and contacting displacements of the capacity in the plane of cross section from the element of the wind load have been defined.

Keywords: aerodynamics; cylindrical silo; internal forces; membrane theory of shells; radial displacements; wind loads

1 INTRODUCTION

Definition of the state of tension of the silos constructions is an important engineering problem. Calculation of the construction depends on the character of the external load. The main asymmetric semi-uniform load for storage containers is wind load. It is radially applied external load that is evenly distributed along the length of capacity, but it is changeable in the cross-section according to the corresponding law.

Similar problems were studied earlier, but they have a rather conditional character towards the nature of the wind load or they refer to the shell calculations in general without the emphasis on the deflective mode of distinct elements [2, 3].

1.1 Defining the Unsolved Aspects of the Problem

According to the general theory of shell rotation it is known that any load can be decomposed in trigonometric series of the finite length [4, 5], for which functional connections between parameters of the load and the deflective mode already exist. By contrast, the wind load is well approximated near cosines. Decomposition of the wind load into finite trigonometric series will simplify the calculation by examining every element separately.

1.2 The Aim of the Article

The aim of this paper is to calculate silos and analysis of displacement taking into consideration deflective mode of vertical stiffening ribs that receive wind load together with the body and take part in transferring arising efforts on the basis.

2 RESEARCH RESULTS

According to the design norms of different countries of the world, including NBS (National Building Standards) [1], uneven distribution of the wind load around the perimeter of cylindrical capacities is described by the function of aerodynamic coefficient $C_{aer}(\varphi)$. This function is represented in the normative literature in tables (graphs) [6, 7] or analytically using decimal logarithms [8, 9]. It is the cause of many inconveniences in capacity calculations. It can be eliminated by decomposing the function $C_{aer}(\varphi)$ into trigonometric series.

$$C_{aer}(\varphi) = a_0 + a_1\cos(\varphi) + a_2\cos(2\varphi) + \ldots + a_k\cos(k\varphi) + \ldots + a_m\cos(m\varphi). \quad (1)$$

There are graphs and diagrams of the aerodynamic coefficient correspondingly in Fig. 1 when it is decomposed into 5-7 elements. In Tab. 1, there are coefficients of this decomposition, computed by the method of the least square according to the graph of norms [1].

Table 1 Quantities of coefficients a_k during the series development $C_{aer}(\varphi)$ according to $\cos(k\varphi)$

№	a_0	a_1	a_2	a_3	a_4	a_5
5	-0.380	0.326	0.686	0.478	0.040	н
6	-0.380	0.337	0.686	0.489	0.040	-0.114
7	-0.378	0.337	0.690	0.489	0.044	-0.114
8	-0.378	0.338	0.690	0.490	0.044	-0.113
9	-0.377	0.338	0.692	0.490	0.046	-0.113
5	a_6	a_7	a_8	ξ_p	ξ_h	ξ_s
6	н	н	н	8.01	0.77	1.32
7	н	н	н	5.27	0.72	1.37
8	-0.048	н	н	3.63	0.70	1.42
9	-0.048	-0.016	н	2.88	0.70	1.44
5	-0.046	-0.016	-0.021	1.65	0.69	1.45

From the drawing we can see that 5 or 6 elements in series are sufficient for practical calculations accuracy. The attention needs to be directed to the recommendation norms [1] which are not the only ones, for example [10], which, respectively, influence the quantitative assessment of series coefficients (1). However, this question requires further

research of the wind effect both on separate capacities and capacities as a part of silos stock.

Decomposition of aerodynamic coefficient and wind load, respectively, into finite trigonometric series allows a significant simplification of the solution of the calculation problem of cylindrical capacities, since in this case calculation can be carried out for every element of the load separately. Following is the equation of equilibrium for capacity according to the momentless theory [11]

$$\begin{aligned} &\frac{D_w}{2}\frac{\partial N_{p,k}(x)}{\partial x}+\frac{\partial S_k(x,\varphi)}{\partial \varphi}=0,\\ &\frac{\partial N_{h,k}(\varphi)}{\partial \varphi}+\frac{D_w}{2}\frac{\partial S_k(x,\varphi)}{\partial x}=0,\\ &N_{h,k}(\varphi)=\frac{W_k D_w}{2}, \end{aligned} \tag{2}$$

where $N_{h,k}$ and $N_{p,k}$ are linear longitudinal efforts in radial and meridional (longitudinal) directions; S_k is a linear shearing force; A_k is an amplitude value of k element.

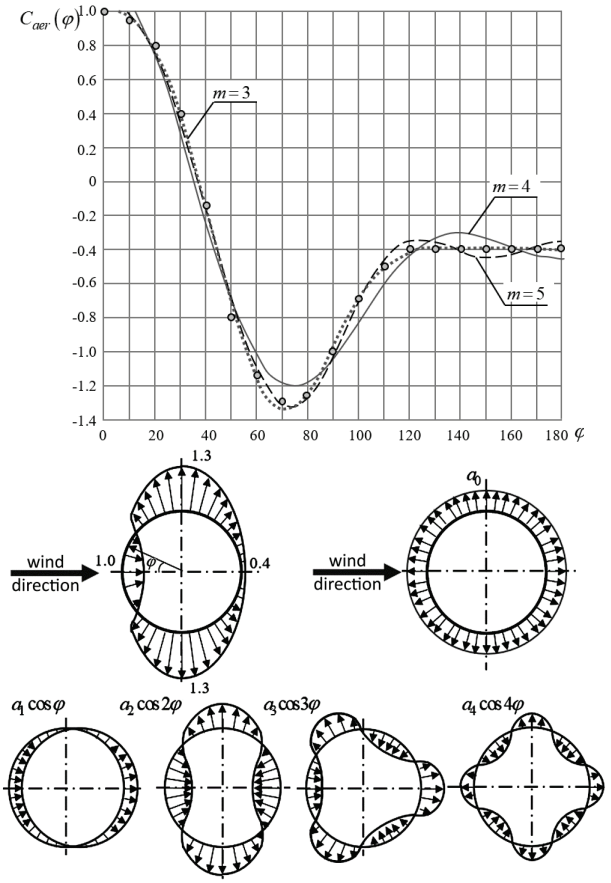

Figure 1 Series development of the aerodynamic coefficient of the wind load

From the system of differentiate Eqs. (2) we will get unknown efforts

$$S_k(x,\varphi)=(kA_k x+C_1)\sin(k\varphi), \tag{3}$$

$$N_{p,k}(x)=\left[\frac{k(kA_k x^2-C_1 x)}{D_w}+C_2\right]\cos(k\varphi), \tag{4}$$

where C_1 and C_2 are arbitrary constants, which are defined from the boundary condition $N_{p,k}(x)\wedge S_k(x,\varphi)=0$ when x = 0, if to count x from the top of the capacity.

When we find out that arbitrary constants under the given boundary conditions are equal to zero, we get

$$S_k(x,\varphi)=kA_k x\sin(k\varphi), \tag{5}$$

$$N_{p,k}(x,\varphi)=\frac{k^2 A_k x^2\cos(k\varphi)}{D_w}, \tag{6}$$

$$N_{h,k}(\varphi)=A_k D_w\cos(k\varphi)/2. \tag{7}$$

Full efforts from the influence of the wind load will be expressed as a sum of Eqs. (5)-(7) according to the accepted amount of m elements of trigonometric series (1). After this, it is easy to get the maximum value of efforts $S_{\max}(x)$, $N_{p,\max}(x)$ and $N_{h,\max}$. It is likely that functions $N_p(x, \varphi)$ and $N_h(\varphi)$ peak when φ = 0, therefore for $N_{p,\max}(x)$ and $N_{h,\max}$ we can write down

$$N_{p,\max}(x)=w_p x^2\xi_p/D_w,\qquad \xi_p=\sum_{k=0}^{m}k^2 a_k, \tag{8}$$

$$N_{h,\max}=w_p D_w\xi_h,\qquad \xi_h=\frac{1}{2}\sum_{k=0}^{m}a_k, \tag{9}$$

where w_p is a design value of the wind load excluding the coefficient C_{aer}.

According to the classic rules of the search of the function extremum, the maximum condition of $\varphi_{\max}$ of the effort $S_{\max}(x)$ is established. Calculations show that depending on the number of elements of the m series (1) $\varphi_{\max}$ varies from 37° to 41°, which correspond to the meaning of the coefficient ξ_s = 1.32 - 1.45 (Tab. 1). For maximum effort $S_{\max}$ we have an equation

$$S_{\max}(x)=w_p x\xi_s,\qquad \xi_s=\sum_{k=0}^{m}ka_k\sin(k\varphi_{\max}). \tag{10}$$

By examining in details expressions from (8) to (10), we can pay attention to a rather wide diapason of the change of the coefficient ξ_p compared to coefficients ξ_h and ξ_s, depending on the number of m elements of the series $C_{aer}(\varphi)$. At the same time, if coefficients ξ_h and ξ_s approach to some constant value, the same cannot be said about the coefficient ξ_p. It is explained by limitation of the momentless theory which is prone to more "smooth" change of external load; however, if the parameter m increases, we will have another nature.

Efforts $S(x,\varphi)$ and $N_h(\varphi)$ are less dependent from the smooth change of the load (outside of the border effect), since the energy of bending (the capacity is under the cross

bend) mainly received by vertical stiffener ribs. Therefore, it makes sense that it is some boundary value for the coefficient ξ_p, which allows finding acceptable results using the Eq. (8). Basis of such value is given in the next paragraph of this section.

Numerical assessment can be given to normal tensions in laminas of the body under efforts $N_{h,\max}$ and $S_{\max}$ to understand how they correlate with tensions from the pressure of the bulk material when $x = H_w$. The maximum value of the diameter is set to $D_w = 40$ m and the height to $H_w = 40$ m of the capacity and it is taken into account that the design value of the wind load w_p excluding aerodynamic coefficient C_{aer} rarely exceeds value of 1 kPa. Consequently, we get that even when $t_w = 1$ mm hoop tensions $N_{h,\max}/t_w$ does not exceed 3 kN/cm^2, and the sheer stress $S_{\max}(x)/t_w$ - 6 kN/cm^2. If the designed situation, which connected to the wind load, is current for the empty capacity, these efforts are not supplement spectrum of tensions from the pressure of the bulk material and we can neglect them in calculations.

The capacity displacement can be defined because of the load $W_k = A_k \cos(k\varphi)$. In order to do this, geometric equations of the cylindrical shell assuming non-stretchability of its middle line in annular direction and absence of the shear line in it are used. Taking into account (4), we can write down

$$\begin{aligned}
&\frac{\partial u(x,\varphi)}{\partial x} = \frac{N_{p,k}(x,\varphi)}{Et_{w,ef}},\\
&\frac{\partial v(x,\varphi)}{\partial \varphi} + w(x,\varphi) = 0,\\
&\frac{2}{D_w}\frac{\partial u(x,\varphi)}{\partial \varphi} + \frac{\partial v(x,\varphi)}{\partial x} = 0.
\end{aligned} \tag{11}$$

Conditional thickness of the $t_{ef,x}$ capacity in the cross-section, which was input in the first expression of the Eq. (11), is taking into account that the change of the longitudinal deformation of the capacity occurs due to both deformations of vertical stiffener ribs and deformations of borders of the body. This defines conditional thickness using actual thickness of the capacity's body and correlation of planes of the cross-section of vertical stiffener ribs and the body of the capacity

$$t_{ef,x} = t_w + \frac{A_p n_p}{\pi D_w} = t_w\left(1 + \frac{A_p n_p}{\pi D_w t_w}\right) = t_w(1+\alpha_{wp}) \tag{12}$$

where $\alpha_{wp} = A_p n_p / (\pi D_w t_w)$ is the ratio of planes of cross-sections of all vertical stiffener ribs and the wall of the capacity.

If all dependences that are needed are substituted and a series of algebraic manipulations is done, we get

$$\begin{aligned}
&\frac{\partial u(x,\varphi)}{\partial x} = \frac{k^2 x^2}{Et_w}\frac{1}{D_w(1+\alpha_{wp})}A_k\cos(k\varphi),\\
&\frac{\partial v(x,\varphi)}{\partial \varphi} + w(x,\varphi) = 0,\\
&\frac{2}{D_w}\frac{\partial u(x,\varphi)}{\partial \varphi} + \frac{\partial v(x,\varphi)}{\partial x} = 0,
\end{aligned} \tag{13}$$

where u, v and w are longitudinal, annular and radial displacements of the body.

Integrating by x and φ and defining arbitrary constants under the condition $x = H_w - u(\cdot) = v(\cdot) = w(\cdot) = 0$, after arithmetic manipulations and similar consolidation, we get (to reduce it, it is denoted by $y = x / H_w$):

$$u_k(y,\varphi) = \frac{G_H}{2\Delta_w}\left(1-y^3\right)a_k k^2\cos(k\varphi), \tag{14}$$

$$v_k(y,\varphi) = G_H\left(y - y^4/4 - 0.75\right)a_k k^3\sin(k\varphi), \tag{15}$$

$$w_k(y,\varphi) = -G_H\left(y - \frac{y^4}{4} - \frac{3}{4}\right)a_k k^4\cos(k\varphi), \tag{16}$$

where $y = x/H_w$ is a non-dimensional high-rise level, G_H is a conventional deflection

$$G_H = \frac{2w_p H_w^2 \Delta_w^2}{3(1+\alpha_{wp})Et_w}. \tag{17}$$

For full displacements of the capacity's body (radial or linear) in the plane of the cross-section we get an equation

$$\begin{aligned}
&w_{\Sigma,k}(y,\varphi) = G_H\left(y - \frac{y^4}{4} - \frac{3}{4}\right)\times\\
&\times a_k k^4\sqrt{\cos^2(k\varphi) + \frac{1}{k^2}\sin^2(k\varphi)}.
\end{aligned} \tag{18}$$

Maximum values of all displacements under load $W_k = A_k\cos(k\varphi)$ are realized when $y = 0$, that means at the top of the capacity

$$\begin{aligned}
&u_{k,\max} = \frac{G_H}{2\Delta_w}a_k k^2\cos(k\varphi),\\
&w_{k,\max} = \frac{3G_H}{4}a_k k^4\sqrt{\cos^2(k\varphi) + \frac{1}{k^2}\sin^2(k\varphi)}.
\end{aligned} \tag{19}$$

Full displacements from the influence of the wind load are analogous to full efforts. It means adding by using separate harmonicas k. Mainly, we are interested in maximum values for $u(\bullet)$ and $w_\Sigma(\bullet)$ when $\varphi = 0$, then after simplifications we get

$$u_{\max} = \frac{G_H}{2\Delta_w}\xi_p,$$
$$w_{\Sigma,\max} = \frac{3G_H}{4}\xi_w, \quad (20)$$
$$\xi_w = \sum_{k=0}^{m} k^4 a_k.$$

According to the data from Tab. 1, numeric value of the coefficient ξ_w corresponds to $m = 5 - \xi_w \approx 60.3$; m = $6 - \xi_w \approx -10.1$; $m = 7 - \xi_w \approx -71.2$; $m = 8 - \xi_w \approx -109$; $m = 9 - \xi_w \approx -192$.

Analysis of the obtained results raises doubt about the accuracy of the value of full displacements.

It must be pointed out that the results, which were obtained above, refer to capacities that have constant thickness of body and ribs in height. In case of the changeable thickness, we have to decompose the exponent $\exp\left[\varepsilon_w(x/H_w)\right]$ into the power series, restraining first four elements when $\varepsilon_w \le 1.5$. Meanwhile, to describe functional dependences $t_w(x)$ and $t_p(x)$, the one and the same exponent of the degree ε_w must be used This claim is not too idealistic, since in real storage containers the thickness of vertical ribs and the wall simultaneously and monotonously decrease with the height.

3 CONCLUSION

1. To calculate cylindrical silos influenced by the wind load we offer to decompose function of the aerodynamic coefficient into the finite trigonometric series. It simplifies the solution significantly, since this calculation can be conducted for each element separately.

2. Coefficients of the given decomposition were calculated using the graph of norms.

3. According to the equation of equilibrium by using the momentless theory, expressions for maximum value of linear longitudinal efforts in radial and meridional (longitudinal) direction and linear shearing force were obtained.

4. The thesis about maximum shearing force was set up. Meaning of the incidence angle varies between 37° - 41°, depending on the number of components of the trigonometric series.

5. From the analysis of design factors series, the opportunity of using the momentless theory to evaluate changes of linear efforts in radial direction and shearing forces was presented. There is a boundary meaning of the design factor for linear efforts in meridional direction that allows finding acceptable results according to the proposed formula.

6. Quantitative assessment of the normal tension in laminas of the silos body (for maximum values of the diameter D_w = 40 m and the height H_w = 40 m) was made from the influence of maximum linear efforts and their connection with tension from the pressure of the bulk material at the top of the capacity.

7. The expressions needed to define full radial and contacting displacements of the capacity in the plane of cross section from the element of the wind load were gotten.

8. Recommendations about the calculation of silos with changeable thicknesses of body laminas and stiffening ribs in height were given.

4 REFERENCES

[1] DBN V.1.2-2:2006. Systema zabezpechenniana diinostita bezpeky budivelnykh obiektiv. Navantazhennia i vplyvy. Normy proektuvannia, Ministry for Regional Development, Building and Housing of Ukraine, Kyiv, 2006, 83 p. (in Ukrainian)

[2] Kolkunov, N. (1972). *Osnovyi raschyota uprugih obolochek: monografiya*, Moscow: Vyisshaya shkola, 296 p. (in Russian)

[3] Korobov, L., Zharkov, A., & Shernik, A. (2006). *Dyimovyie i ventilyatsionnyie trubyi vyisotoy 200-500 metrov, kak prostranstvennyie sooruzheniya*, Moscow: Kompaniya Sputnik, 246 p. (in Russian)

[4] Flyugge, V. (1961). *Statika i dinamika obolochek*, Moscow: Gosudarstvennoe izdatelstvo literaturyi po stroitelstvu i arhitekture, 304 p. (in Russian)

[5] Goldenveyzer, A. (1976). *Teoriya uprugih tonkih obolochek*, Moscow: Nauka, 512 p. (in Russian)

[6] ASCE 7-10. (2010). Minimum Design Loads for Buildings and Other Structures, Virginia: American Society of Civil Engineers, 65 p.

[7] Schelokov, Ya., Duzhih, F., Osolovskiy, V., & Ladyigichev, M. (2007). *Sooruzhenie promyishlennyih dyimovyih trub: spravochnoe izdanie*. Kniga 1. Konstruktsii, raschetyi, ekspertiza, Moscow: Teplotehnik, 336 p. (in Russian)

[8] Makhinko, A. (2012). *Imovirnisnyi rozrakhunok bashtovykh opor zviazku*, Poltava: PoltNTU, 410 p. (in Ukrainian)

[9] ISO 4354:2009 Wind Actions on Structures, Geneva: Switzerland: International Organization for Standardization, 2009, 68 p.

[10] Zdravkovich, M. (2003). *Flow around Circular Cylinders*, New York: Oxford Universiti press, Vol. 2, 314 p.

[11] Lessing, E., Lileev, A., & Sokolov, A. (1970). Listovyie metallicheskie konstruktsii, Moscow: Stroyizdat, 490 p. (in Russian)

Authors' contacts:

Oleksandr LAPENKO, Doctor of Technical Sciences, Professor
National Aviation University
Kosmonavta Komarova 1, 03058 Kyiv, Ukraine
+380662006727, my-partner@ukr.net

Anton MAKHINKO, Doctor of Technical Sciences, Senior Scientist
ETUAL LLC
1, Bortnytska street, Petropavlivske, Boryspil district, Kiev, 08341, Ukraine
+380503272785, Pasargada1981@gmail.com

Natalia MAKHINKO, Candidate of Technical Science
National Aviation University
Kosmonavta Komarova 1, 03058 Kyiv, Ukraine
+380503045072, Pasargada1985@gmail.com

ISSN 1846-6168 (Print), ISSN 1848-5588 (Online)
https://doi.org/10.31803/tg-20180921100632

Original scientific paper

INVESTIGATION ON THE INFLUENCE OF PARAMETER UNCERTAINTIES IN THE POSITION TRACKING OF ROBOT MANIPULATORS

Habib GHANBARPOUR ASL, Kerim Youde HAN

Abstract: This paper presents a novel trajectory tracking method for robot arms with uncertainties in parameters. The new controller applies the robust output feedback linearization method and is designed so that it is robust to the variation of parameters. Robustness of the algorithm is evaluated when the parameters of the system are floating over 10 percent up and down. An Unscented Kalman Filter (UKF) is applied for state and parameter estimation purposes. As the considered system has 8 unknown parameters while only 5 of them are independent parameters, UKF is applied only to the augmented system with independent parameters. Three types of simulations are applied depending on sensor groups – first with both position and joint sensors, second with only position sensors and third with only joint sensors. The observation of parameters in these groups is discussed. Simulation results show that when both position sensors and joint sensors are used, all the parameters and states are observable and good tracking performances are obtained. When only position sensors are used, the accuracy of the estimated parameters is reduced, and low tracking performances are revealed. Finally, when only joint sensors are applied, the lengths of robot arms are unobservable, but other parameters related to the dynamic system are observable, and poor tracking performances are given.

Keywords: path following; parameter uncertainty; robot control; robust control; sensor fusion; unscented Kalman filter

1 INTRODUCTION

The robot arm (also called Robot manipulator) is a type of mechanical device which is usually programmable, and it usually has similar functions to a human arm. Traditionally, many Proportional-Derivative (PD) or Proportional-Integral-Derivative (PID) controllers were designed for controlling robot arms. Takegaki et al. [1] and Arimoto [2] designed simple PI and PID feedback controllers. A PD controller with stability robustness in the presence of parameter uncertainty in the gravitational torques vector was presented by Hsia in [3]. However, these controllers are difficult to use in determining the appropriate PID gains in the cases of nonlinear and unknown controlled plants. The fixed PID parameters in these controllers may often deteriorate control performances, and while these controllers are enough for the general control, they usually result in weak robustness and poor performances due to the nonlinearity characteristics of robot arms. Research works on nonlinear PD or PID controllers of robot arms such as [4-6] were proposed for these purposes. Huang et al. [6] proposed a nonlinear PD controller with gravity compensation that is globally asymptotically stable in position control and a comparison was made between their proposed controller and the conventional PD controller, which showed that a faster response velocity and higher position accuracy were obtained by the former. Davoud et al. [7] proposed fractional order PID controllers by applying evolutionary algorithms (particle swarm optimization (PSO), the genetic algorithm and estimations of the distribution algorithm) and better tracking results were obtained compared to the normal PID controllers. Nevertheless, the nonlinearity of the kinematics and the dynamics of robot arms is inherited in the robot itself, which means that even if a well precisely calibrated model-based controller may give good tracking performance for a given robot model [8], the difficulty of having an exact model of a robot arm makes the calibrated controllers unable to adapt to any changes and uncertainties in its model and environment. Under these circumstances, every time the robot arm picks up some tools of different dimensions, unknown orientations or gripping points, the overall kinematics and dynamics of the robot arm will also change, which requires the derivation of a new robot arm model, as well as the designing of a controller. It is also not possible for the robot arm to grip the tool at the same grasping point and orientation site, even if the same tool is used again. To solve these problems, many controllers with stronger robustness have been developed, such as back-stepping control [9], neural network control [10-12], fuzzy logic control [13], adaptive control [14, 15], sliding mode control [16, 17] and robust control [18, 19]. These controllers can achieve more accurate trajectory tracking results with faster convergent speed even under presence of various disturbances. Among these controllers, the focus of this paper will be concentrated on the adaptive and robust controller design of the robot arm. An important point in adaptive control is that the tracking error will converge regardless of whether the trajectory persistently exists or not [20, 21]. Many adaptive controllers [22-25] were designed for robot arms. However, these adaptive controllers all assumed that the kinematics of the robot arm was known in advance, and no uncertainties in kinematics and dynamics of robot arms were considered. To deal with uncertainty issues, Cheah et al. [26] developed an adaptive controller that can give concurrent adaptation to both kinematics and dynamic uncertainties of the robot arm by measuring its end-effector position, joint angles and joint velocities. Torres et al. [27] developed a controller that added an adaptive scheme to the standard robust controller in order to improve its performance, especially when unknown parameters or unknown variable loading exist. Yin et al. [28] applied the dynamic linearization technique and designed a controller that used only the input/output data of robotic manipulator systems. This paper will present a new adaptive control-based tracking method of a robot arm when there are

uncertainties in robot arm parameters. The output linearization method will also be applied so that the proposed controller will be robust to the variation of the parameters. In order to estimate the states and parameters, UKF is applied. The standard UKF was introduced in [29], and the implementation of this filter was proposed numerically with robustness in [30, 31]. Different combinations of sensors are to be used for validating the effectiveness of the proposed adaptive and robust controller. The rest of this paper is organized as follows: in Section 2, the problem is defined and the adaptive robust inverse controller is designed. UKF is used in Section 3 to estimate the states and parameters of the robot arm. Section 4 gives a numerical example to validate the effectiveness of the proposed controller. Conclusions and future research are given in Section 5.

2 PROBLEM DEFINITION AND CONTROLLER DESIGN

In general, the dynamics of a robot manipulator is given in the form as follows:

$$M(\theta)\ddot{\theta} + C\left(\theta, \dot{\theta}\right) + G(\theta) = u \tag{1}$$

Where $\theta \epsilon \mathcal{R}_n$ denotes the set of configuration variables of the robot arm, $u \epsilon \mathcal{R}_n$ is the torques applied at the joints. $M(\theta)$ is the moment of the inertia matrix, $C(\theta, \dot{\theta})$ is the Coriolis/centripetal vector, and $G(\theta)$ is the gravity vector. The objective of the design problem here is to develop a suitable controller so that the robot arm can track the desired trajectory as close as possible.

As a starting point, we apply the input-output linearization method, where the model of the system is summarized in its state space representation form as follows [32]:

$$\begin{aligned} \dot{\theta} &= \omega \\ \dot{\omega} &= M^{-1}(u - f) \\ z &= g(\theta) \end{aligned} \tag{2}$$

where $f = C\left(\theta, \dot{\theta}\right) + G(\theta)$ is the summation of Coriolis/centrifugal and gravity effect, and z is the output of the system representing the position of the end-effector (forward kinematic). By taking the derivative of the output functional equation in terms of the time *t*, it results in

$$\dot{z} = \frac{\partial g(\theta)}{\partial \theta}\dot{\theta} = J\dot{\theta} \tag{3}$$

Here, *J* is the Jacobian matrix of the robot arm. Substitute $\dot{\theta}$ in the Eq. (2) into Eq. (3) and take the derivative of $\dot{z}$ in terms of time *t* again, which results in the following representation:

$$\ddot{z} = \dot{J}\dot{\theta} + J\ddot{\theta} = \dot{J}\omega + JM^{-1}(u - f) \tag{4}$$

Meanwhile, let us define the output error dynamics as:

$$\dot{e} = z_{ref} - z \tag{5}$$

where z_{ref} is the desired reference path that is to be tracked. By doing so, the output error will include an integrator, which will increase the type of the system and let the error converge to zero in a steady state condition. Differentiate (5) twice and substitute (3) into (5), which will lead to

$$\ddot{e} = \ddot{z}_{ref} - \dot{J}\omega - JM^{-1}(u - f) \tag{6}$$

Let us suppose that the desired error dynamic equation is given by

$$\dddot{e} + K_2\ddot{e} + K_1\dot{e} + K_0 e = 0_{n\times n} \tag{7}$$

Here, K_0, K_1 and K_2 are assumed to be $n \times n$ matrices, so the characteristic equation is $Is^3 + K_2 s^2 + K_1 s + K_0 = 0$, where I is a $n \times n$ unit matrix. Substitute (6) into (7), it results in

$$u = MJ^{-1}\left(\ddot{z}_{ref} - \dot{J}\omega + K_2\ddot{e} + K_1\dot{e} + K_0 e\right) + f \tag{8}$$

By selecting proper values for K_0, K_1 and K_2, the error dynamics become stable, and the controller can be defined in terms of (8). In real situations, however, the error dynamics will not be of the form of (7) due to parameter and state errors. Thus, input function can be defined as:

$$u = \tilde{M}\tilde{J}^{-1}\left(\ddot{z}_{ref} - \dot{\tilde{J}}\tilde{\omega} + K_2\ddot{\tilde{e}} + K_1\dot{\tilde{e}} + K_0\tilde{e}\right) + \tilde{f} \tag{9}$$

Where $\tilde{M}$, $\tilde{J}$, $\dot{\tilde{J}}$, and $\tilde{f}$ are the approximated or estimated values of M, J, $\dot{J}$ and f, and $\tilde{e} = e + \Delta e$, $\tilde{\omega} = \omega + \Delta\omega$, Δe and $\Delta\omega$ are the errors of the output and angular velocity estimation. Next, substitute (9) into (6), it results in

$$\ddot{e} = \ddot{z}_{ref} - \dot{J}\omega - JM^{-1}\left[\tilde{M}\tilde{J}^{-1}\left(\ddot{z}_{ref} - \dot{\tilde{J}}\tilde{\omega} + K_2\ddot{\tilde{e}} + K_1\dot{\tilde{e}} + K_0\tilde{e}\right) + \tilde{f} - f\right] \tag{10}$$

Rearranging (10) results in

$$\begin{aligned} &\dddot{e} + \tilde{I}K_2\ddot{\tilde{e}} + \tilde{I}K_1\dot{\tilde{e}} + \tilde{I}K_0\tilde{e} = \Delta u \\ &\Delta u = (I - \tilde{I})\ddot{z}_{ref} + \left(\tilde{I}\dot{\tilde{J}} - \dot{J}\right)\omega + \tilde{I}\begin{pmatrix}\dot{\tilde{J}}\Delta\omega - K_2\Delta\ddot{e} \\ +K_1\Delta\dot{e} + K_0\Delta e\end{pmatrix} - JM^{-1}(\tilde{f} - f) \end{aligned} \tag{11}$$

where $\tilde{I} = JM^{-1}\tilde{M}\tilde{J}^{-1}$. If there is not any error in the parameters or states of the system, the matrix $\tilde{I}$ should be a unit matrix I, and Δu will be zero. The stability of error dynamics is affected only by the matrix $\tilde{I}$. When errors appear in the parameters and states, the input of error equation will be Δu (non-zero function). Therefore, for the robustness of the proposed controller Eq. (9), we need an estimator to estimate the parameters and states of the system so that the tracking error will go to zero.

The values of K_0, K_1 and K_2 can be selected for system stability when parameters are varied in the range. By doing so, we have a stable control system, and errors will arise in the steady state due to an unknown input error. In order to reduce the steady state errors, in Section 3, an unscented Kalman filter will be applied to estimate the states and parameters of the robot arm system.

At this stage, for calculating the controller gains that are represented in the Eq. (7), first we convert that equation in the state space form.

$$\begin{bmatrix}\ddot{e}\\ \dot{e}\\ \dot{e}\end{bmatrix} = A\begin{bmatrix}\ddot{e}\\ \dot{e}\\ e\end{bmatrix} + B\mathcal{U},\ A = \begin{bmatrix}0 & 0 & 0\\ I & 0 & 0\\ 0 & I & 0\end{bmatrix}, B = \begin{bmatrix}\tilde{I}\\ 0\\ 0\end{bmatrix} \quad (12)$$

here

$$\mathcal{U} = K\begin{bmatrix}\ddot{e}\\ \dot{e}\\ e\end{bmatrix} = [K_2 \quad K_1 \quad K_0]\begin{bmatrix}\ddot{e}\\ \dot{e}\\ e\end{bmatrix} \quad (13)$$

The matrix A, does not have uncertainty, but the matrix B is an uncertain matrix. The matrix B can be written as:

$$B = B_0 + \Delta B,\ \Delta B = DFE,\ F^TF \le I \quad (14)$$

Here, the matrices D, E and F are the known matrices. One can determine the gain K through the solution of the linear matrix inequality equation represented in (15) [34].

$$\begin{bmatrix}(AS + BW) + (AS + BW)^T + \varepsilon DD^T & (EW)^T\\ EW & -\varepsilon I\end{bmatrix} < 0 \quad (15)$$

If the Eq. (15) has a feasible solution, in terms of variables $(\varepsilon > 0, S, W)$, then the state feedback law represented by (13) is robustly stabilizing the system (12) with gain

$$K = [K_2 \quad K_1 \quad K_0] = WS^{-1} \quad (16)$$

Consequently, the beefcake (9) can guarantee the stability of the system (1), but the system will have a steady state error. For reducing steady state errors, we need to estimate the parameters of the system.

3 STATE AND PARAMETER ESTIMATION

In this section, a two degree of freedom robot arm is taken into consideration, the schematic diagram of which is given in Fig. 1. The manipulator has 8 unknown constant parameters, which are $L_1, L_2, m_1, m_2, r_1, r_2, I_1$ and I_2, representing lengths, masses, radius and the moment of inertia of the first and second link, respectively. r_1 and r_2 are the positions of the center of mass, m_1 and m_2 are the masses of links. The kinetic and potential energy equations are given by the following equation

$$T = \frac{1}{2}[\dot{\theta}_1 \quad \dot{\theta}_2]\begin{bmatrix}\alpha + 2\beta c_2 & \delta + \beta c_2\\ \delta + \beta c_2 & \delta\end{bmatrix}\begin{bmatrix}\dot{\theta}_1\\ \dot{\theta}_2\end{bmatrix}, V = 0, L = T - V \quad (17)$$

T, V and L represent the kinetic energy, potential energy and Lagrangian of the manipulator, and $c_i = cos\theta_i, i = 1.2$. For simplicity, in this paper, time-based parameters will only be written with the parameters themselves, but omitting time t in notation. For instance, $\theta_i = \theta_i(t)$. Meanwhile, α, β and δ are represented by [33]:

$$\begin{aligned}\alpha &= I_1 + I_2 + m_1r_1^2 + m_2(L_1^2 + r_2^2)\\ \beta &= m_2L_1r_2\\ \delta &= I_2 + m_2r_2^2\end{aligned} \quad (18)$$

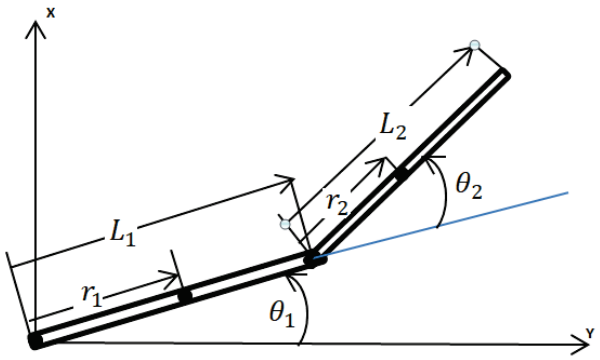

Figure 1 Robot arm parameters

By substituting the Lagrangian $L = T$ into Lagrange's equations, matrices M, C and G will become the function of $p^s = [\alpha \ \beta \ \delta]^T$. By discretizing the dynamic Eq. (2) by the 4th order of the Runga Kutta method, the system equation is then given as

$$\theta_k = f(\theta_{k-1}, u_{k-1}, p^s_{k-1}), p^s_k = p^s_{k-1} \quad (19)$$

Let us suppose that $x_k = [\theta_k^T \ (p_k^s)^T]^T$ is the state of the augmented system. The model of the augmented system (14) is then considered as:

$$x_k = \boldsymbol{f}(x_{k-1}, u_{k-1}) \quad (20)$$

For identification and control purposes, two types of sensors are considered. One of them is the joint sensor and the other one is the position sensor. The modeling of these sensors is as follows:

$$z_k = [I_{2\times2} \quad 0_{2\times3}]x_k = g(x_k) \quad (21\text{-}1)$$

$$y_k = \begin{bmatrix}L_1c_1 + L_2c_{12}\\ L_1s_1 + L_2s_{12}\end{bmatrix} = h(x_k, p^m) \quad (21\text{-}2)$$

where $c_i = cos\theta_i, s_i = sin\theta_i, c_{12} = \cos(\theta_1 + \theta_2)$ and $s_{12} = \sin(\theta_1 + \theta_2)$. z_k and y_k are the output of joint sensors and position sensors respectively; $p^m = [L_1 \ \ L_2]^T$ is the unknown parameter that appears in the position sensor output.

If only two sensors are used for measuring the angles of links, (20) will be the system equation and (21-1) will be the measurement equation. Therefore, in the best condition, p^s will be identifiable (when the inputs are suitable) and p^m will not appear in any measurement of the system equation. Consequently, it remains unidentifiable. As a result, tracking errors will arise in the position control of the end-effector due to the errors which arise from L_1 and L_2, and that makes it impossible to get zero tracking errors without applying external sensors or measuring the end-effector's position.

When the position sensor is available, (20) acts as a system dynamic and (21-1) and (21-2) are the measurement equations, in which case both p^s and p^m will be active, and they can both be identified in the best condition. Consequently, when both the joint and position sensors are available, tracking errors will be reduced. Let us put two unknown parameter vectors of p^s and p^m into a vector form $p = [(p^s)^T \quad (p^m)^T]^T$, and consider a random walk model [31] for the unknown parameter vector. Then the augmented system model is

$$\begin{aligned} \theta_k &= \boldsymbol{f}(\theta_{k-1}, u_{k-1}, p_{k-1}) \\ p_k &= p_{k-1} + w_k \\ z_k &= g(x_k) + v_k \\ y_k &= h(x_k, p) + \vartheta_k \end{aligned} \tag{22}$$

Where w_k and v_k and ϑ_k are zero mean white noise signals with the covariances of $E[w_k(w_k)T] = Q_k$, $E[v_k(v_k)T] = R_v$ and $E[\vartheta_k(\vartheta_k)T] = R_\vartheta$, respectively. $X_k = [\theta_k^T \quad p_k^T]^T$, as an augmented state space representation of the system in (22), can be re-written as:

$$\begin{aligned} X_k &= F(X_{k-1}, u_{k-1}) + Gw_k \\ z_k &= HX_k + v_k \\ y_k &= h(X_k) + \vartheta_k \end{aligned} \tag{23}$$

where $H = [I_{2\times2} \quad 0_{2\times7}]$, and $G = \begin{bmatrix} 0_{4\times5} \\ I_{5\times5} \end{bmatrix}$. Due to the fact that the filter falls off reducing the covariance of the system, some noises are added here for holding the robustness of the system, which will increase the covariance of unknown parameters.

The following method will provide an augmented UKF method for parameter and state estimation.

Table 1 Unscented Kalman Filter

- Initialization:
  $\hat{X}_0 = E(X_0), P_0 = E[(X - X_0)(X - X_0)^T]$
- for $k = 1 \ldots \infty$
- set $t = k - 1$
- calculate sigma points
  $x_t = [\hat{X}_t \quad \hat{X}_t + \gamma S_t \quad \hat{X}_t - \gamma S_t]$
- time update equations

$$x_{i,k|t} = F(x_{i,t}, u_{k-1})$$
$$\hat{X}_k^- = w_i^m x_{i,k|t}$$
$$P_k^- = \sum_{i=1}^{2l} w_i^c [x_{i,k|t} - \hat{X}_k^-][x_{i,k|t} - \hat{X}_k^-]^T + GQ_kG^T$$
$$\mathcal{Y}_{i,k|t} = h(x_{i,k|t})$$
$$y_k^- = \sum_{i=1}^{2l} w_i^m \mathcal{Y}_{i,k|t}$$

- When position sensor data is available:

$$P_{\hat{y}_k\hat{y}_k} = \sum_{i=1}^{2l} w_i^c [\mathcal{Y}_{i,k|t} - y_k^-][\mathcal{Y}_{i,k|t} - y_k^-]^T + R_\vartheta$$
$$P_{\hat{x}_k\hat{y}_k} = \sum_{i=1}^{2l} w_i^c [x_{i,k|t} - \hat{X}_k^-][\mathcal{Y}_{i,k|t} - y_k^-]^T$$
$$K_k = P_{\hat{x}_k\hat{y}_k}(P_{\hat{y}_k\hat{y}_k})^{-1}$$
$$\hat{X}_k = \hat{X}_k^- + (y_k - y_k^-)$$
$$P_k = P_k^- - K_k P_{\hat{y}_k\hat{y}_k} K_k^T$$
$$\hat{X}_k^- = \hat{X}_k, \qquad P_k^- = P_k$$

- When joint sensor data is available:

$$P_{\hat{z}_k\hat{z}_k} = HP_k^- H^T + R_v$$
$$K_k = P_k^- H^T (HP_k^- H^T + R_v)^{-1}$$
$$\hat{X}_k = \hat{X}_k^- + (z_k - H\hat{X}_k^-)$$
$$P_k = P_k^- - P_k^- H^T P_{\hat{z}_k\hat{z}_k} HP_k^-$$

End for

Where l is the summation of the lengths of states and parameters, w_i^m and w_i^c are a set of scales weights as follows:

$$w_0^m = \frac{\lambda}{\lambda+l}, w_0^c = \frac{\lambda}{\lambda+l} + (1 - \tilde{\alpha}^2 + \tilde{\beta}) \tag{24-1}$$

$$w_i^m = w_i^c = \frac{\lambda}{2(\lambda+l)}, \quad i = 1, \ldots, 2l \tag{24-1}$$

where $\lambda = l(\tilde{\alpha}^2 - 1)$ and $\gamma = \sqrt{l + \lambda}$ are the scaling parameters. The constant $\tilde{\alpha}$ determines the spread of the sigma points around the estimated state and is usually set to $10^{-4} \leq \tilde{\alpha} \leq 1$, $\tilde{\beta}$ is used to add prior knowledge of the distribution of the state (for Gaussian distribution, $\tilde{\beta} = 2$ is optimal). S is the square root matrix of P (Choleski factor of P).

4 EXAMPLE APPLICATION

In this section, the MATLAB simulation will be used to demonstrate the effectiveness of the proposed controller. We will start with a two-link robot arm whose system model is given by (25).

$$\begin{bmatrix} \alpha + 2\beta c_2 & \delta + \beta c_2 \\ \delta + \beta c_2 & \delta \end{bmatrix} \begin{bmatrix} \ddot{\theta}_1 \\ \ddot{\theta}_2 \end{bmatrix} + \begin{bmatrix} -\beta s_2 \dot{\theta}_2 & -\beta s_2(\dot{\theta}_1 + \dot{\theta}_2) \\ \beta s_2 \dot{\theta}_1 & 0 \end{bmatrix} \begin{bmatrix} \dot{\theta}_1 \\ \dot{\theta}_2 \end{bmatrix} = \begin{bmatrix} u_1 \\ u_2 \end{bmatrix} \tag{25}$$

Let us consider the parameters of this robot arm that are given by the values in the Tab. 2.

Table 2 Robot arm parameters

Parameter	Unit	Value
L_1	m	0.5
L_2	m	0.5
r_1	m	0.2
r_2	m	0.25
m_1	kg	1.5
m_2	kg	1
I_1	$kg - m^2$	0.15
I_2	$kg - m^2$	0.1

The initial conditions of the system are given in Tab. 3.

Table 3 State parameters without errors

Parameter	Unit	Value
θ_1	rad	0
θ_2	rad	0.5π
ω_1	rad/sec	0
ω_2	rad/sec	0

The independet parameters that are calculated from Tab. 2, through (18), are represented in the Tab. 4.

Table 4 States as calculated parameters without errors

Calculated Parameters	Unit	Value
α	$kg-m^2$	0.6225
β	$kg-m^2$	0.125
δ	$kg-m^2$	0.1625

From the basic 8 parameters given in Tab. 2, three independent parameters of α, β and δ that are defined in (18) will be calculated as 0.6225, 0.1250 and 0.1625 respectively as given in Tab. 4. Let us suppose that all independent parameters have their own uncertainties, and let us suppose that the estimation of parameters and states are shown in the Tab. 5.

Table 5 Estimated parameters of the robot arm

Parameter	Unit	Error range or standard deviation	Mean Value
$\hat{L}_1$	m	± 0.05	0.45
$\hat{L}_2$	m	± 0.05	0.55
$\hat{\alpha}$	$kg-m^2$	± 0.06	0.6845
$\hat{\beta}$	$kg-m^2$	± 0.01	0.1375
$\hat{\delta}$	$kg-m^2$	± 0.01	0.1463
$\hat{\theta}_2$	rad	0.01	0.001
$\hat{\theta}_2$	rad	0.01	$0.5\pi+0.003$
$\hat{\omega}_1$	rad/sec	0.01	0.02
$\hat{\omega}_2$	rad/sec	0.01	0.03

The Standard Deviation (STD) of the sensors' noises used in this simulation example is also given in Tab. 6.

Table 6 Standard deviation of sensors

Joint sensors	Joint 1	0.01 rad
	Joint2	0.01 rad
Position sensors	x-axis	0.05 m
	y-axis	0.05 m

To design the controller's gain, here we apply the Monte Carlo simulation method. For this purpose, we generate 10 thousand time parameters of the system with uniform distribution within the range given in Tab. 5 for determining the structured uncertain model represented by (14), and then the controller gain is calculated as

$$K = \begin{bmatrix} -3.7156 & -0.0000 & -2.3804 & -0.0000 & -0.4145 & -0.0000 \\ -0.0000 & -3.7156 & 0.0000 & -2.3804 & 0.0000 & -0.4145 \end{bmatrix}$$

In order to test the robustness of the controller, by generating the above-mentioned data, and by calculating $\tilde{M}$ and $\tilde{J}$, we can find the poles of random selected systems. The poles of this system are shown in Fig. 2.

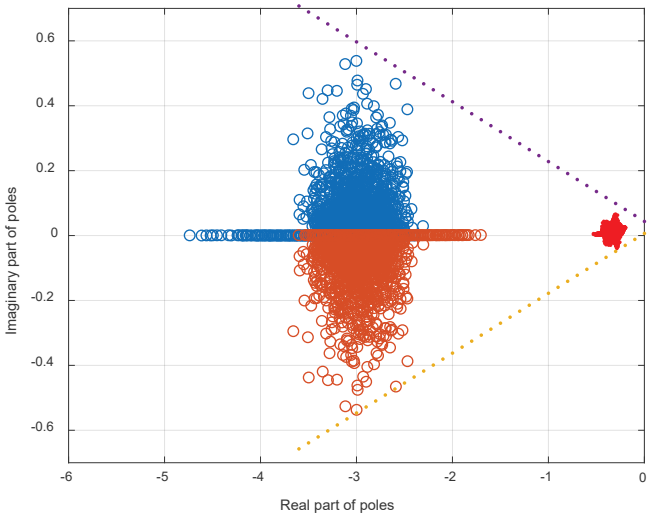

Figure 2 Poles of the uncertain system

It is seen that the nominal poles of a closed-loop system are two repeated poles at −2.9575, −0.4154 and −0.3235. The slowest pole is −0.29, the fastest pole is −4.8 and the minimum damping of the system is 0.95 for an uncertain closed-loop system. These conditions are acceptable.

It is worth mentioning that, when the filter identifies all parameters after some time, the poles of the system will approach the nominal poles. Hence, the best way for the robot arm to give small tracking errors is to give more time to the filter for identifying the parameters of system. When the error estimations of α, β and δ approach zero, the roots of the closed-loop system approach the nominal poles. Meanwhile, when the parameter errors of L_1 and L_2 approach zero, the tracking error will decrease.

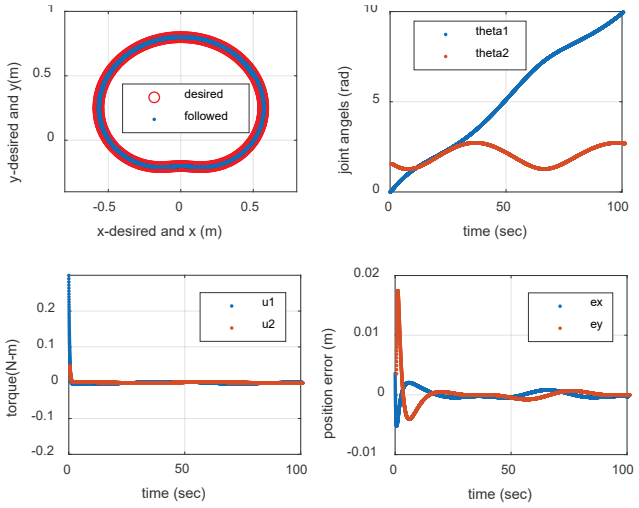

Figure 3 Trajectory Tracking of Robot Arm

Furthermore, to evaluate the power of the system in path tracking, a desired path is generated for tracking purposes. The equation of the desired path is in its polar coordinated form, which is characterized by $= 0.5 + 0.3sin\theta$, $r = 0.5 + 0.3sin\theta$, $\theta = \theta 0 + \omega t$, $\omega = \omega_0 + \dot{\omega}cos(0.01t)$, $\omega_0 = 0.1rad$, $\dot{\omega} = 0.01rad/sec$, $\theta_0 = 0.7854$. When all

parameters of the robot are known, and the measurements are perfect, performances of the controller are presented in Figure 3. The desired and tracked path of the robot is given in Figure 3.a. Figure 3.b also shows that the first arm is rotated more than one time, but the second arm is oscillated between $1.28 - 2.74rad$. Figures 3.c and 3.d show that the applied torques and tracking errors of the robot are always lower than $0.3\ N - m$ and $0.02m$ respectively. In all graphs, the blue and red colors represent the first and second parameters respectively.

The first analysis will be made when both joint angles and position sensors are applied. The position tracking error and position estimating error is represented in Fig. 4.a and Fig. 4.b respectively. Here, the minimum position error is $0.025m$ and finally, it reduces to a very small value that is lower than $1 \times 10^{-3}\ m$. The joint angles and angular velocities and those 3δ bounds are shown in Fig. 5. Errors are in 3δ bounds, which is why the filter worked well. Fig. 6 represents the estimation of unknown parameters, the STD of parameters, errors of α, β, δ and errors of L_1 and L_2. It is shown that all parameters of the system are estimated correctly and the standard deviation of all parameters is close to zero. Therefore, in this case, good estimation and tracking are obtained.

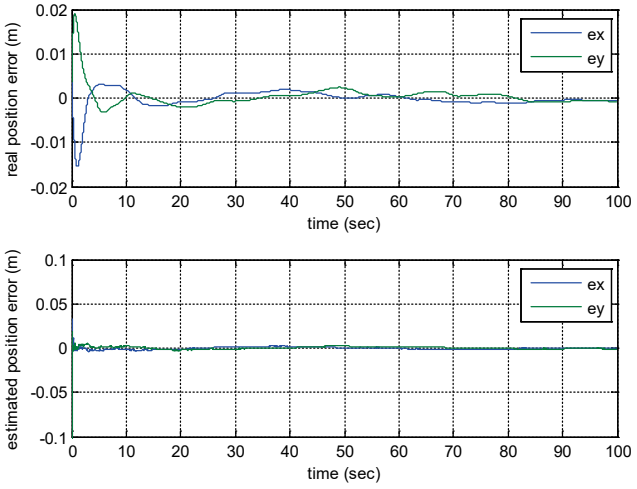

Figure 4 Errors of Position and Estimated Position

The second simulation is done when there is only a position sensor, so the robot arm cannot find two solutions of inverse dynamics (elbow up and down) without using the historical data of the position sensor. Furthermore, it needs to have small errors in the initial condition of the robot arm angles. The position errors and position estimation errors are shown in Fig. 7. Their maximum position error is near 0.02m. The joint angles errors and its 3δ bounds and angular velocities of joint angles and its 3δ bounds are represented in Fig. 8. The errors of joint angles and angular velocities are higher than in the previous case. Nevertheless, all estimations are in the 3δ bounds. In Fig.9, the estimated parameters, STD of parameters, estimation error of α, β, δ and estimation error of L_1 and L_2 are shown. The results show that the estimation errors of parameters are larger than of the previous case, but all errors are finally bounded, which indicates that tracking only with position sensors results in bounded errors.

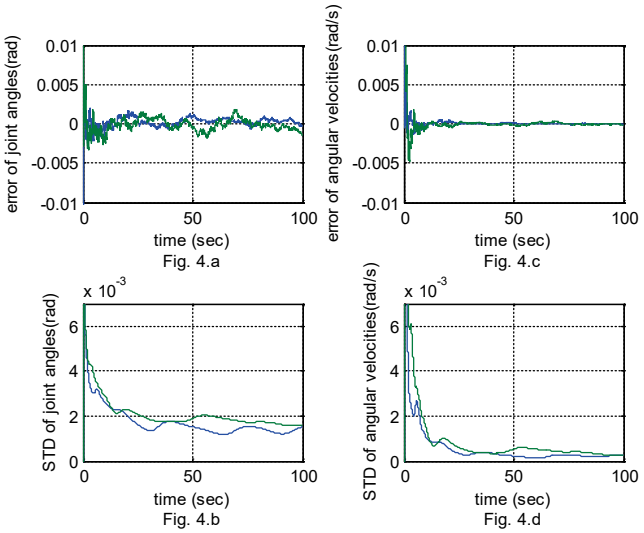

Figure 5 Joint Angle and Joint Angle Rates

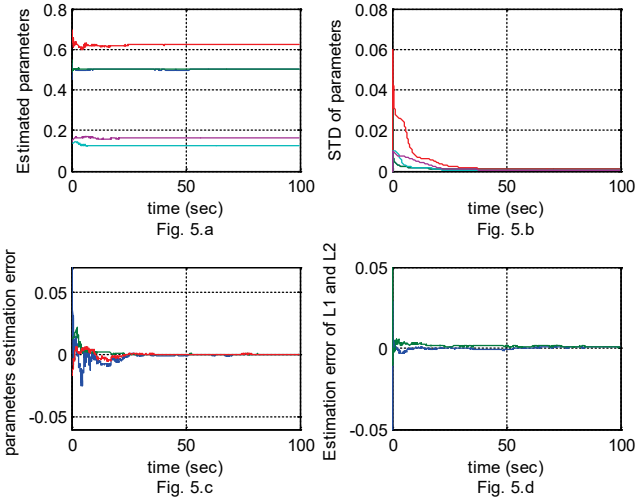

Figure 6 Estimated Parameters and Errors

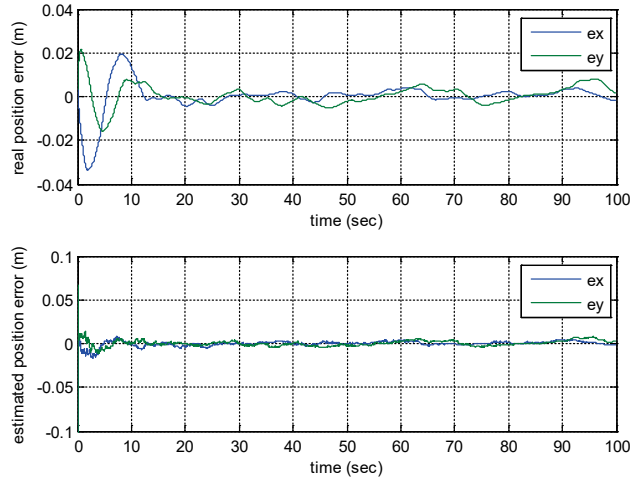

Figure 7 Errors of Position and the Estimated Position

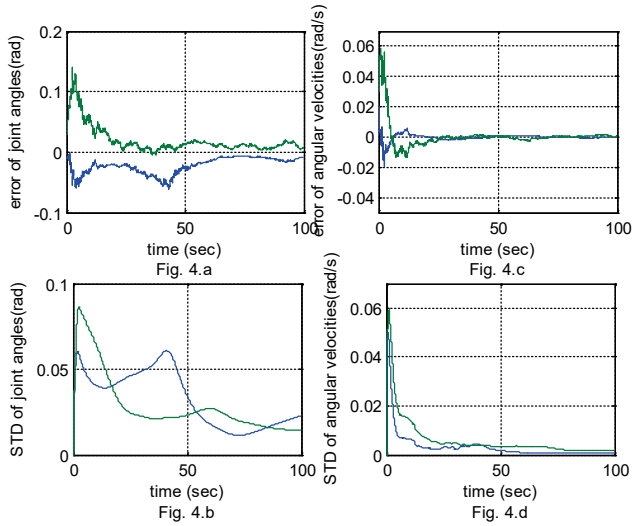

Figure 8 Joint Angle and Joint Angle Rates

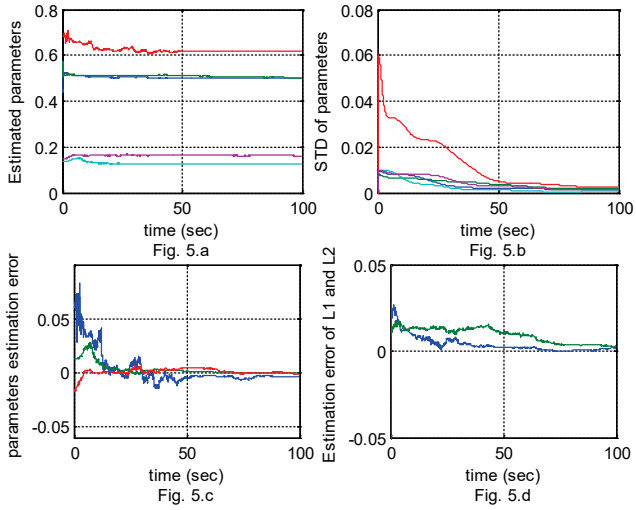

Figure 9 Estimated Parameters and Errors

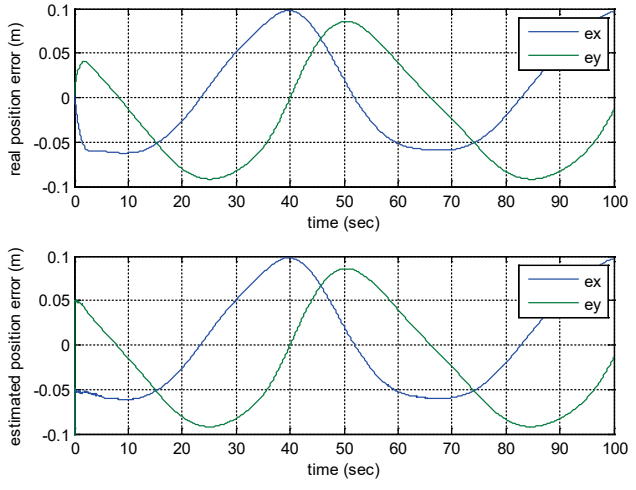

Figure 10 Errors of Position and the Estimated Position

In the third case, only joint sensors are used. The results of position tracking and estimation are shown in Fig. 10. The joint angle and angular velocities and those 3δ bounds are represented in Fig. 11. The estimated parameters and those 3δ bounds are shown is Fig. 12. The results show that position tracking errors are large, but the errors of joint angles and joint velocities are very small and in 3δ bounds. In addition to that, the parameter errors, standard deviation of errors, estimation errors of α, β, δ and estimation errors of L_1 and L_2 are represented in Fig. 12. It shows that errors of α, β, δ are small, but the filter is not able to estimate the value of L_1 and L_2. Therefore, large position tracking errors will always appear due to the errors of L_1 and L_2, and then these parameters are not identifiable.

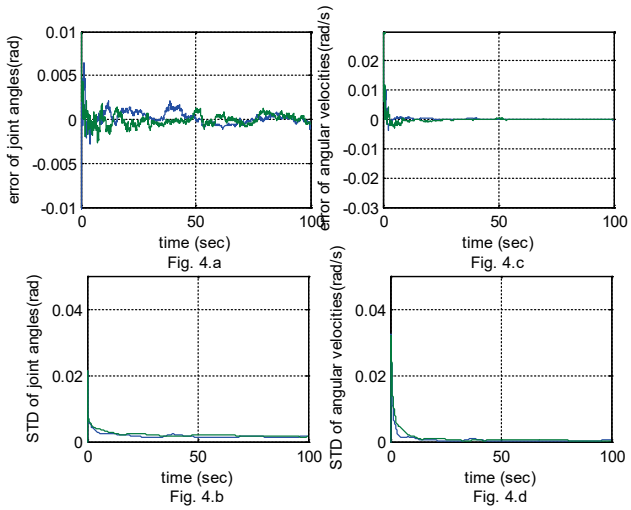

Figure 11 Joint Angle and Joint Angler Rates

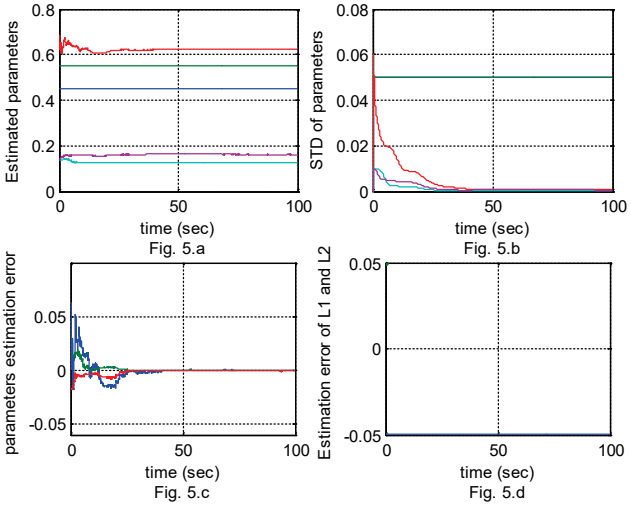

Figure 12 Estimated Parameters and Errors

4 CONCLUSIONS

In this paper, a new adaptive robust inverse control algorithm is developed for the position tracking of the end-effector of a 2 DOF robot arm. Analyses were done on this controller under uncertain conditions. It has been shown that the stability of the controller depends only on the independent parameters of the system, and under the considered range of parameters, the proposed controller is stable. To achieve better tracking results, all independent

parameters need to be identified. An augmented UKF is used for state and parameter estimation purposes. This filter is able to identify all parameters and states when joint sensors, as well as an external position sensor, are used to measure the position of the end-effector, which is how the best tracking performance is achieved. When only the external position sensor is available, all states are observable, but parameters have large errors. Nonetheless, tracking errors are getting very close to zero. Finally, when only joints sensors are present, but without any external sensors, states become observable but L_1 and L_2 are not observable and poor tracking results are obtained due to the error which arises from estimating the position of the end-effector. It is worthwhile to mention that when only a position sensor is present, errors of the initial condition will be important because two solutions will appear in this case. These two solutions are of the link up and down. When the initial condition does not have large errors, the algorithm will converge to the true condition. Future work can be carried out to apply the proposed analyzing method to robot manipulators with a higher DOF to finalize the role of position sensors in robot manipulator position tracking problems.

4 REFERENCES

[1] Takegaki, M. & Arimoto, S. (1981). A new feedback method for dynamic control of manipulators. *Journal of Dynamic Systems, Measurement, and Control*, *103*(2), 119-125. https://doi.org/10.1115/1.3139651

[2] Youcef-Toumi, K. & Wu, S. T. (1992, June). Robustness and stability analysis of time delay control. In *American Control Conference, 1992* (pp. 2691-2695). IEEE. https://doi.org/10.23919/ACC.1992.4792631

[3] Hsia, T. C. (1994). Robustness analysis of a PD controller with approximate gravity compensation for robot manipulator control. *Journal of Robotic Systems*, *11*(6), 517-521. https://doi.org/10.1002/rob.4620110606

[4] Kelly, R. & Carelli, R. (1996). A class of nonlinear PD-type controllers for robot manipulators. *Journal of Robotic Systems*, *13*(12), 793-802. https://doi.org/10.1002/(SICI)1097-4563(199612)13:12<793::AID-ROB2>3.0.CO;2-Q

[5] Seraji, H. (1998). A new class of nonlinear PID controllers with robotic applications. *Journal of Robotic Systems*, *15*(3), 161-181. https://doi.org/10.1002/(SICI)1097-4563(199803)15:3<161::AID-ROB4>3.0.CO;2-O

[6] Huang, J., Yang, C., & Ye, J. (2014). Nonlinear pd controllers with gravity compensation for robot manipulators. *Cybernetics and Information Technologies*, *14*(1), 141-150. https://doi.org/10.2478/cait-2014-0011

[7] Fani, D. & Shahraki, E. (2016). Two-link robot manipulator using fractional order PID controllers optimized by evolutionary algorithms. *Biosciences Biotechnology Research Asia*, *13*(1), 589-598. https://doi.org/10.13005/bbra/2075

[8] Craig, J. J. (1989). Introduction to robotics. Addison-Wesley, New York.

[9] Oh, J. H. & Lee, J. S. (1999). Control of flexible joint robot system by backstepping design approach. *Intelligent Automation & Soft Computing*, *5*(4), 267-278. https://doi.org/10.1080/10798587.1999.10750607

[10] Shuzhi, S. G., Hang, C. C., & Woon, L. C. (1997). Adaptive neural network control of robot manipulators in task space. *IEEE transactions on industrial electronics*, *44*(6), 746-752. https://doi.org/10.1109/41.649934

[11] Cheng, L., Hou, Z. G., & Tan, M. (2009). Adaptive neural network tracking control for manipulators with uncertain kinematics, dynamics and actuator model. *Automatica*, *45*(10), 2312-2318. https://doi.org/10.1016/j.automatica.2009.06.007

[12] Al Ashi, M. M. (2014). Trajectory Tracking Control of A 2-DOF Robot Arm Using Neural Networks. *MS. c, Islamic University of Gaza, Electrical Engineering Department*.

[13] Goléa, N., Goléa, A., Barra, K., & Bouktir, T. (2008). Observer-based adaptive control of robot manipulators: Fuzzy systems approach. *Applied Soft Computing*, *8*(1), 778-787. https://doi.org/10.1016/j.asoc.2007.05.011

[14] Seo, D. & Akella, M. R. (2009). Non-certainty equivalent adaptive control for robot manipulator systems. *Systems & Control Letters*, *58*(4), 304-308. https://doi.org/10.1016/j.sysconle.2008.11.008

[15] Craig, J. J., Hsu, P., & Sastry, S. S. (1987). Adaptive control of mechanical manipulators. *The International Journal of Robotics Research*, *6*(2), 16-28. https://doi.org/10.1177/027836498700600202

[16] Zeinali, M. & Notash, L. (2010). Adaptive sliding mode control with uncertainty estimator for robot manipulators. *Mechanism and Machine Theory*, *45*(1), 80-90. https://doi.org/10.1016/j.mechmachtheory.2009.08.003

[17] Jin, M., Lee, J., Chang, P. H., & Choi, C. (2009). Practical nonsingular terminal sliding-mode control of robot manipulators for high-accuracy tracking control. *IEEE Transactions on Industrial Electronics*, *56*(9), 3593-3601. https://doi.org/10.1109/TIE.2009.2024097

[18] Bascetta, L. & Rocco, P. (2010). Revising the robust-control design for rigid robot manipulators. *IEEE Transactions on Robotics*, *26*(1), 180-187. https://doi.org/10.1109/TRO.2009.2033957

[19] Kolhe, J. P., Shaheed, M., Chandar, T. S., & Talole, S. E. (2013). Robust control of robot manipulators based on uncertainty and disturbance estimation. *International Journal of Robust and Nonlinear Control*, *23*(1), 104-122. https://doi.org/10.1002/rnc.1823

[20] Arimoto, S. (1996). *Control Theory of Non-Linear Mechanical Systems: A Passivity-Based and Circuit-Theoretic Approach (Oxford Engineering Science Series)*. Oxford University Press.

[21] Slotine, J. J. E. & Li, W. (1987). On the adaptive control of robot manipulators. *The international journal of robotics research*, *6*(3), 49-59. https://doi.org/10.1177/027836498700600303

[22] Ortega, R. & Spong, M. W. (1989). Adaptive motion control of rigid robots: A tutorial. *Automatica*, *25*(6), 877-888. https://doi.org/10.1016/0005-1098(89)90054-X

[23] Sadegh, N. & Horowitz, R. (1990). Stability and robustness analysis of a class of adaptive controllers for robotic manipulators. *The International Journal of Robotics Research*, *9*(3), 74-92. https://doi.org/10.1177/027836499000900305

[24] Whitcomb, L., Arimoto, S., Naniwa, T., & Ozaki, F. (1996). Experiments in adaptive model-based force control. *IEEE Control Systems*, *16*(1), 49-57. https://doi.org/10.1109/37.482150

[25] Lee, K. W. & Khalil, H. K. (1997). Adaptive output feedback control of robot manipulators using high-gain observer. *International Journal of Control*, *67*(6), 869-886. https://doi.org/10.1080/002071797223839

[26] Cheah, C. C., Liu, C., & Slotine, J. J. E. (2006). Adaptive tracking control for robots with unknown kinematic and

dynamic properties. *The International Journal of Robotics Research*, *25*(3), 283-296. https://doi.org/10.1177/0278364906063830

[27] Torres, S., Méndez, J. A., Acosta, L., & Becerra, V. M. (2006). Adaptive robust controller for robot manipulators: experiments on a PUMA 560 robot. *IFAC Proceedings Volumes*, *39*(15), 437-442. https://doi.org/10.3182/20060906-3-IT-2910.00074

[28] Yanling, Y. (2015). Model free adaptive control for robotic manipulator trajectory tracking. *The Open Automation and Control Systems Journal*, *7*(1). https://doi.org/10.2174/1874444301507010358

[29] Julier, S., Uhlmann, J., & Durrant-Whyte, H. F. (2000). A new method for the nonlinear transformation of means and covariances in filters and estimators. *IEEE Transactions on automatic control*, *45*(3), 477-482. https://doi.org/10.1109/9.847726

[30] Van Der Merwe, R. & Wan, E. A. (2001). The square-root unscented Kalman filter for state and parameter-estimation. In *Acoustics, Speech, and Signal Processing, 2001. Proceedings (ICASSP'01). 2001 IEEE International Conference on*, Vol. 6, 3461-3464. https://doi.org/10.1109/ICASSP.2001.940586

[31] Asl, H. G. & Pourtakdoust, S. H. (2007). UD covariance factorization for unscented Kalman filter using sequential measurements update. *World Academy of Science, Engineering and Technology*, *34*, 368-376.

[32] Khalil, H. K. & Grizzle, J. W. (2002). *Nonlinear systems* (Vol. 3). Upper Saddle River, NJ: Prentice hall.

[33] Murray, R. M. (2017). *A mathematical introduction to robotic manipulation*. CRC press. https://doi.org/10.1201/9781315136370

[34] Obaiah, M. C. (2014). *Multiobjective output feedback controller compare with IMC-based PID controller* (Doctoral dissertation).

Authors' contact:

Habib GHANBARPOUR ASL, Assistant Professor
University of Turkish Aeronautical Association
Department of Mechatronics
Bahçekapı Mahallesi, Okul Sk. No:11, 06790 Etimesgut/Ankara, Turkey
Tel: +905060214718,
E-mail: hghanbarpourasl@thk.edu.tr, habib.ghanbarpour@gmail.com

Kerim Youde HAN, Assistant Professor
Çankaya University
Department of Mechatronics
Yukarıyurtçu Mahallesi Eskişehir Yolu 29. Km, Mimar Sinan Caddesi No: 4, 06790 Etimesgut, Turkey
Tel: +905422047928,
E-mail: kerimyoudehan@gmail.com

ISSN 1846-6168 (Print), ISSN 1848-5588 (Online)
https://doi.org/10.31803/tg-20181112104935

Original scientific paper

MINIMUM-TIME PATH PLANNING FOR ROBOT MANIPULATORS USING PATH PARAMETER OPTIMIZATION WITH EXTERNAL FORCE AND FRICTIONS

Habib GHANBARPOUR ASL

Abstract: This paper presents a new minimum-time trajectory planning method which consists of a desired path in the Cartesian space to a manipulator under external forces subject to the input voltage of the actuators. Firstly, the path is parametrized with an unknown parameter called a path parameter. This parameter is considered a function of time and an unknown parameter vector for optimization. Secondly, the optimization problem is converted into a regular parameter optimization problem, subject to the equations of motion and limitations in angular velocity, angular acceleration, angular jerk, input torques of actuators', input voltage and final time, respectively. In the presented algorithm, the final time of the task is divided into known partitions, and the final time is an additional unknown variable in the optimization problem. The algorithm attempts to minimize the final time by optimizing the path parameter, thus it is parametrized as a polynomial of time with some unknown parameters. The algorithm can have a smooth input voltage in an allowable range; then all motion parameters and the jerk will remain smooth. Finally, the simulation study shows that the presented approach is efficient in the trajectory planning for a manipulator that wants to follow a Cartesian path. In simulations, the constraints are respected, and all motion variables and path parameters remain smooth.

Keywords: constrained optimization; dynamic constraints; minimum-time robot path planning; path parameter optimization; trajectory tracking

1 INTRODUCTION

In the field of robotics, there is a need for the tracking of a known path for robot manipulators in the Cartesian space with maximum velocity or minimum-time algorithms for their economic benefits. Minimum-time path planning problems for robotic manipulators have widely been studied in the past, especially for industrial applications. Many techniques have been proposed in the past for this problem; however, due to factors such as non-linearity, coupling dynamics, and torque limitation, the task of finding a minimum-time path for robot manipulators is quite complicated. Therefore, an efficient motion planning technique for robot manipulators to move along a pre-defined trajectory is required. The most notable earliest studies in the domain of minimum-time path planning along a specified path were [1-3]. Additionally, ref. [4] is also included in one of the earliest studies in this domain, which presents an analysis of time-optimal trajectories in the case of fixed initial and final positions. In another study of the same era, the authors present a method to compute robotic paths in cases of closed kinematic chain mechanisms [5]. The earliest works in this domain also included solutions to the problem of minimum-time robotic manipulator motion along a specified geometric path, considering constraints such as force and torque [6]. That was the first attempt of its kind to address the minimum-time problem involving constraints. The minimum-time trajectory planning was similarly discussed in [7, 8]. Bobrow took the research further and devised a technique to find a collision-free path to obtain a minimum-time motion of a robotic manipulator [9]. Bobrow used B-spline polynomials and nonlinear equations of motion to produce optimal trajectories in the Cartesian space of the manipulator. These early studies paved the way for progress in robotics research and gave rise to further advancements in this domain. Bobrow's uses of B-spline polynomials to produce optimal trajectories were further investigated by researchers [10], most recently in [11]. Furthermore, minimization of the spline curve path was studied in [12-14]. More notable studies which contributed to further advancements in the research include techniques for making the robot manipulator learn from the previous path devised in [15], where waypoints are determined with the help of a robot manipulator tracking the path. This procedure of specifying a set of waypoints for path planning for robot manipulators is further elaborated in [16, 17], where previous path velocities are estimated for trajectory generation, and several continuous trajectories are considered between two points in a path so that they are blended. That is also referred to as point-to-point trajectory motion in other studies, such as in [18, 19], where a method for generating a smooth, time-optimal trajectory is presented. In [19], the authors used the third derivative of the path parameter with respect to time as an input, and it limits the torque rate in order to achieve the smoothness of the path. The point-to-point trajectory motion was investigated in [20], where the authors generated trajectories in joint space for the point-to-point motion. In this study, the authors also considered the constraints of the actuators' velocity, acceleration and jerk limits while calculating the minimum-time path [21, 22]. In more recent studies, the type of path that a robot manipulator needs to follow between given waypoints, such as a straight-line path, cubic spline or a circular path, are included in the path planning techniques. This consideration has been taken into account in [22]. In addition to considering the path type, the point-to-point motion planning also includes the polynomial coefficients of the constraints such as the position, velocity, acceleration and jerk constraints, as presented in [23-26]. Moreover, recent studies, namely [27, 28], focus on the user-defined trajectories for path planning, as well as on the development of a commercial robotics software. Many previous

researchers have also focused on iterative and geometric methods as well as on optimal switching structures in accordance with Pontryagin's Maximum Principle, as mentioned in [8, 29]. Other approaches have applied B-spline cubical methods for trajectory planning as mentioned in [30-32]. The optimization of the point-to-point minimum-time path problem has also been analyzed using the Sequential Quadratic Programming (SQP) method, as mentioned in [33]. For the purpose of optimization, the above-mentioned method involves the determination of minimum transmission time with electromagnetic constraints such as kinematics. Building up to that, [34] uses a similar approach with a dynamic programming algorithm in order to solve the minimum-time optimization problem. The dynamic programming approach has also been applied in [35]. After the early advancements in this domain, an ample amount of research has been undertaken on the constrained motion of robots. For example, [36, 37] propose a method to find the minimum-time considering the constraints of a jerk or higher order derivatives of position. Other studies presenting an approach for minimum-time calculation subject to kinematic constraints can be found in [38-40]. Another approach for a robot arm with path planning is the connection of straight-lines with circular arcs, perturbations about a straight-line with a Fourier series and cubic Bezier splines, as suggested in [41]. Furthermore, solutions to the path planning problem with end-effector constraints for robotic manipulators have also been studied, as presented in [42]. Another approach to path planning with torque constraints includes either the bang-bang trajectory or the bang-singular-bang trajectory as presented in [43]. Other interesting approaches for solving the path planning problem include a continuous genetic algorithm for path generation of robotic manipulators in a Cartesian space as presented in [44]. More recently, the robotic methodologies of a point-to-point trajectory planning have also been applied in other applications, as mentioned in [45]. Other examples using trajectory planning include agricultural field machines [46] and trajectory generation for animal movement [47]. Most significant studies on robotic manipulators include those, which estimate the minimum path and generate trajectories while handling any kinematic constraints on the velocity and acceleration [48-50]. This study proposes a path planning mechanism, whereby trajectories are generated in the operational space subject to certain dynamic constraints. The studies, which have been hitherto mentioned, do not usually consider the factors of external force and friction while calculating the minimum path for robotic manipulators. However, there is some significant research focusing on external forces as well as friction as factors influencing the calculation of the minimum path for a robotic manipulator. For example, [51, 52] present studies on robotic manipulators being controlled by DC motors, and considering the forces and friction generated by the motors that are dependent upon the kinematic constraints of velocity and acceleration.

A few of these studies have presented an approach for trajectory tracking control with taking into account the actuator dynamics [53]. However, most recent studies have found it necessary to include actuator dynamics and constraints as a part of the trajectory tracking control. For example, [54] proposed a trajectory tracking mechanism where geometrical constraints, impulsive force constraints, torque constraints, maximum acceleration and velocity constraints are considered. Another interesting study in this regard [55] compares different frameworks of trajectory tracking controllers for unmanned vehicles, where nonlinearity of the dynamics, uncertainties, noise, disturbances and several constraints are considered. The actuating machines usually used for robotic manipulators are DC motors. Hence, the actuator dynamics mostly consist of the force, energy and friction required for the DC motors which are attached to the manipulators [56]. However, there is some significant research focusing on external forces as well as friction as factors influencing the calculation of the minimum path for a robotic manipulator.

In this paper, the minimum-time path planning problem for a parametric approach to the solution of path planning in robotic manipulators uses a manipulator's path description, dynamic relations, and other defined constraints. Thus, an optimization strategy has been devised for path planning considering the mentioned constraints. The paper is presented in the following manner: Section 2 describes and illustrates the dynamics of the robotic manipulator. The problem is formulated and presented in Section 3, and the approach to solving the problem of optimization of a robotic manipulator is presented in Section 4. Afterward, the results of the simulation and path planning are presented and discussed in Section 5. Finally, a summary and conclusion of the paper are presented in Section 6.

2 DYNAMIC MODELLING OF THE MANIPULATOR

If we suppose that the manipulator's joint angles are represented by a vector q, the joint angle velocity vector will be $\dot{q}$, and $\ddot{q}$ will be the angular acceleration vector. The dynamic equation of the motion of the robot manipulator can be written as [49, 50]:

$$M(q)\ddot{q} + C(q,\dot{q})\dot{q} + G(q) = T \tag{1.1}$$

The total torque T is then given by:

$$T = T_{ext} + T_c + T_f \tag{1.2}$$

where $M(q) \in R^{n\times n}$is the inertia matrix and $C(q,\dot{q}) \in R^{n\times n}$is a matrix that contains the information of centrifugal and Coriolis torques. Here, C is not a unique matrix, but $C(q,\dot{q})\dot{q}$ is a unique vector. $G(q) \in R^{n\times n}$ is the gravity torque, T is the vector of total torques, and n is the number of joints angles. $T_{ext}, T_c,$ and T_f are the external force, control and friction torques, respectively. The external torque T_{ext} can be modelled as [49]:

$$T_{ext} = J^T F_{ext} \tag{2}$$

where $F_{ext}$is the external force at the robot's end-effector, and $J^T$is the transpose of the Jacobian matrix. We consider

that the external force is generated by friction between the end-effector and task plane and its direction is along the opposite direction of the end-effector's velocity. We can consider a model such as:

$$F_{ext} = -\mu v f_n \hat{n}_v \tag{3}$$

where v is the norm of the velocity vector of the end-effector, $f_n$is a normal force which is perpendicular to the surface which contains the velocity vector and the end-effector's link, μ is the friction coefficient, and $\hat{n}_v$ is a unit vector along the velocity vector tangent to the path. The joint angle friction torque is thus modeled as [49, 50]:

$$T_f = K_c sign(\dot{q}) + K_v \dot{q} \tag{4}$$

where $K_c$is a diagonal matrix which contains the coulomb friction coefficients for any joint, and K_v is another diagonal matrix that contains the viscous friction coefficients of the joint angles. There are a number of constraints due to the limitations of the robot manipulator. These constraints can be divided into two groups, the first of which is related to kinematics constraints, such as the constraints in joint angles, angular velocity, angular acceleration, jerk and higher time derivatives of the joint angles. We can consider limitations for the higher time derivatives of the joint angles. The second group is related to the constraints on the actuators. Many researchers consider $\dot{q}$ and $\ddot{q}$ to have constraints, but when the actuator is able to generate more torque, it will be able to generate higher jerk and acceleration, so the limitations on the time derivatives of the joint angles come from the actuators. Consequently, the added limitations on the time derivatives of the joint angles will cause more limitation on the robot, which is why we will not use the actual potential of the robot. Here, we will consider the transmission of rotation between the actuators and the arm of the robot as being guaranteed by the mechanical transmission system of the gears. Although this mechanism reduces the angular velocity of the motor, it increases the generated torque of the motor, thus [49]:

$$\begin{aligned} &T_c = NT_m, N = diag([N_1, \dots, N_n]) \\ &\dot{q} = N^{-1}\dot{q}_m \end{aligned} \tag{5}$$

where N is the diagonal matrix of the transmission gear system, $T_m$the vector of motor's torque, and $\dot{q}_m$ is the speed of the motor. When the joint angle motors are DC motors, and using Kirchhoff's voltage law for armature windings as represented in Fig. 1, the equations of the DC motor become [52]:

$$\begin{aligned} &\dot{I} = L^{-1}\left(-RI - K_{bemf}\dot{q}_m + U\right) \\ &T_m = K_m I \end{aligned} \tag{6}$$

where $L = diag([L_1, L_2, \dots, L_n])$is a diagonal matrix which contains the element of motor inductances and $R = diag([R_1, R_2, \dots, R_n])$is a matrix which contains armature resistances, $K_{bemf} = diag([K_{bemf_1}, K_{bemf_2}, \dots, K_{bemf_n}])$ is the back electromotive force constant matrix, $U = (U_1, U_2, \dots, U_n)$ is the input voltage vector, $I = (I_1, I_2, \dots, I_n)$ is the armature current of each DC motor, and $K_m = diag([K_1, K_2, \dots, K_n])$ is the motor torque constant matrix. By substituting Eq. (6) into Eq. (5), we find that:

$$\begin{aligned} \dot{T}_c &= AT_c + B\dot{q} + DU \\ A &= diag\left(\left[-\tfrac{R_1}{L_1}, -\tfrac{R_2}{L_2}, \dots, -\tfrac{R_n}{L_n}\right]\right) \\ B &= diag\left(\left[-\tfrac{K_{m_1}K_{bemf_1}N_1^2}{L_1}, -\tfrac{K_{m_2}K_{bemf_2}N_2^2}{L_2}, \dots, -\tfrac{K_{m_n}K_{bemf_n}N_n^2}{L_n}\right]\right) \\ D &= diag\left(\left[\tfrac{K_{m_1}N_1}{L_1}, \tfrac{K_{m_2}N_2}{L_2}, \dots, \tfrac{K_{m_n}N_n}{L_n}\right]\right) \end{aligned} \tag{7}$$

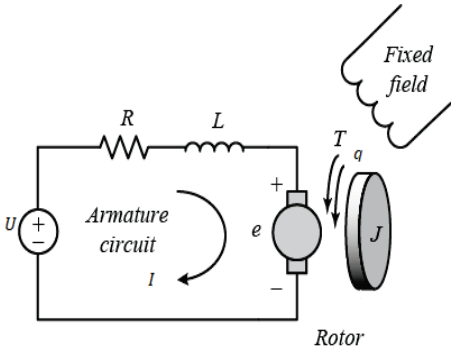

Figure 1 DC motor equivalent circuit.

As a result, the augmented equations of the motion of the manipulator can be summarized as:

$$T_c = M\ddot{q} + C\dot{q} + G(q) - T_{ext} - T_f \tag{8}$$

By calculating the time derivative of Eq. (8), we have:

$$\dot{T}_c = \dot{M}\ddot{q} + M\dddot{q} + \dot{C}\dot{q} + C\ddot{q} + \frac{\partial G}{\partial q}\dot{q} - \dot{T}_{ext} - \dot{T}_f \tag{9}$$

Eq. (7) is rearranged as:

$$U = D^{-1}(\dot{T}_c - AT_c - B\dot{q}) \tag{10}$$

Here, $\dot{T}_{ext}$ and $\dot{T}_f$ are calculated using Eq. (2), thus:

$$\dot{T}_{ext} = \dot{J}^T F_{ext} + J^T \dot{F}_{ext} \tag{11}$$

When the normal force is constant, by calculating the time derivative of F_{ext} using Eq. (3), we obtain:

$$\dot{F}_{ext} = -\mu \dot{v} f_n \hat{n}_v - \mu v f_n \dot{\hat{n}}_v \tag{12}$$

where $\hat{n}_v$ and $\dot{\hat{n}}_v$ are the unit vector of velocity and its time derivative, respectively. Consequently, when the desired joint angles and their first, second and third time derivatives are known, to calculate U, we need to calculate T_c using the desired path, after which Eq. (9) is used to calculate $\dot{T}_c$. Finally, by using Eq. (10), U is calculated. The constraints of the motors are as follows [52]:

$$|\dot{q}_{m_i}| \le \bar{\dot{q}}_{m_i} \tag{13.1}$$

$$|I_i| \le \bar{I}_i \tag{13.2}$$

$$|U_i| \le \bar{U}_i \tag{13.3}$$

$$|\dot{I}_i| \le \bar{\dot{I}}_i \tag{13.4}$$

$$\sqrt{\frac{1}{t_f}\int_0^{t_f} {I_i}^2(t)\,dt} \le \bar{I}_{c_i},\ (i = 1, 2, \dots, n) \tag{13.5}$$

where n is the number of joint angles, and $\bar{\dot{q}}_{m_i}$, $\bar{I}_i$, $\bar{U}_i$, $\bar{\dot{I}}_i$, $\bar{I}_{c_i}$, are the maximum admissible motor speed, current, feeding voltage, the time derivative of current and braked motor current, respectively. Finally, we have to convert these constraints into robot manipulator constraints:

$$|\dot{q}_i| \le N^{-1}\bar{\dot{q}}_{m_i} \tag{14.1}$$

$$|T_{c_i}| \le NK_m\bar{I}_i \tag{14.2}$$

$$|\dot{T}_{c_i}| \le NK_m\bar{\dot{I}}_i \tag{14.3}$$

$$\sqrt{\frac{1}{t_f}\int_0^{t_f} {T_{c_i}}^2(t)dt} \le N^2{K_m}^2\bar{I}_{c_i}^{\ 2},(i = 1, 2, \dots, n) \tag{14.4}$$

where $\dot{q}_i, T_{c_i}$, $\dot{T}_{c_i}$ and $\sqrt{\frac{1}{t_f}\int_0^{t_f} {T_{c_i}}^2(t)dt}$ are the angular velocity of joint angles, the control torque, the time derivative of the control torque, and the guaranteed term for harmless overtaking of the permanent operating range [33].

3 DEFINITION OF THE PARAMETRIC TRAJECTORY OPTIMIZATION PROBLEM

We are interested in performing a task with the manipulator in the minimum-time. Therefore, the cost function can be expressed as:
Cost function:

$$J = \int_0^{t_f} dt = t_f \tag{15.1}$$

Subject to the constraints:

$$\begin{aligned} T_c &= M\ddot{q} + C\dot{q} + G(q) - T_{ext} - T_f \\ \dot{T}_c &= \dot{M}\ddot{q} + M\dddot{q} + \dot{C}\dot{q} + C\ddot{q} + \frac{\partial G}{\partial q}\dot{q} - \dot{T}_{ext} - \dot{T}_f \\ U &= D^{-1}(\dot{T}_c - AT_c - B\dot{q}) \\ |\dot{q}_i| &\le N^{-1}\bar{\dot{q}}_{m_i} \\ |T_{c_i}| &\le NK_m\bar{I}_i \\ |\dot{T}_{c_i}| &\le NK_m\bar{\dot{I}}_i \\ \sqrt{\frac{1}{t_f}\int_0^{t_f} {T_{c_i}}^2(t)dt} &\le N^2{K_m}^2,\qquad (i = 1, 2, \dots, n) \end{aligned} \tag{15.2}$$

where M and C are functions of q and $\dot{q}$, respectively. Therefore, the time derivatives of these matrices are:

$$\begin{aligned} \dot{M} &= \sum_{i=1}^{n} \frac{\partial M}{\partial q_i}\dot{q}_i \\ \dot{C} &= \sum_{i=1}^{n} \frac{\partial C}{\partial q_i}\dot{q}_i + \sum_{i=1}^{n} \frac{\partial C}{\partial \dot{q}_i}\ddot{q}_i \end{aligned} \tag{16}$$

Let us suppose that the purpose of path planning is to track a desired path in the Cartesian space that is parameterized by γ. The position of end-effector r is the function of the path parameter (γ).

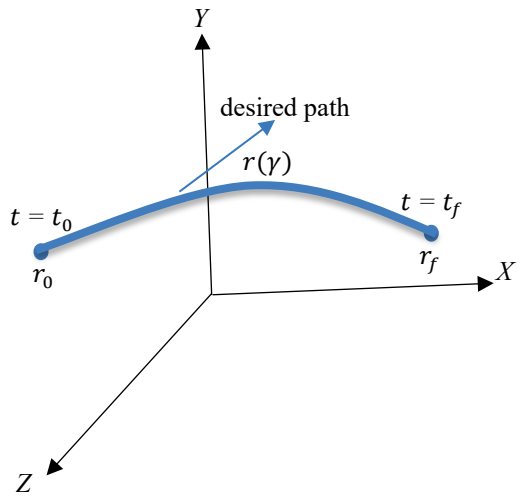

Figure 2 Trajectory planning along a parameterized path.

In Fig. 2, the coordinates of the start and stop points are r_0 and r_f. When the robot is at the starting point, for simplicity γ is $\gamma(t_0) = 0$, and at the stopping point, it is $\gamma(t_f) = \gamma_f$. The aim of an optimization problem is to find $\gamma(t)$ to minimize the cost function equation Eq. (15.1) by considering the constraints equation Eq. (15.2). In this paper, a polynomial approach is taken to convert the function optimization problem into a parameter optimization problem. Therefore, the approach will be a suboptimal solution. However, $\gamma(t)$ has a number of constraints due to the limitations of a manipulator. Firstly, we know that γ has two constraints due to the definition of the path at the initial and the final times as:

$$\begin{aligned} \gamma(t_0) &= \gamma(0) = 0 \\ \gamma(t_f) &= \gamma_f \end{aligned} \tag{17}$$

To find other constraints, we have to find the relation between the kinematic constraints in the Cartesian space and the joint space. Therefore, we start by finding the relation between the velocity, acceleration, and jerk as functions of time in the Cartesian space, thus:

$$\dot{r} = \mathrm{v} = r'\dot{\gamma}$$

$$\ddot{r} = a = r''\dot{\gamma}^2 + r'\ddot{\gamma} \tag{18}$$

$$\dddot{r} = \mathcal{J} = r'''\dot{\gamma}^2 + 2r''\ddot{\gamma} + r'\dddot{\gamma}$$

Here, v, a, and $\mathcal{J}$ are the velocity, acceleration and jerk of the end-effector, respectively. The relation between kinematic parameters in the Cartesian space and the joint space are:

$$\mathrm{v} = J\dot{q}$$

$$a = \dot{J}\dot{q} + J\ddot{q} \tag{19}$$

$$\mathcal{J} = \ddot{J}\dot{q} + 2\dot{J}\ddot{q} + J\dddot{q}$$

where J, $\dot{J}$, and $\ddot{J}$ are the Jacobian, first and second time derivatives of the Jacobian matrix at any time, respectively. It is desirable for the velocity, acceleration and jerk to be zero at the initial time. Therefore, by using Eq. (18), $\dot{q}$, $\ddot{q}$, $\dddot{q}$, will be zero. These conditions are simple in the view of the actuators for starting because the commands of the actuator will not jump to the maximum. Hence, if at the starting point the velocity, acceleration and jerk in the Cartesian space are zero, then the time derivatives of the path parameter $\dot{\gamma}(0)$, $\ddot{\gamma}(0)$ and $\dddot{\gamma}(0)$ will be zero. Therefore, the initial conditions for $\gamma(t)$ are:

$$\gamma(0) = 0$$

$$\dot{\gamma}(0) = 0 \tag{20}$$

$$\ddot{\gamma}(0) = 0$$

$$\dddot{\gamma}(0) = 0$$

It is necessary to define the final conditions for the path parameter. We know that γ_f is known by the definition of the path, hence again, in order to have zero velocity, zero acceleration, and zero jerk in the Cartesian and joint spaces, the final condition for $\gamma(t)$ will be:

$$\begin{aligned} \gamma(t_f) &= \gamma_f \\ \dot{\gamma}(t_f) &= 0 \\ \ddot{\gamma}(t_f) &= 0 \\ \dddot{\gamma}(t_f) &= 0 \end{aligned} \tag{21}$$

For a suboptimal solution, let us suppose that the function $\gamma(t)$ is approximated by a time series as:

$$\gamma(t) = \sum_{i=4}^{n} a_i\, t^i \tag{22}$$

In the above format, all initial conditions will satisfy, but the final conditions will not satisfy. Because of the simplicity, for the satisfaction of the final conditions, we will consider a model for $\gamma(t)$ to be:

$$\gamma(t) = A\gamma_1(t) + B\gamma_2(t) + C\gamma_3(t) + D\gamma_4(t) \tag{23}$$

Here, $A, B, C,$ and D are constant and unknown parameters and γ_1, γ_2, γ_3 and γ_4 have a format as in Eq. (22); therefore, they will satisfy the initial conditions:

$$\begin{aligned} \gamma_1(t) &= \sum_{i=4}^{n} a_i\, t^i \\ \gamma_2(t) &= \sum_{i=4}^{n} b_i\, t^i \\ \gamma_3(t) &= \sum_{i=4}^{n} c_i\, t^i \\ \gamma_4(t) &= \sum_{i=4}^{n} d_i\, t^i \end{aligned} \tag{24}$$

Therefore, when a_i, b_i, c_i, and $d_i, (i = 4, \dots, n)$, and t_f are known, we are able to calculate $A, B, C,$ and D as:

$$\begin{aligned} &A\gamma_1(t_f) + B\gamma_2(t_f) + C\gamma_3(t_f) + D\gamma_4(t_f) = \gamma_f \\ &A\dot{\gamma}_1(t_f) + B\dot{\gamma}_2(t_f) + C\dot{\gamma}_3(t_f) + D\dot{\gamma}_4(t_f) = 0 \\ &A\ddot{\gamma}_1(t_f) + B\ddot{\gamma}_2(t_f) + C\ddot{\gamma}_3(t_f) + D\ddot{\gamma}_4(t_f) = 0 \\ &A\dddot{\gamma}_1(t_f) + B\dddot{\gamma}_2(t_f) + C\dddot{\gamma}_3(t_f) + D\dddot{\gamma}_4(t_f) = 0 \end{aligned} \tag{25}$$

In Eq. (25), there are four unknown parameters $A, B, C,$ and D, when $\gamma_1, \gamma_2, \gamma_3$ and γ_4 at the final time are known. Therefore, for the satisfaction of the final conditions, we can then write:

$$\begin{bmatrix} A \\ B \\ C \\ D \end{bmatrix} = \begin{bmatrix} \gamma_1(t_f) & \gamma_2(t_f) & \gamma_3(t_f) & \gamma_4(t_f) \\ \dot{\gamma}_1(t_f) & \dot{\gamma}_2(t_f) & \dot{\gamma}_3(t_f) & \dot{\gamma}_4(t_f) \\ \ddot{\gamma}_1(t_f) & \ddot{\gamma}_2(t_f) & \ddot{\gamma}_3(t_f) & \ddot{\gamma}_4(t_f) \\ \dddot{\gamma}_1(t_f) & \dddot{\gamma}_2(t_f) & \dddot{\gamma}_3(t_f) & \dddot{\gamma}_4(t_f) \end{bmatrix}^{-1} \begin{bmatrix} \gamma_f \\ 0 \\ 0 \\ 0 \end{bmatrix} \tag{26}$$

Hence, when $A, B, C,$ and D are selected from Eq. (26), the initial and final conditions will always be satisfied. Consequently, $\gamma(t)$ will be a function of the unknown vector as:

$$\gamma(t) = \gamma(x,t)$$
$$x = [a_4, \dots, a_n, b_4, \dots, b_n, c_4, \dots, c_n, d_4, \dots, d_n, t_f]^T \quad (27)$$

Here, x is an unknown vector that has to be found by the minimization of the cost function in Eq. (15.1) subjected to the constraint Eq. (15.2). Therefore, the objective function Eq. (15.1) and constraints Eq. (15.2) will updated as:
Cost function:

$$J(x) = [0_{1x4(n-4)}\ 1]x$$

The constraint equations are:

$$T_c = M\ddot{q} + C\dot{q} + G(q) - T_{ext} - T_f$$

$$\dot{T}_c = \dot{M}\ddot{q} + M\dddot{q} + \dot{C}\dot{q} + C\ddot{q} + \frac{\partial G}{\partial q}\dot{q} - \dot{T}_{ext} - \dot{T}_f$$

$$U = D^{-1}\left(\dot{T}_c - AT_c - B\dot{q}\right)$$

$$|\dot{q}_i| \le N^{-1}\bar{\dot{q}}_{m_i} \quad (28)$$

$$\left|T_{c_i}\right| \le NK_m\bar{I}_i$$

$$\left|\dot{T}_{c_i}\right| \le NK_m\bar{\dot{I}}_i$$

$$\sqrt{\frac{1}{t_f}\int_0^{t_f} {T_{c_i}}^2(t)dt} \le N^2{K_m}^2{\bar{I}_{c_i}}^2, (i = 1, 2, \dots, n)$$

4 MANAGING THE CONSTRAINTS OF THE OPTIMIZATION PROBLEM

The purpose of the optimization problem is to minimize the final time subjected to the dynamic of the manipulator. As mentioned previously, parameters are unknown.

Here they are collected in the vector x. Therefore, the objective function can be written as:

$$J(x) = x_{\hat{N}+1} = t_f \quad (29)$$

Here, $\hat{N}$ is the number of unknown parameters for the modelling of $\gamma(t)$; therefore, $4(n-4) = \hat{N}$. However, there are a number of constraints due to the limitations related to the angular velocity and the motor input voltages, and the torques of the motors. These constraints may appear at any time. We can manage the constraints of the problem at any time by adding the previous constraints. A simple method of doing this is to divide the time between the initial and final time with known and constant m incremental times. The constraints listed in Table 1 are divided into two types. The first type consists of differential equations and the second type consists of normal nonlinear or linear inequality equations.

In this paper, we suggest rewriting every constraint without solving the differential equations. We know that some constraints may appear at all times, hence we can manage the constraints of the problem at any time by adding to the previous constraints. A simple method for doing so is to generate new constraints for any time interval. Therefore, when the vectors x and t_f are known, we can divide the t_f to m incremental times as:

$$\Delta t = \frac{t_f}{m}, t_k = \Delta tk, (k = 0, \dots, m) \quad (30)$$

To prepare the constraints as a function of the unknown vector x, the initial time x_0 is first generated as a random vector. This random vector will guarantee the initial and final condition of the path parameter, but it is necessary for it to be tuned for other constraints. Tab. 1 shows the processes of the generating of constraints for each time as listed in Tab. 1.

Table 1 Managing constraints for the optimization problem at time t_k

Initial time	*- Initial estimate of the final time* $t_f(0)$ *- Generating a random vector* x
For $(k = 1, \dots, m)$	*- using of x, calculate* $\gamma_k, \dot{\gamma}_k, \ddot{\gamma}_k, \dddot{\gamma}_k$ *- using Eq. (18), calculate* $r_k, \dot{r}_k, \ddot{r}_k, \dddot{r}_k$ *- Calculate:* $q_k = q(r_k)$ J_k *and* $\dot{J}_k$ $\dot{q}_k = {J_k}^{-1}{r_k}'\dot{\gamma}_k\dot{J}_k$ $v = J_k\dot{q}_k$ *- Calculate:* $M_k(q_k), C_k(q_k, \dot{q}_k), G_k, T_{ext_k}, T_{f_k}$ $\ddot{q}_k = {J_k}^{-1}(-\dot{J}_k\dot{q}_k + {r_k}''{\dot{\gamma}_k}^2 + {r_k}'\ddot{\gamma}_k)$ $T_{c_k} = M_k\ddot{q}_k + C_k\dot{q}_k + G_kq_k - T_{ext_k} - T_{f_k}$ *- Calculate:* $\dot{M}_k(q_k, \dot{q}_k), \dot{C}_k, \dot{G}_k, \dot{T}_{ext_k}, \dot{T}_{f_k}$ $\dddot{q}_k = {J_k}^{-1}(-{J_k}^{-1}\dot{q}_k - 2\dot{J}_k\ddot{q}_k + {r_k}'''{\dot{\gamma}_k}^2 + 2{r_k}''\ddot{\gamma}_k + {r_k}'\dddot{\gamma}_k)$ $\dot{T}_{c_k} = \dot{M}\ddot{q} + M\dddot{q} + \dot{C}\dot{q} + C\ddot{q} + \frac{\partial G}{\partial q}\dot{q} - \dot{T}_{ext}$ $U_k = D^{-1}(\dot{T}_{c_k} - AT_{c_k} - B\dot{q}_k)$ *Constraints are:* $C_k = \begin{Bmatrix} U_k - \overline{U} \\ \underline{U} - U_k \\ T_{c_k} - \overline{T}_c \\ \underline{T_c} - T_{c_k} \\ \dot{q}_k - \bar{\dot{q}} \\ \underline{\dot{q}} - \dot{q}_k \\ \dot{T}_{c_k} - \bar{\dot{T}}_c \\ \underline{\dot{T}_c} - \dot{T}_{c_k} \\ \gamma_k \ge 0 \\ \dot{\gamma}_k \ge 0 \end{Bmatrix} \le 0$

In Tab. 1, $\overline{a}$ and $\underline{a}$ are respectively used to represent the maximum and minimum of the parameter a. Therefore, the size of constraints at each step will increase. There are ten constraints in each t_k, hence the size of the constraint vector at the end will be $10(m\ +\ 1)$. In Eq. (28), there is an integral equation for any motor. This integral can be approximated as:

$$\Delta t \sum_{i=1}^{N} {T_{c_i}}^2 = N\Delta t{\bar{T}_{c_i}}^2 \quad (31)$$

Therefore, at the end of each iteration, another constraint will be added to the previous constraints.

5 SIMULATION STUDY

Simulations in the MATLAB environment were used to test the performance of the proposed algorithm. A model of the SCARA robot (Selective Compliance Assembly Robot Arm) used in the simulation study are given in ref. [33]. However, there are some additional parameters and small changes that we considered in the simulations. The model of the manipulator (represented in Fig. 3) that is considered for the simulation is:

$$\begin{bmatrix}(3.78+0.272\cos q_2+0.022\sin q_2)+(0.08+0.136\cos q_2+0.011\sin q_2) & 0\\ (0.08+0.136cosq_2+0.011\sin q_2) & 0.08\end{bmatrix}\begin{bmatrix}\ddot{q}_1\\ \ddot{q}_2\end{bmatrix}+\begin{bmatrix}(0.011\cos q_2-0.136\sin q_2)+(\dot{q}_2+\dot{q}_1)+0.07 & (0.011\cos q_2-0.136\sin q_2)\dot{q}_1\\ (0.011cosq_2-0.136sinq_2)\dot{q}_1 & 0.013\end{bmatrix}\begin{bmatrix}\dot{q}_1\\ \dot{q}_2\end{bmatrix}=\begin{bmatrix}T_{c_1}\\ T_{c_2}\end{bmatrix}+\begin{bmatrix}0.62sign\dot{q}_1\\ 0.17sign\dot{q}_2\end{bmatrix}+\begin{bmatrix}K_{v_1} & 0\\ 0 & K_{v_2}\end{bmatrix}\begin{bmatrix}\dot{q}_1\\ \dot{q}_2\end{bmatrix}+\begin{bmatrix}T_{ext_1}\\ T_{ext_2}\end{bmatrix} \quad (32\text{-}1)$$

The position of the end-effector is a function of the length of the robot arm and joint angles, thus:

$$r=\begin{bmatrix}x\\ y\end{bmatrix}=\begin{bmatrix}L_1cosq_1+L_2cos(q_1+q_2)\\ L_1sinq_1+L_2sin(q_1+q_2)\end{bmatrix} \quad (32\text{-}2)$$

By using the above forward kinematic, the inverse kinematic of the robot is:

$$q_1=\tan^{-1}\left(\frac{y}{x}\right)-\tan^{-1}\left(\frac{K_2}{K_1}\right) \quad (33)$$

$$q_2=\tan^{-1}\left(\frac{\sin(q_2)}{\cos(q_2)}\right) \quad (34)$$

where K_1, K_2, $\sin(q_2)$ and $\cos(q_2)$ are:

$$K_1=L_1+L_2\cos(q_2),\ K_2=L_2\sin(q_2)$$

$$\sin q_2=\pm\sqrt{1-\cos{q_2}^2}$$

$$\cos q_2=\frac{x^2+y^2-{L_1}^2-{L_2}^2}{2L_1L_2}$$

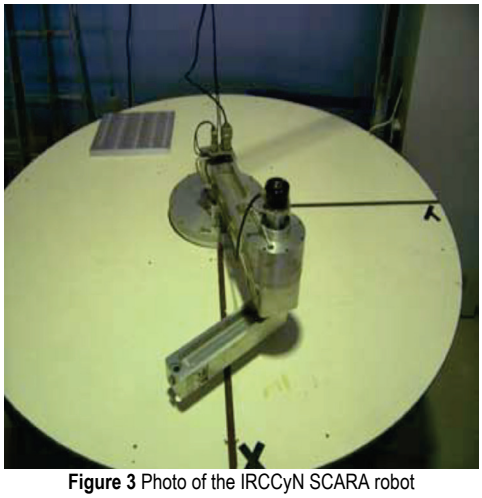

Figure 3 Photo of the IRCCyN SCARA robot

The parameters of the robot are presented in Tab. 2.

Table 2 Parameters of the IRCCyN SCARA robot.

Task N°	μ	K_v	K_c	$L\ (m)$
1	0.2	0.4	0.01	0.21
2	0.2	0.3	0.01	0.3

The normal force is $f_n = 0.1N$. The electro-mechanical constraints of the actuators are presented in Tab. 3.

Table 3 Electro-mechanical constraints of the SCARA robot.

Axis	$\bar{U}$ (volt)	q (deg)	$\bar{\dot{q}}$ (rad · s^{-1})
1	20	0-270	1.5
2	20	0-180	2

The purpose of the simulations is to plot Fig. 3 with a pencil attached to the end-effector. Hence, there is the desired path, and the end-effector has to track that path. Here, the Cartesian path as a function of the path parameter is considered to be:

$$r=\begin{bmatrix}\rho\sin(\gamma)\\ 0.5\rho\cos(\gamma)\end{bmatrix} \quad (35)$$

Then, the derivative of r with respect to the path parameter (γ) are listed as follows:

$$r'=\begin{bmatrix}\rho'\sin(\gamma)+\rho\cos(\gamma)\\ 0.5\rho'\cos(\gamma)-0.5\rho\sin(\gamma)\end{bmatrix} \quad (36)$$

$$r''=\begin{bmatrix}\rho''\sin(\gamma)+2\rho'\cos(\gamma)-\rho sin(\gamma)\\ 0.5\rho''\cos(\gamma)-\rho'\sin(\gamma)+0.5\rho\cos(\gamma)\end{bmatrix} \quad (37)$$

$$r'''=\begin{bmatrix}\rho'''\sin(\gamma)+3\rho''\cos(\gamma)-3\rho'\sin(\gamma)+\rho\cos(\gamma)\\ 0.5\rho'''\cos(\gamma)-1.5\rho''\sin(\gamma)-0.5\rho'\cos(\gamma)-\rho\sin(\gamma)\end{bmatrix} \quad (38)$$

Here ρ, ρ', ρ'', ρ''', are:

$$\rho=0.4-0.1\gamma cos(\gamma),\ (0\le\gamma\le 200^0)$$

$$\rho'=-0.1cos(\gamma)+0.1\gamma sin(\gamma)$$

$$\rho''=0.2\,sin(\gamma)+0.1\gamma cos(\gamma)$$

$$\rho'''=-0.4\,sin(\gamma)-0.1\gamma cos(\gamma)$$

The desired path is presented in Fig. 4 and the starting and stopping points are:

$$r_0=\begin{bmatrix}0\\ 0.2\end{bmatrix}m,\ r_f=\begin{bmatrix}-0.1965\\ -0.2699\end{bmatrix}m$$

The desired path, start-point and end-point in the Cartesian space are shown in Fig. 4. To provide an approximation for γ as a function of time, n in Eq. (22) is set to be $n = 10$. The Taylor expansion will contain terms up to t^{10} and $a_i = b_i = c_i = d_i = 0, (i = 1, \dots, 4)$. The number of unknown parameters for the representation of γ is (4×6) and by adding t_f, there will be $(4 \times 6 + 1) = 25$ unknown parameters. To initialize the unknown parameters, we use a

normal distribution to generate the coefficients of the path parameter. Moreover, the initial estimation of the final time is considered to be (17) seconds. The time between (0 and 17) seconds is divided into (5000) points; then, as mentioned in Tab. 1, the number of constraints is (50 000). For any iteration, when the time is increasing, the number of constraints will increase. After running the optimization algorithm, the final time is found to be (14.4296) seconds and the results below are found. The path parameter and its first, second and third time derivatives are presented in Figs. 5 and 6.

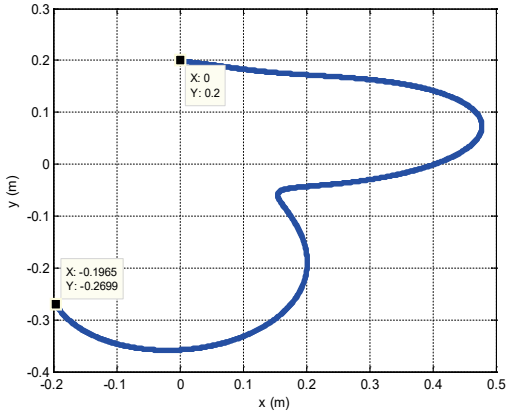

Figure 4 Desired path along the x and y axes

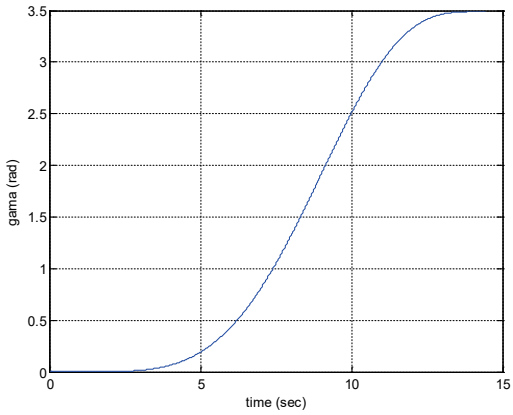

Figure 5 Optimal path parameter

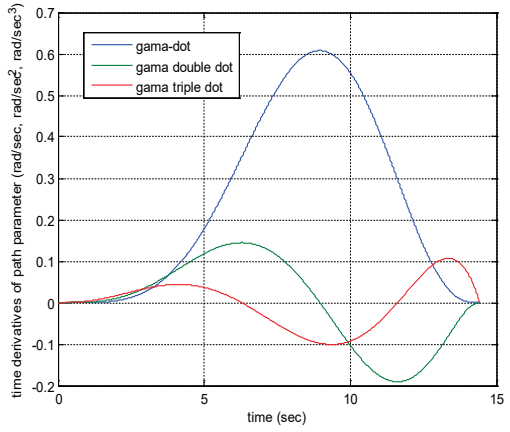

Figure 6 Time derivatives of the path parameter

Fig. 5 shows that the path parameter starts at zero and stops at (200 deg = 3.4907 rad). The path parameter has a smooth graph and Fig. 6 shows the first three-time derivatives of the path parameter. Those parameters are smooth and have zero values at the start and stop points. In addition to that, the first-time derivative has a positive value. Consequently, γ is an increasing function. Then, when the time increases, the end-effector always goes toward the final point and it does not have any backward motion. However, the other derivatives are sometimes positive and sometimes they are negative because the system changes the acceleration along the Cartesian path.

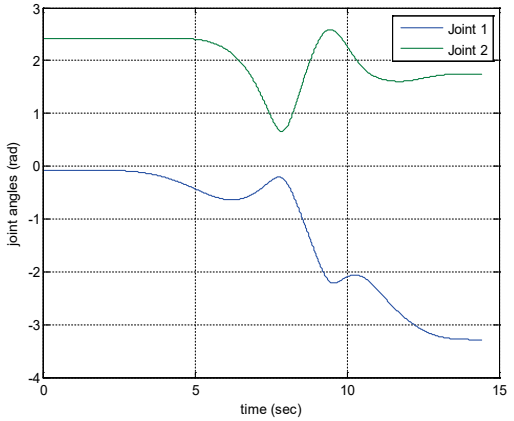

Figure 7 Time history of joint angles

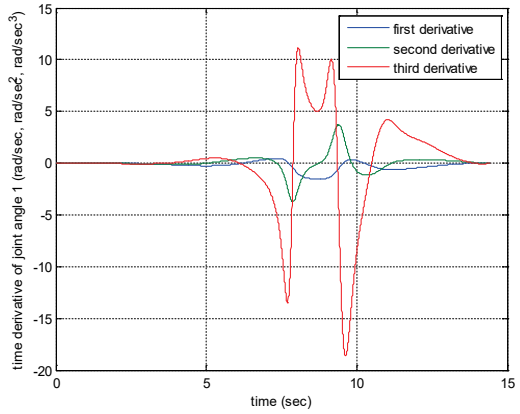

Figure 8 Time derivative of the first joint.

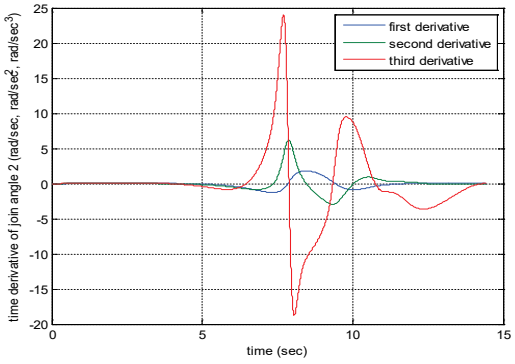

Figure 9 Time derivative of the second joint.

Fig. 7 shows the joint angles and Figs. 8 and 9 show the first, second and third time derivatives of the joint angles. We can see that the time derivatives of the joint angles are smooth and at the initial and final times, they are equal to zero. The figures show that the angular velocity of the joint angles has positive and negative values, which is why the robot changes its angular velocity. The absolute values of the maximum angular velocities are $\begin{bmatrix} 1.5 \\ 1.757 \end{bmatrix}$ rad, and are in the defined range, as presented in Tab. 2.

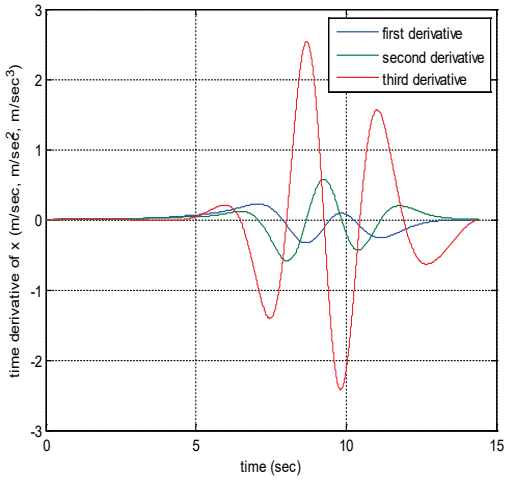

Figure 10 Velocity, acceleration and jerk along the x direction in the Cartesian-space

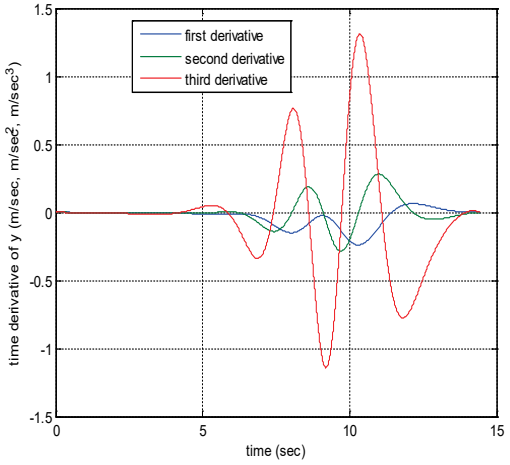

Figure 11 Velocity, acceleration and jerk along the y direction in the Cartesian-space

Figs. 10 and 11 show that the third time derivatives of position have zero values at the initial and the final times and are smooth graphs; and then the end-effector moves smoothly in the Cartesian space.

Fig. 14 shows the feeding voltage of the motors, which are smooth factions and have zero values at the start and stop points. We can see that the robot uses maximum voltages for link one, which is (20) volts and uses (15.161) volts for the second links. Therefore, the feeding voltages are in the range.

6 CONCLUSIONS

In this work, a new technique based on path parameter optimization is used for the path planning problem in the Cartesian space with external forces and frictions. The actuators of the robot are modeled as permanent magnet DC motors with a consideration of their constraints. By dividing the time between the start and stop times to known portions, the path parameter optimization problem is converted to the optimization of a function subject to certain equality and inequality constraints. A MATLAB simulation is used for the path planning of a two-degree robot manipulator with a desired path in the Cartesian space. The path parameter is used in the formulation of the desired path as a function of time. A polynomial model is considered for the path parameter so that it can guarantee constraints at the start and stop points. Consequently, the three first-time derivatives of the joint angles and the position of the end-effector will be zeros. Additionally, the voltages, torques and time derivatives of the torques are zeros at boundary conditions. It is shown that the approach can hold all constraints related to the actuators and other kinematics constraints between the initial and final times. The method was suboptimal due to the consideration of a polynomial model for the path parameter and it will not be a global optimum point for the problem. The best advantages of the method are all the dynamic and kinematic parameters which remain smooth, and it is practically more important that we be able to automatically control the start and stop conditions. Computer simulation results show the satisfactory performance responses of the method on a robotic manipulator path planning.

7 REFERENCES

[1] Bobrow, J. E., Dubowsky, S., & Gibson, J. S. (1985). Time-optimal control of robotic manipulators along specified paths. *The International Journal of Robotics Research*, 4, 3-17. https://doi.org/10.1177%2F027836498500400301

[2] Shin, K. G. & McKay, N. D. (1986). Selection of near-minimum time geometric paths for robotic manipulators. *IEEE Transactions on Automatic Control*, June 1986, 31, 501-511. https://doi.org/10.1109/TAC.1986.1104316

[3] Lin, C. S., Chang, P. R., & Luh, J. Y. S. (1983). Formulation and optimization of cubic polynomial joint trajectories for industrial robots. Automatic Control, IEEE Transactions 1983 on, 28(12), 1066-1074. https://doi.org/10.1109/TAC.1983.1103181

[4] Hans, P. G., Lino, G., Stephan, A. R. H., & Christopher, H. O. (1985). *Time-optimal motions of robots in assembly tasks*. IEEE-Institute of Electrical and Electronics Engineers, Inc., 1985. Fort Lauderdale, FL, USA, USA1 December 1985, 982-989. https://doi.org/10.1109/CDC.1985.268647
Luh, J. & Zheng, Y. F. (1985). Computation of input generalized forces for robots with closed kinematic chain mechanisms. *IEEE Journal of Robotics and Automation, 1*(2), 95-103. https://doi.org/10.1109/JRA.1985.1087008

[5] Shin, K. G. & Mckay, N. D. (1985). Minimum time control of robotic manipulators with geometric path constraints. *IEEE Transactions on Automatic Control, AC* 30, 531-541.

[6] Dubowsky, S., Norris, M. A., & Shiller, Z. (1986). Time optimal trajectory planning for robotic manipulators with

obstacle avoidance: A CAD approach. In IEEE International Conference on Robotics and Automation 1986, San Francisco, California, 1906-1912. https://doi.org/10.1109/ROBOT.1986.1087434

[7] Pfeiffer, F. & Johanni, R. (1986). A concept for manipulator trajectory planning. In *Proceedings of the International Conference on Robotics and Automation*, 3, 1399-1405.

[8] Bobrow, J. E. (1988). Optimal robot plant planning using the minimum-time criterion. *IEEE Journal on Robotics and Automation*, 4, 443-450. https://doi.org/10.1109/56.811

[9] Cao, B., Dodds, G. I., & Irwin, G. W. (1994). Time optimal and smooth constrained path planning for robot manipulators. *Proceedings of the International Conference on Robotics and Automation*, Minneapolis, 43(2), 1853-1858. https://doi.org/10.1109/ROBOT.1994.351191

[10] Gang, L. & Chao, Y. (2016). A fast approach for time-optimal and smooth trajectory planning of robot manipulators. *Journal of Harbin Institute of Technology, (New Series), 23*(5).

[11] Lepetic, M., Klancar, G., Skrjanc, I., & Matko, D. et al. (2003). Time-optimal path planning considering acceleration limits. Robotics and Autonomous Systems, 45, 199-210. https://doi: 10.1016/j.robot.2003.09.007

[12] Cao, B., Dodds, G., & Irwin, G. (1997). Constrained time-efficient and smooth cubic spline trajectory generation for industrial robots. In IEEE Proceedings Control Theory and Applications, 144, 467-475. https://doi.org/10.1049/ip-cta:19971494

[13] Chang, Y. H., Lee, T. T., & Liu, C. H. (1992). On-line approximate cartesian path trajectory planning for robotic manipulators. *IEEE Transactions on Systems, Man, and Cybernetics, 22*(3), 542-547. https://doi.org/10.1109/21.155953

[14] Murray, J. J. & Lovell, G. (1989). Dynamic modelling of closed-chain robotic manipulators and implications for trajectory control. *Robotics and Automation, IEEE Transactions on*, 5(4), 522-528. https://doi.org/10.1109/70.88066

[15] Shiller, Z., Chang, H., & Wong, V. (1996). The practical implementation of time-optimal control for robotic manipulators. *Robotics and Computer-Integrated Manufacturing, 12*(1), 29-39. https://doi.org/10.1016/0736-5845(95)00026-7

[16] Lloyd, J. & Hayward, V. (1993). Trajectory generation for sensor-driven and time-varying tasks. International Journal of Robotics Researches 1993, 12(4), 380-393. https://doi.org/10.1177%2F027836499301200405

[17] Volpe, R. (1993). Task space velocity blending for real-time trajectory generation. Proceedings of IEEE International Conference on Robotics and Automation, Atlanta, GA, 2-6 May 1993, 680-687. https://doi.org/10.1109/ROBOT.1993.291880

[18] Sciavicco, L. & Siciliano, B. (1996). Modelling and control of robot manipulators. The McGraw-Hill Companies Inc. 1996, New York.

[19] Constantinescu, D. & Croft, E. A. (2002). Smooth and time-optimal trajectory planning for industrial manipulators along specified paths. *Journal Robotic System, 17*(5), 233-249. https://doi.org/10.1002/(SICI)10974563(200005)17:5%3C233::AID-ROB1%3E3.0.CO;2-Y

[20] Sandor G. N. & Erdman A. G. (1985). Advanced mechanism design; Analysis and synthesis. Prentice-Hall, *Mechanism and Machine Theory, 2*(1), 81.

[21] Shiller, Z. (1994). On singular time-optimal control along specified paths. *IEEE Transactions on Robotics and Automation, 10*(4), 561-566. https://doi.org/10.1109/70.313107

[22] Kardos, E. S. & Kiss, B. (2009). Continuous-curvature paths for mobile robots. *Periodica Polytechnic Electrical Engineering, 53*(1-2), 63-72.

[23] Bianco, C. G. L. & Piazzi, A. (2010). Minimum-time trajectory planning of mechanical manipulators under dynamic constraints. *International Journal Control, 75*(13), 967-980. https://doi.org/10.1080/00207170210156161

[24] Kim, K. W., Kim, H. S., Choi, Y. K., & Park, J. H. (1997). Optimization of cubic polynomial joint trajectories and sliding mode controllers for robots using evolution strategy. *Proceedings of the 23rd International Conference on Industrial Electronics Control and Instrumentation IECON 1997*, 3, 1444-1447. https://doi.org/10.1109/IECON.1997.668531

[25] Aurelio, P. & Antonio, V. (2000). Global minimum-jerk trajectory planning of robot manipulators. *IEEE Transactions on Industrial Electronics, 47*(1), 140-149. https://doi.org/10.1109/41.824136

[26] Gasparetto, A. & Zanotto, V. (2009). Optimal trajectory planning for industrial robots. *Advances in Engineering Software*, 41, 548-556. https://doi.org/10.1016/j.advengsoft.2009.11.001

[27] Incerti, G. (2015). Motion planning of SCARA robots for trajectory tracking. *Excellence in Research and Innovation for Humanity, Part I.* Rome Italy, 17(5). https://10.13140/RG.2.2.29780.40321

[28] Zhao, Y. & Tsiotras, P. (2013). Speed profile optimization for optimal path tracking. *American Control Conference (ACC)*, 1171-1176. https://doi.org/10.1109/ACC.2013.6579994

[29] Wang, C. H. & Horng, J. G. (1990). Constrained minimum-time path planning for robot manipulators via virtual knots of the cubic B-spline functions. IEEE Transactions on Automatic Control, 35(5), 573-577. https://doi.org/10.1109/9.53526

[30] Sakamoto, K. & Kawamura, A. (1993). Trajectory planning using optimum Solution of variational problem. *Power Conversion Conference*, Yokohama, Japan, 666-671. https://doi.org/10.1109/PCCON.1993.264177

[31] Macfarlane, S. & Croft, E. A. (2003). Jerk-bounded manipulator trajectory planning: Design for real-time applications. *IEEE Transactions on Robotics and Automatic, 19*(1), 42-52. https://doi.org/10.1109/TRA.2002.807548

[32] Chettibi, T. & Lemoine, P. (2007). Generation of point-to-point trajectories for robotic manipulators under electro-mechanical constraints. *International Review of Mechanical Engineering (I.RE.M.E.), 1*(2), 131-143.

[33] Murray, J. J. & Lovell, G. (1989). Dynamic modelling of closed-chain robotic manipulators and implications for trajectory control. *Robotics and Automation, IEEE Transactions on, 5*(4), 522-528. https://doi.org/10.1109/70.88066

[34] Kröger, T. & Wahl, F. M. (2010). On-line trajectory generation: Basic concepts for instantaneous reactions to unforeseen events. *IEEE Transactions on Robotics, 26*(1), 94-111. https://doi.org/10.1109/TRO.2009.2035744

[35] Sahar, G. & Hollerbach, J. M. (1986). Planning of minimum-time trajectories for robot arms. *The International Journal of Robotic Research*, 5, 90-100. https://doi.org/10.1177%2F027836498600500305

[36] Haschke, R., Weitnauer, E., & Ritter, H. (2008). On-line planning of time-optimal, jerk-limited trajectories. In *Proceedings IEEE/RSJ International Conferences on Intelligent Robots and Systems (IROS) 2008*, Nice, France, 3248-3253. https://doi.org/10.1109/IROS.2008.4650924

[37] Guarino Lo Bianco, C., & Piazzi, A. A. (2001). *Semi-infinite optimization approach to optimal spline trajectory planning of mechanical manipulators, semi-infinite programming: Recent*

advances. Goberna M. A. and Lopez M. A. (Eds.), Springer Verlag 2001, 271-297.

[38] Dijk, van, N. J. M., Wouw, van de, N., Pancras, W. C. M., & Nijmeijer, H. (2007). Path-constrained motion planning for robotics based on kinematic constraints. In *Proceedings of the ASME International Design Engineering Technical Conferences and Computers and Information in Engineering Conference (IDETC/CIE) 2007*, 4-7 September 2007, Nevada, USA,1-10.

[39] Dongmei, X., & Daokui, Q., Fang, X. (2006). Path constrained time-optimal robot control. In *Proceedings of the International Conference on Robotics and Biomimetics*, 1095-1100. https://doi.org/10.1109/ROBIO.2006.340081

[40] Tangpattanakul, P. & Artrit, P. (2009). Minimum time trajectory of robot manipulator using harmony search algorithm. In *Proceedings of the IEEE 6th International Conference on ECTI-CON 2009*, 354-357. https://doi.org/10.1109/ECTICON.2009.5137025

[41] Martin B. J. & Bobrow, J. E. (1995). Determination of minimum-effort motions for general open chains. In *IEEE International Conference on Robotics and Automation*, 1160-1165, Piscataway, New Jersey. https://doi.org/10.1109/ROBOT.1995.525437

[42] Abo-Hammoura, Zaer, S., Nasir M. Mirza., Sikander M. Mirza., & Muhammad, A. (2002). Cartesian path generation of robot manipulators using continuous genetic algorithms. *Robotics and Autonomous Systems*, 41, 179-223.

[43] Yao, Z. & Gupta, K. (2007). Path planning with general end-effector constraints. *Robotics and Autonomous Systems*, 55, 316-327. https://doi.org/10.1109/IROS.2005.1545305

[44] Ardeshiri, T., Norrlof, M., Lofberg, J., & Hansson, A. (2011). Convex optimization approach for time-optimal path tracking of robots with speed dependent constraints. In 18th IFAC World Congress, Milano, Italy. https://10.3182/20110828-6-IT-1002.01136

[45] Oksanen, T. & Visala, A. (2009). Coverage path planning algorithms for agricultural field machines. *Journal of Field Robotics, 26*(8), 651-668. https://doi.org/10.1002/rob.20300

[46] Technitis, G., Othman, W., Safi, K., & Weibel, R. (2015). From A to B, randomly: A point-to-point random trajectory generator for animal movement. *International Journal of Geographical Information Science, 29*(6), 912-934. https://doi.org/10.1080/13658816.2014.999682

[47] Park, F. C., Bobrow J. E., & Ploen, S. R. (1995). A lie group formulation of robot dynamics. *International Journal of Robotics Research, 14*(6), 609-618. https://doi.org/10.1177/027836499501400606

[48] Khalil, W. & Dombre, E. (2002). *Modelling identification and control of robots*. London, U. K. HPS.

[49] Plédel, P. & Bestaoui, Y. (1995). Actuator constraints in point-to-point motion planning of manipulators. *Proceedings of the 34th Conferences on Decision and Control*, New Orleans, LA, 1009-1010. https://doi.org/10.1109/CDC.1995.480220

[50] Bianco, C. & Ghilardelli, F. (2014). Real-time planner in the operational space for the automatic handling of kinematic constraints. *IEEE Transactions on Automatic Sciences and Engineering, 11*(3), 730-739. https://doi.org/10.1109/TASE.2014.2310813

[51] Moojin, K., Wonkyu, M., Daesung, B., & Ilhan, P. (2004). Dynamic simulations of electro-mechanical robotic systems driven by DC motors. *Robotica*, 22, 523-531.

[52] Spong, M. W. & Vidyasagar, M. (2008). Robot dynamics and control. John Wiley and Sons 2008.

[53] Cho, B. H., Choi, B. S., & Lee, J. M. (2006). Time-optimal trajectory planning for a robot system under torque and impulse constraints. *International Journal of Control Automation and Systems, 4*(1), 10-16.

[54] Calzolari, D., Schürmann, B., & Althoff, M. (2017). Comparison of trajectory tracking controllers for autonomous vehicles. In *Intelligent Transportation Systems (ITSC) 2017, IEEE 20th International Conference on*, 1-8.

[55] Leena, N. & Saju, K. K. (2016). Modelling and trajectory tracking of wheeled mobile robots. *Procedia Technology*, 24, 538-545.

LIST OF SYMBOLS

M	Inertia matrix
$q, \dot{q}$	Joints of position and velocity
$\ddot{q}$	Joint of acceleration
$\dddot{q}$	Joint of jerk
C	Coriolis centrifugal torque
G	Gravity torque
n	The number of joints
T_m	$[n \times 1]$ Vector of the motor torque constant
N	$[n \times n]$ Matrix of the gear transmission ratio
T	$[n \times 1]$ Total torques
T_c	Control torque
T_{ext}	External torque
T_f	Friction torque
F_{ext}	External force
J	Jacobian matrix
v	Normal velocity
f_n	Normal force
μ	Friction coefficient
$\hat{n}_v$	Unit vector along the velocity vector
K_c	Coulomb friction coefficient of the joint
K_v	Viscous friction coefficient of the joint
$\dot{q}_m$	Motor speed
I	Armature current in the motor
L	Armature inductance of the motor
R	Armature resistance of the motor
U	Armature voltage of the motor
K_{bemf}	Back electromotive force of the DC motor
K_m	Motor torque constant matrix
$\bar{U}$	Maximum of the motor voltage
$\bar{\dot{q}}_m$	Maximum of speed motor
$\bar{I}$	Maximum current in the motor
$\bar{I}_c$	Maximum armature current
$\underline{T_c}$	Minimum control torque
$\underline{U}$	Minimum motor voltage
$\underline{\dot{q}}$	Minimum joint velocity
J	Cost function in the objective function
v	Velocity of the end-effector
a	Acceleration vector
$\mathcal{J}$	Jerk vector (i.e., derivative of acceleration)
γ_0, γ_f	Path parameter at zero and final times
r_0, r_f	Initial position and final positions
t_0, t_f	Start and final times

Author's contacts:

Habib GHANBARPOUR ASL, Assistant Professor
University of Turkish Aeronautical Association
Department of Mechatronics
Bahçekapı Mahallesi, Okul Sk. No: 11, 06790 Etimesgut/Ankara, Turkey
Tel: +905060214718
E-mail: hghanbarpourasl@thk.edu.tr, habib.ghanbarpour@gmail.com

ISSN 1846-6168 (Print), ISSN 1848-5588 (Online)
https://doi.org/10.31803/tg-20181011124610

Original scientific paper

BIG DATA FOR PRODUCT INNOVATION IN MANUFACTURING: EVIDENCE FROM A LARGE-SCALE SURVEY

Jasna PRESTER, Mihaela JURIĆ

Abstract: The article analyses big data usage in the Croatian manufacturing sector. Big data usage is still low but present. We analysed the influence of six sources of big data and their influence on share of returns generated by new products using two step OLS regression analysis. The results are robust but they show that some sources have positive and some have negative effects on share of returns generated by new products. Based on the most recent research of scholarly papers we define big data and show a clear research gap by linking big data and innovation. That is, only six papers deal with big data and innovation. In five papers big data comes from social media data, and in the remaining one paper they use data from sensors but predominantly to reduce cost or support the product. Therefore, we contribute by closing this research gap of linking big data and innovation.

Keywords: Big data; Croatia; EMS Survey; Manufacturing; Product innovation

1 INTRODUCTION

Big data is a buzz word that appeared approximately in 2005 according to three most recent scientific papers on big data literature research [1-3]. The current Google trends show even greater numbers than reported in [2, p. 97]. For the current state please see Fig. 1.

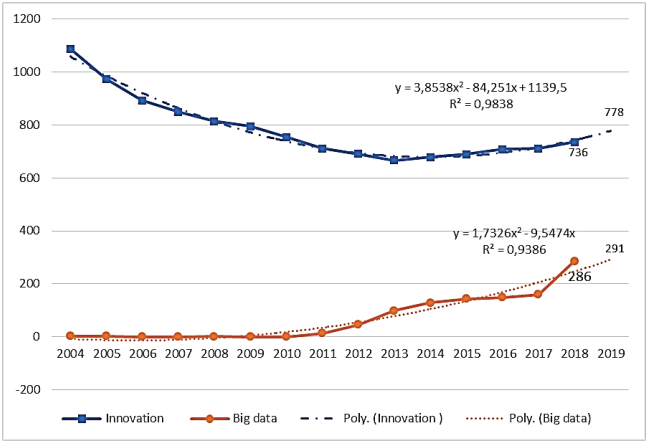

Figure 1 Goggled: Innovation and Big data cumulative per year

Big data is defined by 5V, namely; volume, variety, velocity, veracity, value [1-2]. However, for the purpose of this paper we adopted the description given by [2]: "extremely large amount of structured, semi structured or unstructured data continuously generated from diversified sources, which inundates business operations in real time and impacts on decision-making through mining insightful information from rambling data. For research clarity, big data includes large structured datasets and unstructured data in the form of text (e.g. documents, natural language), web data (e.g. web structure, web usage, web content), social media data (e.g. virtual network), multimedia data (e.g. image, audio, video), and mobile data (e.g. sensor, geographical location, application)." According to [2] who analysed more than 300 scholarly peer reviewed papers, only 6 papers deal with big data and innovation. We analysed all six of them: four of them use social data for innovation [4-7], one focuses the research on product defects discovery [8], and one uses social data for smart cities thus not directly related to product innovation [9]. Most papers, according to [2], focus on a specific problem that is solved by big data. Therefore, there is a clear gap in literature that is simultaneously using big data (but not social data) and innovation. We start the paper by explaining in more details what big data is, mostly based on three prominent literature reviews [1-3], which all investigated more than 150 scholarly journals. Then we briefly define innovation to a larger extent as defined by the OSLO manual [10]. In the methodology section, we describe the model, variables and data gathering methodology. Next, we present results and discussion. Finally, we conclude the article.

2 BIG DATA

The literature is abundant with grand terms of how big data will revolutionize innovation [11], the fourth industrial/scientific revolution [12], the next frontier for innovation [13], "transforming processes, altering corporate ecosystems, and facilitating innovation" [3]. However, as [3] states, potential adopters of 'big data' are struggling to better understand the concept and therefore capture the business value from 'big data'. A recent report by McKinsey on big data shows the current state of big data in US, showing that manufacturing by far exceeds the data gathered when compared to other sectors [14]. This is illustrated in Fig. 2.

However, recent report by McKinsey [15] shows that despite the largest chunk of data being in manufacturing, only 20-30% of that data is actually used for improvement (p. 2). According to [2], a clear path towards management and usage of this data is an urgent need. But big data is not without challenges. Data has to be collected in a systematized way in order to be processed. The processing of data is a challenge

in itself [1]. So far, [1] identified the following processing methods: descriptive analytics scrutinizes data and information to define the current state of a business situation in a way that developments, patterns and exceptions become evident, in the form of producing standard reports, ad hoc reports, and alerts [16]; inquisitive analytics is about probing data to certify/reject business propositions, for example, analytical drill downs into data, statistical analysis, factor analysis [17], predictive analytics is concerned with forecasting and statistical modelling to determine the future possibilities [18]; prescriptive analytics is about optimization and randomized testing to assess how businesses enhance their service levels while decreasing the expenses[16]; and preemptive analytics is about having the capacity to take precautionary actions on events that may undesirably influence the organizational performance, for example, identifying the possible perils and recommending mitigating strategies far ahead in time [19]. We overtook these definitions from [1] because all five data analysis processes would be beneficial for either innovation of the product or modifying a product based on the failure data recorded by either sensors or other data capturing techniques. This now brings to the question of what is defined as innovation.

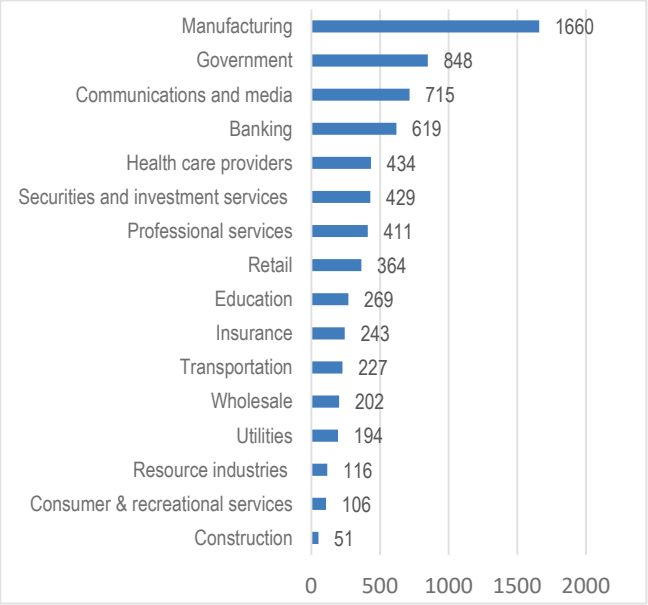

Figure 2 Data stored in Petabytes US, 2009 [14]

3 INNOVATION

Every innovation starts with an idea [20]. An "idea" is an opportunity to create value through further investment [21] or a recognized opportunity [22]. An idea may be recognizing a new need; a new modified product providing a solution to an existing need; an existing solution that could meet needs from new markets; and ideas evolve over the course of the innovation process [23]. An idea/ideas emerge through iterative process after identifying a problem [24], or opportunity identification [25]. And these sources of information will differ depending on the type of innovation [22].

According to Oslo manual (OECD 2005, 32) [10] product innovations are divided into improved products and products new to the market or radically new products. An improved product "is an existing product whose performance has been significantly enhanced or upgraded. A simple product may be improved (in terms of better performance or lower cost) through use of higher-performance components or materials, or a complex product which consists of a number of integrated technical sub-systems may be improved by partial changes to one of the sub-systems".

A new product "is a product whose technological characteristics or intended uses differ significantly from those of previously produced products. Such innovations can involve radically new technologies, can be based on combining existing technologies in new uses, or can be derived from the use of new knowledge".

In this analysis we define New products as both of these categories, even though in the questionnaire there is an additional question regarding these "Radically new products".

4 HYPOTHESES

According to the previous paragraph on innovation, it is evident that sources of idea coming from big data are not explored enough. Usual sources of ideas for innovation [10] (p. 78-80) can be internal sources of information (R&D, marketing, and production departments etc.) or external sources (customer/user, supplier, research units, conferences, scientific papers etc.). In this paper we investigate the sources of ideas coming from the usage of big data, which is stored in the manufacturing plant. Specifically, we explored data coming from providing remote support to customers, data coming from Sensor or remote control, data coming from the Enterprise Resource Planning software (ERP), data coming from exchange with supply chain partners (SCM), data coming from automation of flow of goods and storage, identification systems such as bar codes, RFID tags, etc., which for simplicity we abbreviated to (RFID), and data coming from digital devices used to program equipment which we abbreviated to Mobile programing. All these data sources fall into mobile big data as defined by [2]. All this data is supposed to enable companies to detect potential problems of the current product and enable and give ideas how to improve a product either incrementally giving raise to what Oslo manual calls Improved products or radically new products which Oslo manual defines as New products.

The model we propose is fairly simple. Each of these six sources will improve revenues from new products.

H1: data coming from Remote support will enhance share of revenues generated by new products

H2: data coming from Sensor or remote control will enhance share of revenues generated by new products

H3: data coming from ERP system will enhance share of revenues generated by new products

H4: data coming from SCM system will enhance share of revenues generated by new products

H5: data coming from RFID system will enhance share of revenues generated by new products

H6: data coming from Mobile programing system will enhance share of revenues generated by new products

These hypotheses will be tested through two step OLS regression analysis. Therefore, here is the place to introduce control variables.

4.1 Size of the Company

There is a difference in innovation output in small and large firms [26-28]. Bigger companies have larger and better R&D background, more staff, suppliers, customers that are all sources of innovative ideas. Size of a company is considered as a contingency because size of a company in terms of number of employees does not change overnight and depends also on labour market and overall conditions of the economy. Therefore, size of the company is considered as a control variable and a contingency; it is expected that larger companies will have more benefit in terms of generated revenues from new products. Therefore, H7 is as follows:

H7: Larger companies obtain higher share of return from new products

4.2 Complexity of the Product

Complexity is usually measured in number of components, newness, or number of functions designed into the product [29-31]. However, [32] in their research found that this complexity also brings in new growth opportunities (58% of responders), and possible competitive advantage (59.4% of responders). [33] researched product complexity in new product development (NPD). Although, as [32] show, complexity of the product should increase new product potential developments, [33] found no impact of complexity on new product performance measures. The impact of complexity on manufacturing performance has not been clearly articulated in the previous empirical studies despite the widely expected negative relationship between them [34]. For example, [35] and [36] show that the higher the complexity of products is, the more complicated the supply chain is, and with that the risk of operating performance failures raises. [37] show that the more complex the product is, it might lead to poor delivery performance. [38] observe that the lead time increases with the number of parts. By analogy, complexity would also impact new product performance. Therefore, [32], [33] show that complexity might increase the chance of better innovative results, but also that it might bring problems to supply chain and consequently prolong the period of generating positive results. Therefore, we will hypothesize that H8 is as follows:

H8: complexity of the new product positively affects share of return from sales of new products.

5 METHODOLOGY

The research data was collected using the European Manufacturing Survey (EMS), coordinated by the Fraunhofer Institute for Systems and Innovation Research – ISI, the largest European survey of manufacturing activities [39]. The survey's questions deal with manufacturing strategies, application of innovative organizational and technological concepts in production, cooperation issues, production off-shoring, servitisation, and questions of personnel deployment and qualification. In addition, data on performance indicators such as productivity, flexibility, quality and returns are collected. The survey is conducted among manufacturing companies (NACE Revision 2 codes from 10 to 31) having at least 20 employees. The EMS project researches the whole manufacturing sector through a condensed eight-page questionnaire. To collect valid data permitting international comparisons, the EMS consortium employs various procedures recommended by the Survey Research Centre designed to avoid problems arising from the use of different languages and specific national terminology. First, a basic questionnaire is developed in English, which is then translated to the language of a country and then back to English to check consistency. Second, in each participating country pre-tests are conducted. Third, identical data harmonization processes are applied [40]. The sample used in the present paper consists of 105 Croatian manufacturing companies with over 20 employees. The questionnaire was sent to 1275 Croatian Chief Operating Officers who were asked to help in responding to the survey. A response rate of 8% was achieved, which is satisfactory for such large-scale voluntary surveys. The data collection was conducted in 2015.

6 RESULTS

We firstly analyse the sample using descriptive statistics. That is, we show the sample in terms of researched industries, size categories of companies and complexity of the produced product.

Distribution of industries, size of companies and complexity are given in Tab. 1 and Figs. 3-6.

Representativeness according to size and industry was performed and it was valid for both industry and size. That enables us to generalize conclusions for the whole Croatian manufacturing sector.

In the sample, 30.5% of companies are small with less than 50 employees, medium-sized companies having 50 to 249 employees are represented by 44.8% of companies, and 24.8% companies are large companies.

NACE code is not usually a good descriptor of complexity of the product, so additional analysis was performed in order to describe the sample in terms of complexity of the product they provide.

In the sample, 33.3% of companies produce simple products of not many parts, 41.2% of companies produce products of medium complexity, and 25.5% of companies produce complex products.

Fig. 5 shows share of revenues generated by new products depending on the complexity of the product.

From Fig. 5 it can be already seen that the Hypothesis H8 is confirmed, that more complex products can obtain higher share of revenues from new products.

Table 1 Distribution of the sample by industry

No	Sector (NACE rev. 2) - 2 digits	Frequency	%
10	Manufacture of food products	11	10.5
11	Manufacture of beverages	2	1.9
12	Manufacture of tobacco products		
13	Manufacture of textiles	10	9.5
14	Manufacture of wearing apparel	2	1.9
15	Manufacture of leather and related products	3	2.9
16	Manufacture of wood and of products of wood and cork, except furniture; manufacture of articles of straw and plaiting materials	5	4.8
17	Manufacture of paper and paper products	4	3.8
18	Printing and reproduction of recorded media	5	4.8
19	Manufacture of coke and refined petroleum products		
20	Manufacture of chemicals and chemical products	1	1
21	Manufacture of basic pharmaceutical products and pharmaceutical preparations		
22	Manufacture of rubber and plastic products	3	2.9
23	Manufacture of other non-metallic mineral products	8	7.6
24	Manufacture of basic metals		
25	Manufacture of fabricated metal products, except machinery and equipment	26	24.8
26	Manufacture of computer, electronic and optical products	1	1
27	Manufacture of electrical equipment	4	3.8
28	Manufacture of machinery and equipment n.e.c.	13	12.4
29	Manufacture of motor vehicles, trailers and semi-trailers	1	1
30	Manufacture of other transport equipment	2	1.9
31	Manufacture of furniture	4	3.8
	Total	105	100

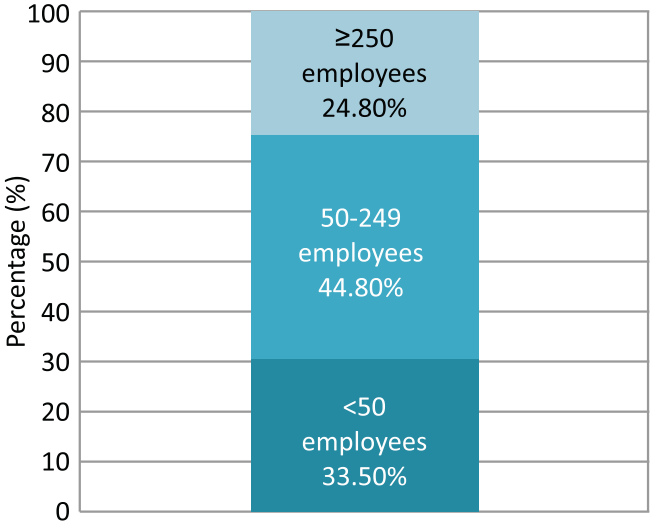

Figure 3 Percentage of companies by size

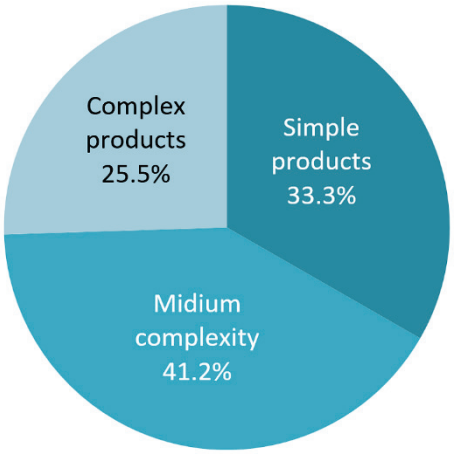

Figure 4 Percentage by complexity of produced products

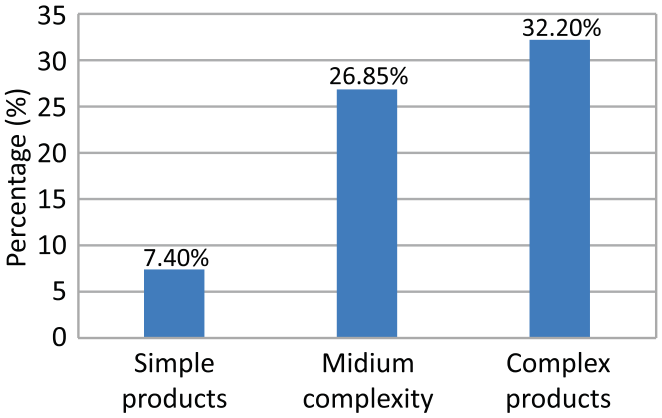

Figure 5 Share off revenues by new products (%)

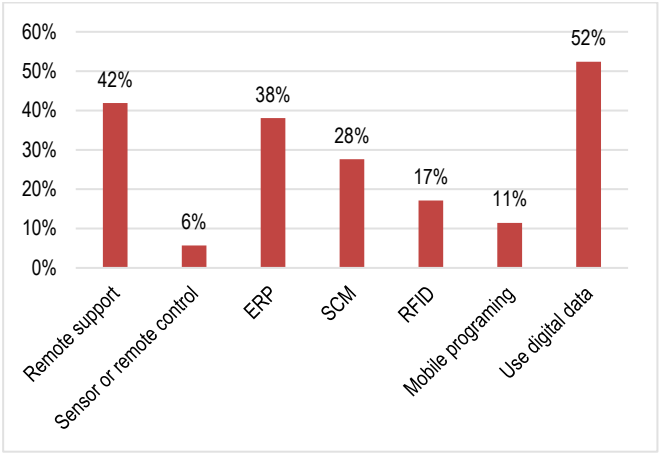

Figure 6 Percentage of companies using digital source

Fig. 6 presents the percentage of companies using the digital source of data. The 7th column displays the question "Do you use your digital data" and it can be seen that 52% of companies do use their digital data. However, the question has limitations because it was not possible to ask for which purpose they use data (marketing, operations or like).

Tab. 2 presents the results of the regression analysis.

Looking at overall results of the regression analysis $R = 0.526$ with significance $p = 0.024$ we can conclude that the model is significant. Coefficient of determinacy R^2 shows

that 15.6% of share of revenues are generated by these sources of innovation ideas.

Table 2 Results from the regression analysis

	Standardized Beta	*Sig.*
(Constant)		0.615
Number of employees	-0.127	0.355
Complexity	0.287	0.019
NACE Code	0.09	0.47
Remote support	-0.021	0.864
Sensor or remote control	-0.092	0.462
ERP	0.233	0.08
SCM	-0.165	0.196
RFID	-0.198	0.142
Mobile programing	0.01	0.935
Data usage from digital sources	0.07	0.562
R	0.526	
R^2	0.156	
F	2.291	
Sig.	0.024	
a Dependent Variable: Share of revenues by new products (%)		

Two step regression analysis first evaluates the influence of control variables. In our case that was size of the company, complexity of the product produced and NACE code. The control variables show that only complexity of the product matters and therefore the hypothesis H8 is confirmed. Hypothesis H7 that larger companies will have a higher share of revenues by new products is not confirmed, that is shares of revenues from the new products do not depend on size of the company, is not confirmed which is in line with [41], who show that even small companies with limited resources are able to successfully innovate. Control variables account to only $R = 0.229$, $R^2 = 5.2\%$, not significant $p = 0.170$, $F = 1.710$.

Contrary to our hypotheses, only usage of data from Enterprise Resource Planning software has most influence on revenues from new products. Although significance is over the limit of $p = 0.05$, this hypothesis H3 has to be rejected. Data coming from remote support H1, data coming from sensors and remote control H2, data coming from digital exchange of information from suppliers and customers H4 and data coming from identification devices (shortened RFID) all have to be rejected because they show a negative sign, i.e., this data for some reason negatively affects share of revenues generated by new products. However, results cannot be generalised as the significances are over the limit of $p = 0.05$. One hypothetical explanation might be that this data is still dominantly used for solving current operational problems and it has not yet been analysed as prescribed in [1] and thus this negative sign. If this data was analysed as prescribed by [1], then maybe the effects of analysing this data would be positive on share of revenues generated by new products. Even though this was not put in the form of a hypothesis, Data usage from digital sources has a small but positive, although not significant effect. However, even this percentage is low (only 52% of companies analyse their digital data), which is in line with McKinsey's report [15] that although manufacturing generates and stores most data as compared to other industries (see Fig. 2), they are still not using it to their full potential.

To try to interpret these results we have to go back to the definition of "Big data" as given by [2]. They name sources of big data as Text, Web data, Social media data, Multimedia data and Mobile data. Of the five named sources of big data we have researched only the last source – mobile data (sensors, geographical location, and application). If one looks at Fig. 6, sensor and remote control source of data, one sees that this source of data is still very low (only 6% of companies gather data through this channel of data generation). Also, although the percentages are larger for sources of data from Enterprise Resource Planning and exchange of data with supply chain partners (SCM), the percentages are still very low (28%). It would be expected that in current days all of the companies, large and small, would have had installed an Enterprise Resource Planning system which is obviously still not the case (only 38% of companies use it). One possible explanation for this is that the research was conducted in 2015 and maybe the percentage in the next round, which is scheduled for this year (the survey is based on a three-year period), would be higher.

The limitation of the study is that, at the time the study was conducted, the question regarding what they use collected data for was not included in the questionnaire. This should be included in the next round as it may represent a source of competitive priority.

7 CONCLUSION

In this work we have shown on grounds of literature research that there is a clear gap in researching big data for usage for innovation. Also, most big data used in literature are Web data, Text data, and Social media data and only a small part of this big data is coming from mobile data (sensors, GPS or application). Therefore, in this work we have closed this gap by providing an analysis of how big data in Croatian manufacturing enhances or reduces share of revenues by new products as a measure of a successful innovation.

Of our 8 hypotheses only one has been partially confirmed (H3) – Enterprise Resource Planning systems positively affect share of revenues generated by new products, and H8 has been fully confirmed (Producers of complex products obtain better share of revenues from new products), while other hypotheses had to be rejected. They have shown a negative sign, contrary to our hypotheses, although the coefficients were not significant at p=0.05. Based on descriptive data we hypothesized that the rejection of these hypotheses is for one in low level of usage of big data, and it is probably more used for problem solving than for analysing this data for new potential improvements and new products. This is actually in line with current research that manufacturing is still not using the full potential of the data it gathers as suggested in McKinsey's report [15].

Some general conclusion and advice to managers is to invest more into some kind of ERP system and to analyse this data, as those two sources showed positive effect on share of revenues generated by new product. As for the other four sources of data (Remote support, Sensors and Remote control, Supply Chain Management Software and

Identification devices (abbreviated RFID), it might be useful to analyse the data after the problem is solved. As it seems now, the data is used for solving operational problems and maybe not enough effort is put into post analysis of this data as described in McKinsey's report [15].

Acknowledgement

This research is conducted by Grant O-1861-204-3535 Building Competitiveness of Croatian Manufacturing financed by Croatian Science Foundation.

8 REFERENCES

[1] Sivarajah, U., Kamal, M. M., Irani, Z., & Weerakkody, V. (2017). Critical analysis of Big Data challenges and analytical methods. *Journal of Business Research*, 70, 263-286. https://doi.org/10.1016/j.jbusres.2016.08.001

[2] Sheng, J., Amankwah-Amoah, J., & Wang, X. (2017). A multidisciplinary perspective of big data in management research. *International Journal of Production Economics*, 191, 97-112. https://doi.org/10.1016/j.ijpe.2017.06.006

[3] Wamba, S. F., Akter, S., Edwards, A., Chopin, G., & Gnanzou, D. (2015). How 'big data' can make big impact: Findings from a systematic review and a longitudinal case study. *International Journal of Production Economics*, 165, 234-246. https://doi.org/10.1016/j.ijpe.2014.12.031

[4] Abrahams, A. S., Fan, W., Wang, G. A., Zhang, Z., & Jiao, J. (2015). An integrated text analytic framework for product defect discovery. *Production and Operations Management*, 24(6), 975-990. https://doi.org/10.1111/poms.12303

[5] Chan, H. K., Wang, X., Lacka, E., & Zhang, M. (2016). A mixed-method approach to extracting the value of social media data. *Production and Operations Management*, 25(3), 568-583. https://doi.org/10.1111/poms.12390

[6] Mount, M. & Martinez, M. G. (2014). Social media: A tool for open innovation. *California Management Review*, 56(4), 124-143. https://doi.org/10.1525/cmr.2014.56.4.124

[7] Qi, J., Zhang, Z., Jeon, S., & Zhou, Y. (2016). Mining customer requirements from online reviews: A product improvement perspective. *Information & Management*, 53(8), 951-963. https://doi.org/10.1016/j.im.2016.06.002

[8] Zhan, Y., Tan, K. H., Li, Y., & Tse, Y. K. (2016). Unlocking the power of big data in new product development. *Annals of Operations Research*, 1-19.

[9] Jun, C. N. & Chung, C. J. (2016). Big data analysis of local government 3.0: Focusing on Gyeongsangbuk-do in Korea. *Technological Forecasting and Social Change*, 110, 3-12. https://doi.org/10.1016/j.techfore.2015.11.007

[10] Mortensen, P. S. & Bloch, C. W. (2005), *Oslo Manual-Guidelines for Collecting and Interpreting Innovation Data: Proposed Guidelines for Collecting and Interpreting Innovation Data*. Organisation for Economic Cooperation and Development, OECD.

[11] Gobble, M. M. (2013). Big Data: The Next Big Thing in Innovation. *Research Technology Management, 56*(1), 64-66. https://doi.org/10.5437/08956308X5601005

[12] Strawn, G. O. (2012). Scientific Research: How Many Paradigms? *Educause Review, 47*(3), 26.

[13] Manyika, J., Chui, M., Brown, B., Bughin, J., Dobbs, R., Roxburgh, C., & Byers, A. H. (2011). Big data: the next frontier for innovation, competition and productivity: *McKinsey Global Institute.*

[14] McKensey, (2011). *Big data: The next frontier for innovation, competition, and productivity*. https://www.mckinsey.com/business-functions/digital-mckinsey/our-insights/big-data-the-next-frontier-for-innovation, p. 259, Accessed 01.09.2018.

[15] McKinsey, (2016). *The Age Of Analytics: Competing In Adata-Driven World.* https://www.mckinsey.com/business-functions/mckinsey-analytics/our-insights/the-age-of-analytics-competing-in-a-data-driven-world, p. 136. Accessed 01.09.2018.

[16] Joseph, R. C. & Johnson, N. A. (2013). Big data and transformational government. *IT Professional, 15*(6), 43-48. https://doi.org/10.1109/MITP.2013.61

[17] Bihani, P. & Patil, S. T. (2014). A comparative study of data analysis techniques. *International journal of emerging trends & technology in computer science, 3*(2), 95-101.

[18] Waller, M. A. & Fawcett, S. E. (2013). Data science, predictive analytics, and big data: a revolution that will transform supply chain design and management. *Journal of Business Logistics, 34*(2), 77-84. https://doi.org/10.1111/jbl.12010

[19] Smith, M., Szongott, C., Henne, B., & Von Voigt, G. (2012). Big data privacy issues in public social media. In *Digital Ecosystems Technologies (DEST), 2012 6th IEEE International Conference on*, 1-6. https://doi.org/10.1109/DEST.2012.6227909

[20] Chandra, M. & Neelankavil, J. P. (2008). Product development and innovation for developing countries: potential and challenges. *Journal of Management Development, 27*(10), 1017-1025. https://doi.org/10.1108/02621710810916277

[21] Terwiesch, C. & Ulrich, K. T. (2009). I*nnovation tournaments: Creating and selecting exceptional opportunities*. Harvard Business Press.

[22] Florén, H. & Frishammar, J. (2012). From preliminary ideas to corroborated product definitions: Managing the front end of new product development. *California Management Review, 54*(4), 20-43. https://doi.org/10.1525/cmr.2012.54.4.20

[23] Kornish, L. J. & Ulrich, K. T. (2014). The importance of the raw idea in innovation: Testing the sow's ear hypothesis. *Journal of Marketing Research, 51*(1), 14-26. https://doi.org/10.1509/jmr.12.0401

[24] Harvey, S. (2014). Creative synthesis: Exploring the process of extraordinary group creativity. *Academy of Management Review, 39*(3), 324-343. https://doi.org/10.5465/amr.2012.0224

[25] Koen, P. A., Bertels, H. M., & Kleinschmidt, E. J. (2014). Managing the Front End of Innovation—Part II: Results from a Three-Year Study. *Research-Technology Management, 57*(3), 25-35.

[26] Krawczyk, M. (2013). Sources of Information for Innovative Activity of Enterprises. Types, Importance, Measurement. *Oeconomia Copernicana*, 1, 5-18. https://doi.org/10.12775/OeC.2013.001

[27] Varis, M. & Littunen, H. (2010). Types of innovation, sources of information and performance in entrepreneurial SMEs. *European Journal of Innovation Management, 13*(2), 128-154. https://doi.org/10.1108/14601061011040221

[28] Laursen, K. & Salter, A. (2006). Open for innovation: the role of openness in explaining innovation performance among UK manufacturing firms. *Strategic management journal, 27*(2), 131-150. https://doi.org/10.1002/smj.507

[29] Griffin, A. (1997). The effect of project and process characteristics on product development cycle time. *Journal of Marketing Research*, 24-35. https://doi.org/10.1177/002224379703400103

[30] Murmann, P. A. (1994). Expected development time reductions in the German mechanical engineering industry. Journal of Product Innovation Management: *An International*

Publication of the Product Development & Management Association, 11(3), 236-252. https://doi.org/10.1111/1540-5885.1130236

[31] Novak, S. & Eppinger, S. D. (2001). Sourcing by design: Product complexity and the supply chain. *Management science, 47*(1), 189-204. https://doi.org/10.1287/mnsc.47.1.189.10662

[32] Kim, J. & Wilemon, D. (2012). Complexity and the Multiple Impacts on New Product Development: Results from a Field Study. *International Journal of Innovation and Technology Management, 9*(06), 1250043. https://doi.org/10.1142/S0219877012500435

[33] Caniato, F. & Größler, A. (2015). The moderating effect of product complexity on new product development and supply chain management integration. *Production Planning & Control, 26*(16), 1306-1317. https://doi.org/10.1080/09537287.2015.1027318

[34] Park, K. & Kremer, G. E. O. (2015). Assessment of static complexity in design and manufacturing of a product family and its impact on manufacturing performance. *International Journal of Production Economics*, 169, 215-232. https://doi.org/10.1016/j.ijpe.2015.07.036

[35] Paulonis, D. & Norton, S. (2008), Managing Global Supply Chains: McKinsey Global Survey Results. https://autoassembly.mckinsey.com/html/knowledge/quarterly/McKQ_ManagingGlobalSupplyChains.asp, Accessed 1.10.2015.

[36] Burkett, M. (2008). Technology: Keep it Simple--But Not to Simple. *Supply Chain Management Review*, 12(7), p. 12.

[37] Vachon, S. & Klassen, R. D. (2002). An exploratory investigation of the effects of supply chain complexity on delivery performance. *IEEE Transactions on engineering management*, 49(3), 218-230. https://doi.org/10.1109/TEM.2002.803387

[38] Ferrer, G. & Ketzenberg, M. E. (2004). Value of information in remanufacturing complex products. *IIE transactions*, 36(3), 265-277. https://doi.org/10.1080/07408170490274223

[39] ISI, (2015), European Manufacturing Survey (EMS). http://www.isi.fraunhofer.de/isi-en/i/projekte/fems.php, Accessed 10. 04. 2018.

[40] Bikfalvi, A., Jäger, A., & Lay, G. (2014). The incidence and diffusion of teamwork in manufacturing–evidences from a Pan-European survey. *Journal of Organizational Change Management*, 27(2), 206-231. https://doi.org/10.1108/JOCM-04-2013-0052

[41] De Massis, A., Audretsch, D., Uhlaner, L., & Kammerlander, N. (2018). Innovation with Limited Resources: Management Lessons from the German Mittelstand. *Journal of Product Innovation Management*, 35(1), 125-146. https://doi.org/10.1111/jpim.12373

Authors' contacts:

Jasna PRESTER, PhD, Professor
University of Zagreb,
Faculty of Business & Economics,
Trg J. F. Kennedy 6, 10000 Zagreb, Croatia
jprester@efzg.hr

Mihaela JURIĆ, univ. spec. oec., PhD candidate
University of Rijeka,
Faculty of Economics and Business,
Infodom d.o.o.
Ul. Andrije Žaje 61, 10000 Zagreb, Croatia
mihaela.juric@infodom.hr

ISSN 1846-6168 (Print), ISSN 1848-5588 (Online)
https://doi.org/10.31803/tg-20190116100550

Original scientific paper

CONTROL OF A NON-HOLONOMIC MOBILE ROBOT SYSTEM WITH PARAMETRIC UNCERTAINTY

Hassan ZARABADIPOUR, Zahra YAGHOUBI

Abstract: In this paper, the control of a mobile robot system via a feedback linearization controller and anti-control of chaos with parametric uncertainty is researched. Anti-control is also applied to convert non-chaotic systems to chaotic ones and to create chaos dynamic. The synchronization of system errors with a chaotic gyroscope system is researched for energy reduction and performance improvement. In the other words, control effort is based on synchronizing the error system with chaos for decreasing control cost. The combination of these techniques yields high efficiency and global convergence of trajectories, even in the presence of parametric uncertainty, which has been shown by simulation. Finally, the energy of control signals is calculated and compared for showing the energy reduction.

Keywords: anti-control of chaos; feedback linearization controller; non-holonomic mobile robot; parametric uncertainty

1 INTRODUCTION

Recently, the controller of non-holonomic systems became a challenging area for engineers; however, a lot of work has been done in this field. Non-holonomic systems have non-holonomic constraints on velocities. Constraints are considered in wheeled mobile robots [1]. The control of a non-holonomic system is more difficult than that of a holonomic system. Non-holonomic control problems are studied in [2]. The time-varying adaptive control based on backstepping for uncertain non-holonomic chained systems was studied in [3]. There are two approaches for mobile robot control: one of them is stabilization and the other is trajectory tracking, which means the control of robots to track a desired trajectory. Many researchers pay attention to tracking [4-6]. The Lyapunov function is used for designing a tracking controller in [2]. Feedback linearization for tracking is studied in [7], backstepping in [8-9], the sliding mode control in [10], adaptive control in [11], fuzzy control in [12, 13], neural network control in [14], etc.

The mechanical system is synchronized with a chaotic system to control the system in [15]. The chaotification or anti-control of chaos means that a non-chaotic system is to be chaotified. Recently, the application of chaos in control attracts a lot of attention. Some features, such as initial conditions and limitations, are creating complexity in chaotic systems.

Due to the global stability of the chaos system, it is used in this paper, and errors of the states of the system are synchronized with a small ratio of the chaotic system, so that the states of the system can follow the reference path. In this paper, this concept of the anti-control of chaos is used, which refers to the synchronization of the error system with chaotic system.

The gyroscope system is studied in several research papers because of its applications in navigational, aeronautical and space engineering [17, 18]. There are different types of the linear/nonlinear gyroscope which has periodic or chaotic motions [19, 20].

The organization of this paper is as follows: in section 2, the chaotic gyroscope system is introduced, in section 3, mobile robot dynamics are described, sections 4 and 5 deal with the feedback linearization controller for nonlinear systems and mobile robot, in section 6, the control of mobile robot systems with feedback linearization via the anti-control of chaos is researched, in section 7, the linearization controller for the mobile robot with parametric uncertainty is studied, the simulation results are provided in section 8 and finally, the conclusion is provided in the last section.

2 CHAOTIC GYROSCOPE SYSTEM

The gyroscope is modelled as follows and the scheme of it is shown in Fig. 1(c) [21]:

$$\ddot{\theta} + \alpha_1^2 \frac{(1-\cos\theta)^2}{\sin^3\theta} - \beta_1 \sin\theta + c_1\dot{\theta} + c_2\dot{\theta}^3 = f \sin\omega t \sin\theta \quad (1)$$

Where $f \sin\omega t$ is defined as parametric excitation, the linear and nonlinear damping terms are $c_1\dot{\theta}$ and, $c_2\dot{\theta}^3$ and $\alpha_1^2 \frac{(1-\cos\theta)^2}{\sin^3\theta} - \beta_1 \sin\theta$ is a nonlinear force.

By giving $x_1 = \theta$, $x_2 = \dot{\theta}$ and $g(\theta) = \alpha_1^2 \frac{(1-\cos\theta)^2}{\sin^3\theta} - \beta_1 \sin\theta$, Eq. (1) can be rewritten as follows:

$$\begin{aligned} \dot{x}_1 &= x_2 \\ \dot{x}_2 &= -g(x_1) - c_1 x_2 - c_2 x_2^3 + f \sin\omega t \ \sin(x_1) \end{aligned} \quad (2)$$

Where the parameters are defined as follows: $32 < f < 36$, $\alpha_1^2 = 100$, $\beta_1 = 1$, $c_1 = 0.5$, $c_2 = 0.05$, and $\omega = 2$. Fig. 1(a) and

1(b) illustrates the irregular motion exhibited by this system for f = 35.5 and the initial conditions of $(x_1, x_2) = (1, -1)$.

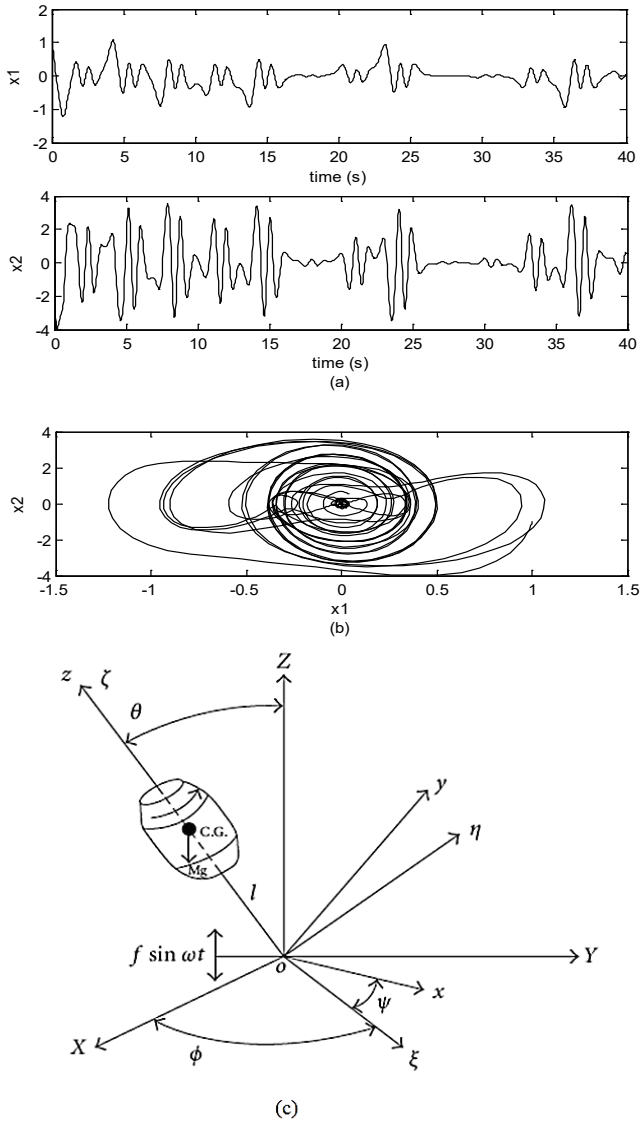

Figure 1 (a) Time series of x1 and x2, (b) Phase Portrait of a gyroscope, (c) A schematic diagram of a symmetric gyroscope

3 MOBILE ROBOT KINEMATICS AND DYNAMICS

The mobile robot system is modelled as follows:

$$\begin{bmatrix} \dot{x} \\ \dot{y} \\ \dot{\theta} \end{bmatrix} = \begin{bmatrix} \cos\theta & 0 \\ \sin\theta & 0 \\ 0 & 1 \end{bmatrix} . \begin{bmatrix} v \\ \omega \end{bmatrix} \tag{3}$$

Where the control inputs of v and ω are the forward and angular velocities, as shown in Fig. 2(a). The non-holonomic constraint, which comes from the non-slip condition, is described as follows [24]:

$$\dot{x}\,\sin\theta + \dot{y}\,\cos\theta = 0 \tag{4}$$

Let us assume that $(x_r, y_r, \theta_r, v_r, \omega_r)^{\mathrm{T}}$ are the references, hence the following equations are satisfied:

$$\begin{bmatrix} \dot{x}_r \\ \dot{y}_r \\ \dot{\theta}_r \end{bmatrix} = \begin{bmatrix} \cos\theta_r & 0 \\ \sin\theta_r & 0 \\ 0 & 1 \end{bmatrix} . \begin{bmatrix} v_r \\ \omega_r \end{bmatrix} \tag{5}$$

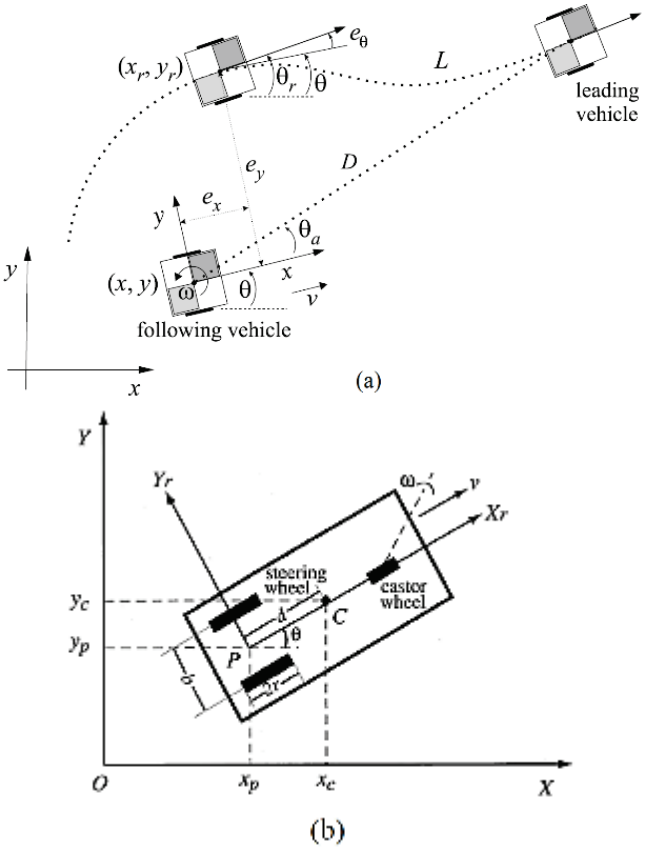

Figure 2 (a) Illustration of error transformation where the following vehicle follows the path of the leading vehicle at the distance L [24]; (b) Mobile robot with two actuated wheels

Where the control inputs references are derived as follows:

$$v_r = \sqrt{\dot{x}_r^2 + \dot{y}_r^2} \quad , \qquad \omega_r = \frac{\dot{x}_r\,\ddot{y}_r - \dot{y}_r\,\ddot{x}_r}{\dot{x}_r^2 + \dot{y}_r^2} \tag{6}$$

Fig. 2(a) shows the error when the real vehicle follows the reference vehicle. The error system is described as follows [24]:

$$e = \begin{bmatrix} e_x \\ e_y \\ e_\theta \end{bmatrix} = \begin{bmatrix} \cos\theta & \sin\theta & 0 \\ -\sin\theta & \cos\theta & 0 \\ 0 & 0 & 1 \end{bmatrix} . \begin{bmatrix} x_r - x \\ y_r - y \\ \theta_r - \theta \end{bmatrix} \tag{7}$$

By differentiating Eq. (7), the nonlinear error model of the system is obtained as follows:

$$\begin{bmatrix}\dot{e}_x\\ \dot{e}_y\\ \dot{e}_\theta\end{bmatrix}=\begin{bmatrix}v_r\cos e_\theta\\ v_r\sin e_\theta\\ \omega_r\end{bmatrix}+\begin{bmatrix}-1 & e_y\\ 0 & -e_x\\ 0 & -1\end{bmatrix}\begin{bmatrix}v\\ \omega\end{bmatrix} \tag{8}$$

For the dynamic model, Eq. (9) is added to Eq. (3):

$$\begin{cases}\dot{v}=\dfrac{1}{m\,r}(\tau_1+\tau_2)\\ \dot{\omega}=\dfrac{b}{2I\,r}(\tau_1-\tau_2)\end{cases} \tag{9}$$

Where m is the mass and I the moment inertia of mobile robot with the radius of the rear wheels r and the length the between wheels b, τ_1 and τ_2 are the control torques of each rear wheel as it is shown in Fig. 2(b).

The error $(e_x, e_y, e_\theta)^T$ converges to zero with control laws for v and ω, and this is a tracking control problem.

4 FEEDBACK LINEARIZATION CONTROLLER FOR MIMO NONLINEAR SYSTEMS

The general system is considered as follows:

$$\begin{cases}\dot{x}=f(x)+\sum_{i=1}^{m}g_i.u_i\\ y=[h_1,\ldots,h_m]^T\end{cases} \tag{10}$$

$$\dot{y}_k=L_f(h_k)+\sum_{i=1}^{m}L_{g_i}(h_k)u_i \tag{11}$$

r_k is the relative degree and $L_f(h)$ is the lie bracket [f, h].

For some i, $L_{g_i}(L_f^{r_k-1}(h_k))\neq 0$.

$J(x)$ is the decoupling matrix and the $m\times m$ matrix is defined as follows:

$$J(x)=\begin{bmatrix}L_{g_1}(L_f^{r_1-1}(h_1)) & \ldots & L_{g_m}(L_f^{r_1-1}(h_1))\\ \ldots & \ldots & \ldots\\ L_{g_1}(L_f^{r_m-1}(h_m)) & \ldots & L_{g_m}(L_f^{r_m-1}(h_m))\end{bmatrix} \tag{12}$$

Where r_k is the relative degree, $L_f(h)$ is the lie bracket [f,h] and $J(x)$ is assumed to be non-singular.

Let the $m\times 1$ be a vector y^r:

$$y^r=\begin{bmatrix}\dfrac{d^{r_1}y_1}{dt^{r_1}}\\ \ldots\\ \dfrac{d^{r_m}y_m}{dt^{r_m}}\end{bmatrix} \tag{13}$$

$$l(x)=\begin{bmatrix}L_f^{r_1}(h_1)\\ \ldots\\ L_f^{r_m}(h_m)\end{bmatrix} \tag{14}$$

Therefore,

$$y^r=l(x)+J(x),\ u=v \tag{15}$$

Where $l(x)$ is the $m\times 1$ vector and v is the $m\times 1$ input. A decoupled set of equations are given as follows:

$$\begin{cases}\dfrac{d^{r_1}y_1}{dt^{r_1}}=v_1\\ \ldots \qquad so \qquad y\Leftrightarrow v\\ \dfrac{d^{r_m}y_m}{dt^{r_m}}=v_m\end{cases} \tag{16}$$

The input v is designed by methods such as: pole placement method, LQR, etc. For example,

$$\begin{aligned}&v=-c_0y-c_1\dot{y}-c_2\ddot{y}\ldots\\ &\Rightarrow y^{(r)}+c_{r-1}y^{(r-1)}+\ldots+c_0y=0\end{aligned} \tag{17}$$

The control, u, is given as:

$$u=J^{-1}(v-l) \tag{18}$$

5 FEEDBACK LINEARIZATION CONTROLLER FOR MOBILE ROBOT

The feedback linearization controller will be designed for the system described by Eq. (3), as shown in Fig. 3.

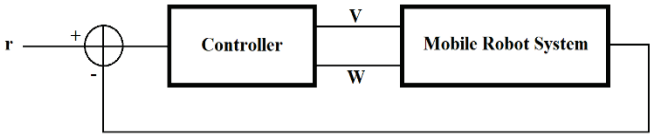

Figure 3 Block diagram of the control system.

If we define $y_1=x_1$ and $y_2=x_2$ as outputs, then we have:

$$\begin{bmatrix}\dot{y}_1\\ \dot{y}_2\end{bmatrix}=\begin{bmatrix}\cos\theta & 0\\ \sin\theta & 0\end{bmatrix}\begin{bmatrix}v\\ \omega\end{bmatrix} \tag{19}$$

$J(x)=\begin{bmatrix}\cos\theta & 0\\ \sin\theta & 0\end{bmatrix}$ is singular and its rank is one.

Let us suppose that $v=x_3$, $\dot{v}=\dot{x}_3=u_1$, $\omega=u_2$.

The states have been extended as:

$$\begin{cases}\dot{x}_1=x_3\cos\theta\\ \dot{x}_2=x_3\sin\theta\\ \dot{x}_3=\dot{v}=u_1\\ \dot{\theta}=\omega=u_2\end{cases} \tag{20}$$

Take $y_1=x_1$ and $y_2=x_2$.

$$\begin{bmatrix}\ddot{y}_1\\ \ddot{y}_2\end{bmatrix}=\begin{bmatrix}\cos\theta & -x_3\sin\theta\\ \sin\theta & x_3\cos\theta\end{bmatrix}\begin{bmatrix}u_1\\ u_2\end{bmatrix} \tag{21}$$

The relative degree of the system is 2 and the matrix $J(x)$ is $J(x)=\begin{bmatrix}\cos\theta & -x_3\sin\theta\\ \sin\theta & x_3\cos\theta\end{bmatrix}$, which is non-singular for $x_3\neq 0$.

Let us suppose

$$\begin{cases}\ddot{y}_1=V_1\\ \ddot{y}_2=V_2\end{cases} \tag{22}$$

The control, *u*, is obtained as:

$$\begin{bmatrix}u_1\\ u_2\end{bmatrix}=J^{-1}(x)\begin{bmatrix}V_1\\ V_2\end{bmatrix}=\begin{bmatrix}\cos\theta & \sin\theta\\ \frac{-1}{x_3}\sin\theta & \frac{1}{x_3}\cos\theta\end{bmatrix}\begin{bmatrix}V_1\\ V_2\end{bmatrix} \tag{23}$$

Now $(V_1,\ V_2)^{\mathrm{T}}$ can be obtained by using the pole placement technique in Eq. (17) and $\dot{v}=u_1$.

It should be noted that, by using the pole placement method, the mobile robot converges faster or more slowly to the desired path depending on the occasion of poles.

6 FEEDBACK LINEARIZATION CONTROLLER FOR A MOBILE ROBOT BY USING THE ANTI-CONTROL OF CHAOS (CHAOTIFICATION)

In this section, the errors of states track the chaotic gyroscope system with a small amplitude, but in section 5, error signals are converged to zero, as shown in Fig. 4. The coefficient α is used to reduce the magnitude of chaotic systems and $10^{-10}\leq\alpha\leq 1$.

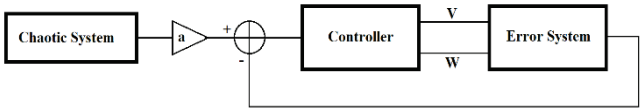

Figure 4 Block diagram of the control system

Thus, the error system in Eq. (8) is studied by using the feedback linearization technique. $y_1=e_y$ and $y_2=e_\theta$ are defined as outputs.

$$\begin{bmatrix}\dot{y}_1\\ \dot{y}_2\end{bmatrix}=\begin{bmatrix}0 & -e_x\\ 0 & -1\end{bmatrix}\begin{bmatrix}v\\ \omega\end{bmatrix}+\begin{bmatrix}v_r\sin e_\theta\\ \omega_r\end{bmatrix} \tag{24}$$

$J(x)=\begin{bmatrix}0 & -e_x\\ 0 & -1\end{bmatrix}$ with rank one is singular.

Let $v=u_1$, $\omega=x_4$, $\dot{\omega}=\dot{x}_4=u_2$.

The states have been extended as:

$$\begin{cases}\dot{e}_x=v_r\cos e_\theta-u_1+e_y\,x_4\\ \dot{e}_y=v_r\sin e_\theta-e_x\,x_4\\ \dot{e}_\theta=\omega_r-x_4\\ \dot{x}_4=\dot{\omega}=u_2\end{cases} \tag{25}$$

Assuming that $y_1=e_y$ and $y_2=e_\theta$.

$$\begin{bmatrix}\ddot{y}_1\\ \ddot{y}_2\end{bmatrix}=\begin{bmatrix}x_4 & -e_x\\ 0 & -1\end{bmatrix}\begin{bmatrix}u_1\\ u_2\end{bmatrix}+\begin{bmatrix}(-2\,v_r\,x_4+v_r\,\omega_r)\cos e_\theta-e_y\,x_4^2+\dot{v}_r\sin e_\theta\\ \dot{\omega}_r\end{bmatrix} \tag{26}$$

The relative degree of the system is 2 and the matrix $J(x)$ is $J(x)=\begin{bmatrix}x_4 & -e_x\\ 0 & -1\end{bmatrix}$ that is non-singular for $x_4\neq 0$, and

$l(x)=\begin{bmatrix}(-2v_r\,x_4+v_r\,\omega_r)\cos e_\theta-e_y\,x_4^2+\dot{v}_r\sin e_\theta\\ \dot{\omega}_r\end{bmatrix}$

The control, *u*, is obtained by using Eq. (22):

$$\begin{bmatrix}u_1\\ u_2\end{bmatrix}=J^{-1}(x)\left(\begin{bmatrix}V_1\\ V_2\end{bmatrix}+l(x)\right)= \tag{27}$$
$$=\begin{bmatrix}\frac{1}{x_4}\left(V_1+(2v_r\,x_4-v_r\,\omega_r)\cos e_\theta+e_y\,x_4^2-\dot{v}_r\sin e_\theta-e_x\,(V_2-\dot{\omega}_r)\right)\\ -(V_2-\dot{\omega}_r)\end{bmatrix}$$

Designing $(V_1,V_2)^T$ by using pole placement technique in Eq. (17) and $\dot{\omega}=u_2$.

7 FEEDBACK LINEARIZATION CONTROLLER FOR A MOBILE ROBOT WITH PARAMETRIC UNCERTAINTY

In this section, nonlinear control laws are proposed for the control of the mobile robot motion described by Eq. (3) and Eq. (9). Feedback control for τ_1 and τ_2 in the presence of uncertainty in the parameter *m* is derived.

Assuming that $y_1 = x$ and $y_2 = \theta$. The relative degrees are 2 and the control signals without the anti-control of chaos are obtained as:

$$\begin{bmatrix}\tau_1\\ \tau_2\end{bmatrix} = \begin{bmatrix}\frac{r\,m}{2\cos\theta}(V_1 + v\,\omega\sin\theta) + \frac{r\,I}{b}V_2\\ \frac{r\,m}{2\cos\theta}(V_1 + v\,\omega\sin\theta) - \frac{r\,I}{b}V_2\end{bmatrix} \tag{28}$$

The control signals with the anti-control of chaos with the Eqs. (8) and (9) are obtained as Eq. (29):

$$\begin{bmatrix}\tau_1\\ \tau_2\end{bmatrix} = \begin{bmatrix}-\frac{r\,m}{2}(V_1 - \dot{v}_r\cos e_\theta + v_r\,\omega_r\sin e_\theta - 2v_r\,\omega\,\sin e_\theta + \omega^2 e_x) - (\frac{r\,I}{b} + \frac{r\,m}{2}e_y)(V_2 - \dot{\omega}_r)\\ -\frac{r\,m}{2}(V_1 - \dot{v}_r\cos e_\theta + v_r\,\omega_r\sin e_\theta - 2v_r\,\omega\,\sin e_\theta + \omega^2 e_x) + (\frac{r\,I}{b} - \frac{r\,m}{2}e_y)(V_2 - \dot{\omega}_r)\end{bmatrix} \tag{29}$$

8 SIMULATION RESULTS

8.1 Control of the Mobile Robot

Feedback linearization control is applied to a mobile robot system with a different desired reference and the results are shown in Fig. 5. Reference paths are Circle (circular reference: (x_r = cos *t*, y_r = sin *t*), Sine wave (x_r = *t*, y_r = sin *t*) and Sinc wave (x_r = *t*, y_r = sin *t*/*t* = sinc *t*). In these cases, poles=−100 were chosen for the linear controller.

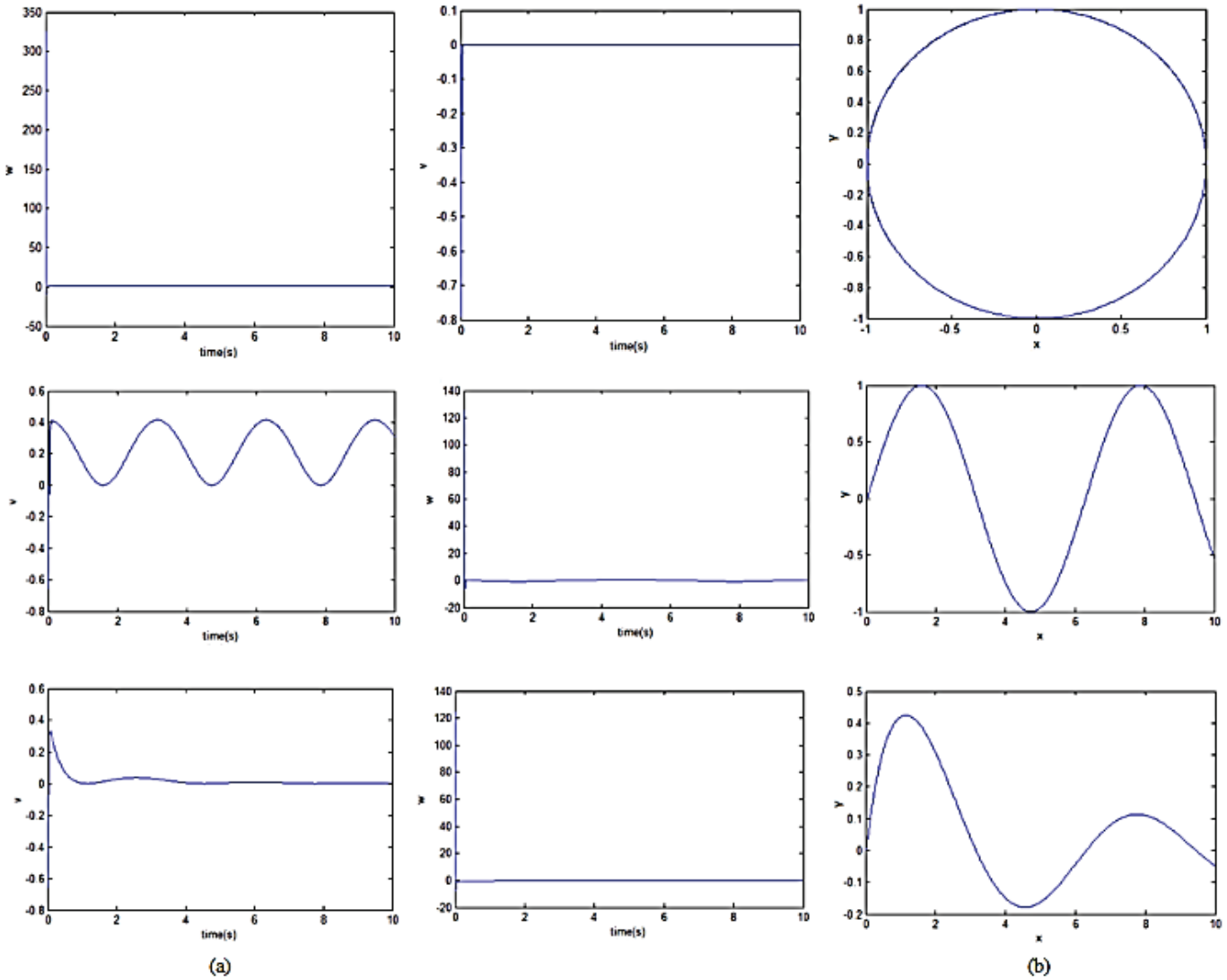

Figure 5 Control signals for references and path following

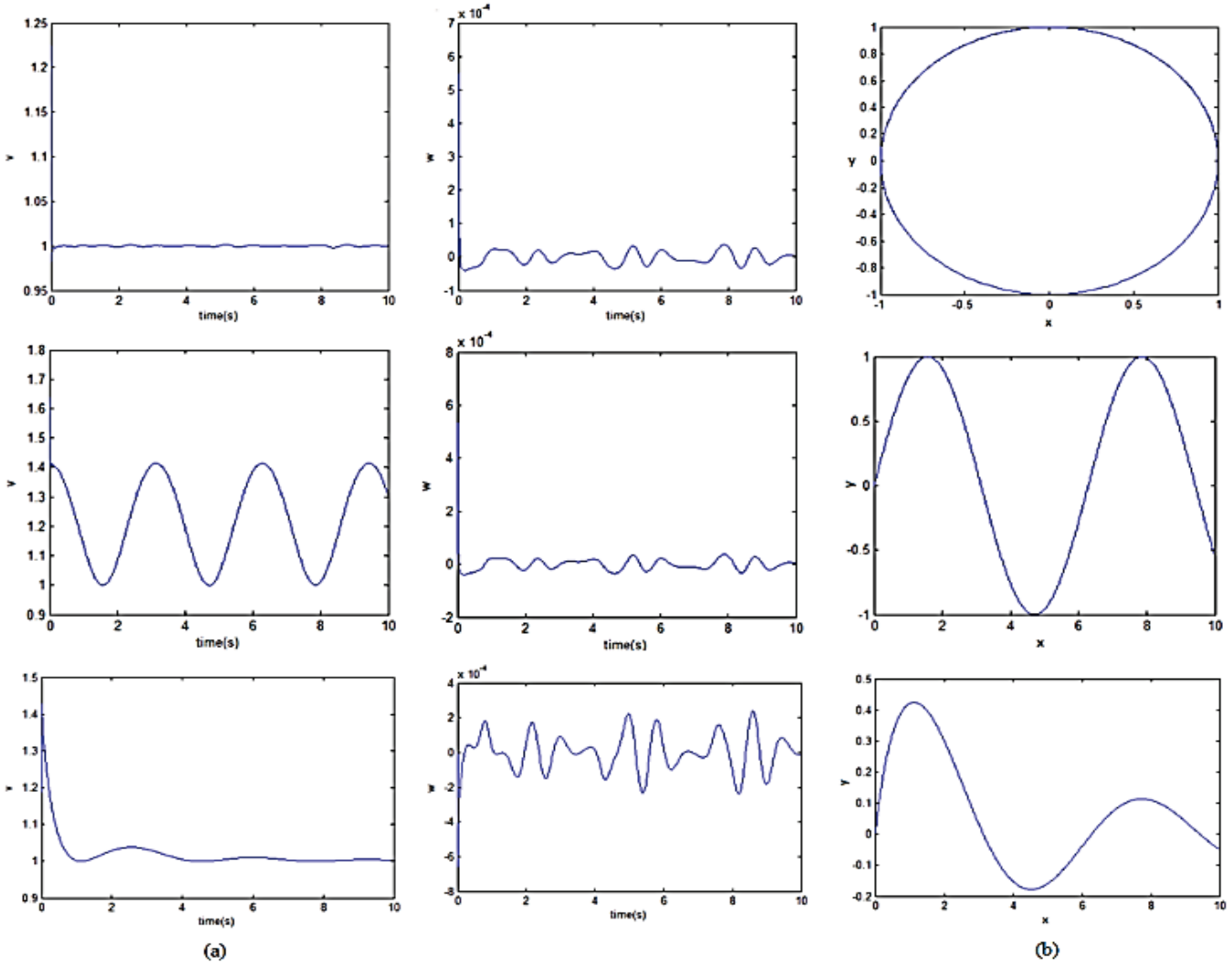

Figure 6 Control signals for references and path following

8.2 Anti-control of Chaos for Controlling the Mobile Robot

The mobile robot system is controlled via the anti-control of chaos with a different desired reference, and they are shown in Figure 6. In these cases, poles=−150 were chosen for the linear controller. As shown in Fig. 4, the two states of the mobile robot system and the error system are synchronized with the two states of chaotic gyroscope systems.

8.3 Mobile Robot Control with Parametric Uncertainty

In this section, the performance of the feedback linearization controller with parametric uncertainty is illustrated. The parameters were adopted as follows for the circle reference: m = 10 kg, I = 1.25 kgm^2, b = 1 m and r = 0.1 m.

The parameter m with uncertainty is in Fig. 7.(a), a poor tracking of variables x and y by using the feedback linearization controller in the presence of parametric uncertainty is shown, while in Fig. 7(d), the feedback linearization controller with the anti-control of chaos was applied to better tracking. Fig. 7(b) and 7(c) shows control signals and 7(d) shows the tracking comparison of the feedback linearization controller with the anti-control of chaos, whether in the presence of parametric uncertainty or not.

8.4 Energy Comparison

In this paper, the main purpose is the reduction of energy or control cost with synchronization error system with chaos system. The energy is defined as follows, which it means the integral of signals squared (area under the curve):

$$energy = \sum (v^2 + \omega^2) \tag{30}$$

The energy comparison is shown in Tab. 1. It is shown that the anti-control of chaos causes the energy reduction.

Table 1 Energy comparison.

Control	circle	sine wave	sinc wave
feedback linearization control	15683	31415	30890
anti-control of chaos	592.08	818.55	565.29

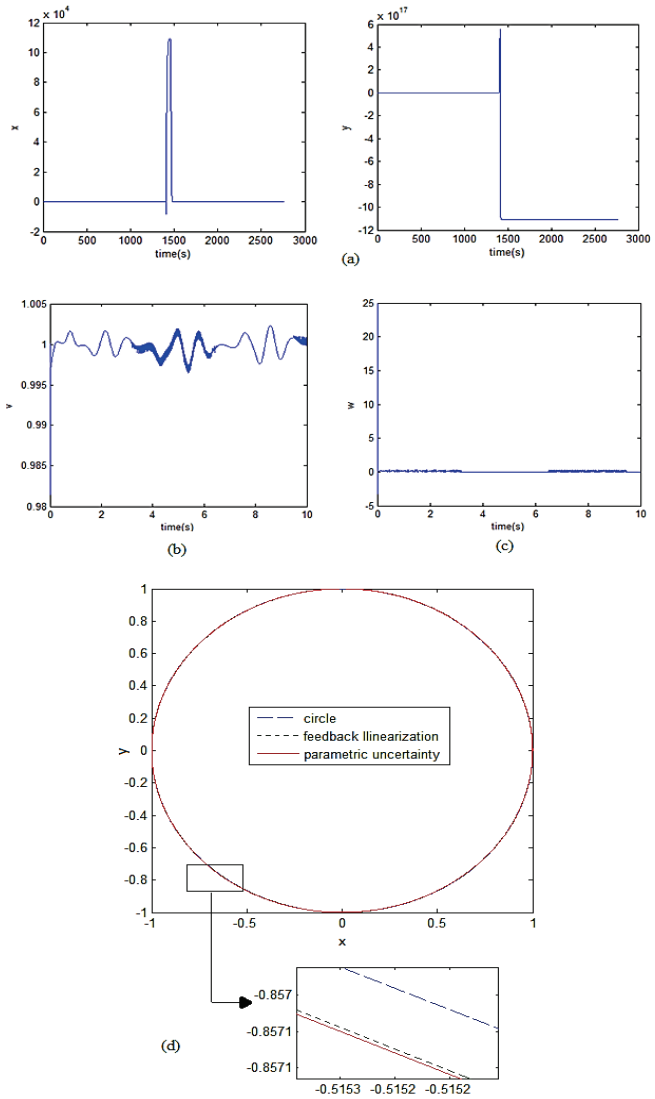

Figure 7 Path following in the presence of parametric uncertainty. (a) Using the feedback linearization controller. Feedback linearization controller with the anti-control of chaos: (b) Control signal (v), (c) Control signal (ω), (d) Path following.

9 CONCLUSION

In this paper, the control of the mobile robot system has been researched in two different ways, and the feedback linearization controller has been used in both of them. Different desired references have been applied for a better comparison. Due to the positive feature of chaotic systems such as energy improvement and control cost, the errors of the states of the mobile robot system are synchronized with the chaotic system.

While the desired tracking error is permanently zero, the control effort is based on the convergence of the error to zero, which is a somewhat strict way of dealing with the issue. The fact is that although by decreasing the error, the desired control is obtained, but too much control cost should be applied, while the anti-control of chaos solves this problem.

The non-linear control laws that yield convergence of the trajectories in the presence of parametric uncertainty have been derived. Simulation results are proposed to illustrate the effectiveness of the proposed controller.

10 REFERENCES

[1] Bloch, A. M., Baillieul, J., Crouchand P., & Marsden, J. E. (2003). *Nonholonomic mechanics and control*. New York, Berlin, Heidelberg. https://doi.org/10.1007/b97376

[2] Kanayama, Y., Kimura, Y., Miyazakiand, F., & Noguchi, T. (1990). A Stable Tracking Control Method for an Autonomous Mobile Robot. *IEEE International Conference on Robotics and Automation*, 384-389. https://doi.org/10.1109/ROBOT.1990.126006

[3] Jiang, Z. P. & Pomet, J. B. (1996). Global stabilization of parametric chained systems by time-varying dynamic feedback. *International Journal of Adaptive Control and Signal Processing*, 10, 47-59. https://doi.org/10.1002/(SICI)1099-1115(199601)10:1<47::AID-ACS385>3.0.CO;2-7

[4] Dierks, T. & Jagannathan, S. (2009). Asymptotic Adaptive Neural Network Tracking Control of Nonholonomic Mobile Robot Formations. *Journal of Intelligent and Robotic Systems, 56*(1), 153-176. https://doi.org/10.1007/s10846-009-9336-8

[5] Lee, J. H., Lin, C., Lim, H., & Lee, J. M. (2009). Sliding Mode Control for Trajectory Tracking of Mobile Robot in the RFID Sensor Space. *IJCAS, 7*(3), 429-435. https://doi.org/10.1007/s12555-009-0312-7

[6] Michalek, M., Dutkiewicz, P., Kielczewski, M., & Pazderski, D. (2009). Trajectory Tracking for a Mobile Robot with Skid-Slip Compensation in the Vector-Field-Orientation Control System. *AMCS, 19*(4), 547-559. https://doi.org/10.2478/v10006-009-0043-1

[7] d'Andrea-Novel, B., Campion, G., & Bastin, G. (1995). Control of a nonholonomic wheeled mobile robot by state feedback linearization. *IJRR, 14*(6), 543-559. https://doi.org/10.1177/027836499501400602

[8] Jinag, Z. P. & Nijmeijer, H. (1997). Tracking Control of Mobile Robots: A Case Study in Backstepping. Automatica, 33, 1393-1399.

[9] Lee, T. C. & Tai, K. (2011). Tracking Control of Unicycle-Modeled Mobile robots using a Saturation Feedback Controller. *IEEE T CONTR SYST T., 9*(2), 305-318.

[10] Yang, J. M. & Kim, J. H. (1999). Sliding Mode Control for Trajectory of Nonholonomic Wheeled Mobile Robots. *IEEE T-RO, 15*(3), 578-587.

[11] Pourboghrat, F. & Karlsson, M. P. (2002). Adaptive Control of Dynamic Mobile Robots with Nonholonomic Constraints. *Computers and Electrical Engineering*, 28, 241-253. https://doi.org/10.1016/S0045-7906(00)00053-7

[12] Imen, M., Mansouri, M., & Aliyari, Sh. M. (2011). Tracking Control of Mobile Robot Using ANFIS. *IEEE International Conference on Mechatronics and Automation*, August 7-10, Beijing, China, 422-427. https://doi.org/10.1109/ICMA.2011.5985695

[13] Wang, S. D. & Lin, C. K. (2000). Adaptive Tuning of the Fuzzy Controller for Robots. *Fuzzy Sets Systems, 110*(2), 351-363. https://doi.org/10.1016/S0165-0114(98)00078-5

[14] Yildirim, S. (2004). Adaptive Robust Neural Controller for Robots. *Robotics and Autonomous Systems, 46*(1), 175-184. https://doi.org/10.1016/j.robot.2003.11.008

[15] Chen, H. K. & Lee, Ch. I. (2004). Anti-control of chaos in rigid body motion. CS&F, 21, 957-965. https://doi.org/10.1016/j.chaos.2003.12.034

[16] Chen, G. & Dong, X. (1988). *From chaos to order: Perspectives, methodologies and applications*. World Scientific, Singapore, 50-51.
[17] Chen, H. K. (2002). Chaos and chaos synchronization of a symmetric gyro with linear-plus-cubic damping. *JSV, 255*(4), 719-740. https://doi.org/10.1006/jsvi.2001.4186
[18] Farivar, F., Aliyari, Sh, M., Nekoui, M. A., & Teshnehlab, M. (2012). Chaos control and generalized projective synchronization of heavy symmetric chaotic gyroscope systems via Gaussian radial basis adaptive variable structure control. *CS&F*, 45, 80-97. https://doi.org/10.1016/j.chaos.2011.10.008
[19] Ge, Z. M. (2002). *Chaos control for rigid body systems*. Taipei. GauLih Book Company.
[20] Lei, Y., Xu, W., & Zheng, H. (2005). Synchronization of two chaotic nonlinear gyros using active control. Physics Letters A. 343, 153-158. https://doi.org/10.1016/j.physleta.2005.06.020
[21] Farivar, F., Aliyari, Sh. M., Nekoui, M. A., & Teshnehlab, M. (2009). Chaos synchronization of uncertain nonlinear gyros via hybrid control. *IEEE/ASME international conference on advanced intelligent mechatronics*, 1365-1370. https://doi.org/10.1109/AIM.2009.5229879
[22] Yau, H. T. (2008). Synchronization and anti-synchronization coexist in twodegree- of-freedom dissipative gyroscope with nonlinear inputs. *Nonlinear Analysis Real World Applications, 9*(5), 2253-2261. https://doi.org/10.1016/j.nonrwa.2007.08.002
[23] Van, D. R. & Chen, H. K. (2003). Chaos and chaos synchronization of a symmetric gyro with linear-plus-cubic damping. *JSV, 268*(3), 632-636. https://doi.org/10.1016/S0022-460X(03)00343-2
[24] Klančar, G., Matko, D., & Blažič, S. (2010). A control strategy for platoons of differential drive wheeled mobile robot. RAS, 59, 57-64.

Authors' contacts:

Hassan ZARABADIPOUR, PhD, Associate Professor
Department of Electrical Engineering
Imam Khomeini International University
Qazvin, Iran
hzarabadi@eng.ikiu.ac.ir

Zahra YAGHOUBI, M.Sc.
Department of Electrical Engineering
Imam Khomeini International University,
Qazvin, Iran
z_yaghoubi@aut.ac.ir

ISSN 1846-6168 (Print), ISSN 1848-5588 (Online)
https://doi.org/10.31803/tg-20190114182836

Preliminary communication

PROPOSED CHANGES TO THE CROTIS TOPOGRAPHIC MODEL FOR THE BASIC PACKAGE AND THE OBJECT ENTITY OF HYDROGRAPHY

Ivan LANDEK, Saša CVITKOVIĆ, Milan REZO

Abstract: In 1992, the State Geodetic Administration started with the development of cartography in the Republic of Croatia. After making a certain number of studies, STOKIS (the Official Topographic-Cartographic Information System) was defined. Topographic and cartographic data models were then defined by STOKIS. According to the STOKIS guidelines, the Croatian topographic information system (CROTIS) was developed as a data model and on the basis of CROTIS, the Basic Topographic Database (TTB) was established. One thematic entity contained in CROTIS 2.0, and whose data is often used, is the object entity of Hydrography. This article will provide an insight into the need to expand/correct the TTB data model in relation to the underlying basic package and the object entity of Hydrography, all in line with international standards and the INSPIRE directive.

Keywords: CROTIS; hydrography; topography; TTB

1 INTRODUCTION

Previously, in the former state, the Republic of Croatia was one of the six federal republics until gaining independence (1991) and international recognition (1992). In the former state, the production of topographic maps in the scale of 1:25 000 (TM25>TK25) and smaller was exclusively under the jurisdiction of the federal military authority, respectively in the institution responsible for this activity, which was the Military Geographic Institute (MGI>VGI) in Belgrade. The Republic Geodetic Administration in Croatia could only order a certain number of printed copies of topographic maps (only civilian publications). After the proclamation of independence, the Republic of Croatia was without the possibility of printing and updating the topographic maps because the reproductive originals were still only in MGI>VGI [11]. Later, during the Homeland War, copies of some remaining maps were used [12].

Major changes in space caused by war events, the demographic changes, as well as the general progress of the society, followed by strong technological development and excessive spending of natural resources, have significantly influenced the awareness of the priceless value of the space we live in. Therefore, thoughtful use, purposeful planning and systematic environmental protection of the space we live in have become very important tasks of the modern society. In this process, information about the space we live in is extremely important [13]. In the past, spatial data were mainly in the form of cartographic representation, and more recently, digital data is being used in the form of spatial databases for various designing, spatial planning, making of various studies etc.

In 1992, the Republic of Croatia began with the independent development of topographic cartography. The State Geodetic Administration (SGA>DGU), in cooperation with other relevant experts from the academia and private companies that had a long-standing experience in the production of large scale maps, has launched several studies and the designing of a future topographic and cartographic system. The result of these activities is the creation of the official topographic and cartographic information system in 1993 which was named STOKIS. The current STOKIS data model is shown in Fig. 1 [2].

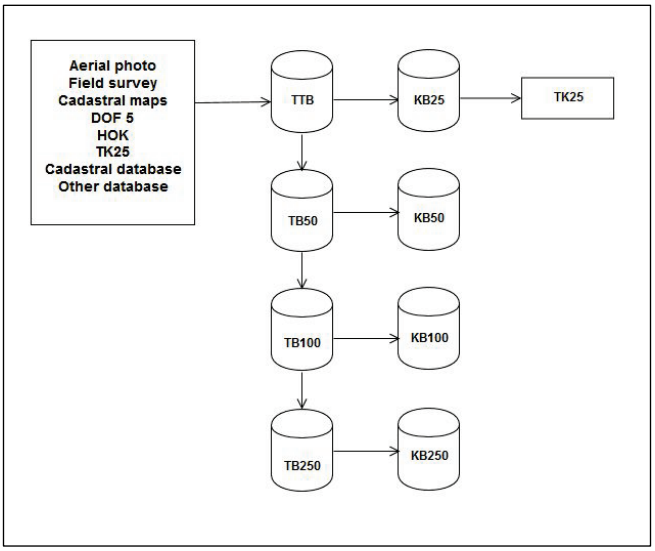

Figure 1 STOKIS Data Model

According to Article 23 of the Ordinance on Topographic Survey and State Maps Designs [1], the basic principles for the establishment of topographic and cartographic databases conforming to STOKIS are laid down, and Article 25 specifies the creation of topographic databases (TTB). Article 26 of the Ordinance clarifies the model of the creation of cartographic databases (KB).

After the establishment of STOKIS, an analysis was carried out to make the model of the data, which would be the most suitable for the current situation in the Republic of Croatia.

For a research of the state of geospatial data in the Republic of Croatia [5], a large number of experts were hired to collect data on the need and usage of geospatial information in different fields. When the research and analysis of the collected data were done, the Croatian Topographic Information System of the Republic of Croatia (CROTIS) was proposed and adopted [6].

Based on the Croatian Topographic Information System (CROTIS), in the period from 2003 to 2010, the Basic Topographic Database (TTB) was established. TTB is the basis for the first edition of the Topographic Map at a scale of 1:25 000 (TK25), as well as for all topographic maps that will be developed in the future. During the creation of the basic topographic database, a deficit of objects in the data model was noticed. This paper aims to supplement the existing data model to better classify the collected data into certain thematic entities or classes. The intention is to reduce the possibility that there is an object on the ground and that when data is collected, we do not know where to place it or we do not have where to place it (we do not have an object entity or class and we cannot assign a value to the attribute). The proposal for improvement is based on the experience and comments/suggestions from the data collection process and the creation of a Basic Topographic Database by the contractors and employees of SGA who have been working on data quality control.

2 DEVELOPMENT OF THE CROATIAN TOPOGRAPHIC INFORMATION SYSTEM (CROTIS)

The official topographic-cartographic information system [4] is the fundamental document in which the strategy of multiannual cartographic development in the Republic of Croatia has been written. After the establishment of STOKIS, an analysis has been carried out to make the model of the data which would be the most suitable for the current situation in the Republic of Croatia. CROTIS is the basic document for topographic data that prescribes the classification of topographic data in their collection, processing, accuracy, topological relations and exchange of topographic data. Data which is obtained by photogrammetric restitution and topological processing is stored in the Basic Topographic Database (TTB). TTB was established in the year 2003, and at the end of 2010, the first initial upload of TTB data for the entire territory of the Republic of Croatia was completed [3].

The first version of the CROTIS data model was made based on the ATKIS (Amliches Topographisch-Kartographishes Informationssystem – German Official Topographic Cartographic Information System) data model. ATKIS is a project of the Working Committee of the Surveying Authorities of the Laender of the Federal Republic of Germany, consisting of one Digital Topographic Model (DLM) and Multiple Digital Cartographic Models (DKM), and is annex to classical analogue (printed) maps. The Republic of Croatia did not have any experience about the production of topographic maps at the scale larger than the 1:5000 scale (Croatian Basic Map - HOK). Parallel with the independence of the Republic of Croatia in the year 1991, analyses for the most suitable data model for the Republic of Croatia began. After the analysis and the production of numerous studies in cooperation with the professors at the Faculty of Geodesy in Zagreb, the staff of the State Geodetic Administration and the experts in the field of cartography, it was concluded that ATKIS was the most appropriate data model and according to it, a data model for the Republic of Croatia should be established. In the period between 1990 and 1996, several studies were produced which provided the basic determinants for the topographic data model named CROTIS 1.0. The CROTIS 1.0 data model (Tab. 1) is a defined and standardized data model for the collecting, processing, accuracy, topological relations and exchange of topographic data [3].

Table 1 CROTIS 1.0, CROTIS 1.2, CROTIS 2.0 data model object entities

CROTIS 1.0	CROTIS 1.2	CROTIS 2.0
1000 Permanent geodetic	~~1000 Permanent geodetic~~	
2000 Buildings, commercial and public objects	2000 Buildings, commercial and public objects	Buildings
3000 Utility lines	3000 Utility lines	Utility lines
4000 Transport	4000 Transport	Transport
5000 Vegetation and land types	5000 Vegetation and land types	Land cover and land use
6000 Waters	6000 Waters	Hydrography
7000 Relief	7000 Relief	Relief
8000 Administrative and territorial division, boundaries	~~8000 Administrative and territorial division, boundaries~~	
9000 Geographical names	1000 Geographical names	Geographical names

The data model consisted of 9 object entities, 31 object groups, and 101 object types. Object entities that made up the first CROTIS 1.0 document were: permanent geodetic points, buildings, commercial and public objects, utility lines, transport, vegetation and land types, waters, relief, administrative and territorial division, boundaries and geographical names (toponyms) (Tab. 1).

After the CROTIS 1.0 data model, the version CROTIS 1.1 was created [15]. By conducting additional analyses and due to the technological progress, it was concluded that the EXPRESS exchange format was to be accepted, which was a universal exchange format at that time. CROTIS 1.1. was created in 2002. In the CROTIS 1.1 data model, 9 object entities were kept, as well as in the CROTIS 1.0 data model.

Subsequently, the CROTIS 1.2 data model was created. (Tab. 1) In it, the object entities of permanent geodetic points, as well as the administrative and territorial division and boundaries, were extracted and maintained in separated databases. The CROTIS 1.2. data model was adopted in 2006 [3].

Having in mind the technological advances in the field of spatial data and EU directives, new occurrences in the development of spatial data happened. At that time, the Republic of Croatia had a pre-accession agreement with the European Union and all the information regarding spatial data was closely followed. The EU issued the INSPIRE 2007/2/EC Directive of the European Parliament and the Council of the European Union on 14 March 2007. The CROTIS 2.0 data model [7] was largely aligned with the INSPIRE directive and adopted in 2014 [8]. The basic idea of the Directive is to share (exchange) spatial data among all interested parties, and considering the fact that the scope of the INSPIRE themes is very extensive, CROTIS 2.0 met the

basic components of the concepts of interoperability and harmonization – also known as the components of interoperability [9].

In CROTIS 2.0 (Tab. 1), the data model was modified so that Relief (3D) was excluded and the object entity of Vegetation and Land Type was renamed into Land Cover and Land Use. Compared to the previous versions of the data model, this version was minimally expanded with new content. The newly created object classes, attributes, and values are the result of a new approach to objects grouping, a new catalog of objects and aligning names with definitions, all in order to minimize the number of unidentified objects. Furthermore all object classes that are an integral part of the Digital Relief Model (DRM) are also omitted from the Relief object entity. Major changes were also made in the former entity of Vegetation and Land Types, and the Land Use Class was introduced as a special layer within an entity which conceptually differs from other classes within the Coverage and Land Use. The biggest change occurred in the way of displaying area objects, since the data collection was adapted to primitive graphic elements (point, line), so the area objects consisted of boundaries (lines) that contained the attributes of the area object. In the new model, each object can have one of the three predefined geometries (point, line, polygon) and contains all the attributes provided by the model [14]. In addition to the definition of object entities, attributes and classes, in the new model, attribute values definitions are also provided. In the CROTIS 2.0 model, the abstract object of upper-class "CROTIS objects" has been introduced, which is the carrier of the basic attributes of all classes in the model, for example the unique identifier, accuracy of collection, origin, life cycle of the object and so on [3].

CROTIS 2.0 is a topographic model similar to the topographic models of the Kingdom of Denmark and the Netherlands [10], in which topographic databases are in the scale of 1:10 000 [3].

3 CROATIAN TOPOGRAPHIC INFORMATION SYSTEM – CROTIS 2.0

The Croatian topographic information system (CROTIS 2.0) consists of seven object entities, namely: Geographical Names, Buildings, Transport, Land Cover and Land Use, Utility, Relief and Hydrography (Fig. 2).

The object entity of Geographical Names consists of the class: GeographicalName, and the list of allowed attribute values of the class: GeographicalNameCategoryType and GeographicalNameType.

The object entity of Buildings consists of the following classes: Abstract Buildings, Buildings, BuiltBarriers, SmallStructures, PurposeType, BigStructures, VerticalLevelType, BuiltBarrierType, OtherStructuresType, BuildingType and Building.

The components of the object entity of Transport consist of the following classes: Transport Elements, Curve Transport Elements, Road Axis, Surface Transport Elements, Traffic Area, Rail and the list of allowed attributes of the class: Road Category Type, Transport Category Type, Rail Type, Type of Transport Element Value, Type of Pavement Value, Type of Road Axis, Type of Traffic Area Value, Rail Category Type.

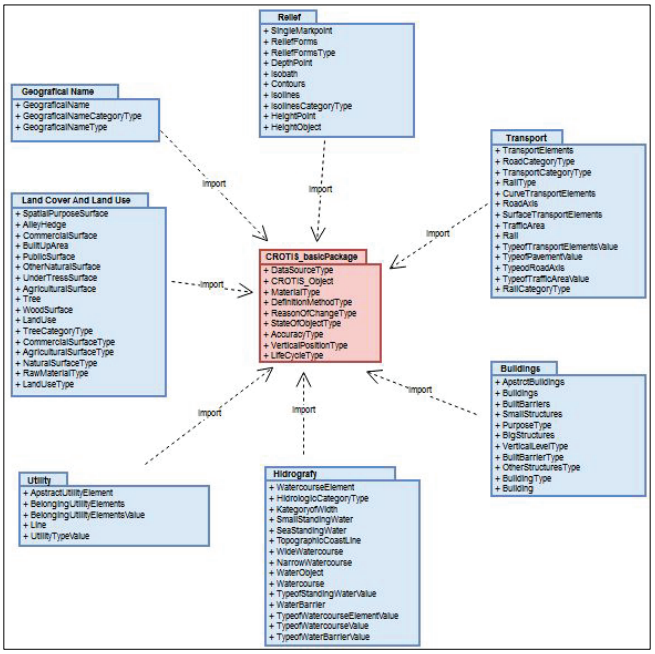

Figure 2 CROTIS 2.0 object entities

The object entity of Land Cover and Land Use consists of the following classes: Spatial Purpose Surface, Alley Hedge, Commercial Surface, Built-up Area, Public Surface, Other Natural Surface, Under Tree Surface, Agriculture Surface, Tree, Wood Surface, Land Use, and the list of allowed attributes of the class: Tree Category Type, Commercial Surface Type, Agricultural Surface Type, Natural Surface Type, Raw Material Type, Land Use Type.

According to the topographic data model of CROTIS 2.0, the object entity of Utility consists of the class: Abstract Utility Element, Belonging Utility Element, Line, and the list of allowed attributes of the class: Belonging Utility Element Value, Utility Type Value.

The object entity of Relief consists of the following classes: Single Mark Point, Relief Forms, Depth Point, Isobath, Contours, Isolines, Height Point, Height Object, and the list of allowed attributes of the class: Relief Forms Type, Isolines Category Type.

Finally, the object entity of Hydrography consists of the following classes: Watercourse Element, Sea Standing Water, Small Standing Water, Topographic Coast Line, Wide Watercourse, Narrow Watercourse, Water Object, Watercourse, Water Barrier, and the list of allowed attributes of the class: Hydrologic Category Type, Type of Standing Water Value, Type of Watercourse Element Value, Type of Watercourse Value, Type of Water Barrier Value.

All listed object entities contain a basic package consisting of the following upper-class: FeatureType CROTIS_Object and dataType Life Cycle Type and the list of allowed attributes of the upper-class: enumeration Accuracy Type, enumeration Definition Method Type, code list Vertical Position Type, code List Material Type, code

List Dana >source Type, code list Reason of change type and code list State of Object Type. (Fig. 3).

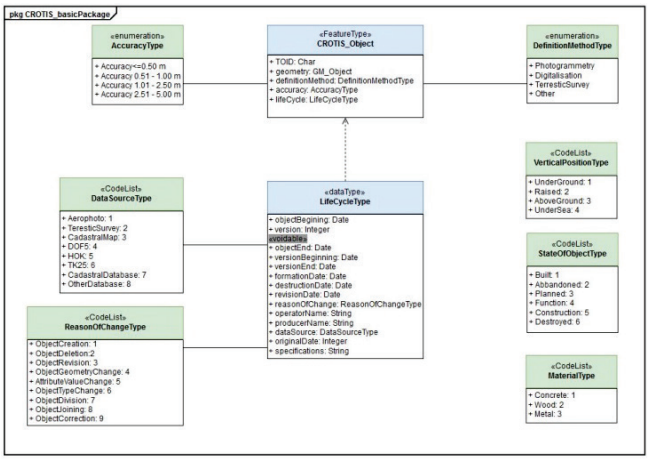

Figure 3 CROTIS 2.0_basic package

The article depicts images with diagrams marked with different colors which have the following meaning:

- red color – base Package (entity)
- blue color – upper-class or class
- green color – list of allowed values of the upper-class or class attribute.

4 PROPOSED IMPROVEMENT OF THE CROATIAN TOPOGRAPHIC INFORMATION SYSTEM – CROTIS 2.1

The CROTIS 2.0 topographic data model is largely in line with the INSPIRE 2007/2/EC directive. However, a careful analysis has shown some inconsequence that we will present and propose the correction of, thereby improving CROTIS 2.0. The proposal of a new upgraded topographic information system will be labeled as CROTIS 2.1.

4.1 CROTIS 2.1_basicPackage

Changes to the CROTIS 2.0 topographic model in relation to CROTIS 2.1 topographic model will be explained in an italic text.

The CROTIS 2.1_basicPackage does not differ from the CROTIS 2.0_basicPackage in the number and title of classes and upper-class, and it contains the following upper-classes: FeatureType CROTIS_Object and DataType LifeCycleType, and a list of allowed values of the upper-class attributes: AccuracyType, DefinitionMethodType, VerticalPositionType, StateOfObjectType, MaterialType, ReasonsOfChangeType and DataSourceType (Fig. 4).

In the CROTIS 2.1_basicPackage topographic model (Fig. 4), the following improvements are proposed:

In the code list (CodeList), the StatusOfObjectType excludes attribute values and codes: Abandoned: 2 and InFunction: 4. This part is unnecessary since the primary purpose of collecting data in TTB is not to know whether or not a building is in use or not or whether it is in function. This type of information is collected and maintained by other institutions. If the object is in function, the assumption is that the object is built, and that the attribute already exists.

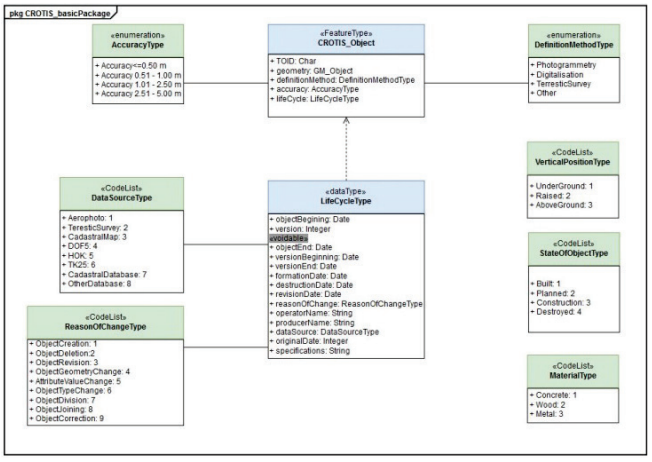

Figure 4 CROTIS 2.1_basic package

Therefore, in the CROTIS 2.1_basicPackage topographic data model (Fig. 4), the code list (CodeList) of the StatusOfObjectType should consist of the following attribute values and codes:

Built: 1, Planned: 2, InDevelopment: 3, Destroyed: 4.

In the CROTIS 2.1_basicPackage topographic data model (Fig. 4), in the code list (CodeList) of the Vertical PositionType, the proposition is to exclude the values and codes of the value of the attribute: UnderSea: 4, as these data are under the responsibility of the Croatian Hydrographic Institute (CHI), and additionally, the majority of the data collected and maintained in TTB is from photogrammetric images where the data below the sea cannot be detected and collected. Data which is available to the CHI are very specific and required for a smaller and more specific group of users.

Therefore, in the CROTIS 2.1_basicPackage topographic data model (Fig. 4), the code list (CodeList) of VerticalPositionType consisted of the following attribute values and codes:

UnderGround: 1, Raised: 2, AboveGround: 3

The upper-class feature type of CROTIS_Object and the data type of LifeCycleType, as well as the list of allowed values of the upper-class attribute values, AcurracyType, VerticalPositionType, StateOfObjectType, MaterialType, ReasonOfChangeType and DataSourceType (Fig. 4), will all remain the same, except for the above-mentioned changes, as it is the case in the CROTIS 2.0 _basicPackage topographic data model (Fig. 3).

4.2 CROTIS 2.1_ object entity Hydrography

The object entity of Hydrography is intended for storing and displaying all waters: streams and stands, underwater objects, natural and built objects on watercourses that in any way affect water flow or retain water. Fig. 5 depicts in detail

the object entity of Hydrography according to the CROTIS 2.0 data model.

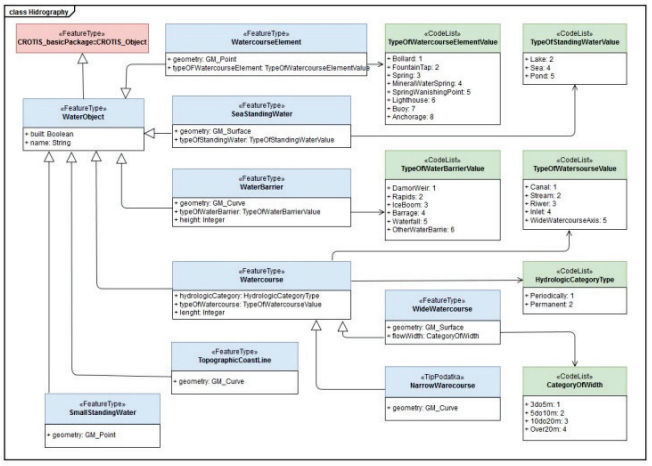

Figure 5 CROTIS 2.0_Hydrography

In the topographic data model of CROTIS 2.1, the object entity of the Hydrography (Fig. 6), the proposal is to add, in the class feature type of Watercourse, the value of attribute navigability: Boolean.

Thus, in the topographic model of CROTIS 2.1, the object entity of Hydrography (Fig. 6) in the class of FeatureType Watercourse would consist of the following titles and attribute types:
hydrologicCategory: HydrologicCategoryType, typeOfWatercourse: typeOfWatercourseValue length: Integer, navigability: Boolean.

In the topographic data model of CROTIS 2.1, the object entity of Hydrography (Fig. 6), the proposal is to add, in the code list the HydrologicCategoryType, the value and attribute value codes: Dry: 3.

Thus, in the topographic model of CROTIS 2.1, the object entity of Hydrography (Fig. 6), the CodeList HydrologicCategoryType would contain the following values and attribute values codes:

Periodically: 1, Permanent: 2, Dry: 3

In the topography model of CROTIS 2.1, the object entity Hydrography (Fig. 6), the proposal is to add, in the CodeList TypeOfWatercourseElementValue, the value and attribute value codes: Puddle: 9.

Thus, in the topographic model of CROTIS 2.1, the object entity of Hydrography (Fig. 6), the CodeList TypeOfWatercourseElementValue would contain the following values and attribute values codes:

Bollard: 1, FountainTap: 2, Spring: 3, MineralWaterSpring: 4, SpringWanishingPoint: 5, Lighthouse: 6, Buoy: 7, Anchorage: 8, Puddle: 9

In the topography model of CROTIS 2.1, the object entity of Hydrography (Figure 6), the proposal is to add, in the CodeList TypeOfStandingWaterValue, the values and attribute value codes: Plash: 6.

Thus, in the topographic model of CROTIS 2.1, the object entity of Hydrography (Fig. 6), the CodeList TypeOfStandingWaterValue would contain the following values and attribute values codes:

Lake: 2, Sea: 4, Pond: 5, Plash: 6

In the topographic data model of CROTIS 2.1, the object entity of Hydrography (Fig. 6), the proposal is to delete the value and attribute value codes in the CodeList CategoryOfWidthType: 5do10m: 2.

The cartographic key for TK25 and Product Specifications for TTB define that narrow watercourses up to 3 m in width are displayed as line objects; watercourses from 3 to 10 m width are defined as surface watercourses and are displayed on TK25 as line objects; watercourses up to 10 to 20 m in width are line objects that are displayed with a special type of line; and objects wider than 20 m are displayed as areas. Therefore, the attribute value of an object from 5 to 10 m in width is unnecessary.

Thus, in the topographic model of CROTIS 2.1, the object entity of Hydrography (Fig. 6), the CodeList CategoryOfWidthType would contain the following values and attribute values codes:

3 to 10m: 1, 10 to 20m: 2, over20m: 3

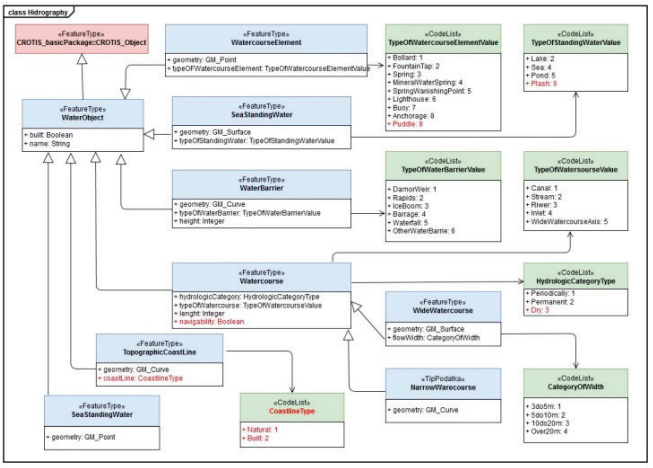

Figure 6 CROTIS 2.1_Hydrography

5 CONCLUSION

After the creation of the Official Topographic Cartographic Information System, STOKIS, as the basic document for the development of cartography in the Republic of Croatia, the Croatian Topographic Information System (CROTIS) was established in 1996. By establishing CROTIS, a topographic data model was defined.

Several versions of the topographic data model were made, including CROTIS 1.0, CROTIS 1.1, CROTIS 1.2 and finally CROTIS 2.0. The last version of the topographic data model, CROTIS 2.0, is in large proportion in line with the

INSPIRE 2007/2/EC Directive. In the topographic data model of CROTIS 2.0, certain object classes have been replicated from one object entity to another object entity, and some object classes have been omitted because the State Geodetic Administration does not have the jurisdiction for it and the classes have not been collected for the Basic Topographic Database (TTB). According to the proposition from the topographic data model, the object entity of Geographical Names and the object entity of Utility Lines are excluded and those object entities will be placed in separate databases. This would be similar to CROTIS 1.2, when the object entities of Permanent Geodetic Points and of Administrative and Territorial Division and Boundaries were excluded and placed in a separate database.

From a detailed analysis of the topographic data model of CROTIS 2.0, and based on the experience in data collection and processing, a number of suggestions were made to improve the topographic data model. The proposal for improvement is given for the CROTIS basic package and for the thematic entity of Hydrography. For the basic package, the proposed change is in the StateOfObjectType code list. For the object entity of Hydrography it is given in the FeatureType Watercourse, and the proposal is to add the attribute of Navigability. It is also proposed to change the Code List for the TypeOfWatercourseElementValue, TypeOfStandingWaterValue, and HydrologicCategoryType. It is strongly advised to continue in the future a close cooperation with all interested parties (institutions) and to supplement and harmonize the existing data model with other spatial data users' data models. Advances in technologies that use spatial data create a growing need for spatial data both in the geometric and attributive form. Therefore, it is evident that this proposed cooperation is simply necessary and unavoidable.

6 REFERENCES

[1] Narodne novine. (2008). Pravilnik o topografskoj izmjeri i izradbi državnih karata, Narodne novine broj 107/08, Zagreb.

[2] Racetin, I. (2013). STOKIS u hrvatskoj pravnoj regulativi, *Geod. list*, 2, 135-144.

[3] Landek, I. (2017). Unapređenje modela topografskih podataka Republike Hrvatske, *doktorska disertacija*, Zagreb

[4] Frančula, N. & Lovrić, P. (1993). *Službeni topografsko-kartografski informacijski sustav – Idejni projekt*, Državna geodetska uprava, Zagreb.

[5] Radić, Z. (1994). Restrukturiranje i reprogramiranje geodetsko-prostornog sustava Republike Hrvatske s tehnološkom dogradnjom njegova informacijskog sustava (u novim uvjetima samostalne, suverene države koja se uključuje u evropske sustave), Podprojekt provedba brzih promjena i konceptualna rješenja restruktuiranog geodetsko-prostornog sustava Republike Hrvatske (GEOPS), Državna geodetska uprava, Zagreb.

[6] Biljecki, Z. (1996). *CROTIS – topografsko informacijski sustav Republike Hrvatske*, Državna geodetska uprava, Zagreb.

[7] Divjak, D. (2013). *Prijedlog poboljšanja postojećeg sustava na temelju dosadašnjih projekta i iskustava*, Državna geodetska uprava, Zagreb.

[8] Divjak, D. (2014). *Hrvatski topografsko informacijski sustav 2.0 (CROTIS 2.0)*, Državna geodetska uprava, Zagreb.

[9] Landek, I., Marjanović, M., & Šimat, I. (2014). Model podataka Hrvatskog topografsko informacijskog sustava CROTIS 2.0. *Časopis Kartografija i geoinformacije*, Zagreb, 2015, 30-51.

[10] Ključanin, S., Poslončec-Perić, V., Ponjavić, M., Karabegović, A., & Landek, I. (2014). *Strategija razvoja službene kartografije u Federaciji Bosni i Hercegovini*, Dokument Federalne uprave za imovinsko-pravne poslove, Sarajevo.

[11] Ćosić, S., Alilović, M., Frangeš, S., & Landek, I. (2012). *Topografske karte na području Hrvatske*, Državna geodetska uprava, Zagreb.

[12] Biljecki, Z. (1995). *Studija o nadomještanju reprodukcijskih izvornika i obnavljanja sadržaja topografskih zemljovida*, Državna geodetska uprava, Zagreb

[13] Križaj, E. (1992). *Studija o ustrojstvu službenoga topografsko kartografskog informacijskog sustava Republike Hrvatske*, Državna geodetska uprava, Zagreb

[14] Mallgren, W. R. (1982). Formal specification of graphic data types. *ACM Transactions of Programming Language and System, 4*(4), 687-710. https://doi.org/10.1145/69622.357191

[15] Biljecki, Z. (2009). *Implementacija rezultata projekta CROTIS-GML u postojeći document CROTIS 1.1*, Državna geodetska uprava, Zagreb

Ivan LANDEK, PhD
State Geodetic Administration
Gruška 20, 10000 Zagreb, Croatia
Tel.+38516165422, ivan.landek@dgu.hr

Saša CVITKOVIĆ, B.Sc. in Geodesy
State Geodetic Administration
Gruška 20, 10000 Zagreb, Croatia
Tel.+38516165464, sasa.cvitkovic@dgu.hr

Milan REZO, PhD
Faculty of Geotehnical Engineering
Hallerova aleja 7, 42000 Varaždin, Croatia
Tel.+38542408900, mrezo@gfv.hr

ISSN 1846-6168 (Print), ISSN 1848-5588 (Online)
https://doi.org/10.31803/tg-20181206205307

Preliminary communication

OPTIMIZATION OF THE STRUCTURE OF INSULATING COMPOSITE MATERIALS

Zeljko KOS, Valerii VYROVOI, Volodymyr SUKHANOV, Mykhailo ZAVOLOKA, Aleksandr GOKHMAN, Iryna GRYNYOVA

Abstract. The article deals with the interdependent relationship between the properties of a structure and the properties of a material, which sets the task of reducing them, even they are indistinguishable, to a certain integrity. The object of research and analysis in the article is a building structure, which is seen as an open self-organized complex structural system. In the main part, the processes of the formation of structures are considered, as well as the classification of structural elements. The article concludes with structural changes related to the self-support and self-development of the network of active elements, which allow the manifestation of adaptation effects and the design-system to function during the normalized period. The importance of self-organization processes during the development and operation of construction systems allow us to attribute it to a self-organizing system. Thus, the building structure can be represented as an open and complex self-organizing system.

Keywords: construction systems; open system; self-organized complex; self-organization processes; structural organization

1 INTRODUCTION

Operable in adverse conditions, construction structures leave the safe operation mode by changing the properties of the material from which they are made. The main task is to combine the relationships between the properties of the structure and the properties of the material, down to indistinguishability, into a certain integrity. Identifying ways to solve this problem may be due to the attraction of the ideas and methods of the system approach [1]. The object of the research and analysis is the building structure, which is seen as an open complex of the structural self-organized system.

The rationale for such a representation is based on the following:

- it is an integral object;
- it consists of subsystems, which are in certain relationships and connections with each other;
- construction is strictly focused on the implementation of the target laid down in target functions;
- properties of the construction do not reduce to the properties of its components.

Continuing the justification for the allocation of the structure in the form of a system, we can conclude the following:

- the structure-system, being an element of a system of structural systems, creates an uninterrupted structural series of systems of any complexity;
- the representation of the design-system in the system-systems and in megasystems allows us to consider the issues of a rational use of material and technical resources, taking into account the environmental requirements, both at the construction stage and in the period of individual structures, structures and urban complexes, from unified technical and economic positions;
- the design-system, being a node of interstructural interactions in the system-structure-systems, determines by its state the safe functioning of the entire system;
- the implemented structure is in the design-system and so are the properties of the material, allowing the material to enter into all structural levels of hierarchical systems.

The representation of the design in the form of a priori system involves its structural design [2]. This gives rise to another interpretation of the history of the change in the parameters of the structure and, consequently, of the properties of the system design.

For a different interpretation, the functioning of system designs should be presented as continuous structural transitions, under which the homeostasis of the system is preserved under the conditions of external and internal factors, under the permissible limits of variation of structural parameters.

The fact of continuous change in indicators and structure parameters allows us to present the structure as a function of motion, which defines a certain range of material properties and determines the functional state of the system design. The intensity of the structural transformation of the material when exposed to an operational load structure depends on the initial qualitative composition and the quantitative relationships of structural elements [3, 4]. The outcomes of structure parameters are a certain set of structural elements at the time of putting the structure into operation. At this point, the structure of the contraction-system has already passed a certain history of formation and development. The beginning of this history falls on the technological period of obtaining the design – the period of the birth and formation of the system.

The technological period is a relatively short period in comparison with the life of the structures. During this period, efforts of designers, engineers and technologists were realized. Prior to this, the disparate models began to merge into a finished model construction system.

The process period is information-intensive. This is due to the concentration of information on the requirements for a product and the information databases that predecessors accumulated on the technological-technical and economic factors for the rational way of producing a concrete

construction structure, both in the industrial method and under construction conditions.

The functioning of designs systems is seen as an ongoing process of structural transformation that depends on the prehistory of the structural design, which sets the technologist with the following tasks:

- the selection of the design-system model of the structure based on the options of its interaction with the environment during the maintenance period;
- the determination of the dominant elements of the structure, which should ensure the safe operation of the structure-system under the influence of external and internal factors;
- the design of concrete compositions and the designation of technological modes for obtaining a concrete mixture, taking into account the geometric parameters of the structure in order to create the required set of structural elements by their qualitative composition and quantitative ratio;
- the assignment of the design technology production system with a desired set of physical and mechanical properties.

The elements of the structure are classified in 3 categories according to the speed of their reaction to external and internal effects. The three categories are conservative, metastable and active, as the active structural elements have taken cracks and internal interfaces [5]. Their activity is manifested in the following manners:

- the presence of cracks creates in the surrounding material an uneven distribution of internal deformations and stresses, in which stresses relax near the cracks with the concentration at the mouth along the crack front;
- volumetric deformations caused by internal and external factors appear on the shores of cracks and internal interfaces, which leads to their partial dissipation and redistribution between individual subsystems;
- the specificity of cracks is the ability to spontaneously concentrate the stresses caused by almost any external influences, which leads to a change in their parameters and, consequently, to structural changes in individual subsystems and the entire system design.

Thus, the history of the functioning of the structure-system is directly connected with the history of the self-development of the network of active elements of the structure at all levels of structural heterogeneities. By taking for granted the reality of active elements in the design of the system structure, you can get answers to legacy issues:

- why the destruction of the structure takes place when the required quality evidence is provided;
- why with the medium, far from critical, deformations and stresses, localized zones of appearance to the development of cracks appear;
- why cracks grow in the compression zone;
- why cracks as a phenomenon, as a rule, are absent in the calculation schemes;
- why calculations do not take into account the residual (technological, initial, hereditary) deformations;
- why in the analytical methods there are no data on the influence of the material structure on the redistribution and dissipation of the deformation energy;
- how the structure of the structure material is combined;
- how to realize the structure of the product by using the material structure;
- how the structure of the material actually participates in the structural design and operation of the structure.

The process of the formation of structures in their history can be viewed as a kind of scenario for the formation and modification of the properties of CBM (composite building materials). In this case, the scenario itself, as a certain plot scheme, should include a detailed description of the emergence, development and implementation, significant for the system of events. Due to the fact that practically for all CBMs, the organization of the structure begins with interparticle interactions, the task is to manage the mechanisms of directed "guidance" of structure elements that are responsible for the safe operation of the final consumer product.

The structure of CBM is formed as a result of rather complex phenomena associated with the occurrence of diverse chemical, physical and mechanical processes. Any process should be studied in the dynamics of its development, which poses the problems of a reasonable choice of dynamic models that enable the describing of the mechanisms of the formation of dynamic structures with the definition of structural elements, the appearance and development of which determines the functional state of the CBM. Under the elements of the structure in the present context are integral components which implement the objectives that contribute to achieving the specified functions and levels of each structural material as a whole.

The principal difference in the mechanisms of organization of cluster structures of disperse systems (CBM models), depending on the qualitative and quantitative compositions of the particles of the disperse phase, leads to the manifestation of equifinality effects – from different initial states, various qualitative elements of the structure are formed in different ways in the system. In this case, the final act of the three possible scenarios for the organization's structure is the formation in the beginning of a structurally disordered system periodically arranged structural units – clusters of various levels of structural inhomogeneities. As a result of such local cooperative interaction in the system, what is spontaneously formed is a fundamentally new structure for the elements of the inter-cluster interface system.

With the advent of new elements of the structure, the history of the dominant influence of interparticle interactions on the ends of the processes of structure formation ends. The period of further structural design by CM cluster-cluster interactions through intercluster interfaces that require the use of other structural dynamic models. Scenarios for the formation of a microstructure naturally fit into other

storylines of the formation of structures at other levels of structural heterogeneity. The polystructural organization of CBM assumes the coexistence and interdependent influence of structural features of fundamentally dissimilar levels of heterogeneity, which must be taken into account when designing and producing materials and products based on mineral binders.

One of the ways to ensure the safe functioning of the system-design in the system-structure system with the negative effect of the operating environment is to maintain interrelated relationships of active elements at all levels of the subsystems. This can be achieved by directing the organizational structure based on the self-organization phenomena in the process during the manufacture of structures. By the time the design begins to work, a certain set of active elements at all levels of structural heterogeneity should be created in the system with similar ones in the material. A specific set of design involves an interconnectivity and interdependence network of active elements based on their interaction and self-support during the period of a system of external and internal loads. Thus, the principle of self-organization of the system during the entire period of its functioning will be realized, which makes it possible to manifest the whole complex of adaptation mechanisms and, therefore, to avoid crisis situations for systems of situations.

In previous works on this topic [6, 7, 11], the temperature method proposed by us allows us to reliably identify a number of structural inhomogeneities, without resorting to more expensive and time-consuming methods of defectoscopy, such as ultrasound and X-ray. Based on the research conducted in this work, it can be concluded that according to the Wiedemann-Franz law, there will be less heat loss on the surface of the heat-insulating material if the material has both a low thermal conductivity and high specific electrical conductivity. However, this is only possible when using composite materials from an insulator and a conductor.

2 THE METHODOLOGY OF THE RESEARCH

Experimental work was carried out on the model of structural cells of concrete, taking into account the interaction of the matrix material with reinforcement (Fig. 1a), porous (Fig. 1b) and dense aggregates (Fig. 1c) with fillers.

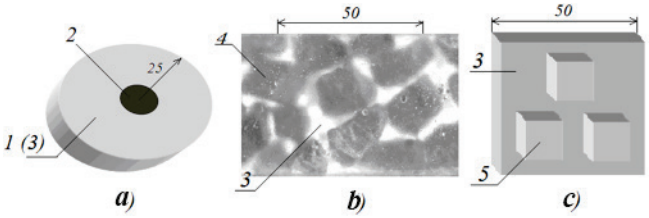

Figure 1 Models of the structural cells of concrete

a) a fragment of reinforcement in the matrix material (concrete), b) coarse aggregate in a cement matrix, c) square-shaped aggregate in the matrix material, 1 - cement stone; 2 - armature; 3 - epoxy resin; 4 - expanded clay gravel; 5 - fillers of a square shape.

The matrix material used the cement paste with W / C = 0.27 to examine the nature of the cracking of cured matrix material during its interaction with various nature and shape of aggregates. To analyze the influence of the kind of aggregates on the formation of the fields of local and integral deformations, an optically sensitive epoxy resin of the ED-20 type with the hardener polyethylene polyamine was used as the matrix.

Condition of development of residual deformations carried graph – analytical method, the method of photoelasticity and speckle – interferometry [7, 8]. A schematic diagram of the interferometer for quantitative and qualitative analysis of deformations in models of structural cells in a three-dimensional measurement is shown in Fig. 2.

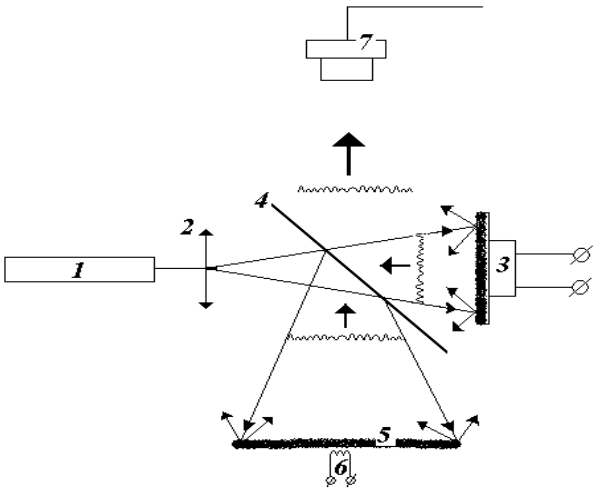

Figure 2 Scheme speckle – interferometer: 1 - helium neon laser, 2 - beam expander, 3 - diffuse diffuser fixed on piezoceramics, 4 - semitransparent mirror, 5 - sample, 6 - heater (tungsten helix about 10×5 mm in size), 7 - camera.

The procedure for carrying out the experiment was as follows: the local temperature was supplied by a 10×5 mm heater from the bottom in the geometric center of the model of structural cells. At the same time, the change in surface temperature was monitored with an accuracy of 0.5 °C with an interval of 5 s and deformations occurring on the surface of the models with an accuracy of 0.03 μm.

3 ANALYSIS OF THE EFFECT OF LOCAL HEATING ON THE NATURE OF THE DEVELOPMENT OF DEFORMATIONS

In the article [9, 10] it is told that when local or unilateral change of volume associated with a local or homogeneous change of the humidity and temperature of the samples and products "deformation waves" appear and develop, which are distributed throughout the sample and the product. It was suggested that the material of the article perceiving the energy of the arising deformations transfers it to neighboring parts with a partial distance. As a result, standing waves with variable amplitudes and period are formed,

which can develop as the volume of local sections changes. A similar pattern of occurrence and development of deformation processes must occur at the level of concrete structural inhomogeneities.

Experimental results showed that the development of deformation processes in the models of structural cells of concrete begins almost simultaneously with the supply of thermal energy. Local and thermal deformations cause the deformation of adjacent volumes of a material and appear on the opposite surface without changing its temperature. A local increase in volume causes the development of deformations of neighboring areas, forming a kind of "deformation wave". The nature of the formation of a deformation wave in a sample of a structurally homogeneous material is shown in Fig. 3

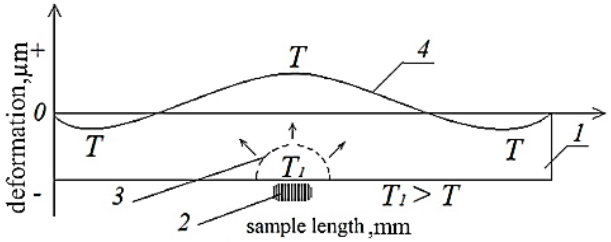

Figure 3 The mechanism of the formation of deformation waves at the local heating of the sample: 1 - sample; 2 - heater; 3 - zone of development of temperature deformations; 4 - change of deformations; T - initial temperature; T1 - temperature change.

In the case of using materials with a certain structural organization, the transfer of deformation energy from one kind of structural inhomogeneities to other will be determined by the state of the interface between the components and their deformation characteristics. This changes the appearance of emerging deformation waves. Fig. 4 shows the mechanism of the formation of deformation waves during the local heating of a sample made of a multicomponent material.

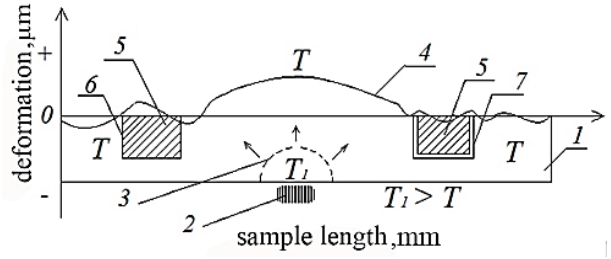

Figure 4 Formation of a deformation wave for the local heating of a sample and a structurally inhomogeneous material: 1 - sample; 2 - heater; 3 - zone of development of temperature deformation; 4 - change of deformations; 5 - structural component with increased deformation characteristics; 6 - perfect adhesion on interphase interfaces; 7 - absence of adhesion forces, bonds on interphase interfaces; T1 - temperature change.

With perfect adhesion of the matrix material to the surface of the structural inhomogeneity (under the condition $E_M < E_{CH}$, where is E_M - the modulus of elasticity of the matrix, and E_{CH} - the modulus of elasticity of the structural component), the deformation energy varies, which affects the nature of the basic deformation wave. In the case of weakened adhesion, the matrix material "sags" on the inclusion, causing half the appearance of local deformations. It can be assumed that similar perturbations of the deformation wave with the local heating of the structurally inhomogeneous material will occur when it meets the shores of the cracks and internal interfaces. The initial local and integral deformations, both at the level of the structural heterogeneities of the material and at the levels of the sample or article, should have a special effect on the character of the development and the type of deformation waves. An example of the emergence and development of the deformation wave is instantaneous volume "portraits" of the deformation state, which arose when local models of structural concrete cells were heated in Figs. 5, 6 and 7.

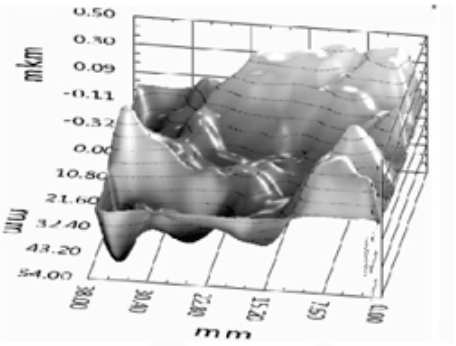

Figure 5 Deformations of the surface of models of structural cells of concrete with fittings

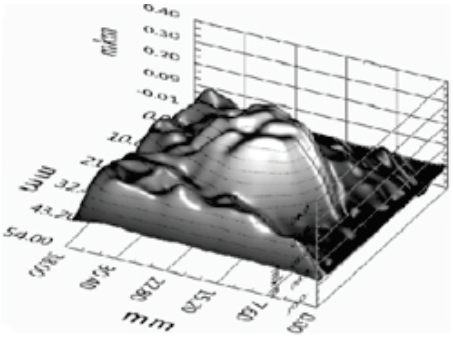

Figure 6 Deformations of the surface of models of structural cells of concrete with expanded clay gravel

The comparison of the deformation state of the model obtained by the speckle-interferometry method after the local temperature supply by the nature of the residual strain distribution obtained by the grapho-analytical method and the photoelasticity method made it possible to determine the effect of residual deformations, the state of the interfaces between the matrix and inclusions, and the type and orientation of the inclusion on the formation deformation waves. This allowed us to recommend this method, after

improvement, to detect, fix and quantify structural heterogeneities of complexly organized materials.

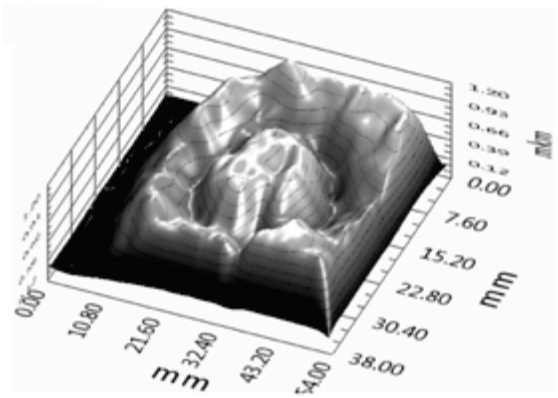

Figure 7 Deformations of the surface of models of structural cells of concrete with a low-modulus filler

The analysis of the kinetics of the formation and propagation of deformation waves made it possible to conclude that the arising deformation perturbations superimposing on the existing non-uniform deformation fields change their general form. In the material there are spontaneously zones, regions, and extent (streams) of material with increased density. It is logical to assume that the transfer of thermal energy will occur through the zones of material with increased density, which will lead to local thermal deformations and, as a consequence, to the formation of deformation microwaves, the latter entering into a component part of the basic deformation waves. In addition to that, the wave process of changing the deformation state should be considered one of the main factors affecting the formation of heat transfer conditions. The coexistence of the zones of different density in the matrix material assumes the formation of heat flows in the form of separate channels or streams, the runoff of which will be determined by the zones of maximum density. Such a stream pattern of heat fluxes will form a kind of percolation cluster in the sample, design and product. Changing the form of percolation clusters due to directed structure formation and "guidance" of residual deformations in the material can be regulated by heat transfer processes in the enclosing structures.

4 CONCLUSIONS

The conducted research has shown that when local heat is applied to complex materials, deformation waves arise that pass through the entire sample obtained from these materials. The velocity of propagation of deformation waves is higher than the rate of transfer of thermal energy, which leads to the spontaneous formation of density fluctuations in the material. The formation of density gradients assumes that complex trajectories of heat fluxes are formed in the material, the changing of which makes it possible to change the thermal protective properties of heat-insulating and heat-insulating is a structural materials. Moreover, structural changes related to self-support and self-development of the network of active elements enable the manifestation of adaptation effects, which allows the design-system to function during the normalized period. The importance of the processes of self-organization during the creation and operation of the system-design allows it to be attributed to a self-organizing system. Thus, the building structure can be represented as an open and complex self-organizing system. Based on the experiments conducted on the formation of the structure of heterogeneous materials, it is possible to predict and produce composite materials with desired properties. In the future, plans are to study the influence of structural inhomogeneities in the form of an interface (cracks), local media and capillary-compacted porous structure of materials to improve their thermal performance.

5 REFERENCES

[1] Prangishvili, I. V. (2000). *System approach and system-wide regularities*. Moscow, "SYNTHEGA".
[2] Capra, F. (2004). *Hidden connections*. Moscow, Publishing house "Sofia".
[3] Vyrovoi, V. N., Dorofeev, V. S., & Sukhanov, V. G. (2010). *Composite building materials and structures. Structure, self-organization of a property*. Odessa, Publishing house "TPP".
[4] Sukhanov, V. G., Vyrovoi, V. N., & Korobko, O. A. (2016). *Structure of the material in the structure of the structure*. Odessa, Polygraph.
[5] Sukhanov, V. G., Vyrovoi, V. N., Cheriega, A. S., Elkin, A. V., & Dorofeev, A. V. (2011). The role of faults in the destruction of material structures. *Modern designs from metal and wood*, 15, 141-148.
[6] Vyrovoi, V. N., Zavoloka, M. V., & Sukhanov, V. G. (2017). Formation of knowledges system in educational process: Scientific and methodological basis for teaching natural sciences and engineering in higher education, 49, 187-193.
[7] Vyrovoi, V. N., Zhukovsky, O. K., & Gokhman, A. R. (2016). The mechanism of formation of deformation waves under thermal gradient conditions. *Bulletin of OSACEA*, 62, 61-68.
[8] Nay J. 1991Physical properties of crystals and their description by means of tensors and matrices. Moscow, The World, 1967.
[9] Grigoriev, I. S. & Meilikhov, E. Z. (1991). *Physical quantities*. Moscow, Energoatomizdat.
[10] Zavoloka, Yu. M. & Vyrovoi, V. N. (1997). Features of heat transfer processes in heterogeneous materials. Scientific and Practical Conference. *Problems of building thermal physics and energy saving in buildings*, 3, 313.
[11] Zhukovsky, V. K., Gokhman, A. R., Zavoloka, Yu. M., & Vyrovoi, V. N. (2012). Investigation of the stress-strain state of composite building materials by the method of speckle-interferometry. *Bulletin of OSACEA*, 47, 139-147.

Authors' contacts:

Zeljko KOS, PhD
University North
Jurja Križanića 31b, 42000 Varazdin, Croatia
+38598757989, zeljko.kos@unin.hr

Valerii VYROVOI, Doctor of Technical Science, Professor
Odessa State Academy of Civil Engineering and Architecture
4, Didrikhson str., Odesa, Ukraine
vyrovoy@ukr.net

Volodymyr SUKHANOV, Doctor of Technical Science, Professor
Odessa State Academy of Civil Engineering and Architecture
4, Didrikhson str., Odesa, Ukraine
ecostroy_odessa@ukr.net

Mykhailo ZAVOLOKA, PhD, Professor
Odessa State Academy of Civil Engineering and Architecture
4, Didrikhson str., Odesa, Ukraine
+380674852564, lab.psk.ogasa@ukr.net

Aleksandr GOKHMAN, Doctor of Physical and Mathematical Sciences, Professor
South Ukrainian National Pedagogical University named after K. D. Ushynsky
26, Staroportofrankivska str., Odesa, Ukraine
+380967274242, alexander.gokhman@gmail.com

Iryna GRYNYOVA, postgraduate
Odessa State Academy of Civil Engineering and Architecture
4, Didrikhson str., Odesa, Ukraine
+380939799301, irene.grinyova@gmail.com

ISSN 1846-6168 (Print), ISSN 1848-5588 (Online)
https://doi.org/10.31803/tg-20180802210608

Preliminary communication

THE CANTILEVER BEAMS ANALYSIS BY THE MEANS OF THE FIRST-ORDER SHEAR DEFORMATION AND THE EULER-BERNOULLI THEORY

Dino KLJUČANIN, Abaz MANĐUKA

Abstract: The effect of the Timoshenko theory and the Euler-Bernoulli theory are investigated in this paper through numerical and analytical analyses. The investigation was required to obtain the optimized position of the pipes support. The Timoshenko beam theory or the first order shear deformation theory was used regarding thick beams where the shearing effect of the beam is considered. The study of the thin beams was performed with the Euler-Bernoulli theory. The analysis was done for stainless steel AISI-440C beams with the rectangular cross-section. The steel beams were a cantilever and stressed under varying point-centred load.

Keywords: AISI-440C; Cantilever; Euler-Bernoulli beam theory; First order shear deformation theory; Timoshenko beam theory

1 INTRODUCTION

The importance of beam theories applications can be seen in many engineering fields. Their use comprises applications in machine design, mechatronics, the design of components, etc. These theories are used in the analysis of thin and thick beams. The thick beam theory was introduced by Timoshenko. It is based on shear deformation that takes place due to the bending of the beam.

In order to optimize design and to obtain the most precise results, various cases of the pipes supports were examined. The piping requires various location positioning due to terrain specification. In order to minimize the required materials and to achieve the best aesthetic, the behaviour of end pinned beams is investigated. The examination is done through numerical and analytical methods. One of the mistakes that is made in practice is neglecting of the shearing component in the material that happens in certain cases regarding the beam geometry. For FEM analysis, one of the latest numerical algorithms will be used (NASTRAN). This paper will determine the optimal positioning of the beam and present the comparison of the results obtained through analytical and numerical analyses. In order to obtain the best results and avoid neglecting of the aforementioned shearing component of this type of beams, the Euler-Bernoulli and Timoshenko Beam theories are applied in certain cases.

The Euler-Bernoulli theory has been successfully applied in engineering practice. This theory served as the base to formulate a theory for the finite displacement in the beam and post-buckling analysis [1]. Ghosh used this theory as a base for developing and implementing a solution for shape memory polymers [2]. Xue and Khawaja successfully applied the Euler-Bernoulli theory in the analytical study of sandwich structures [3]. The Euler-Bernoulli theory in fractional form is successfully used in the experimental analysis for micro-beams [4].

Labuschagne et al. have shown analysis of the Euler-Bernoulli and Timoshenko beam theories alongside with two-dimensional elasticity theory where the Timoshenko theory application had the most desirable results [5]. In the numerical and analytical study, the Timoshenko shear deformation theory was used as a foundation for the investigation of the vibrational performances in continuous beam [6]. For bending analysis of the cantilever isotropic beam, this theory was utilized as a base for the development of the theory for the displacements and stress [7]. Tessler et al. have done the refinement of the Timoshenko Beam theory for sandwich beams using Zigzag Kinematics [8]. The Timoshenko theory was used with Eringen nonlocal elasticity theory to form differential transformation method for the analysis of the thick nano-beams vibrations [9].

The accuracy of the Timoshenko theory is governed by the shear correction factor. Regardless of the shear correction factor three approaches i.e. two shear stress approaches and Saint-Venant are used for evaluation of shear correction factor [10]. Birman and Bert highlighted the importance of shear correction factor and evaluated its function for six methods in sandwich structures [11]. The effect of the different approaches used for shear coefficient can affect the accuracy in terms of natural frequencies [12].

2 THICK AND THIN BEAM THEORIES

The calculation of the observed values is done taking into consideration the stress caused by momentum made by the static force and the shear in the observed cross-section. The force is applied in the direction y and along the horizontal axis of the cantilever beam. A displacement occurring with respect to x can be determined as Eq. (1):

$$\frac{\mathrm{d}w}{\mathrm{d}x} = \frac{P}{A \cdot G \cdot k} + \frac{\mathrm{d}\varphi}{\mathrm{d}x} \tag{1}$$

Taking into consideration the angle of rotation which can be determined as Eq. (2)

$$\frac{\mathrm{d}\varphi}{\mathrm{d}x} = \frac{Px}{EI} \tag{2}$$

For the boundary condition for the value of x_1 and x_2, this equation can be expressed as Eq. (3) and Eq. (4), or in the final form given with Eq. (5):

$$\mathrm{d}\varphi = \int_{x_2}^{x_1} \frac{Px}{EI}\mathrm{d}x \tag{3}$$

$$\varphi(x) = \frac{P}{EI}\int_{x_2}^{x_1} x\mathrm{d}x \tag{4}$$

$$\varphi(x) = \frac{1}{2}\left(\frac{Px_1^{\,2}}{EI} - \frac{Px_2^{\,2}}{EI}\right) \tag{5}$$

After the integration is finished, and if the maximum distance of the beam is denoted as l, the final term for the angle of rotation with respect to x will have the form expressed with Eq. (6):

$$\varphi(x) = \frac{1}{2}\left(\frac{Pl^2}{EI} - \frac{Px^2}{EI}\right) \tag{6}$$

After all conditions for integration are obtained, the main equation can be written as Eq. (7):

$$w(x) = \int_x^l \frac{P}{A\cdot G\cdot k}\mathrm{d}x + \frac{1}{2}\int_x^l\left(\frac{Pl^2}{EI} - \frac{Px^2}{EI}\right)\mathrm{d}x \tag{7}$$

Integration with respect to dx will transform the aforementioned equations to final forms Eq. (8) and Eq. (9):

$$w(x) = \frac{P}{A\cdot G\cdot k}(l-x) + \frac{P}{6EI}\left(2l^3 - 3l^2x + x^3\right) \tag{8}$$

$$w(x) = P\left(\frac{(l-x)}{A\cdot G\cdot k} + \frac{\left(2l^3 - 3l^2x + x^3\right)}{EI}\right) \tag{9}$$

Where: E – Young's modulus of elasticity (GPa); G – Shearing modulus (MPa); K – Timoshenko coefficient (-); I – Inertia moment (mm^4); A – The cross-section of the observed beam (mm^2); P – Force acting on the element (N).

The phenomenon of the thick beams was developed by Timoshenko and this theory was named after him. The principle of this theory is in the fact that beams that are considered thick, or that are of length twenty times shorter than their thickness, perform differentially from thin beams. The basic assumption is predicted by the Euler-Bernoulli theory, which states that sections of the beam plane remain perpendicular to the longitudinal direction.

The deformation which happens due to bending of the beam can only be correct for the long and thin beams. In the case of thick beams, shear deformation must be taken into consideration. In this study, the force was pointed in the following distances 130 mm, 260 mm, 390 mm, 520 mm and at the end, i.e. 650 mm from the fixed support. The end values of the applied forces are shown in Tab. 1.

Table 1 Values of the applied force

F1	F2	F3	F4	F5
(N)	(N)	(N)	(N)	(N)
4414.5	3433.5	2452.5	1471.5	882.9

3 NUMERICAL SIMULATION

Analysis was based on stainless steel beams with squared-rectangular cross-sections, as it is shown in Fig. 1. Used steels have many advantages compared to other commercial steels. Due to their high chromium content, they have good corrosion resistance. These steels are also used in applications such as medical equipment, kitchen hardware, transport systems of fluids, and structural parts. As a structural part, these steels are widely used due to their ability to sustain harsh outdoor conditions without any maintenance.

All beams were made of stainless structural steel with properties shown in Tab. 2. In order to obtain results for this type of load by FEM, NASTRAN algorithm was used. This algorithm was developed by NASA (NASA Stress Analysis) and was used as an addition to Autodesk Inventor stress analysis tools.

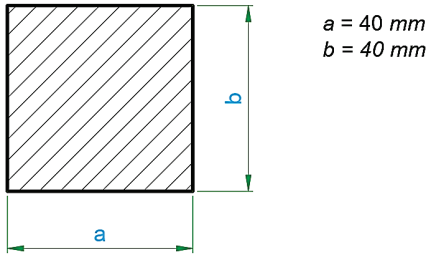

Figure 1 Cross section of the examined beams

The meshing setup was made for 15 mm element size as it is shown in Fig. 2. In order to increase the accuracy of performed analysis, parabolic element order was used. The cross-section of the beam was quadratic with dimensions of 40 × 40 mm. The Timoshenko theory was applied on the beam with a length of 650 mm, while the Euler-Bernoulli theory was applied to the beam with a length of 950 mm.

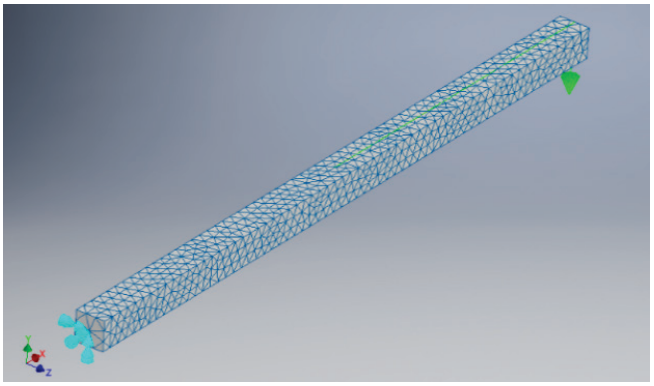

Figure 2 Boundary condition of the numerical model

Table 2 Properties of the used material - AISI 440C

Designation	E	G	n	K
Unit	(GPa)	(MPa)	-	-
Value	206.7	83900	0.27	0.833

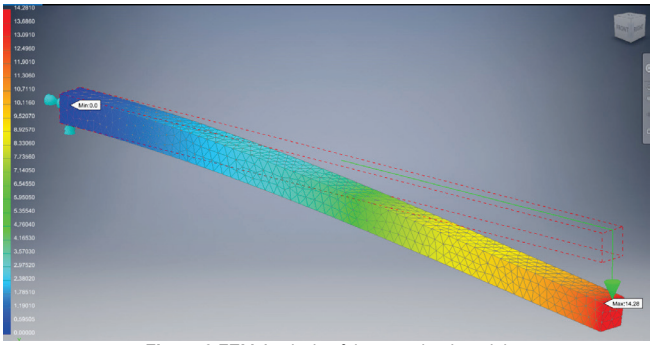

Figure 3 FEM Analysis of the examined model

Investigation of the non-supported cantilever beams included a fixed setup of the support (Fig. 2.) with no translation and rotation as the boundary condition and remote force according to the specified length in the x, y, z coordinate system. A detail from the experimental run is shown in Fig. 3.

4 RESULTS EVALUATION – ANALYSIS COMPARISON

Nastran module was used as an add-in module in Autodesk Inventor stress analysis environment. The results were obtained for each case that consisted of various distances at which the values of the aforementioned forces were applied. The analytical results in the case of the Timoshenko theory obtained for all the distances of the applied forces are shown in Tab. 3.

The analytical analysis and calculation of the second beam displacement with the length of 950 mm, were done by means of the Euler-Bernoulli theory and the results for all the examined cases of applied forces are shown in Tab. 4.

Table 3 Analytical results for the first beam

Case No.	Dist (mm)	d1 (mm)	d2 (mm)	d3 (mm)	d4 (mm)	d5 (mm)
1	130	0.513208	0.399162	0.285116	0.171069	0.102642
2	260	1.906193	1.482594	1.058996	0.635398	0.381239
3	390	3.95901	3.07923	2.19945	1.31967	0.791802
4	520	6.451715	5.018001	3.584286	2.150572	1.290343
5	650	9.164365	7.127839	5.091314	3.054788	1.832873

Table 4 Analytical results for the second beam

Case No.	Dist. (mm)	d1 (mm)	d2 (mm)	d3 (mm)	d4 (mm)	d5 (mm)
1	190	1.602212	1.246165	0.890118	0.534071	0.320442
2	380	5.951072	4.628612	3.306151	1.983691	1.190214
3	570	12.359919	9.613271	6.866622	4.119973	2.471984
4	760	20.142091	15.666070	11.190050	6.714030	4.028418
5	950	28.610924	22.252941	15.894958	9.536975	5.722185

In the case of FEM simulation, the same conditions were applied in both cases of the end pinned beams. The aforementioned setup was used with respect to the real character of the point centred perpendicular load. The results obtained through numerical analysis are shown in Tab. 5.

Table 5 Numerical results for the first beam

Case No.	Dist. (mm)	d1 (mm)	d2 (mm)	d3 (mm)	d4 (mm)	d5 (mm)
1	130	0.548650	0.427240	0.305140	0.182990	0.109720
2	260	2.471700	1.923000	1.373500	0.824030	0.494350
3	390	4.394800	3.418700	2.441800	1.465000	0.878910
4	520	6.317400	4.913900	3.509900	2.106000	1.263500
5	650	8.240500	6.409600	4.578100	2.746700	1.648100

In order to show the detailed comparison of the beam theories in the case of thick beams, numerical analysis was performed for all the points of the applied loads with the same values and the results are shown in Tab. 6.

Table 6 Numerical results for the second beam

Case No.	Dist. (mm)	d1 (mm)	d2 (mm)	d3 (mm)	d4 (mm)	d5 (mm)
1	190	1.709000	1.329400	0.949320	0.569210	0.341330
2	380	7.709600	5.996200	4.282800	2.569300	1.541400
3	570	13.710000	10.663000	7.616000	4.569200	2.741300
4	760	19.708000	15.328000	10.949000	6.569300	3.941200
5	950	25.708000	19.994000	14.281000	8.568600	5.141300

The used methodologies are compared and standard errors according to the deviation, for the first case, are obtained and presented in Tab. 7. Margin error in the case of the first beam for all runs is presented in Tab. 8.

Table 7 Standard Error for analytical and numerical method for the first beam

Case	SE1	SE2	SE3	SE4	SE5
1	0.017721	0.014039	0.010012	0.0059605	0.003539
2	0.2827535	0.220203	0.157252	0.094316	0.0565555
3	0.217895	0.169735	0.121175	0.072665	0.043554
4	0.0671575	0.0520505	0.037193	0.022286	0.0134215
5	0.4619325	0.3591195	0.256607	0.154044	0.0923865

For the margin error at a confidence level of 90% and an alpha value of 0.1, the standard error is calculated by means of Eq. (10) given as:

$$SE = \frac{SD}{\sqrt{n}} \tag{10}$$

Where: SE – Standard Error: SD – Standard Deviation; n – number of examined values.

Table 8 Margin Error for analytical and numerical method for the first beam

Case	ME1	ME2	ME3	ME4	ME5
1	0.029151	0.023094	0.01647	0.009805	0.005822
2	0.46513	0.362234	0.25868	0.15515	0.093034
3	0.358437	0.279214	0.199333	0.119534	0.071646
4	0.110474	0.085623	0.061182	0.03666	0.022078
5	0.759879	0.590752	0.422119	0.253402	0.151976

In the case of the first beam, two methodologies are compared and characteristic trend lines with corresponding equations are shown in Fig. 4.

In the case of the second beam at the confidence level of 90%, using the same term given with Eq. (10), the standard error is determined and presented in Tab. 9.

Margin error for the second case with the critical value of 1.645 according to the t-test, as it was the case for the first beam, is obtained and presented by means of Tab. 10.

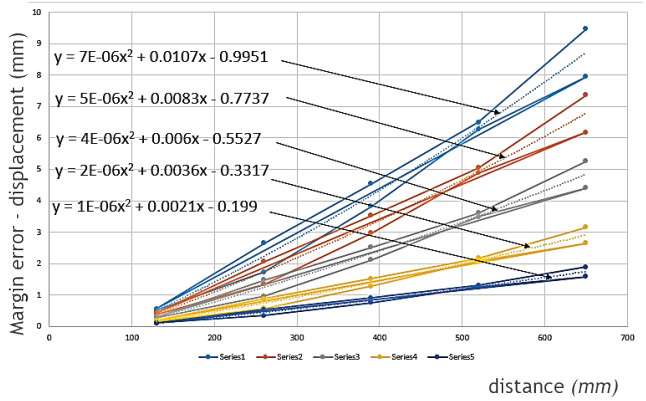

Figure 4 Comparison of the trend lines for analytical and numerical methods in the case of the first beam

Table 9 Standard Error for analytical and numerical method for the second beam

Case	SE1	SE2	SE3	SE4	SE5
1	0.053394	0.0416175	0.029601	0.0175695	0.010444
2	0.879264	0.683794	0.4883245	0.2928045	0.175593
3	0.6750405	0.5248645	0.374689	0.2246135	0.134658
4	0.2170455	0.169035	0.120525	0.072365	0.043609
5	1.451462	1.1294705	0.806979	0.4841875	0.2904425

Table 10 Margin Error for analytical and numerical method for the second beam

Case	ME1	ME2	ME3	ME4	ME5
1	0.087833	0.068461	0.048694	0.028902	0.01718
2	1.446389	1.124841	0.803294	0.481663	0.28885
3	1.110442	0.863402	0.616363	0.369489	0.221512
4	0.35704	0.278063	0.198264	0.11904	0.071737
5	2.387655	1.857979	1.32748	0.796488	0.477778

The comparison of two methodologies for the second beam is done and the trend lines are calculated and presented with corresponding equations for all the cases (Fig. 5).

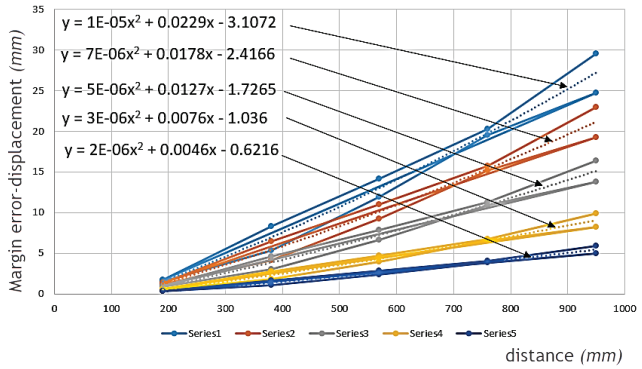

Figure 5 Comparison of the trend lines for analytical and numerical methods in the case of second beam

5 CROSS SECTION ANALYSIS AND ANALYSIS COMPARISON

After the evaluation of the results, the differences between obtained displacements were present. The differences were asymmetrical. A certain cross-section of the support showed major differences for each magnitude of the force. The displacement deviations were present in the observed cross-section regardless of the load. The displacement deviations are shown in Fig. 6.

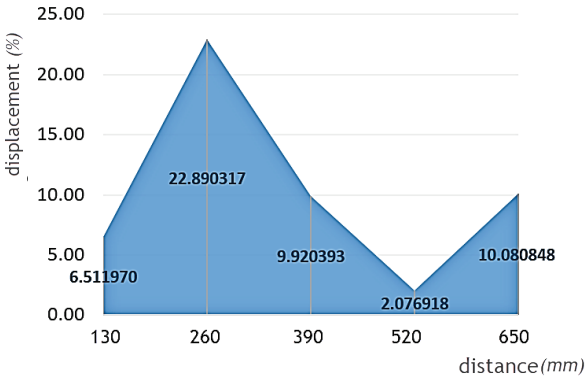

Figure 6 Comparison of the evaluated values for analytical and numerical method (shown in percentage) - Timoshenko theory

Compared results showed displacement deviations distinctions for both cases. The distinctions were the biggest in the first half part of the beam with up to a quartered deviation. Obtained results for the case of the Euler-Bernoulli theory are shown in Fig. 7.

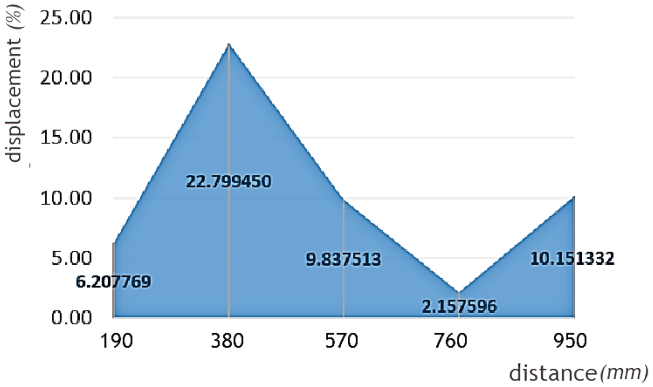

Figure 7 Comparison of the evaluated values for analytical and numerical method (shown in percentage) - Euler-Bernoulli theory

6 DISPLACEMENT APPROXIMATION

Due to different requirements in terms of the pipeline cross-sections, the combined mass of the transportation fluid and the pipes, it was necessary to investigate different values of the force applied. The investigations are done as a part of the development phase of the pipeline construction-setup to obtain the best values of the inclination angle that can provide the optimal fluid transportation. In the analysis of the optimal results for the two chosen supports numerical and analytical analyses were performed.

The numerical analysis showed the results obtained through calculation of analysed cases can be correlated and the relationship between the distance of the applied load and the displacement were linear, which can be seen from the diagram shown in Fig. 8.

The functional dependency for analytical solutions showed a slight deviation from the linear approximation of the displacement character in terms of distance of the load applied. The relation between them can be seen in Fig. 9.

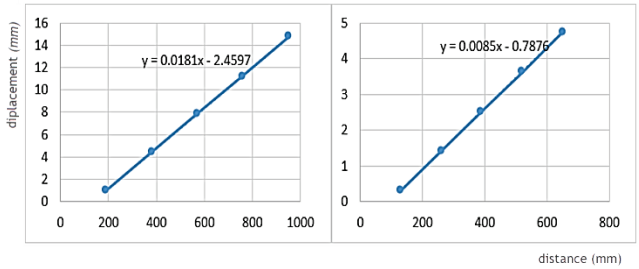

Figure 8 Distance-displacement relation preview - Numerical analysis

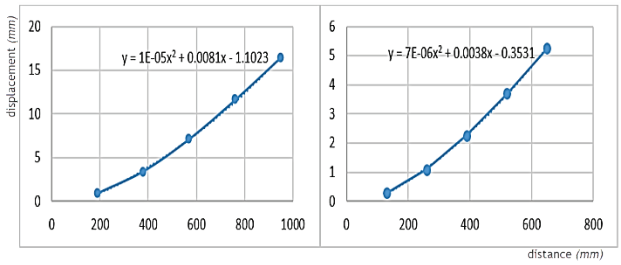

Figure 9 Distance-displacement relation preview – Analytical analysis

7 CONCLUSION

From the results obtained through numerical and analytical analyses, differences that were determined are noticeable and are in the sum range value of maximum 11% for the overall cross-section. The Timoshenko theory applied to thick beam analysis showed better overall fit compared to the Euler - Bernoulli theory. The displacement caused by the force that acted upon the different location on the beam had a linear character on all the evaluated beams.

Differences are more noticeable in the first part of the support and gradually elevated towards perpendicular mid-plane of the support. For the double value of the starting distance, the differences are most obvious with more than 20% for every tested case. The optimal results that provided the most reliable value regarding vertical displacement were the supports with the length of 520 mm and 760 mm for the first and second analysed beams, respectively. Future work is expected to be referenced regarding optimization and application of these theories in modified types of beams with a unique modified cross-section according to the design that is planned to be developed.

8 REFERENCES

[1] Usuki, T. (2008). A theory for the finite displacement of a thin-walled Bernoulli–Euler beam and lateral post-buckling analysis. *Proceedings of the Royal Society of London A: Mathematical, Physical and Engineering Sciences*, 1543-1570. https://doi.org/10.1098/rspa.2007.0256

[2] Gnoshl, P., Reddy, J. N., & Srinivasa, A. R. (2013). Development and implementation of a beam theory model for shape memory polymers. *International Journal of Solids and Structures, 50*(3-4), 595-608. https://doi.org/10.1016/j.ijsolstr.2012.10.024

[3] Xue, H. & Khawaja, H. (2016). Analytical Study of Sandwich Structures using Euler–Bernoulli Beam Equation. *AIP Conference Proceedings: ICNPAA 2016 World Congress - 11th International Conference on Mathematical Problems in Engineering, Aerospace and Sciences*, La Rochelle.

[4] Sumelka, W., Blaszczyk, T., & Liebold, C. (2015). Fractional Euler-Bernoulli beams: theory, numerical study and experimental validation. *European Journal of Mechanics - A/Solids*, 54, 243-251. https://doi.org/10.1016/j.euromechsol.2015.07.002

[5] Labuschagne, A., v. Rensburg, N., & v. d. Merwe, A. (2009). Comparison of linear beam theories. *Mathematical and Computer Modelling, 49*(1-2), 20-30. https://doi.org/10.1016/j.mcm.2008.06.006

[6] Zhang, X., Zhu, M., Wu, Z., & Zhao, M. (2018). Dynamic Analysis of Timoshenko Beam with Arbitrary Constraints and a Further Optimization Based on Least Energy Principle. *Mathematical Problems in Engineering*, vol. 2018. https://doi.org/10.1155/2018/1269738

[7] Jadhav, V. A. & Dahake, A. G. (2016). Bending Analysis of Deep Beam Using Refined Shear Deformation Theory. International Journal of Engineering Research, 5(3), 526-531.

[8] Tessler, A., Sciuva, M. D., & Gherlone, M. (2007). *Refinement of Timoshenko Beam Theory for Composite and Sandwich Beams Using Zigzag Kinematics*, NASA Center for AeroSpace Information, Hampton.

[9] Ebrahimi, F. & Nasirzadeh, P. (2015). A Nonlocal Timoshenko Beam Theory for Vibration Analysis of Thick Nanobeams Using Differential Transform Method. *Journal of Theoretical and Applied Mechanics, 53*(4), 1041-1052. https://doi.org/10.15632/jtam-pl.53.4.1041

[10] Marinetti, A. & Oliveto, G. (2009). On the Evaluation of the Shear Correction Factors: a Boundary Element Approach.

[11] Birman, V. & Bert, C. W. (2002). On the Choice of Shear Correction Factor in Sandwich Structures. *Journal of Sandwich Structures and Materials, 4*(1), 83-95. https://doi.org/10.1177/1099636202004001180

[12] Jensen, J. J. (1983). On the shear coefficient in Timoshenko's beam theory. *Journal of Sound and Vibration, 7*(4), 621-635. https://doi.org/10.1016/0022-460X(83)90511-4

Authors' contacts:

Dino KLJUČANIN, Engr.
University of Zenica
Fakultetska 1,
72000 Zenica, Bosnia and Herzegovina
kljucanin@live.com

Abaz MANĐUKA, PhD
University of Zenica
Fakultetska 1,
72000 Zenica, Bosnia and Herzegovina

ISSN 1846-6168 (Print), ISSN 1848-5588 (Online)
https://doi.org/10.31803/tg-20180911085644

Subject review

ENVIRONMENT IMPACT OF A CONCENTRATED SOLAR POWER PLANT

Mladen BOŠNJAKOVIĆ, Vlado TADIJANOVIĆ

Abstract: More recently, there has been an increasing interest in the use of concentrated solar thermal energy for the production of electricity, but also for the use in cogeneration and trigeneration. In this sense, the increasing use of solar thermal energy in urban areas is expected, and its impact on the environment is inducing an increasing interest. The paper analyses the impact of concentrated solar power technology (linear Fresnel, parabolic trough, parabolic dish, and central tower) on the environment in terms of water consumption, land use, wasted heat, emissions of gases, emissions of pollutants that include the leakage of heat transfer fluid through pipelines and tanks, impact on flora and fauna, impact of noise and visual impact. The impact on the environment is different for different concentrated solar power technologies and depends on whether thermal energy storage is included in the plant. Water is mainly used for cooling the system, but also for cleaning the surface of the mirror. To reduce water consumption, other cooling technologies (e.g. air cooling) are being developed. The available data from the literature show large variances depending on the size of the plant, geographic location and applied technology.

Keywords: concentrated solar power plant; environment impact

1 INTRODUCTION

Solar power production can be achieved in two different ways:
a) by using a photovoltaic technique that enables the conversion of total solar radiation directly into electricity,
b) by applying thermal techniques based on the transformation of solar radiation (direct fraction only) into heat to generate steam used in the turbine as a working fluid, as it is the case with classical thermoelectric power plants.
The basic advantage of the second way is the fact that it is much easier and achievable to store energy in the form of heat at a larger scale than in the form of electricity.
Photovoltaic plants do not provide continuous electricity to the grid causing major network stability risks. Against them, solar thermal power plants can provide 24 h/day of very stable power to the grid thanks to large heat storages they use when there is no solar energy.

The commercial deployment of Concentrated Solar Plants (CSP) started in 1984 in the United States. From 2005 to 2016, electricity production from CSP plants increased from 0.04 GWh to 11.9 GWh. The total capacity of CSP plants on the world level was 5133 MW at the end of 2017.

CSP utilizes mirrors to concentrate the sun's radiation onto a receptor through which heat transfer fluid (HTF) is passing. Heat that is absorbed by the fluid is used to produce vapour which, by applying a conventional thermodynamic cycle (usually Rankin's cycle), is converted into electricity using a steam turbine coupled to an electric generator.

There are several types of CSP plants, and most often, they are classified according to the type of the solar collector used. More than 80% of CSP installed capacity in the world is based on parabolic trough collector technology. However, other types of plants based on linear Fresnel reflectors, central tower and parabolic dishes are also being used [1]. In all CSP parabolic trough plants, conceptual design is very similar, but remarkable differences exist in the plant scale (usually between 20 MWe to 100 MWe), type of the heat transfer fluid, heat transfer mode between the particular parts of the power plant and other operating conditions. Additionally, some power plants may have a thermal storage system which allows them to produce electricity after sunset, thus increasing the total production capacity of the plant (Fig. 1).

In some cases, an auxiliary boiler can be integrated with natural gas or fuel oil to increase production capacity and increase the overall energy efficiency of the system [3].
All CSP systems can extend the time of solar operation to base load by applying larger collector fields and thermal energy storage. Solar heat absorbed during the daytime can be stored in thermal energy storage systems based on molten salt, concrete, ceramics or phase change materials. At night, thermal energy can be recovered from thermal storage to produce electricity continuously. This is an important feature for use in desalination processes, which typically require a continuous steady-state process and constant energy input the whole day. Furthermore, the CSP unit in combination with the classical boiler unit can be used for electricity and heat co-generation. In this case, the plant achieves efficiency up to 85%. Possible applications include the combined production of process heat, district cooling, and seawater desalination. The trend is also about applying trigeneration. One such prototype small-scale solar trigeneration system was built at Orte near Rome (Italy) to meet the needs for heating, electricity and cooling of residential users [4].

Each made-up facility for energy utilization and conversion affects the environment and individual ecosystems on Earth. Since CSP systems are being built more in Europe in areas outside the desert, it is good to know the potential impacts of these facilities on the environment.

This impact on the environment is different in some aspects for different plants and the following is usually analysed:

- Land used
- Water used
- Gas emission to the atmosphere
- Waste emission and impact on water, soil, and air
- Noise emission
- Visual impact.

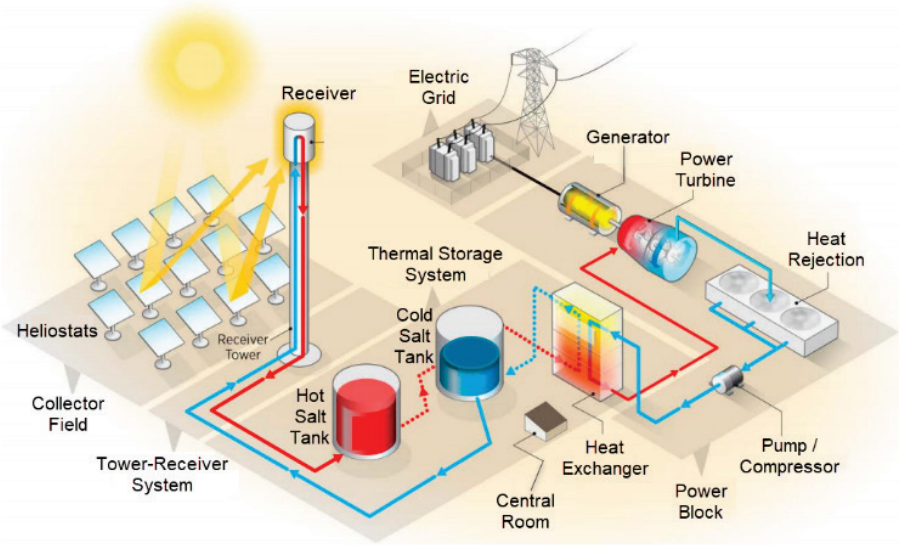

Figure 1 Power tower with direct storage of molten salt. Today's and advanced molten salt projects are conceptually similar, but higher salt temperatures are expected with the sCO_2-Brayton energy cycle [2]

2 THE POTENTIAL ENVIRONMENTAL IMPACT

Studies usually evaluate the life-cycle environmental impacts of CSP plants. The life-cycle analysis (LCA) defines boundary conditions to include processes, such as manufacturing (extraction of raw materials, transport to the factory, component manufacturing processes, transportation to the regional warehouse), construction (land preparation, construction of auxiliary facilities, plant assembly), operation, and maintenance (production of spare parts and their transportation to the site, fuel consumption of maintenance vehicles, water consumption for mirror cleaning), dismantling (energy required to disassemble plant components) and disposal (energy required for transporting waste to landfills, recycling of components, incinerator or the energy required for final disposal).

2.1 Land Used

The land use of solar systems depends strongly on the level of insolation. The land used of a given site decreases with higher insolation, which is why the same system may require up to three times more land for high latitudes than for sites closer to the equator. CSP plants globally require a significant amount of land that must be relatively flat.

There are different metrics for evaluating land-use impacts. Two metrics are most often applied for land use. The first metrics is the total surface area, which corresponds to all land enclosed by the site boundary. The boundaries of the site where the power plant is located are usually specified in blueprint drawings and are usually protected by a fence.

Another metric is the area occupied by individual plant components which comprise land directly occupied by solar arrays, substations, service buildings, access roads, and other infrastructure. This direct-impact area is contained within the total-area border and is smaller than the total area.

Land use is quantified on a basis of capacity (area/MWel) and generation (area/GWh/yr). Capacity-based results are useful for judge land-use and new projects costs, because power plants are often rated in terms of capacity. Results based on generation provide a more consistent comparison between technologies that differ in the capacity factor and enable the evaluation of land-use impacts that vary by solar irradiation, storage options, the way of tracking and applied technology [5].

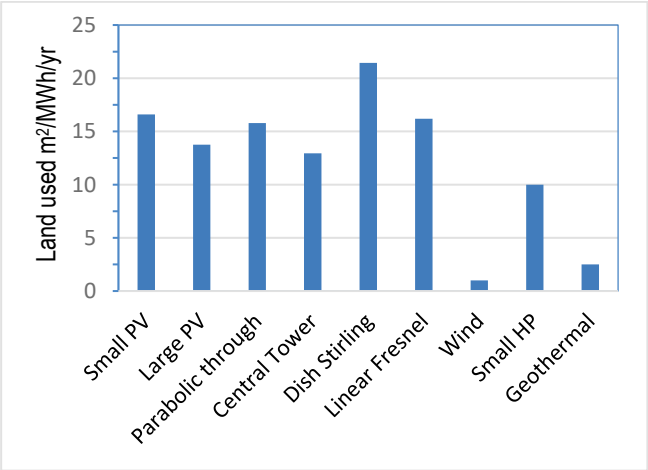

Figure 2 Land used of different technologies [5]

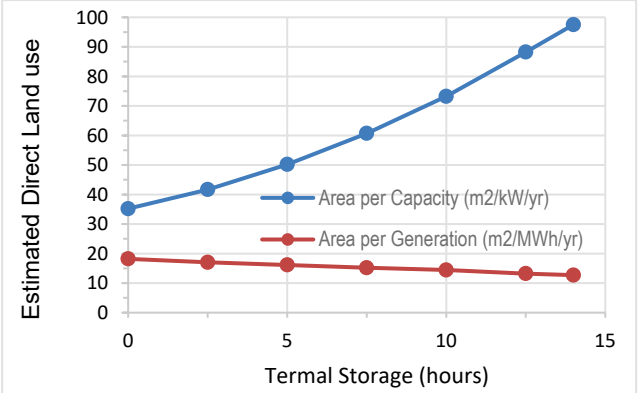

Figure 3 The relationship between CSP thermal storage and direct land-use [6]

Since more recently, more solar power plants have a thermal energy reservoir. In this case, the required surface area increases with the capacity of the reservoir (Fig. 3).

Generally, the land used is higher than for wind power, geothermal power plants, and nuclear power, but lower than for coal, biomass, and hydropower. In the future, growing global energy demand will lead towards lower-quality and open-pit coal mining and oil and gas extraction, using secondary and tertiary recovery technologies (e.g. tight oil and shale gas). This means that the land footprint of non-renewable energy sources will increase over time, while renewable energy sources can be expected to decrease the land footprint.

2.2 Water Use and Consumption

Like other power plants, solar thermal plants have a fairly large water footprint to produce electricity. One part of water is used to produce steam in the thermodynamic cycle, and most of the water (85% to 95%) is intended for cooling. The applied cooling technology largely determines the amount of water the plant has withdrawn. Most of the applied cooling water is returned to the environment, but the quality of that water differs from those taken from the environment and that can be a source of concern.

The consumption of a solar power plant with (once-through) wet cooling is estimated at up to 3.8 m^3/MWh of electricity, which is more than the amount of coal (3.123 m^3/MWh) and the amount of a nuclear power plant (3.055 m^3/MWh) with the same cooling system; but also for gas turbine combined cycle which has the lowest water withdrawal among thermal power plants (0.57 to 1.10 m^3/MWh) using a wet cooling tower (Fig. 4) [7, 8].

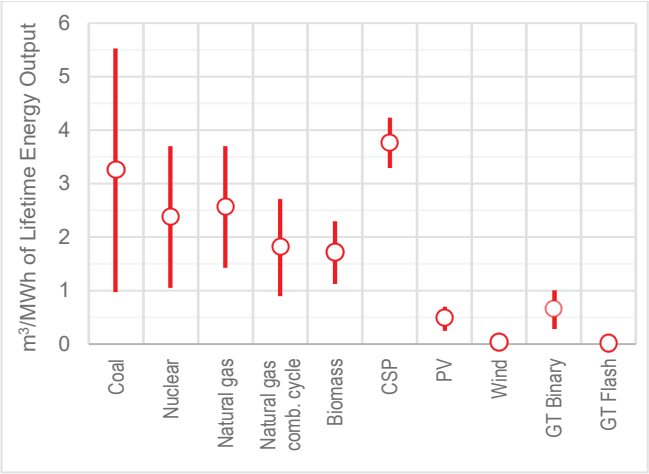

Figure 4 Life-cycle water consumption for power generation [7, 8]

Water is also used to clean mirrors to maintain high surface reflectivity, although water consumption for this purpose is usually hundreds of times lower than for cooling (around 20 litres/MWh). This water consumption is greater in areas where the wind carries dust particles (deserts), hence the surface fouling is larger. Burkhardt et al. [7] present the most comprehensive life cycle assessment of CSP water consumption, showing that solar thermal power plants with a dry cooling system can reduce the life-cycle water consumption of a parabolic through the plant with TES by 80%. However, water savings also include significant compromises. Capital costs are roughly 10 % higher and power consumption is up to 1.5% more than for wet cooling plants.

Some studies point out that the change from wet to dry cooling in a 100 MW parabolic trough a CSP plant can decrease the water consumption from 3.60 m^3/MWh to 0.25 m^3/MWh. However, the application of dry cooling instead of wet increases investment costs and lowers plant efficiency, adding 3.0% to 7.5% to the levelled electricity cost. Moreover, this increases LC GHG emissions and the Cumulative Energy Demand (CED) by 8%. Additionally, dry-cooling technology is less effective at environment temperatures above 38 °C. Finally, there are also CSP designs with small freshwater requirements, such as parabolic dishes with Stirling engines and gas turbine towers.

2.3 Waste

2.3.1 Solid and Non-Hazardous Waste

During the life-cycle of the CSP plant, both maintenance activities and the disposal of waste typical of electricity production will be carried out. Power plant waste includes oily rags, empty containers, broken and rusted metal and machine parts, waste electrical materials and other various solid wastes including the typical waste produced by workers. This waste is classified and managed by a local company authorized to do so. The collection and disposal of waste are carried out in accordance with the appropriate regulatory requirements in order to minimise the safety and health effects.

2.3.2 Hazardous Waste

Different hazardous waste can occur during the operation of a power plant. That waste include waste HTF and solvents, waste oil and oil filters, cleaning rags, used or expired deadline of chemicals from the water treatment system, expired deadline of paints, etc. This hazardous waste is temporarily stored on site in appropriate tanks and is permanently disposed of in the appropriate prescribed manner in accordance with the legal regulations. Workers will be trained to handle all hazardous waste generated in the place.

2.4 Gases Emitted Into the Atmosphere

The US National Renewable Energy Laboratory (NREL) has conducted a comprehensive LCA of renewable energy sources including the CSP technology [9]. In this life-cycle assessment, 42 GHG emissions were identified in thirteen unique references for Fresnel, parabolic trough, power tower, and parabolic dish technologies. Fig. 5 shows the distributions of the published assessment of life-cycle GHG emissions. Although most published estimates of greenhouse gas emissions in the life-cycle range between 14 g and 32 g

CO_2 eq./kWh, there are also some discrepancies that can be seen in Fig. 5, as the analysis also covers solar plants that additionally burn natural gas to generate electricity. These are actually hybrid solar power plants [10].

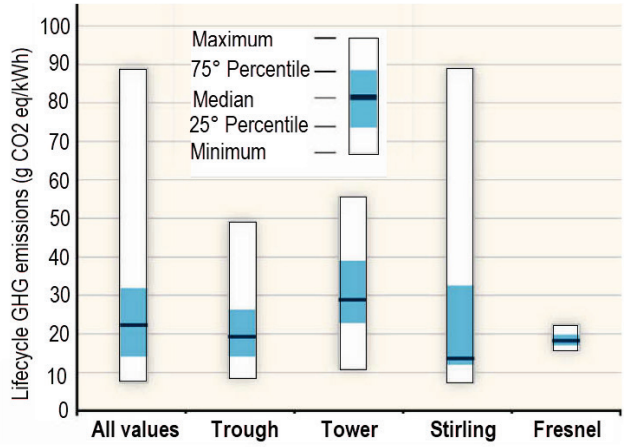

Figure 5 Life-cycle GHG emissions (g CO_2-eq/kWh) of CSP technologies [10]

Phase Extraction and Component Manufacturing takes 12.97% of the total CO_2 production, the construction phase takes 0.02%, the highest CO_2 production is 86.5% in the plant phase, and dismantling and disposal takes 0.51%.

The production of mirrors and galvanized steel contributes to the majority of greenhouse gas emissions associated with the production of solar field components.

The analysis carried out by Kommalapati et al. [11] also includes a large number of plants. The analysis gives results that are twice as high as those previously presented. However, the relative relationship between different technologies is the same, which means that the parabolic dish (Stirling) has the smallest CO_2 emission.

The LCA results also show that plants with TES have approximately twice the life-cycle GHG emissions of the configuration with minimal backup. Plants with dry cooling had slightly higher GHG emissions (5% to 7%) than wet-cooled power plants due to the efficiency penalty of internal fan power consumption.

If the heat transfer system uses nitrogen salts, the plant emits nitrogen oxide (N_2O) into the environment. The emission of this gas is extremely small compared to the carbon dioxide emissions from fossil fuels, but it is certainly not negligible because nitrogen oxide is a stronger greenhouse gas than carbon dioxide and it is necessary to control and solve this problem.

2.5 Wasted Heat

All heat energy-converting systems produce waste heat that can have a significant share (Fig. 6). This applies to CSP generation as well. The waste heat fraction depends on the applied technology.

As seen from Fig. 6, the waste heat in the CSP plant is smaller than for geothermal plants and power plants on natural gas, but it is higher in relation to coal-fired and oil-fired power plants.

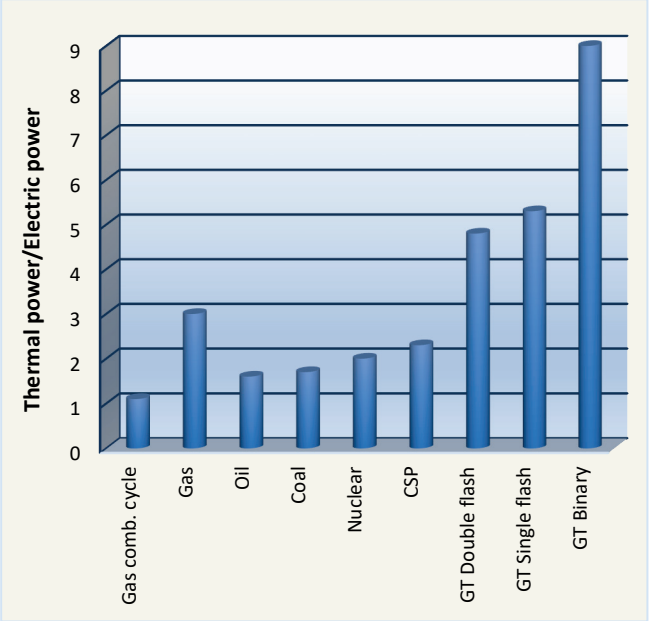

Figure 6 Waste heat (MWt) per unit of electric capacity (MWe) for different processes of power generation [12]

Recently, it became very popular to utilize waste heat in various ways. One application where the heat from CSP could be used is desalinization. This is particularly important for regions with high irradiation that are suitable for CSPs and are faced with a serious deficit of fresh water. Scientists find that in a co-generation plant, where CSPs apply supercritical carbon dioxide cycle, the power cycle could be combined with thermal desalination using waste heat. The desalination process uses only the waste heat because the s-CO_2 cycle rejects heat at 70 °C, the temperature required to integrate with the desalination system.

Additional opportunities for wasted heat use may exist in the industrial sector to meet either the heating needs or cooling purposes.

2.6 Heat Transfer Fluids, Emissions to Soil and Water

The influence of HTF is manifested in the leaking or emitting into the soil, groundwater and surface water, air and human presence. Linear Fresnel, parabolic trough and parabolic dish technologies have a large number of collectors in the solar fields connected by pipelines that contain HTF and therefore occupy a large area. That large part of the surface is under the potential influence of HTF leakage. This fact indicates that the use of HTFs can be dangerous for the environment.

Small leakage (mainly due to evaporation) and accidental spillage may occur at the plant, so effective protection measures should be organized. Leaking not only affects the environment but also the health of people.

Because of this, people must be trained for possible accidents to minimize the impact on nature and humans and all the necessary protective equipment and equipment must be provided.

This aspect is less problematic for the area of heat storage and the area of process equipment due to small area

occupancy. In this case, the inspection surfaces are more accessible and it is possible to place protective surfaces against the ground to prevent significant groundwater contamination if HTF or Heat Storage Media (HSM) is leaking. The central tower system is considered as the middle case, whereby the height of the tower can facilitate dispersion on the large area around the tower. Accidental leakage can occur during HTF circulation in some areas that are not protected by insulation, e.g. the central receiver.

If the CSP plant is placed in a populated place, e.g. on the roof of a building and serves for cogeneration or trigeneration, special attention must be paid to HTF.

2.6.1 Synthetic Oil

Parabolic trough power plants in Spain and California show some leakages of the synthetic oil used in the receiver. The leakage indicator is in the characteristic smell of HTF. Leaks are reduced by new connection elements (ball joints), while soil pollution is recovered by microbial remediation or by removing and replacing large amounts of soil. In areas with surface ponds or shallow groundwater, synthetic oil contaminates the soil and penetrates very quickly in the water to which it is very poisonous. This fact suggests that synthetic oil should be prohibited in the area of very vulnerable aquifers.

2.6.2 Alternative HTFs

HTFs for high-temperature areas have high priority in global research [13]. The results of the research in the past years have led to new systems that do not require synthetic oil, but directly use water/steam as HTF, such as DSG (direct steam production), gases or molten salt mixtures in direct/indirect systems.

Besides the environmental safeguard, the choice of the HTF has various constraints: performances, costs, and plant efficiency. This requires a compromise to meet quality solutions.

Other options involve advanced HTFs, including:

- Pressurised gas, currently under testing
- Systems where molten salt is directly used in solar collectors and energy storage systems, e.g. in a demo plant in Archimedes, Italy
- Use of dense gas-particle suspensions (approximately 50% of solid) in tubes as HTF. This HTF behaves as a liquid with a wide operating temperature range. It remains in a liquid state at almost any temperature (does not freeze) and allows a working temperature increase up to 700 °C and above.
- Adding nanoparticles to the above-mentioned fluids will result in nanofluids that greatly enhance physical and transport properties and have a positive impact on the environment.
- Use of special additives in order to reduce the melting point for molten salt mixtures. The nitrate salts $NaNO_3$ and KNO_3 of the TES are mainly (at about 60%) natural products mined in northern Chile, and the rest are from the chemical industry. Even if the main part of this salt is a natural mineral material, it leaves a significant environmental footprint due to energy consumed for mine extraction, transportation, salt processing and application in TES [14].

2.7 Materials in CSP Plants

CSP plants use a lot of working materials inside their system, far more than the conventional fossil fuel power plants. The main materials used are most often steel, glass, and concrete with a relatively high recycling rate, typically over 95%. Materials that cannot be recycled are mostly inert and can be used for road building or can be land-filled safely. However, there are several toxic materials (compounds) found within the CSP system, most often synthetic organic compounds such as biphenyls and biphenyl ether used in the heat transfer system. These compounds can cause a fire and may, during leakage in the system, reach the ground through which they can reach other parts of the environment and need to be treated as hazardous waste. From the soil, poisonous compounds can be absorbed by plants, and by eating these plants, animals can also absorb them. One of the ways in which they try to solve toxic materials is by replacing them with water or molten salts.

2.8 Impacts on Flora and Fauna

Impacts of CSP plants on the local environment may be associated with creating access roads, building works, and ecosystem disturbance. Construction of facilities, roads and car parks causes the destruction of the local fauna. The extent of destruction depends on the area affected and the type of land use before the construction of the plant.

Construction of the plant can lead to fragmentation of the habitat, which means that species lose the optimal integrity of the ecosystem for their survival. The power plant uses environmental resources (water), thereby reducing the resources necessary for the plants and animals that live there. In Mediterranean areas, plants that are drowned due to lack of water can also contribute to the risk of fire over plants directly affect the vertebral mortality in two ways: collision with the upper parts of the plant (especially with the central tower) and heat stroke or combustion of the surrounding area resulting from the reflection of concentrated solar radiation [15]. Birds rarely collide with the tower of the plant when the visibility is good, but with reduced visibility, a greater number of dead birds have been recorded. Birds can also replace reflective water surface mirrors and, when being convinced of diving into the water, collide with them and become injured. During the operational phase it was noted that the plant and animal world gradually adapt to the new environment. For example, some dwarves are trying to build a nest on the heliostat, and the turkeys returned and feed in the vegetation of the heliostat field.

Building power plants may be a barrier to migratory pathways to local plant and animal populations and thus their chances of survival may be reduced. Likewise, there may be an increase in the number of invasive species to that area. When transporting equipment and materials for the

construction of a plant, the site can be introduced to invasive alien species or species whose natural habitat is not in this ecosystem. Invasive foreign species often have the ability to rapidly propagate and spread and then pose a major threat to domestic species.

Collector arrays in CSP plants affect the profile of wind flow. The mean wind speed is drastically reduced, and the kinetic energy of turbulence grows within the collector field. Reducing wind speed is of great benefit because speed is of primary importance for the desert spread. That is, the collector field acts beneficially in soil protection from erosion.

The collector field in CSP plants also has an influence on the soil temperature below the collector. Depending on where the plant is built, the temperature of the soil in winter may be several °C higher and during the spring and summer several °C lower than the soil temperature outside the collector field (according investigation of Zhiyong Wu et al. [16] in Yanqing, China, temperature difference was from 0.5 °C to 4 °C).

2.9 Potential Noise Sources

Noise from the solar power plant is not significant compared to other types of power plants, such as conventional coal, wind power generation, and gas turbine power plants. The noise from the generating plant of the large-scale trough, Fresnel and power tower plants is unlikely to cause any disturbance to the public since the power block is invariably located at the centre of a large solar field, far from the facility boundary. The effects of noise are greater in the construction phase of the plant, but this impact can be mitigated with the adoption of good work practices. According to the items listed below, the noise is generated in the operation of the plant due to:

- Boiler start-up and operating noises
- Salt and water pumps
- Cooling fans
- Stirling engines
- Waste Water Treatment operations
- Service vehicles (for cleaning mirrors)
- Power transformer noises and
- Transmission line noises.

In the variant of the use of CSP cogeneration and trigger systems, collectors can be placed on the roofs of buildings or factory halls. For this case of CSP application, noise can, though not large, potentially pose a problem for the tenants of the building.

2.10 Visual Intrusion

It is very important to carefully select the location of the solar thermal power plant, as this will be closely related to the visual impact. Due to specific operating requirements of these types of systems, CSP plants are typically placed in regions with a small demographic density and very small visual impact may be introduced as far as natural reserves are avoided. The solar tower system makes a higher visual impact than technologies such as the parabolic trough, dish Stirling and Fresnel, due to the height of the central tower. In terms of new trends in the use of CSP cogeneration and trigeneration systems, collectors can be placed on the roofs of buildings. In this case, the CSP system have a significant visual impact.

3 CONCLUSION

There are different factors that influence the CSP environmental profile, including location, size, applied technology and materials (for construction, HTF, etc.), water use, land use, operation and maintenance needs, etc.

Despite the fact that this kind of power plant has a negative impact on the environment, it is obvious that CSP plants have much better ecological performance than today's fossil power plants. Since they do not use any fuels, there are no oil spillage or methane leaks. On the other hand, the use of materials such as concrete, steel, and glass means the possibility of their recycling.

The problems that need to be solved are the water demand in the dry areas, the use of toxic synthetic oils as a heat transfer fluid and the use of pesticides to limit the growth of vegetation in heliostat fields. For all these problems, there are technical solutions or they are in the development phase.

The impacts of certain applied technologies on the environment are different. Although some CSP technologies are commercialized, they are less mature than conventional fossil fuel power plants. Due to the great interest in this area and the increasing number of research, significant improvements in the efficiency of these systems can be expected, with less environmental impact.

As far as CSPs are concerned, there is a need for further research into Stirling's systems, the effects of storage materials on the ecological profile of the entire CSP plant, water-saving strategies in the cooling system, the application of the Brayton cycle and the application of hybrid solar power plants.

4 REFERENCES

[1] Palgrave, R. (2008). Innovation in CSP. *Renewable Energy Focus, 9*(6), 44-49. https://doi.org/10.1016/S1755-0084(08)70066-8

[2] Mehos, M. at al. (2017). Concentrating Solar Power Gen3 Demonstration Roadmap, Technical Report NREL/TP-5500-67464. https://www.nrel.gov/docs/fy17osti/67464.pdf

[3] Giostri, A., Binotti, M., Astolfi, M., Silva, P., Macchi, E., Manzolini, G. (2012). Comparison of different solar plants based on parabolic trough technology, *Solar Energy*, 86 (5) 1208-1221. https://doi.org/10.1016/j.solener.2012.01.014

[4] Cioccolanti, L., Villarini, M., Tascioni, R., & Bocci, E. (2017). Performance assessment of a solar trigeneration system for residential applications by means of a modeling study. *Energy Procedia*, 126, 445-452. https://doi.org/10.1016/j.egypro.2017.08.211

[5] Ong, S., Campbell, C., Denholm, P., Margolis, R., & Heath, G. (2013). Land-Use Requirements for Solar Power Plants in the United States, Technical Report NREL/TP-6A20-56290

[6] Turchi, C., Mehos, M., Ho, C., & Kolb, G. (2010). Current and Future Costs for Parabolic Trough and Power Tower Systems

in the US Market. NREL/CP-5500-49303. Golden, CO: National Renewable Energy Laboratory.
[7] Burkhardt, J. J., Heath, G. A., & Turchi, C. S. (2011). Life Cycle Assessment of a Parabolic Trough Concentrating Solar Power Plant and the Impacts of Key Design Alternatives. *Environmental Science & Technology*, 45(6), 2457-2464. https://doi.org/10.1021/es1033266
[8] Cho, A. (2010). Energy's tricky tradeoffs. *Science*, 329 (5993), 786-787. https://doi.org/10.1126/science.329.5993.786
[9] Burkhardt, J. J., Heath, G., & Cohen, E. (2012). Life Cycle Greenhouse Gas Emissions of Trough and Tower Concentrating Solar Power Electricity Generation. *Journal of Industrial Ecology*, 16, S93-S109. https://doi.org/10.1111/j.1530-9290.2012.00474.x
[10] Arvizu, D. P., Balaya, L., Cabeza, T., Hollands, A., Jäger-Waldau, M., Kondo, C., Konseibo, V., Meleshko, W., Stein, Y., Tamaura, H., & Xu, R. Z. (2011). In IPCC Special Report on Renewable Energy Sources and Climate Change Mitigation Cambridge, United Kingdom and New York, NY, USA: Cambridge University Press.
[11] Kommalapati, R., Kadiyala, A., Shahriar, M., & Huque, Z. (2017). Review of the Life Cycle Greenhouse Gas Emissions from Different Photovoltaic and Concentrating Solar Power Electricity Generation Systems. *Energies*, 10(3), 350. MDPI AG. https://doi.org/10.3390/en10030350
[12] Rybach, L. (2005). Environmental Aspects of Geothermal Energy Development and Utilisation and Related Legal, Institutional and Social Implications. *World Geothermal Congress (WGC 2005)*. Pre and Post Congress Short Courses. Izmir and Antalya, Turkey, April 2005.
[13] Srivastva, U., Malhotra, R. K., & Kaushik, S. C. (2015). Recent Developments in Heat Transfer Fluids Used for Solar Thermal Energy Applications. *Journal of Fundamentals of Renewable Energy and Application*, 5, 189. https://doi.org/10.4172/2090-4541.1000189
[14] Py, X., Sadiki, N., Olives, R., Goetz, V., & Falcoz, Q. (2017). Thermal energy storage for CSP (Concentrating Solar Power). *The European Physical Journal Conferences*, 148, 00014. https://doi.org/10.1051/epjconf/201714800014
[15] Hernandez, R. R., Easter, S. B., Murphy-Mariscal, M. L., Maestre, F. T., Tavassoli, M., Allen, E. B., Barrows, C. W., Belnap, J., Ochoa-Hueso, R., Ravi, S., & Allen, M. F. (2014). Environmental impacts of utility-scale solar energy. *Renewable and Sustainable Energy Reviews*, 29, 766-779. https://doi.org/10.1016/j.rser.2013.08.041
[16] Zhiyong, Wu, et al. (2014) Environmental impacts of large scale CSP plants in northwestern China, *Environmental Science: Processes and Impacts*, 16, 2432-2441. https://doi.org/10.1039/c4em00235k

Authors' contacts:

Mladen BOŠNJAKOVIĆ, PhD, Assistant Professor
(Corresponding author)
College of Slavonski Brod
Dr. Mile Budaka 1
35000 Slavonski Brod, Croatia
mladen.bosnjakovic@vusb.hr

Vlado TADIJANOVIĆ
Rastušje 42
35107 Podvinje, Croatia
vlado.tadijanovic1@inet.hr

ISSN 1846-6168 (Print), ISSN 1848-5588 (Online)
https://doi.org/10.31803/tg-20180629110602

Professional paper

PROPOSAL FOR A WEB PORTAL MANAGING REGISTRATION FOR STUDENT ACCOMMODATION IN A DORMITORY

Ivor PODUNAVAC, Dominika CRNJAC MILIĆ, Krešimir NENADIĆ

Abstract: A proposal for developing a database model and a web portal for managing registration for student accommodation in a dormitory is given in this paper. The portal has two user profiles and corresponding functionalities; they are intended for users/students and administrators, respectively. In the process of application for student accommodation in a dormitory, every student has to provide data referring to GPA, i.e. academic achievement at school, level of education, university, parents' status, household members, the number of siblings and their school age, and household monthly income. There are also extra conditions that could ensure direct allocation of accommodation at a dormitory. After the application process deadline has expired, the administrator can either accept or decline applications. At the end of the application process, the final ranking list can be published and made accessible. Advantages of using a web portal for the dormitory accommodation election and application process are e.g. better accessibility and the fact that students are exempt from delivering the necessary application documentation personally. In that way, costs are reduced, efficiency at work is increased and the possibility of making errors when entering and processing data is significantly lower.

Keywords: application; database model; dormitory; student; web portal

1 INTRODUCTION

This paper describes the process of development and utilization of a web portal. The developed web portal enables easier application process to potential candidates for student accommodation in a dormitory. Web portal also enables the ranking process, which creates final ranking list of possible dormitory beneficiaries according to the rent price. The ranking is calculated according to high school average grade or passed exams, achieved ECTS (European Credit Transfer and Accumulation System) points, year of studying, social status, etc.

The second section gives a short overview and analysis of current methods of ranking students.

The third section presents technologies used to develop database and web portal.

The fourth section explains development process and related functionalities in web portal.

The fifth section concludes this paper.

This paper is a result of a student graduate thesis written by Ivor Podunavac at Josip Juraj Strossmayer University of Osijek, Faculty of Electrical Engineering, Computer Science and Information Technology in Osijek, Croatia. [1]

2 SHORT OVERVIEW

This section of paper will give insight in the manner the applications are handled without support of ICT (Information Communication Technology).

2.1 Current Methods of Ranking Students against Using New Technologies

Throughout the month of July students and future students have the option to apply for a student dormitory accommodation. First-year students and older have to deliver their application documents personally, while prospective students can send their application documents by mail. The first step in applying for student dormitory accommodation is to pick up the application form at the dormitory. The next step is to fill in the application form and include all the other required documents. The application form requires the following data to be filled in:

- student name and last name,
- name of university and faculty student is applying to,
- total number of achieved ECTS credits,
- number of ECTS credits achieved in current academic year of studying,
- certificate of passed exams, and
- whether the studying program is in a science filed that is marked as deficit on the national level.

The web portal developed as a part of student thesis enables insight in all the required conditions in one place. Another advantage of the web portal is in finishing the application in significantly less time than using paper forms, and web portal user's interface is friendlier. This paper will give a short overview of the older paper-form version of the application process for the dormitory. Work efficiency as well as data processing and creating final rang list will be also mentioned.

Advantage of using new technologies in applying for accommodation can have different groups of beneficiaries, for example high school pupils and students.

Major difference in using new technologies during application process is much easier accessibility, lower costs, and all the relevant data can be processed much faster regarding the server. Applicants can use the web portal functionality on any device with internet connection (a computer, a smartphone or a tablet) and they can finish the application process in several minutes. The only presumption is that all the required documents have already been prepared on the device that will be used for the application process.

2.2 Current State of Accommodation

There are 14 dormitories for student accommodation in eight cities throughout Croatia. Student dormitory in Slavonski Brod has the smallest number of beds - 115, while student dormitory "Stjepan Radić" in Zagreb has the largest number of beds – 4,014. Total sum of all available beds in dormitories for student accommodation across the Republic of Croatia is 11,709. Every year the capacity for student accommodation in dormitories across the Republic of Croatia has maximum occupancy. Every year the total number of applications for student accommodation in dormitories scales about 35-40% above the total available capacity (data acquired by direct inquiry in dormitory in Osijek – similar situation in majority of dormitories). Every summer in Croatia between 15,000 and 17,000 students apply for accommodation in dormitory in a way that they supply all the required paper documents to a certain dormitory they want to apply to. That does not depend on their current residence.

There is a tendency to expand capacity to accommodate more students in dormitories. Two new student dormitories have been opened in the academic year 2017/18. One is in Knin, with a maximum capacity of 78 beds (https://www.veleknin.hr/veleknin/web/index.php/Studentski-dom) and the other one is in Virovitica, with a maximum capacity of 108 beds (http://studom.vsmti.hr/o-domu/1/).

There is a web portal of similar type already in use. It is for student accommodation in dormitories at the University of Zagreb [2]. This web portal has restricted access and allows access only for students of the University of Zagreb. Still, majority of dormitories for student accommodation in the Republic of Croatia do not use the type of application process that will be presented later in this paper. Hence, all students applying for student accommodation in dormitory have to enclose all the required paper documents. There is a problem that students from distant places spend more money for travel expenses and they spend more time for the application process. There is a limited number of available beds so it is possible that some students will not get the desired accommodation. The application process starts after all the applicants enclose all the required documents and the closing date expires. Student centre or student dormitory employees register, manage and process all the supplied data in available software solution for the application process. This is the right place to observe efficiency and profitability of current manner of conducting the application process against the way proposed in this paper. Students could perform the process of registration and filling in the data for themselves. Employees would only have to verify the documents supplied through the web portal. Verification process is required to check that all the applicants supplied all the documents to avoid possible rigging (average grade certificate, some kind of disability or incapacity, year of studying, etc.).

Unlike the way students have applied so far, this is more affordable and cost-effective with regard to minimizing student costs associated with applying, time and cost of data processing, as well as greater control of the data entered. In particular, the ease of use of such a web portal can be emphasized. It is sufficient to have access to the internet and that it is possible to complete the entire application for accommodation in the dormitory within several minutes by simple handling.

3 TECHNOLOGIES USED IN DATABASE MODELLING AND WEB PORTAL DEVELOPMENT

Technologies used in database modelling and web portal development are:

- Cascading Style Sheets (CSS) for styling the content a user can see,
- HTML (HyperText Markup Language) for setting content,
- PHP (PHP: Hypertext Pre-processor) as a server side scrip language to perform all thr functionalities,
- JavaScript (JS) for manipulating and verifying data on the client side, and
- MySQL (Structured Query Language) for manipulating data in the database.

3.1 HyperText Markup Language

HTML is simple to use and easy to learn and these are the main reasons of its worldwide acceptance and popularity. It is intended to be free to use f or any user from its very beginning. Web browsers are applications available to parse and present content from HTML documents [3]. HTML is not a programming language, nor the people using it are programmers. It is simply used to create HTML documents that contain some information for users.

3.2 Cascading Style Sheets

CSS is language for styling content in HTML documents that will be presented to the user in a web browser. [4] CSS can be used to have an impact on the view of particular document elements, such as images, links, text, or the whole page and even on arranging element positions. Styles are usually organized in external files separated from HTML document. In this way, the visual identity of more HTML documents can be changed by editing and changing single CSS document. External CSS files allow more flexibility and control in arranging the document's presentation.

3.3 PHP - Hypertext Pre-processor

PHP is an open-source server-side script language. It allows HTML code to be dynamically generated. Open-source means that anybody may download PHP source code written in programming language C and add new functionalities. PHP is one of the most widely used server-side script languages.

Entire PHP source code has to be written between tags `<?php` and `?>`. There are no restrictions on how many times PHP tags can be used in a PHP document. One has to be careful when using PHP tags to correctly use the opening (`<?php`) and closing tags (`?>`).

3.4 MySQL

MySQL is a free to use, open-source database management system. SQL is a structured language used to generate queries into a database. MySQL databases are of relational type because it is proved to be the best way of storing and searching a vast amount of data. SQL database is the base of almost every information system, i.e. the base of every business subject that needs availability and quality of information.

Every MySQL database can have more than one user with available access. Every user can have predefined access rights. In this manner, good database access settings can significantly reduce the possibility of errors. MySQL as a database management system can operate on wide variety of operating systems. [5]

3.5 Bootstrap Framework

Bootstrap is a free development framework that can make creating a web portal easier. It consists of templates written in HTML and CSS for different components of graphical user interface, as well as JavaScript extensions. That is why it is called a development framework for web applications.

It is compatible with all the web browsers. Some of advantages using Bootstrap in a web portal development are as follows: easier and faster development, easier implementation of web forms, supported responsive design, and its ease of use. There are some deficiencies, such as visual similarities between web applications developed using Bootstrap, library reloading every time a web page is reloaded which leads to slower page loading.

It is not necessary to use Bootstrap in a web page development, but it can save time if a developer uses it.

3.6 JavaScript - Client Side Script Language

JavaScript is the most popular client-side script programming language. It was created with a goal to introduce interactivity to HTML documents. All web browsers support it. Netscape developed JavaScript in 1996. It is interpreting script language, which means that the script code is executed one instruction at a time without compiling whole script code and creating executable file.

JavaScript code is executed on the client side. Code written in JavaScript can be placed in HTML document between tags `<script>` and `</script>` inside the document's head element or inside the body tags. JavaScript code can also be written as an outside code in separate ***.js*** file and included (called) from any HTML document linked to it. [6]

4 WEB PORTAL DEVELOPMENT

This web portal supports two operating modes: user mode and administrator mode. Both are explained further in this section.

4.1 Database Structure

Database is created to enable storing and accessing data for the web portal. All the required information is stored in tables in the database. Database used in this web application is called *studentskidom* (*student dormitory*) and consists of four tables. Tables *rezultati* (*results*) and *dokumenti* (*documents*) have a foreign key referring attribute ID in table *korisnici* (*users*). Foreign key ensures database integrity and prevents deleting data from other tables where foreign key from this table is the primary key in another table. There can be only one primary key per table. Column in the table tagged as primary cannot be empty and has to be unique for the designated table. Primary key value is automatically auto incremented one by one upon inserting a new row into the table. Column (attribute) *idKor* in the table *rezultati* (*results*) is the foreign key and points out the user who applies for student dormitory accommodation. Similar table organization is for table *dokumenti* (*documents*).

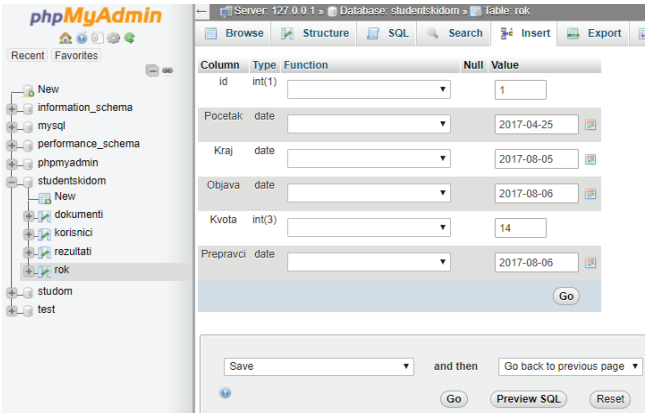

Figure 1 Table *rok* (*deadline*) in database modelled in ***phpmyadmin*** application

Fig. 1 shows the database table *rok* (*deadline*) modelled in free PHP application ***phpmyadmin***. All the tables in database are modelled with the same application because it has a user-friendly interface and it has no requirements for any specific foreknowledge concerning programming.

Table *rezultati* (*results*) stores data about students applying for accommodation (year of studying, faculty, score for each category).

Table *korisnici* (*users*) contains attributes *id*, *name*, encrypted password and unique code given to the user upon registration. Unique code distinguishes users rather than the first and the last name. This mechanism ensures transparency of ranking students who can find and recognize only their result by the given unique code.

Table *dokumenti* (*documents*) consists of document's names attached by the student in the application process. Uploaded documents ensure validity of all the relevant data during the application process. Each document is named according to the unique code given to the user by the web portal.

4.2 User Registration

Before using the web portal, it is necessary to finish the registration process. After the user correctly fills in the required data, they become a registered user and can login and use the web portal's functionality. As mentioned earlier, every new user receives a unique *ID* by calling *uniqid()* function. This function generates a string of characters based on the current system time. During the registration process the user can select their status – a high school graduate or student because there is a difference whether they apply for the first time as a high school graduate or as an older student.

Every user has to enter password required for login to the web portal. The passwords are encrypted by hashing thus making them unrecognizable to other users, including web administrator as well.

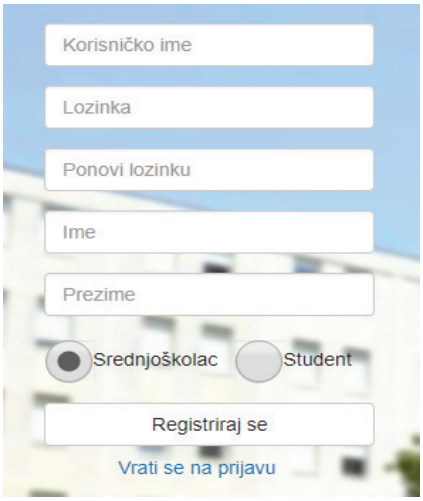

Figure 2 Web portal registration form

Figure 2 shows the registration form included in the web portal. The data required for registering are visible on the register form.

4.3 Accommodation Application Process

Portal home page requires user to enter the username and the password. In the case the user enters valid information (the user is registered and password is correct for that user), the portal will redirect the user to the page for filling in the required data during the application process for student accommodation in the dormitory.

During the login process, every user is assigned to their own session, which differs from other sessions by logged username. Existence of session data is checked in each server-side script. When the session data do not exist, the user is redirected to the login page.

4.4 User Mode Functionality

The user can access the portal's functionalities after the successful login. There is an option to access personal data and fill in the main form. Here is an option for uploading the required documents. Option for dormitory provides basic information about two dormitories for student accommodation in Osijek. A registered user can find results here if the ranking process is completed.

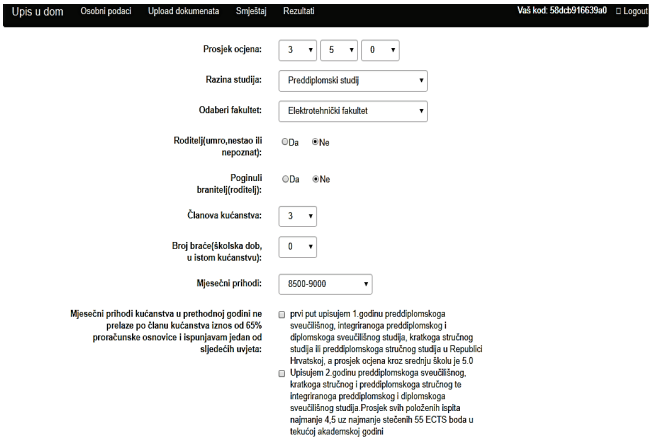

Figure 3 Personal data web form

The web page for personal data filling in process consists of a form that requires filling in the average grade, the level of education (high school graduate or student), the faculty, parents (both parents alive or just for one parent), the number of residents in domicile household, the number of siblings that are pupils or students, and the parents' monthly total income. There are conditions that ensure direct accommodation in the dormitory (a student without both parents, a parent killed in war – both for students with 4.0 or higher average grade, etc.). If the applicant meets some of the above listed conditions, it is required to confirm their status by uploading relevant documents. An applicant can change personal data until the application process deadline expires. The web portal has a functionality that checks all the relevant data by cross-referencing uploaded documents. If the student's application is not valid, there is a short period for making required changes and upload missing documents.

The application form for student accommodation in dormitory has to be filled in as well, alongside the check of all the necessary uploaded documents. The web portal can check ECTS points to ensure the student has the minimum number of ECTS points to apply for student accommodation in a dormitory. The Ministry of Science and Education prescribes the minimum number of required ECTS points.

The required documents have to be in digital form in order to upload them to the server. There can be restrictions to the form of required documents, like PDF (Portable Document Format) or word document (doc or docx).

4.5 Ranking Results

The publication of results is expected in several days after the final deadline expires. All applicants can check and enclose any missing documents in the case administrator rejected the application due to incomplete application data or documentation. The whole process of calculating and ranking applicants is completely automated and performed by PHP server-side scripts.

The applicant can achieve additional 200 points by applying to deficit professions designated by the Ministry of Science and Education.

If the applicant does not have one parent, they can achieve additional 600 points. If they are a child of a defender killed in war, they can achieve additional 200 points.

Each sibling adds additional 150 points. A number of residents in domicile household has to be filled in in the application. If the total income per residence is less than 500 HRK, the applicant achieves the maximum number of 750 points in this part of the application. The number of achieved points is decreased until total house holding income becomes less than 65% of prescribed budget base. If the total house holding income is greater than 1,900 HRK and less than 65% of prescribed budget base (2,162 HRK in the time the web portal was developed), the applicant will achieve the minimum number of 75 points. If the total household income is greater, the applicant will not achieve any points in this category.

Based on the criteria for direct accommodation, each applicant can choose one of the listed conditions, corroborate selected condition by uploading relevant documents related to it, and thus achieve direct accommodation in dormitory regardless the number of achieved points.

There is a PHP server-side script that calculates achieved points based on the applicant's average grade. After this calculation is completed, all points from different categories are added to the total number of achieved points. Ranking list is calculated after the application deadline expires and all the applicant's points are calculated.

There is a PHP function (`prosSum()`) that calculates points for all faculties and for all applicants that are at the same year of studying.

All applications have to be validated by the administrator by checking all the uploaded documents and cross-referencing them with appropriate categories in each applicant's form.

There is a small difference between high school graduate applicants and applicants that are already students. The difference is in the way the points are calculated.

There are two attributes in the table *rezultati* (*results*) – *Pregledan* (*inspected*) and *Valid*. Their default values are set to '0' (zero). After the administrator examines applicant's data and documents, the decision to reject or accept application is made. If the application is rejected, the applicant has several days to complete the application and upload missing documents and fill in the required data.

Figure 4 shows the table for some test application data. The majority of applied users were successful to apply for student accommodation in dormitory, but there are two unsuccessful applications. There were 14 vacancies, which means that 14 applicants will achieve accommodation in the dormitory. Applicants that have direct student accommodation in the dormitory are at the top of the ranking list followed by the rest of applicants ranked by the achieved points. As can be sseen, there are no names on the ranking list but unique IDs provided by the web portal.

Upis u dom | Osobni podaci | Upload dokumenata | Smještaj | Rezultati | Vaš kod: 58eb471351e08 | Logout

	Kod	Prosjek	Deficitarna zanimanja	Bez roditelja	Poginuli branitelj(roditelj)	Braće	Prihodi	Ukupno	Izravan upis	Status
1	58e784af85e4c	784.586	0	600	0	150	0	1534.586	Da	PRIMLJEN
2	5877ddd298a86	1108.483	200	0	0	150	0	1458.483	Da	PRIMLJEN
3	58e4d208ae2b8	1000	0	0	0	0	375	1375	Da	PRIMLJEN
4	58c9969382a89	1089.727	0	600	0	300	525	2514.727	Ne	PRIMLJEN
5	590af750bf6e7	1000	200	600	0	150	225	2175	Ne	PRIMLJEN
6	58e68f087bd6d	924.126	200	600	0	150	225	2099.126	Ne	PRIMLJEN
7	58eb471351e08	884.634	200	0	0	600	375	2059.634	Ne	PRIMLJEN
8	58eb4777d811f	1000	0	600	0	150	300	2050	Ne	PRIMLJEN
9	58eb48e067bbc	1095.261	200	0	0	450	300	2045.261	Ne	PRIMLJEN
10	58c7fc3e0ae21	1260.504	0	0	0	300	375	1935.504	Ne	PRIMLJEN
11	58e4e0828b395	856.444	200	600	200	0	0	1856.444	Ne	PRIMLJEN
12	5877d05852815	1082.569	200	0	0	150	375	1807.569	Ne	PRIMLJEN
13	58e783d0771a4	846.339	0	600	200	150	0	1796.339	Ne	PRIMLJEN
14	58b6a0c075100	1000	0	600	0	150	0	1750	Ne	PRIMLJEN
15	58c7bbe2a98f6	893.157	0	600	200	0	0	1693.157	Ne	NIJE PRIMLJEN
16	5877cf4120383	1172.529	200	0	0	300	0	1672.529	Ne	NIJE PRIMLJEN

Figure 4 Test data rank list

4.6 Administrator Mode Functionalities

An administrator (or administrators) is (are) logged to the web portal as any other user. Authorisation is performed by checking the entered username and password against the data in the users table in database. Fig. 5 shows starting the web page after the administrator is successfully logged in.

Figure 5 Start web page for administrator(s)

The administrator can set options for starting and closing date, incomplete correction deadline date, publishing ranking list date and number of vacancies in dormitory according to the deadline published in the newspapers.

After the applicant has fulfilled all their relevant data and uploaded all the required documents, it remains to wait for expiration deadline date if the application was successful and complete.

4.6.1 Registered Applicants' Checklist

A registered applicants' checklist can be observed as a waiting list. The administrator can see applications rejected due to incomplete documentation or missing data. If the applicant completes their application by uploading additional required documents or filling in the missing data, administrator can confirm the application afterwards. The

opposite result would be rejecting the application because of incomplete documentation or missing data.

If the administrator rejects the application, a popup window will show requiring the administrator to enter additional explanation. This explanation will be shown to the applicant the next time they log in the web portal. The final deadline to complete the application will be shown as well.

Fig. 6 shows the list of applicants the way an administrator can see it. There are lists of documents organized in columns (as shown in Fig. 6) and the administrator can open attached documents (*Otvori*), accept (*Prihvati*) or reject (*Odbij*) the application.

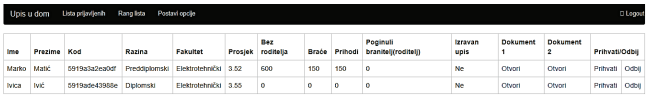

Figure 6 List of applications with relevant actions: open (Otvori), accept (Prihvati) and reject (Odbij)

A ranking list is created and shown in the *Rang lista* (*Ranking list*) option in the menu after the deadline date expires. All applications accepted by the administrator will be shown in the ranking list.

5 CONCLUSION

The developed web portal offers simplicity and a user-friendly environment because it can be accessed by using any available web browser on any device connected to the Internet. The web portal was developed by using modern web technologies like CSS, HTML, PHP, JavaScript, and MySQL was used for database management. This web portal is ready to be used for dormitories in Osijek and with minor changes, it can be used for any student or any high school dormitory.

There are several advantages of using the developed web portal, e.g. applicants are not required to personally deliver their application forms and the required documents; a smaller number of Student Centre employees is required to check out the applications; the process of creating a ranking list is automated and it is performed almost instantly, to name a few.

There is a possibility of communication between applicants and web application administrators by exchanging messages. This enables applicants to be informed of any change in the application process.

The only requirement this web portal imposes is Internet connection. This can be considered as a drawback, but there is a greater number of advantages. Unlike today's application to high school and student dormitories, this approach is more available and cost-efficient. It minimizes the data processing time and the cost of human resources engaged in manually filling in the required data from documentation. It also reduces student costs (e.g. transport) and the possibility of entering incorrect data in the web form.

6 REFERENCES

[1] Podunavac, I. (2017). Model i programska podrška za rangiranje studenata pri upisu u studentski dom (in Croatian), *graduate thesis*, Josip Juraj Strossmayer University of Osijek, Faculty of Electrical Engineering, Computer Science and Information Technology in Osijek. https://zir.nsk.hr/islandora/object/etfos%3A1400
[2] See https://natjecaj.sczg.hr/student
[3] See https://www.mojwebdizajn.net/skriptni-jezici/vodic/html/uvod-u-html.aspx
[4] See https://www.w3.org/Style/CSS/Overview.en.html
[5] See http://php.com.hr/77
[6] See http://razno.sveznadar.info/10-doc-PDF/2_MySQL.pdf
[7] Haverbeke, M. (2011). *Eloquent JavaScript: A Modern Introduction to Programming*, William Pollock, San Francisco.

Authors' contacts:

Ivor PODUNAVAC
Josip Juraj Strossmayer University of Osijek
Faculty of Electrical Engineering, Computer Science and Information Technology in Osijek
Kneza Trpimira 2B, 31000 Osijek, Croatia
ivor.podunavac@etfos.hr

Dominika CRNJAC MILIĆ, Full Professor
Josip Juraj Strossmayer University of Osijek
Faculty of Electrical Engineering, Computer Science and Information Technology in Osijek
Kneza Trpimira 2B, 31000 Osijek, Croatia
+385 31 224 681, dominika.crnjac@ferit.hr

Krešimir NENADIĆ, Associate Professor
Josip Juraj Strossmayer University of Osijek
Faculty of Electrical Engineering, Computer Science and Information Technology in Osijek
Kneza Trpimira 2B, 31000 Osijek, Croatia
+385 31 495 429, kresimir.nenadic@ferit.hr

ISSN 1846-6168 (Print), ISSN 1848-5588 (Online)
https://doi.org/10.31803/tg-20.....

14pt
14pt

ARTICLE TITLE ONLY IN ENGLISH (Style: Arial Narrow, Bold, 14pt)

14pt

Ivan HORVAT, Thomas JOHNSON (Style: Arial Narrow, Bold, 11pt)

11pt
11pt

Abstract: Article abstract contains maximum of 150 words and is written in the language of the article. The abstract should reflect the content of the article as precisely as possible. TECHNICAL JOURNAL is a trade journal that publishes scientific and professional papers from the domain(s) of mechanical engineering, electrical engineering, civil engineering, multimedia, logistics, etc., and their boundary areas. This document must be used as the template for writing articles so that all the articles have the same layout. (Style: Arial Narraw, 8pt)

8pt

Keywords: keywords in alphabetical order (5-6 key words). Keywords are generally taken from the article title and/or from the abstract. (Style: Arial Narraw, 8pt)

10pt
10pt

1 ARTICLE DESIGN
(Style: Arial Narrow, Bold, 10pt)

10pt

(Tab 6 mm) The article is written in Latin script and Greek symbols can be used for labelling. The length of the article is limited to eight pages of international paper size of Letter (in accordance with the template with all the tables and figures included). When formatting the text the syllabification option is not to be used.

10pt

1.1 General guidelines
(Style: Arial Narrow, 10pt, Bold, Align Left)

10pt

The document format is Letter with margins in accordance with the template. A two column layout is used with the column spacing of 10 mm. The running text is written in Times New Roman with single line spacing, font size 10 pt, alignment justified.

Article title must clearly reflect the issues covered by the article (it should not contain more than 15 words).

Body of the text is divided into chapters and the chapters are divided into subchapters, if needed. Chapters are numbered with Arabic numerals (followed by a period). Subchapters, as a part of a chapter, are marked with two Arabic numerals i.e. 1.1, 1.2, 1.3, etc. Subchapters can be divided into even smaller units that are marked with three Arabic numerals i.e. 1.1.1, 1.1.2, etc. Further divisions are not to be made.

Titles of chapters are written in capital letters (uppercase) and are aligned in the centre. The titles of subchapters (and smaller units) are written in small letters (lowercase) and are aligned left. If the text in the title of the subchapter is longer than one line, no hanging indents.

10pt

Typographical symbols (bullets), which are being used for marking an item in a list or for enumeration, are placed at a beginning of a line. There is a spacing of 10pt following the last item:

- Item 1
- Item 2
- Item 3

10pt

The same rule is valid when items are numbered in a list:

1. Item 1
2. Item 2
3. Item 3

10pt

1.2 Formatting of pictures, tables and equations
(Style: Arial Narrow, 10pt, Bold, Align Left)

10pt

Figures (drawings, diagrams, photographs) that are part of the content are embedded into the article and aligned in the centre. In order for the figure to always be in the same position in relation to the text, the following settings should be defined when importing it: text wrapping / in line with text.

Pictures must be formatted for graphic reproduction with minimal resolution of 300 dpi. Pictures downloaded from the internet in ratio 1:1 are not suitable for print reproduction because of unsatisfying quality.

10pt

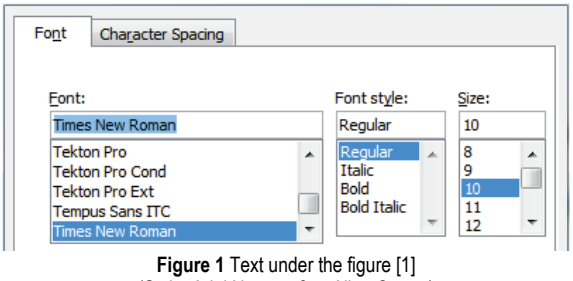

Figure 1 Text under the figure [1]
(Style: Arial Narraw, 8pt, Align Centre)

10pt

The journal is printed in black ink and the figures have to be prepared accordingly so that bright tones are printed in a satisfactory manner and are readable. Figures are to be in colour for the purpose of digital format publishing. Figures in the article are numbered with Arabic numerals (followed by a period).

Text and other data in tables are formatted - Times New Roman, 8pt, Normal, Align Center.

When describing figures and tables, physical units and their factors are written in italics with Latin or Greek letters,

while the measuring values and numbers are written upright.
10pt

Table 1 Table title aligned centre
(Style: Arial Narraw, 8pt, Align Centre)

	1	2	3	4	5	6
ABC	ab	ab	ab	ab	ab	ab
DEF	cd	cd	cd	cd	cd	cd
GHI	ef	ef	ef	ef	ef	ef

10 pt

Equations in the text are numbered with Arabic numerals inside the round brackets on the right side of the text. Inside the text they are referred to with equation number inside the round brackets i.e. ".... from Eq. (5) follows ...." (Create equations with MathType Equation Editor - some examples are given below).
10pt

$$F_{\text{avg}}(t,t_0)=\frac{1}{t}\int_{t_0}^{t_0+t}F\big(q(\tau),p(\tau)\big)\,\mathrm{d}\tau, \tag{1}$$

10pt

$$\cos\alpha+\cos\beta=2\cos\frac{\alpha+\beta}{2}\cdot\cos\frac{\alpha-\beta}{2}. \tag{2}$$

10pt

Variables that are used in equations and also in the text or tables of the article are formatted as *italics* in the same font size as the text.

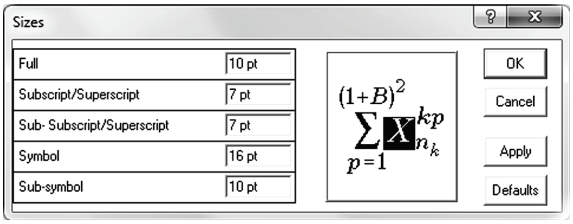

Figure 2 The texts under figures
(Style: Arial Narraw, 8pt, Align Centre)

Figures and tables that are a part of the article have to be mentioned inside the text and thus connected to the content i.e. „ … as shown in Fig. 1…" or „data from Tab. 1…" and similar.
10pt

2 PRELIMINARY ANNOTATION

10pt

Article that is offered for publication cannot be published beforehand, be it in the same or similar form, and it cannot be offered at the same time to a different journal. Author or authors are solely responsible for the content of the article and the authenticity of information and statements written in the article.

Articles that are accepted for publishing are classified into four categories: original scientific papers, preliminary communications, subject reviews and professional papers.

Original scientific papers are articles that according to the reviewer and the editorial board contain original theoretical or practical results of research. These articles need to be written in such a way that based on the information given, the experiment can be repeated and the results described can be achieved together with the author's observations, theoretical statements or measurements.

Preliminary communication contains one or more pieces of new scientific information, but without details that allow recollection as in original scientific papers. Preliminary communication can give results of an experimental research, results of a shorter research or research in progress that is deemed useful for publishing.

Subject review contains a complete depiction of conditions and tendencies of a specific domain of theory, technology or application. Articles in this category have an overview character with a critical review and evaluation. Cited literature must be complete enough to allow a good insight and comprehension of the depicted domain.

Professional paper can contain a description of an original solution to a device, assembly or instrument, depiction of important practical solutions, and similar. The article need not be related to the original research, but it should contains a contribution to an application of known scientific results and their adaptation to practical needs, so it presents a contribution to spreading knowledge, etc.

Outside the mentioned categorization, the Editorial board of the journal will publish articles of interesting content in a special column. These articles provide descriptions of practical implementation and solutions from the area of production, experiences from device application, and similar.
10pt

3 WRITING AN ARTICLE

10pt

Article is written in the English language and the terminology and the measurement system should be adjusted to legal regulations, standards (ISO 80 000 series) and the SI international system of units. The article should be written in third person.

Introduction contains the depiction of the problem and an account of important results that come from the articles that are listed in the cited literature.

Main section of the article can be divided into several parts or chapters. Mathematical statements that obstruct the reading of the article should be avoided. Mathematical statements that cannot be avoided can be written as one or more addendums, when needed. It is recommended to use an example when an experiment procedure, the use of the work in a concrete situation or an algorithm of the suggested method must be illustrated. In general, an analysis should be experimentally confirmed.

Conclusion is a part of the article where the results are being given and efficiency of the procedure used is emphasized. Possible procedure and domain constraints where the obtained results can be applied should be emphasized.
10pt

4 RECAPITULATION ANNOTATION

10pt

In order for the articles to be formatted in the same manner as in this template, this document is recommended for use when writing the article. Finished articles written in MS Word for Windows and formatted according to this

template must be submitted using our The Paper Submission Tool (PST) (https://tehnickiglasnik.unin.hr/authors.php) or eventually sent to the Editorial board of the Technical Journal to the following e-mail address: tehnickiglasnik@unin.hr

The editorial board reserves the right to minor redaction corrections of the article within the framework of prepress procedures. Articles that in any way do not follow these authors' instructions will be returned to the author by the editorial board. Should any questions arise, the editorial board contacts only the first author and accepts only the reflections given by the first author.

10pt

5 REFERENCES (According to APA)

10pt

The literature is cited in the order it is used in the article. Individual references from the listed literature inside the text are addressed with the corresponding number inside square brackets i.e. "… in [7] is shown …". If the literature references are web links, the hyperlink is to be removed as shown with the reference number 8. Also, the hyperlinks from the e-mail addresses of the authors are to be removed. In the literature list, each unit is marked with a number and listed according to the following examples (omit the subtitles over the references – they are here only to show possible types of references):

9pt

[1] See http://www.bibme.org/citation-guide/apa/

[2] See http://sites.umuc.edu/library/libhow/apa_examples.cfm

[3] (Style: Times New Roman, 9pt, according to APA)

[4] Amidzic, O., Riehle, H. J., & Elbert, T. (2006). Toward a psychophysiology of expertise: Focal magnetic gamma bursts as a signature of memory chunks and the aptitude of chess players. *Journal of Psychophysiology, 20*(4), 253-258. https://doi.org/10.1027/0269-8803.20.4.253

[5] Reitzes, D. C., & Mutran, E. J. (2004). The transition to retirement: Stages and factors that influence retirement adjustment. *International Journal of Aging and Human Development, 59*(1), 63-84. Retrieved from http://www.baywood.com/journals/PreviewJournals.asp?Id=0091-4150

[6] Jans, N. (1993). *The last light breaking: Life among Alaska's Inupiat Eskimos*. Anchorage, AK: Alaska Northwest Books.

[7] Miller, J., & Smith, T. (Eds.). (1996). *Cape Cod stories: Tales from Cape Cod, Nantucket, and Martha's Vineyard*. San Francisco, CA: Chronicle Books.

[8] Chaffe-Stengel, P., & Stengel, D. (2012). *Working with sample data: Exploration and inference*. https://doi.org/10.4128/9781606492147

[9] Freitas, N. (2015, January 6). People around the world are voluntarily submitting to China's Great Firewall. Why? Retrieved from http://www.slate.com/blogs/future_tense/2015/01/06/tencent_s_wechat_worldwide_internet_users_are_voluntarily_submitting_to.html
(Style: Times New Roman, 9pt, according to APA)

10pt

10pt

Authors' contacts:

8pt

Full Name, title
Institution, company
Address
Tel./Fax, e-mail

8pt

Full Name, title
Institution, company
Address
Tel./Fax, e-mail

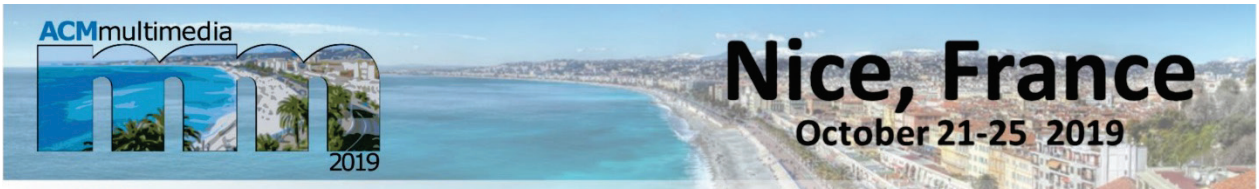

General Chairs
Laurent Amsaleg, CNRS-IRISA
Benoit Huet, EURECOM
Martha Larson, Radboud U.

Program Coordinator
Tat Seng Chua, NUS

Technical Program Chairs
Guillaume Gravier, CNRS-IRISA
Hayley Hung, TU Delft
Chong-Wah Ngo, City U.HK
Wei Tsang Ooi, NUS

Authors' Advocate
Alan Hanjalic, TU Delft

Brave New Ideas Chairs
Yiannis Kompatsiaris, CERTH
Grace Ngai, PolyU

Grand Challenge Chairs
Tao Mei, JD.com
Vivek Singh, Rutgers

Tutorial Chair
Ichiro Ide, Nagoya U.
Giulia Boato, UniTrento

Panels Chairs
Alberto Del Bimbo, U. Firenze
Yu-Gang Jiang, Fudan U.

Workshop Chairs
Yannis Avrithis, Inria
Daniel Gatica Perez, IDIAP

Demo and Video Program Chairs
Qiong Liu, FXPAL
Bart Thomée, YouTube

Doctoral Symposium Chairs
Hervé Bredin, LIMSI
Suzanne Little, DCU

Open Source Chairs
S. Marchand-Maillet, Unige
Klaus Schoeffmann, Klagenfurt U.

Interactive Arts Chairs
Maurice Benayoun, City U.HK
Nathalie Delprat, LIMSI

Sponsorship Chairs
Cathal Gurrin, DCU
Frédéric Jury, GREYC
Qi Tian, Huawei/UTSA

Publicity Chairs
Bogdan Ionescu, PUBucharest
John Smith, IBM TJ Watson
Jinhui Tang, Nanjing U.
Lexing Xie, ANU
Yi Fang, NYU
Silvio J. Guimarães, PUC Minas
Herman Engelbrecht, Stellenbosch U.
Rajiv Ratn Shah, IIIT-Delhi

Web and Social Media Chair
Danny Francis, EURECOM
Dian Tjondronegoro, SCU

Publication Chairs
Wen-Huang Cheng, NCTU

Student Travel Grant Chairs
Chiou-Ting Candy Hsu, NTHU
Georges Quénot, LIG

Culture Chair
Maria Eskevich, CLARIN

Call for Papers

ACM Multimedia is the premier international conference in the area of multimedia within the field of computer science. Multimedia research focuses on integration of the multiple perspectives offered by different digital modalities including images, text, video, music, sensor data, spoken audio. Since 1993, ACM Multimedia has been bringing together researchers and practitioners from academia and industry to present innovative research results and discuss recent advancements. A special part of the conference is the art program, which explores the boundaries of computer science and art. We invite papers submission in four major themes of multimedia:

Engaging users with multimedia
- Emotional and social signals
- Multimedia search and recommendation
- Summarization, analytics and storytelling

Multimedia systems
- Systems and middleware
- Transport and delivery
- Data systems management and indexing

Experience
- Interactions and Quality of Experience
- Art and culture
- Multimedia applications

Understanding multimedia content
- Multimodal fusion and embedding
- Vision and language
- Domain Interpretation

Highlights of ACM Multimedia 2019

- **Scientific inclusiveness**: We focus on top-quality international research that spans the full variety of the field of multimedia research, as represented by our four themes.
- **Scientific quality**: Reviewers follow explicitly formulated reviewer guidelines. Outstanding reviewers will be acknowledged at the conference awards ceremony.
- **Scientific reproducibility**: We are proud to announce that we will, for the first time, implement the ACM reproducibility badge system. More information is available on our website.

Location and venue

The conference will be held in Nice, France, located in the beautiful Côte d'Azur, also known as the French Riviera. Our venue, the Acropolis Convention Centre, is close to the heart of the historical city, and is easily reachable from Nice Airport, which is an international hub.

Important dates

Workshop Proposal Submission	15 February 2019
Regular Papers Submission	1 April 2019
Open Source Competition Submission	20 May 2019
Technical Demos Submission	20 May 2019
Brave New Ideas Submission	20 May 2019
Interactive Artworks Submission	20 May 2019
Doctorial Symposium Submission	20 May 2019
Panel Proposals Submission	20 May 2019
Tutorial Proposals Submission	20 May 2019
Video Program Submission	3 June 2019
Regular Papers Notification	1 July 2019
Grand Challenge Solutions Submission	8 July 2019
Workshop Papers Submission	8 July 2019

Website: http://www.acmmm.org/2019/
Twitter: @ACMMM19

Association for Computing Machinery
SIGMM
EURECOM
Radboud University
UMR IRISA

TEHNIČKI GLASNIK / TECHNICAL JOURNAL – GODIŠTE / VOLUME 13 – BROJ / NUMBER 1

OŽUJAK 2019 / MARCH 2019 – STRANICA / PAGES 1-80

Sveučilište
Sjever

SVEUČILIŠTE SJEVER / UNIVERSITY NORTH – CROATIA – EUROPE

ISSN 1846-6168 (PRINT) / ISSN 1848-5588 (ONLINE)

TEHNICKIGLASNIK@UNIN.HR – HTTP://TEHNICKIGLASNIK.UNIN.HR